

Effect of altered *Cdkn1c* dosage in adipose tissue

Submitted for PhD

2012

Van de Pette. ME

Supervisor: Dr. R John

Cardiff University

Acknowledgements

As far as the body of work is concerned, there are three main people that require due consideration. Firstly, Dr. Simon Tunster, my postdoc and friend for four years. Secondly Dr. Steven Millership who has strangely helped most of all after he left Cardiff university and had moved to Imperial College. Finally to my supervisor, Dr. Rosalind John. Hopefully by the time you will see this (if you read it), I will have thanked you properly in person. I will just say that its' been a wonderful four years and that is almost exclusively due to you three people, with a sizeable bit of help from the staff of the transgenic unit.

To Professor Takahiro Arima (Tohoku University) and Dr. Mark Christian (Imperial College), thank you for allowing me to work in your respective labs during my PhD and I look forward to working with you again in the future. I will also take this opportunity to thank the funding bodies, BBSRC, JSPS and the Gillian Powell Memorial Fund, which have allowed me to conduct the research.

Finally, to my beautiful Steph. You've kept me level headed and semi- in control of things, particularly during the writing up process and a long three months alone in Japan.

Table of Contents	1
Abstract	6
Abbreviations	6
Chapter 1: Introduction	8
Genomic Imprinting	9
gDMR vs. sDMR	11
Imprinting in clusters	12
Dangers of monoallelic expression	12
Appearance and Expansion of Genomic Imprinting	13
Parental Conflict hypothesis	14
Mouse Distal 7- IC1	16
IC2	18
Imprinting disorders of IC1 and 2	18
Cyclin Dependent Kinase Inhibitor 1c	19
Phlda2	21
Slc22a18	22
Adipose tissue- iBAT	23
WAT	26
(Brown) Adipogenesis	28
Thermogenic Programme induction	30
Adipocyte Lineages	30
Imprinted genes and brown fat	32
Preliminary Work	33
Experimental Design	34

Chapter 2: Materials and Methods	37
Mouse Lines	33
Animal Maintenance	39
Genotyping	40
LacZ staining	41
Feeding studies	41
GTT	42
ITT	43
Cold Challenge	44
Dissection and Weighing	44
Embryo dissection	45
MEF culture	45
Confocal microscopy	46
Tissue fixation and sectioning	47
ORO staining	48
H+E staining	49
In situ hybridisation	49
Immunofluorescence	55
TEM	56
RNA extraction	56
gDNA extraction	57
QPCR	59
Bisulphite treatment	60
Western blotting	64

Antibodies	66
Primers	67
Statistical Analysis	69
Chapter 3: iBAT results chapter	70
Imprinted expression of <i>Cdkn1c</i> in iBAT	71
<i>Cdkn1c</i> expression in iBAT	71
Loss of <i>Cdkn1c</i> in iBAT	73
Elevated lipid content in iBAT	76
Critical pathways are disrupted in <i>Cdkn1c</i> ^{-m/+p} iBAT	77
Reduced C/EBP β and Prdm16 disrupts thermogenesis	82
Investigating the consequences of elevated <i>Cdkn1c</i>	85
Effect of <i>Cdkn1c</i> over-expression in iBAT	87
Cellular expression of <i>Cdkn1c</i> in iBAT	90
QPCR analysis of <i>Cdkn1c</i> over-expressing iBAT	92
<i>Cdkn1c</i> functions with <i>Prdm16</i> and C/EBP β in iBAT	96
Co-localisation of Cdkn1c and Prdm16 proteins in iBAT	98
Discussion	101








Chapter 4: <i>Cdkn1c</i> in white adipogenesis	104
<i>Cdkn1c</i> expression in white adipose tissue	105
Increased <i>Cdkn1c</i> alters normal white adipose tissue	108
Induction of thermogenic genes	112
Disruption of adipogenic genes	113
<i>Cdkn1c</i> acts through <i>C/ebpβ</i> and <i>Prdm16</i>	115
MEF culture	118
Discussion	128
Chapter 5: Consequences of over-expression of <i>Cdkn1c</i>	131
Investigating weight gain in <i>Cdkn1c</i> BAC TG mice	132
Examination of fat pad mass in <i>Cdkn1c</i> BAC TG mice	132
Induction of thermogenic genes	136
Elevated core body temperature.	138
Examination of fat pad mass at 1 year of age	140
Glucose and Insulin tolerance	142
Adipose weights	148
High fat diet (BL6)	150
High fat diet (129)	157
Discussion	161

Chapter 6: <i>Cdkn1c</i> expression in adipose tissue	163
<i>Cdkn1c</i> expression across different depots	164
<i>Cdkn1c</i> expression in mice as they age	165
<i>Cdkn1c</i> sDMR and Lit1 gDMR as mice age	167
<i>Cdkn1c</i> expression in response to maternal conditions	169
Discussion	171
Chapter 7: Discussion	174
<i>Cdkn1c</i> in adipogenesis	175
Mechanism for action	176
Loss of expression of <i>Cdkn1c</i>	177
Flexibility of <i>Cdkn1c</i> in iBAT	178
Imprinting of <i>Cdkn1c</i>	178
<i>Cdkn1c</i> and obesity	180
Brown adipose and Parental conflict	181

Supplementary Figure

Bibliography

Colour Coding

Maternally inherited gene	
Paternally inherited gene	
Wild type	
<i>Cdkn1c</i> ^{-m/+p} (knockout)	
5D3	
5A4	
10-15	

Abstract

Genomic imprinting is an epigenetic process in which the instructions for gene activation or gene silencing are initiated in the germline by DNA methylation. Many imprinted genes play key roles regulating fetal growth and placental development. In addition to their prenatal roles, several imprinted genes have been shown to play significant roles post-natally in particularly with respect to regulating behaviour and metabolism.

Cdkn1c, a maternally expressed imprinted gene, codes for the p57^{Kip2} protein which is a cyclin dependent kinase inhibitor, belonging to the same CIP/KIP family as p21 and p27. *Cdkn1c* was shown to be expressed and imprinted in a small population of cells within post natal iBAT and rWAT. Using both loss-of-function and gain-in-expression models, a critical and dosage-related function for *Cdkn1c* in brown adipogenesis was identified, through *Prdm16* and *C/ebpβ*.

Consistent with an increase in mitochondrial uncoupling, mice that over-expressed *Cdkn1c* were found to be protected against diet- and age-induced obesity, in a dosage dependent manner. *Cdkn1c* may therefore represent a novel route towards obesity therapy and corroborates the hypothesis that the brown adipose tissue may represent a key area of genomic conflict in mammals.

Abbreviations

iBAT- interscapular brown adipose tissue	gDNA- genomic Deoxyribonucleic acid
rWAT- retroperitoneal white adipose tissue	mRNA- messenger Ribonucleic acid
mWAT- mesenteric white adipose tissue	DMR- Differentially methylated region
scWAT- inguinal subcutaneous white adipose tissue	sDMR- somatic differentially methylated region
cDNA- complimentary Deoxyribonucleic acid	gDMR- gametic differentially methylated region

IC- Imprinting Centre	Slc22a18- Solute carrier family 22 member 18
IC1- Imprinting Centre 1	Ucp-1- Uncoupling protein 1
IC2- Imprinting Centre 2	PGC-1 α - Peroxisome proliferator-activated receptor gamma coactivator-1 alpha
BWS- Beckwith Wiedemann Syndrome	Prdm16- PR domain containing 16
SWS- Silver-Russell Syndrome	Elov13- elongation of very long chain fatty acids-like 3
C57J/Bl6- Black 6 mouse line	Fsp-27- fat specific protein family member 27
129S2/SvHsd - 129 mouse line	Perilipin- lipid droplet-associated protein
TEM- Transmission Electron Microscopy	aP2- adipocyte fatty acid binding protein
H+E- Haematoxylin and Eosin	Cox II- cyclooxygenase-2
ATP- Adenosine TriPhosphate	MyoD- myogenic differentiation 1
PET- Positron Emission Tomography	Myf5- myogenic factor 5
qPCR- quantitative polymerase chain reaction	pRb- retinoblastoma protein
WT- Wild type.	PPAR γ - Peroxisome proliferator-activated receptor γ
P7- post natal day 7	C/ebp β - Ccaat-enhancer binding protein β
RFLP- restriction fragment length polymorphism	C/ebp α - Ccaat-enhancer binding protein α
E-embryonic day	Cidea- cell death-inducing DFFA-like effector a
(Q) PCR- (quantitative) polymerase chain reaction	RIP140- receptor-interacting protein 140

Gene Abbreviations

Igf2- Insulin like grown factor 2	PPAR α - Peroxisome proliferator-activated receptor α
Igf2r- Insulin like growth factor receptor 2	
Cdkn1c- Cyclin dependent kinase inhibitor 1c	
Phlda2- Pleckstrin homology-like domain family A member 2	

Chapter 1: Introduction

Genomic Imprinting

Genomic imprinting is an epigenetic process in which the instructions for gene activation or gene silencing are initiated in the germline by DNA methylation ¹. Genomic imprinting has so far been described in mammals and in some plants which have independently utilised DNA methylation to generate allele-specific gene expression ². Currently around 100 protein coding genes have been demonstrated to have their expression regulated by imprinting in mice, representing around 0.1% of the genome (Catalogued: MRC Harwell). The majority of these genes are also imprinted in the human genome with some notable exceptions ^{3;4}. Evidence for an imprinting system was implied from work performed in the 1980s on parthogenetic embryos, which possess two maternally inherited copies of the genome from the same mother, gynogenetic embryos which possess two maternally inherited copies from different mothers and androgenetic embryos which possess two paternal copies from the same father. These embryos, while possessing a diploid chromosomal content, failed to reach term ^{5; 6; 7; 8}. It was concluded from these elegant experiments that there must be a difference in the genetic inheritance from either parent that was complimented only by the combination of both the maternal and paternal genomes. It had earlier been shown such an imbalance was unlikely to be found in other vertebrate species ⁹.

Fig 1.1 illustrates the expression pattern of imprinted genes, where one of the parentally inherited genes is silenced while the other remains active. In (a), a classical Mendelian gene is displayed with active expression for the maternally (green) and paternally (blue) inherited alleles. Genes (b) and (c) represent maternally and paternally expressed imprinted genes respectively, with the other parentally inherited copy of the gene silenced. In most cases, this pattern is conserved across members of the same species, where all individuals will display a similar expression pattern.

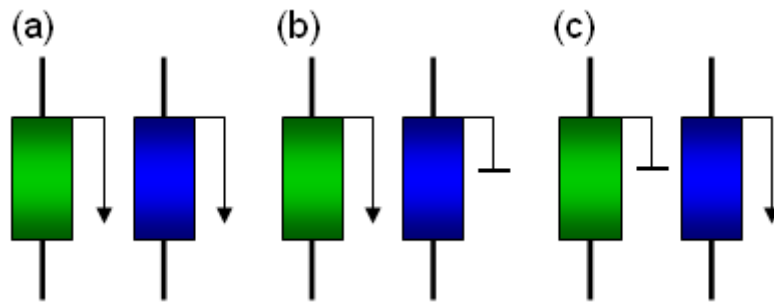


Figure 1.1 Basic Principle of Genomic Imprinting: (a) Bi-allelically expressed gene following a Mendelian pattern of inheritance, (b) Maternally expressed imprinted gene, (c) Paternally expressed Imprinted gene. Mono-allelic expression from the imprinted genes accounts for the majority of expression of that gene, as opposed to (a), where both alleles contribute equally.

This pattern of silencing and expression is controlled by DNA methylation^{10; 11; 12; 13}. All imprinted loci to date contain regions of DNA methylation present on one allele but absent on the other allele¹⁴. These Differentially Methylated Regions (DMRs) are CpG-rich regions of DNA that undergo methylation as a result of the action of the DNA methyltransferase (DNMT) enzymes^{15; 16; 17; 18}. An example of methylation controlling the expression of imprinted genes can be seen below (Fig 1.2). Methylation of the DMR on the maternal allele, often called the Imprinting Centre (IC), is sufficient to control the imprint status of the entire domain^{19; 20; 21}.

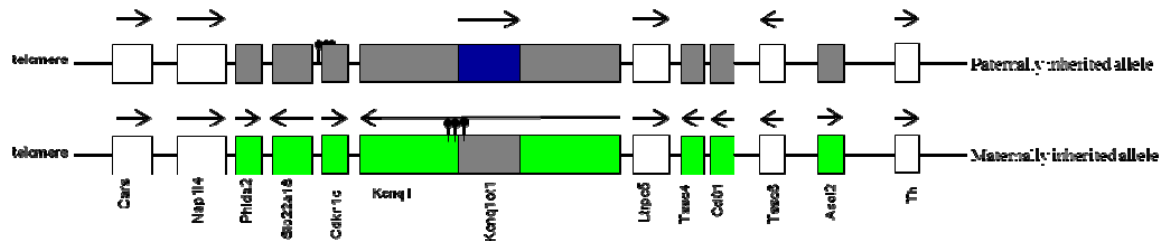


Figure 1.2 Map of IC2 imprinted domain on mouse distal chromosome, a larger cluster of imprinted genes that is located next to, but otherwise functions distinctly, from the IC1. The IC2 is only found to be imprinted in eutherian mammals. White boxes represent bi-allelically expressed genes, green boxes represent maternally expressed imprinted genes and blue box represents paternally expressed imprinted gene. Grey boxes represent the silenced allele. Arrow displays direction of transcription. 3 black lollipops highlight the differentially methylated region (DMR) that controls imprinted expression of the cluster. A differentially methylated region is also found in the promoter region of *Cdkn1c* gene, referred to as a somatic DMR that functions to maintain imprinted expression once it is established.

Gametic differentially methylated region (gDMR) vs. Somatic differentially methylated region (sDMR)

Two types of DMR have been described within imprinted domains (recently reviewed in ²²). DMRs which are initiated in the germline have variously been termed primary DMRs, germline DMRs and gametic DMRs. A number of studies have identified these gDMRs as imprinting centres. This is based on targeted deletion of these discrete regions which has been found to result in loss of imprinting after passage through one parental germline ²². A second type of DMR exists, which is acquired on one parental allele after fertilisation. These are termed secondary or somatic DMRs. An example of a somatic DMR is one spanning the promoter of the *Cdkn1c* gene, where methylation is acquired after monoallelic expression of *Cdkn1c* is established between approximately embryonic day

(E) 6.5 and E8.5²³. These somatic DMRs appear to be important in the maintenance of gene silencing
22; 24; 25

Imprinting in clusters

Imprinted genes are predominantly found in imprinting clusters^{24; 26; 27; 28; 29}. This phenomenon will be described in greater detail later on when exploring the imprinting clusters on mouse distal chromosome 7, including the cluster containing *Cdkn1c*²⁹.

Dangers of monoallelic gene expression

While the parent specific nature of imprinted genes represents a clearly deliberate method of gene dosage regulation, it is also apparent that this method opens the individual to unique dangers from mutation to the single active copy (Fig 1.1). Any changes in this active allele are likely to have an immediate consequence, in contrast to mutations that occur in a single copy of a bi-allelically active gene where the undamaged allele can provide some protection. There is also the possibility that silent mutations can take place in the inactive copy which will manifest only after transmission through one parental germline.

Appearance and Expansion of Genomic Imprinting

As has already been drawn attention to, the genomic imprinting system is believed to be restricted to the mammalian order within vertebrates. Genomic imprinting has also been described in plants. While the two phenomena share mechanistic similarities, there are examples of co-evolution which may have occurred in response to the same evolutionary pressure^{2; 30; 31}.

Much speculation exists with respect to what these evolutionary selective pressures might be. Extant mammals are divided into eutherians, marsupials and monotremes. Monotremes are considered to be the more primitive mammal as they are egg laying mammals and so far imprinting has not been found in the limited examples analysed³². Only three extant species of monotreme remain, located exclusively in Australasia. Unlike the other orders of mammals where offspring begin life within the womb and are nurtured through supplies from the placenta, monotremes instead lay eggs. However, these eggs are not like those laid by birds. Instead they are surrounded by a porous membrane and, as such, some nutrient transfer in the womb does take place³³.

Marsupials, which are now only found in the wild in Australasia and the Americas, have acquired a limited system of genomic imprinting. Of those so far studied, only a subset of genes imprinted in eutherians, such as *Igf2*, are imprinted in marsupials^{34; 35; 36}. This difference in the extent of imprinting has been attributed to differences in reproductive strategies. Although marsupials and eutherians both share the characteristic of giving birth to live young, the marsupial young is born at a less well developed stage and remains dependent on the mother for longer³⁷. Another striking difference between eutherians and marsupials is the structure and invasiveness of the extra embryonic tissues. In marsupials, nutrient transport primarily takes place via membranous extra embryonic tissues (chorio-vitelline placenta). In contrast eutherians switch from this simpler structure at approximately mid gestation to a more complex structure, the chorio-allantoic placenta, which is invasive and, in many mammalian species also in direct contact with maternal blood³⁸. This more complex placenta acts to provide high turnover of supplies supporting extended gestation and the

development of the more mature fetus ³⁹. The difference between the mammalian orders in this context is annotated below (Fig 1.3).



Order	Monotreme	Marsupial	Eutherian
Divergence		160 MYA	125 MYA
Pregnancy	(Limited)	Yes	Yes
Embryogenesis/ Live Young	X	Yes	Yes
Invasive Placenta	X	X	Yes
Imprinting	X	Limited	Yes

Figure 1.3 Comparison of extant mammalian orders with respect to childbirth and genomic imprinting. MYA: Million Years Ago.

Parental Conflict Hypothesis:

The most popular and enduring hypothesis to explain the presence of the imprinting system in eutherian and marsupials is the parental conflict hypothesis. This theory states that

differences in the reproductive contribution made by the two sexes acted as the driving forces for commencement of imprinting. From the point of view of the father, the survival of offspring remains of the utmost importance, so as to continue the genetic line. While this is also the case from the maternal side, allocation of resources to offspring during pregnancy are a factor, as these primarily come from the mother and it is also necessary to ensure her personal wellbeing⁴⁰. Consequently it is thought that there is a selection advantage for the paternal genome to silence genes that limit fetal growth while the maternal genome has responded by silencing genes that act to promote fetal growth (Fig 1.4)^{40; 41; 42}.

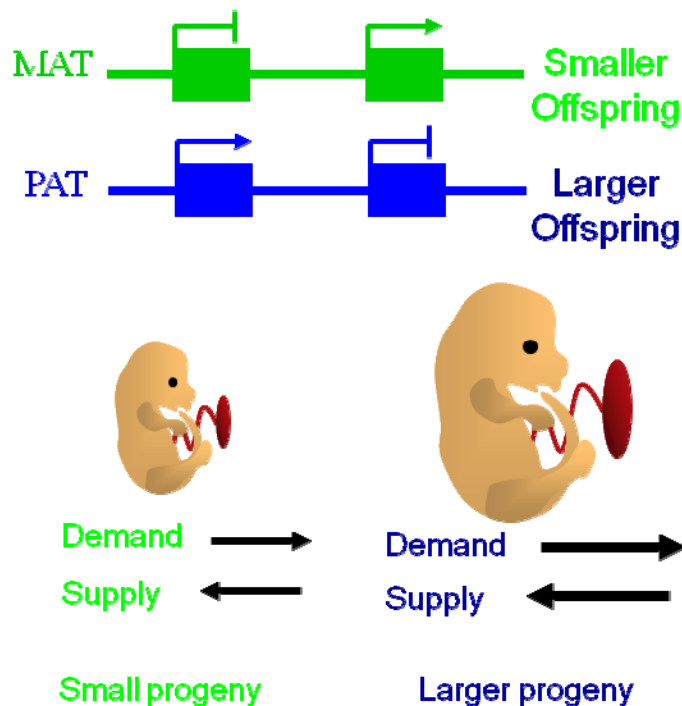


Figure 1.4 Depiction of Parental Conflict Hypothesis. Silencing of genes on the paternally inherited genome result in larger offspring that have improved survival chances. In contrast, silencing of maternally inherited genes will prevent excess nutrient depletion during pregnancy by limiting embryonic growth.

Parental Conflict was based on the observed roles of two of the earliest imprinted genes identified, *Igf2* and the *Igf2r*. In therian mammals studied, *Igf2* is exclusively expressed from the paternally inherited allele in almost all tissue types, while the maternal copy remains silent^{43; 44; 45; 46}. In contrast, *Igf2r* was exclusively found to be expressed from the maternally inherited allele^{3; 44}. Analysis of mouse models and human disease have clearly demonstrated that reduced *Igf2* expression impairs growth, while elevated expression produces overgrowth^{47; 48; 49; 50}. As a reciprocal phenotype to this, loss of *Igf2r* expression presents with, amongst others, perinatal overgrowth in mice⁴⁷. Since this time, a number of imprinted genes have been identified that fit with this pattern. However, not all imprinted genes fit this pattern. For example loss of function of *Nesp55* does not overtly alter fetal growth but instead results in behavioural changes⁵¹. The rationale for adopting the imprinting system may therefore be more complex and several alternative explanations have been put forward^{52; 53; 54}. Parental conflict, however, remains a principle hypothesis associated with the imprinting system and will therefore be utilised in discussing the results of this project.

Mouse Distal Chromosome 7

One of the largest domains of imprinted genes observed in the mouse genome is found on mouse distal chromosome 7, homologous to human chromosome 11p15. Although initially thought to represent a single large domain, it is now known that there are two mechanistically distinct imprinted domains in this region, named IC1 and IC2^{24; 55; 56}.

IC1

The IC1 cluster, which spans *Igf2*, is illustrated below (Fig 1.5). The genes in the IC1 domain were in fact some of the earliest discovered genes that displayed mono-allelic expression, in both mice and humans^{43; 57; 58}. The IC1 domain is thought to be a more ancient imprint since imprinting of *Igf2* occurs in both eutherian and marsupial species^{34; 35; 43; 45}. No such parent specific expression was observed in monotremes³². The presence of imprinting within this cluster of genes prior to the divergence of eutherians and marsupials would suggest that this was one of the earliest imprinting events. The mechanism of imprinting and functions of these imprinted genes will not be discussed in this thesis, as no work has been performed on this cluster.

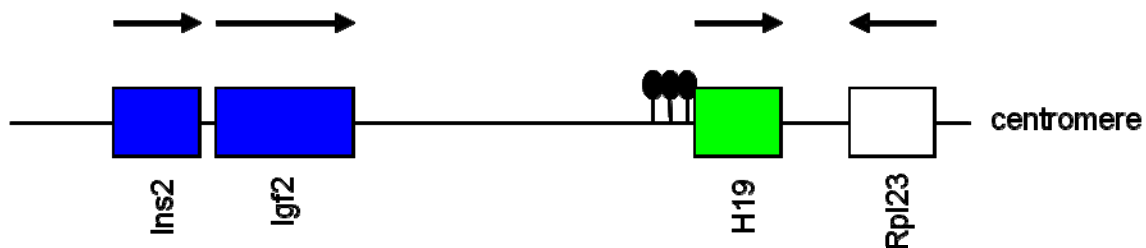


Figure 1.5 Map of IC1 imprinted domain on mouse distal chromosome 7. This cluster represents an evolutionary ancient imprint, with monoallelic expression conserved in marsupials. Blue boxes represent paternally expressed genes, while green are maternally expressed. White box represents a bi-allelically expressed gene. Arrow displays direction of transcription. Black lollipops highlight the differentially methylated region (DMR) that controls imprinted expression of the cluster.

IC2

Located next to the IC1 domain is the larger IC2 imprinted domain, which was previously illustrated (Fig 1.2). In contrast to the IC1 domain, genes within the IC2 domain have been shown to be bi-allelically expressed in marsupials^{34; 36}, implying that imprinted status of this domain was acquired after the divergence of marsupials and eutherians. Imprinted status for the IC2 domain is controlled by a DMR found within the non-coding region of the *Kcnq1* gene. Unlike the enhancer interactions model that has been suggested for the IC1 domain, the IC2 domain appears to work via a non-coding RNA mechanism. The DMR within the IC2 domain, termed KvDMR, contains the promoter of a long non-coding RNA which has been called *Kcnq1ot1* or *Lit1*^{20; 59; 60}. This non protein coding RNA has been demonstrated to be critical for imprinting of the entire cluster, and in its absence, bi-allelic expression is restored in all imprinted genes^{20; 21; 61; 62}.

There is a second DMR within the IC2 domain, depicted in Fig 1.2, which is located over the promoter and gene body of *Cdkn1c*⁶³. Differential methylation at this region is acquired after fertilisation in the mouse^{23; 60} and this DMR is therefore a somatic DMR. Continued methylation at this region is required to maintain the established mono-allelic expression of *Cdkn1c*^{20; 22; 24; 25; 64; 65}

Imprinting Disorders of IC1 and 2

Beckwith-Wiedemann (BWS) and Silver-Russell Syndrome (SRS) are two human imprinting disorders that are believed to primarily arise due to altered imprinting status of the genes on chromosome 11p15^{66; 67; 68; 69; 70}. The syndromes are rare with prevalence of around 1/13,700 and 1/100,000, respectively.

BWS is a childhood overgrowth disorder with additional features including macroglossia, neonatal hypoglycaemia and abdominal wall defects ^{71; 72}. The heterogeneous presentation of symptoms in patients has been attributed to different gene alterations. Familial cases of BWS often possess maternally inherited inactivating mutations of the *CDKN1C* gene ^{73; 74; 75}. Sporadic cases, which make up the vast majority of BWS patients, show far fewer *CDKN1C* mutations ⁷⁰. Instead loss of methylation in the IC2 gametic DMR (Fig 1.2), which would be predicted to result in loss of expression of the IC2 genes including *CDKN1C*, has been found to account for >60% of cases ^{76; 77; 78}. In addition, some patients have maternal uniparental disomy and some show loss of imprinting in the *Igf2* ⁷⁹. Loss of function of *CDKN1C* expression and loss of imprinting of *IGF2* either alone or in combination are likely to be the cause of many of the defects observed in BWS.

SRS is considered to be a reciprocal growth disorder to BWS with many patients showing alterations involving the 11p15 region ^{68; 80; 81; 82}. The major clinical feature associated with the disease is severe growth retardation ^{83; 84}. As with BWS, SRS may originate from mutations in *CDKN1C* and/or *IGF2*. Most recently, micro-duplications in the region that maps to *CDKN1C* have been reported, implicating over expression of *CDKN1C* as a cause of SRS imprinting ^{68; 80; 81; 82; 85}. Similar to BWS, SRS cases display a heterogeneous phenotype implying multiple underlying defects. Overall, it appears that loss of function of *CDKN1C* is present in the majority of cases of BWS while gain-in-expression of *CDKN1C* is present in at least some cases of SRS

Cyclin Dependent Kinase Inhibitor 1c (Cdkn1c)

Cdkn1c codes for the p57^{Kip2} protein which is a cyclin dependent kinase inhibitor, belonging to the same CIP/KIP family as p21 and p27 ^{86; 87; 88}. *Cdkn1c* is located in the IC2 imprinted domain of mouse distal chromosome 7, homologous to human chromosome 11p15. It has been shown to be imprinted in both humans and mice ^{86; 89}, with exclusive expression from the maternally inherited allele in mice and majority expression from the maternal allele in humans. While highly

expressed in the developing embryo and placenta in a specific set of tissues as they exit proliferation^{87; 88; 90}, expression of *Cdkn1c* is down-regulated after birth⁹¹.

The primary function of *Cdkn1c* is to induce growth arrest, through the inhibition of G1/S phase progression in the cell cycle^{87; 88}. However, aside from a general function in attenuating cell cycle progression, *Cdkn1c* has been shown to play roles in directing the differentiation of several cell types, influencing cell migration^{92; 93} and modifying the Actin cytoskeleton^{94; 95}. Regarding a role in differentiation, *Cdkn1c* has been shown to regulate the differentiation of amacrine cells in the retina⁹⁶. In addition, the gene is a positive regulator of dopamine cell differentiation^{97; 98}. Finally, a direct binding interaction between the protein and MyoD protein has been established, and *Cdkn1c* knockout mice display signs of poorly differentiated skeletal muscle^{99; 100; 101}. Included within this role was a positive feedback loop with MyoD, that involved the promotion of *Cdkn1c* expression⁷⁰.

Three independent *Cdkn1c* loss of expression mouse models have been reported^{101; 102; 103}. While some features relevant to BWS were present such as abdominal wall defects, fetal overgrowth, the cardinal feature of the syndrome, was not present. Our more recent studies have revisited the model and demonstrated that, while loss of function results in an increased potential for overgrowth, there is a failure of the *Cdkn1c*-deficient fetuses to maintain their growth trajectory later in development. We attributed this loss of growth potential to severe placental defects. We also noted that *Cdkn1c*-deficient pups in larger litters were not overgrown while those in smaller litter were overgrown by as much as 20%. We suggested that intrauterine competition might account for the difference in overgrowth observed in the mouse model versus the human scenario, rather than the gene functioning differently between the species¹⁰⁴. Adult studies on *Cdkn1c*-deficiency are impaired by the neonatal lethality observed on the C57BL/6 (BL6) strain background^{101; 102; 103} and also, as we reported, on the 129S2/SvHsd (129) background¹⁰⁴. More than 90% of knockout mice die within 24 hours of birth which may be due to a cleft palate that prevents feeding and/or abdominal wall defects.

Using bacterial artificial chromosome-based transgenes (BACs), mouse lines have been generated to study over-expression of *Cdkn1c*. BACs are useful in the studies of over expression

phenotypes since they encompass discrete region of genomic DNA and include both the endogenous promoters and enhancers for the gene of interest. This means that entopic over-expression rather than ectopic mis-expression can be studied ¹⁰⁵. The BAC transgene spanning the *Cdkn1c* locus is 85 kb in size and contains the coding regions for two additional imprinted genes, *Phlda2* and *Slc22a18* ¹⁰⁶. Previous studies on mice carrying one or more copies of this transgene identified a growth restriction phenotype ¹⁰⁷. These mice were studied on a mixed genetic background because on a pure 129 background, the transgene was found to be lethal with no survivors identified after birth ¹⁰⁷. The background for most of the early studies was 75% 129 and 25% BL6. Embryos carrying the transgene were found to be growth restricted during embryogenesis as early as E13.5 and growth restriction was maintained through to birth and into adult life. This growth restriction was found to be dosage dependent, with increased *Cdkn1c* linked to further decreases in body weight ¹⁰⁷. While three genes were present on the transgene, the growth restriction phenotype was attributable to *Cdkn1c* through the use of a modified version of the BAC transgene in which expression of transgenic *Cdkn1c* was interrupted by insertion of β -galactosidase, described in more detail in the material and methods. The conclusion from this study was that *Cdkn1c* represented the major negative regulator of embryonic growth with the IC2 domain.

Phlda2

Located next to *Cdkn1c* on the IC2 domain, *Phlda2* (formerly *Ipl*) encodes a Pleckstrin homology-like domain containing protein that is heavily associated with placental development. As was the case for *Cdkn1c*, *Phlda2* has been shown to exhibit imprinting in eutherians, but not marsupials ^{36; 108}. Expression of *Phlda2* is primarily within the placenta and extra-embryonic membranes ¹⁰⁹. *Phlda2* has been shown to be a potent negative regulator of placental growth in mice, acting on the spongiotrophoblast lineage ^{109; 110; 111}. This role in placental development has been narrowed towards glycogen storage within the placenta that is thought to support later growth of the

fetus¹¹². Imprinting of *Phlda2* results in increased glycogen storage, coinciding with enhanced growth capabilities of the offspring as a result of *Cdkn1c* imprinting.

In humans multiple studies have implicated abnormal expression levels of *PHLDA2* in low birth weight^{94; 113; 114; 115}. The over-expression mouse model was used to demonstrate a direct causal link between elevated *Phlda2* and growth restriction^{97; 110; 111}.

Slc22a18

Slc22a18 is a maternally expressed imprinted gene that displays high expression in the placenta¹¹⁶. The gene encodes a organic cation transporter (solute carrier family 22 (organic cation transporter), member 18), expressed in the placenta, the yolk sac, fetal kidney, liver and intestine¹¹⁶. In the limited work that has been performed on the gene, a change in expression level of the gene was detected in the kidneys of *Aprt*-deficient mice⁹⁸.

Adipose Tissue

Interscapular Brown Adipose Tissue (iBAT)

Brown Adipose tissue was initially described over 400 years ago ¹¹⁷. In rodents, brown adipocytes are primarily located in a distinct depot located between the shoulder blades referred to as interscapular brown adipose tissue (iBAT). Brown adipose is competent to store lipid (Fig 1.6). These stores are multi-locular droplets within the cell. The brown colour, by which this type of adipose tissue is described and which is observable in haematoxylin and eosin (H+E) section, arises from the large mitochondrial count, which can be individually seen in the transmission electron microscope (TEM) images (Fig 1.7).

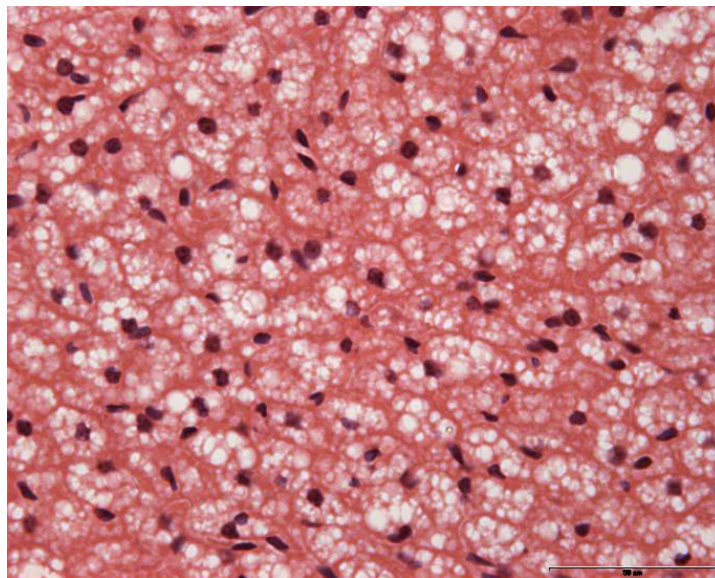


Figure 1.6 H+E stained brown adipocytes from interscapular pad of 10 week old female BL6 mouse. Lipid stores (white) and nucleus (dark purple) are observable in cells. The brown colour results from high mitochondrial population. Photographed under standard light microscopy at 40X magnification.

Clues as to the biological function of the tissue came from studies in the late sixties and seventies and based on the high mitochondrial population of the cell and the unusual membrane potential properties they exhibited. Through a series of experiments it was determined that free fatty acids were providing the major source of metabolic fuel in these adipocytes^{118; 119; 120}. Furthermore, a large proton leak was present within this mitochondrial population^{121; 122; 123; 124}. It was believed that this leak was a determined effort to bypass ATP-synthesis, with free energy given off as a result. Essentially, the free fatty acid stores were being burnt off to provide free energy in the form of heat.

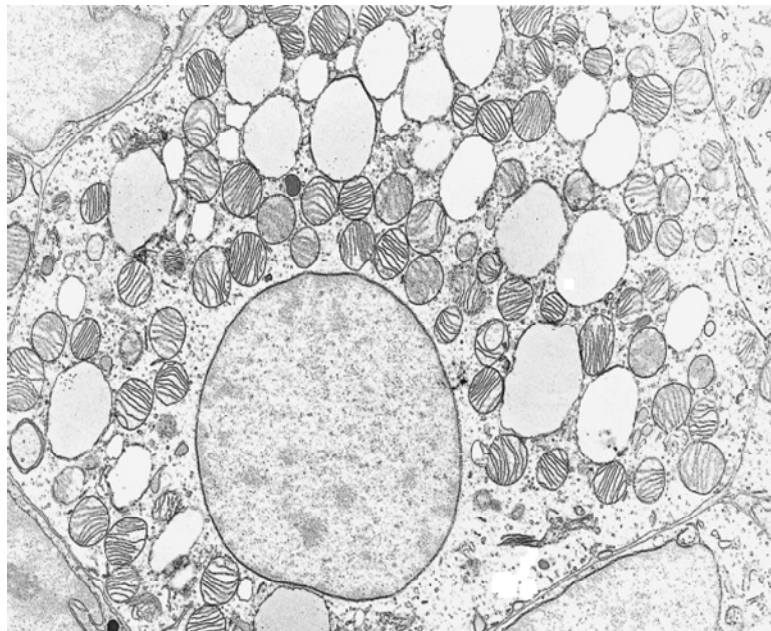


Figure 1.7 Transmission Electron Microscope image of a single brown adipocyte, photographed at X8700 magnification. The nucleus could be seen surrounded by many large mitochondria containing a complex internal membrane structure. Also observable were the multiple lipid droplets (white) within the cell. Reproduced from¹²⁵.

The characterisation of the uncoupling protein 1 (*Ucp-1*) from brown adipose tissue eventually provided an explanation for these phenomena^{126; 127; 128; 129; 130}. *Ucp-1* is a protein that acts to uncouple the electron transport chain through dissipation of the H^+ gradient that spans the inner

mitochondrial membrane. ATP synthase are thus bypassed and the resulting free energy is released in the form of heat. This method of heat generation is termed non-shivering thermogenesis. Winkler and Klingenberg proposed that Ucp-1 spans the mitochondrial membrane, acting as a carrier protein (reviewed ^{131; 132}).

Brown adipose tissue was for an extended period believed to only exist in eutherian mammals. Within mammals, this form of thermoregulation was thought to be absent in monotremes and re-warming rates of echidna hint towards a lack of non-shivering thermogenesis ¹³³. Non-shivering thermogenesis and the occurrence of brown adipose tissue in marsupials remains a highly contentious issue, with multiple reports presenting with conflicting data ^{134; 135; 136; 137}. Consensus now believes that an archaic brown adipocyte-like cell is found in the smallest marsupials, which retain the system of non-shivering thermogenesis throughout life ¹³⁴. Larger marsupials most likely do possess the tissue, though in small quantities and potentially only during immaturity ^{135; 136}. More recent studies on *Ucp-1* conservation across species suggest that, although the gene has been present in vertebra since fish, an acceleration of adaptive evolution occurred in eutherians ¹³⁸.

The detection of brown adipose tissue in adult humans a few years ago was a huge surprise, as it was thought that BAT was lost soon after birth. However, PET scanning of individuals showed all to possess varying amounts of the cell type ¹³⁹. UCP1 positivity confirms the role of these human depots in non-shivering thermogenesis ¹⁴⁰. Prior to these discoveries, brown adipose tissue had largely been viewed as an interesting but otherwise unimportant cell type that was only to be found in small mammals. In light of these discoveries, a host of research avenues has opened up, with a majority focussing on the potential to combat obesity with mitochondrial uncoupling.

White Adipose Tissue (WAT)

While BAT primarily utilises cellular lipid for mitochondrial uncoupling and heat generation, white adipose tissue provides a lipid store. In fact the cell is so specialised at doing this that the vast majority of cellular volume is occupied by a single uni-locular lipid droplet (Fig 1.8). This lipid droplet is so intrusive to the rest of the cellular contents that the nucleus will generally adopt a flattened shape. The full extent of the content can be more easily observed in the TEM image (Fig 1.9), where almost no sub-cellular organelles could be observed.

Due to intermittent restrictions in available food sources, the ability to store energy supplies provides an advantage. From an evolutionary perspective, white adipose tissue is significantly more historic than its brown adipocyte family member that is only observed in the placental mammals. Lipid storage to some degree has been described throughout the eukaryotic family, with most vertebrate organisms found to possess the white adipocyte (reviewed ¹⁴¹).

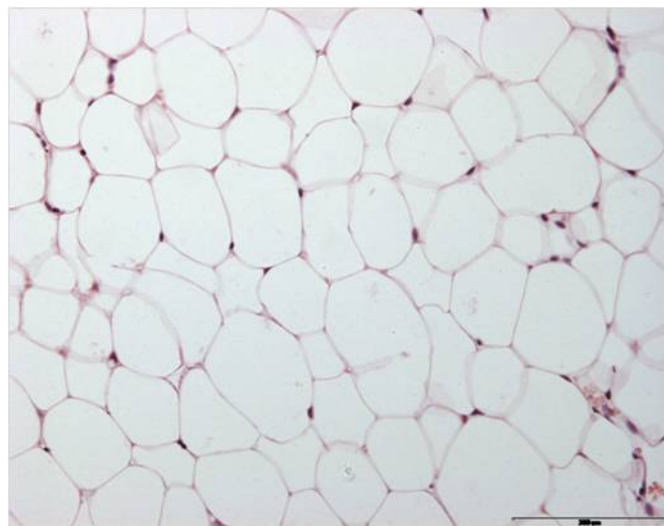


Figure 1.8 H+E image of white adipocytes in epididymal depots from 10 week old C57J/B16 female mouse, image under standard light microscopy at 40X magnification. Scale bar represent 200 μm .

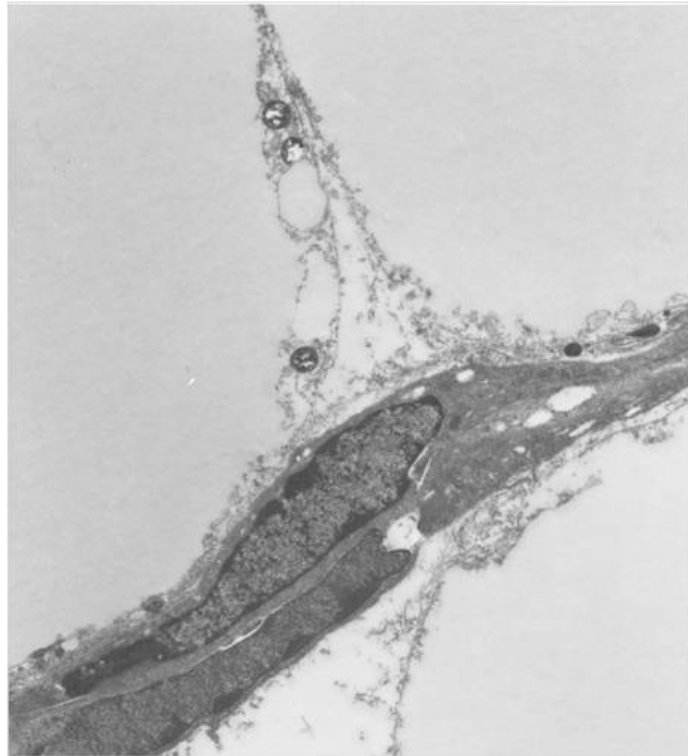


Figure 1.9 TEM image of white adipocytes in epididymal depots from P.7 C57J/B16 female, at 5000X magnification. Uni-locular lipid droplets (white) can be seen with minimal surrounding cytosolic region. Dark organelles are mitochondria.

White adipose tissue is almost exclusively located in the sub cutaneous deposits in reptiles, amphibians and fish. Meanwhile, mammals and many birds share this feature, in addition to possessing significant stores in the visceral areas (reviewed ¹⁴¹). Both groups are the only forms of endotherms, meaning they generate heat through their bodily processes, as opposed to relying on the environment. Clearly generating your own heat will significantly increase the energy intake one must achieve, and these extra lipid stores would help to reduce any strain that would otherwise be put on food gathering. Regarding heat generation, general consensus held that white adipose stores provided insulation to the environment, in a bid to reduce heat loss. Findings that showed little variation between adipose mass of animals from polar regions and the tropics threw doubt on this theory ¹⁴². The picture remains largely unclear as to the true extent that the cell type does play in thermoregulation.

Until quite recently, beyond lipid storage and possible roles in maintaining body temperature, the white adipocyte was not believed to harbour many more biologically significant functions. Perhaps the greatest discovery in dispelling this myth was the cloning of the obese gene, which codes for leptin protein¹⁴³. Since confirmation that the gene was expressed and subsequently secreted from the adipocytes¹⁴, many other secretory factors have been identified. The result is that the adipose organ, comprising both white and brown forms of the adipocyte, has been recognised as an endocrine organ (reviewed⁷²).

(Brown) Adipogenesis

The interscapular brown adipose pad is first identifiable around E15.5 of embryogenesis¹⁴⁴. At birth, iBAT plays a critical role in maintaining body temperature before the development of fur and the insulating layer of subcutaneous white fat (reviewed⁶⁹). In order for correct differentiation of iBAT to occur, a complex signalling cascade must first be achieved, that begins with *C/ebpβ* induction. In fact, it is likely that this signalling cascade is required for both white and brown adipose differentiation. *C/ebpβ* phosphorylation occurs at three separate sites on the protein in two separate events, enabling it to dimerise and attain DNA binding ability^{145; 146; 147} (Fig 1.9).

It has previously been shown that mice lacking *C/ebpβ* display heavily impaired development of adipose pads, resulting in lean and cold sensitive mice^{148; 149}. Given the role of inducing the two major adipogenic transcription factors *C/ebpα* and *PPARγ*, this dependence on *C/ebpβ* expression is not unexpected. Aside from a function in thermogenic program induction that shall be discussed in greater detail later on, there remains a key function for the liver-enriched transcriptional inhibitory (LIP) isoform of *C/ebpβ*. While the activating LAP isoform promotes adipogenesis, the LIP isoform acts to suppress *Ucp-1* expression through direct interaction with its'

promoter¹⁴⁹. These additional functions highlight the dependency of both forms on adipose tissue on *C/ebpβ* expression.

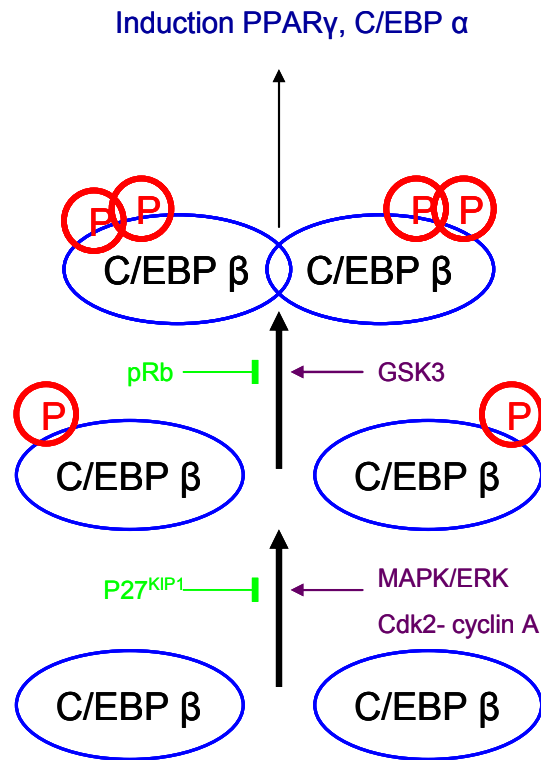


Figure 1.9 Depiction of *C/ebpβ* phosphorylation in differentiating adipocytes. Initial phosphorylation of Thr188 performed by MAPK/ERK, and maintained by Cdk2-cyclin A complexes. Secondary phosphorylation of Ser184 induces di-merisation, activating DNA binding capability and driving cell through S phase. Positive regulators of *C/EBPβ* phosphorylation are shown in purple, while inhibitors are in green.

Downstream of *C/ebpβ* as has already been mentioned are *PPAR γ* and *C/ebpa*. These two, as was the case for *C/ebpβ*, are critical for adipogenesis. *PPAR γ* , often regarded as the master adipogenic regulator is an absolute requirement for differentiation of both white and brown cell types^{150; 151}, while *C/ebpa* is indispensable to white adipogenesis¹⁵². These two work in tandem to activate the expression of all genes required for the formation of mature adipocytes¹⁵³.

Thermogenic Program Induction

In addition to inducing genes that enable lipid storage and turnover amongst other roles, brown adipocytes must successfully acquire the ability to uncouple oxidative phosphorylation in their mitochondria. This function is dependent on *Prdm16* and *C/ebpβ*^{148; 154}, with *Prdm16* acting to both promote the expression of thermogenic genes, and to inhibit white adipogenic genes through direct binding with the CtBP proteins¹⁵⁵.

Recently it has been shown that *Prdm16* and *C/ebpβ* are direct binding partners, inducing expression of downstream genes only when in complex¹⁵⁶. Due to this complex only forming with the active LAP isoform of *C/ebpβ*, activation of gene expression appears to be its' exclusive function. Loss of this complex revert the cell towards a skeletal muscle phenotype¹⁵⁷.

Adipocyte lineages

The proposed pathways leading to formation of mature adipocytes is visualised below (Fig 1.10). The number of question marks within the diagram draws attention to how much work remains to be done before these pathways have been fully elucidated. Furthermore, the adipoblast, which gives rise to the white adipose population, has yet to be identified.

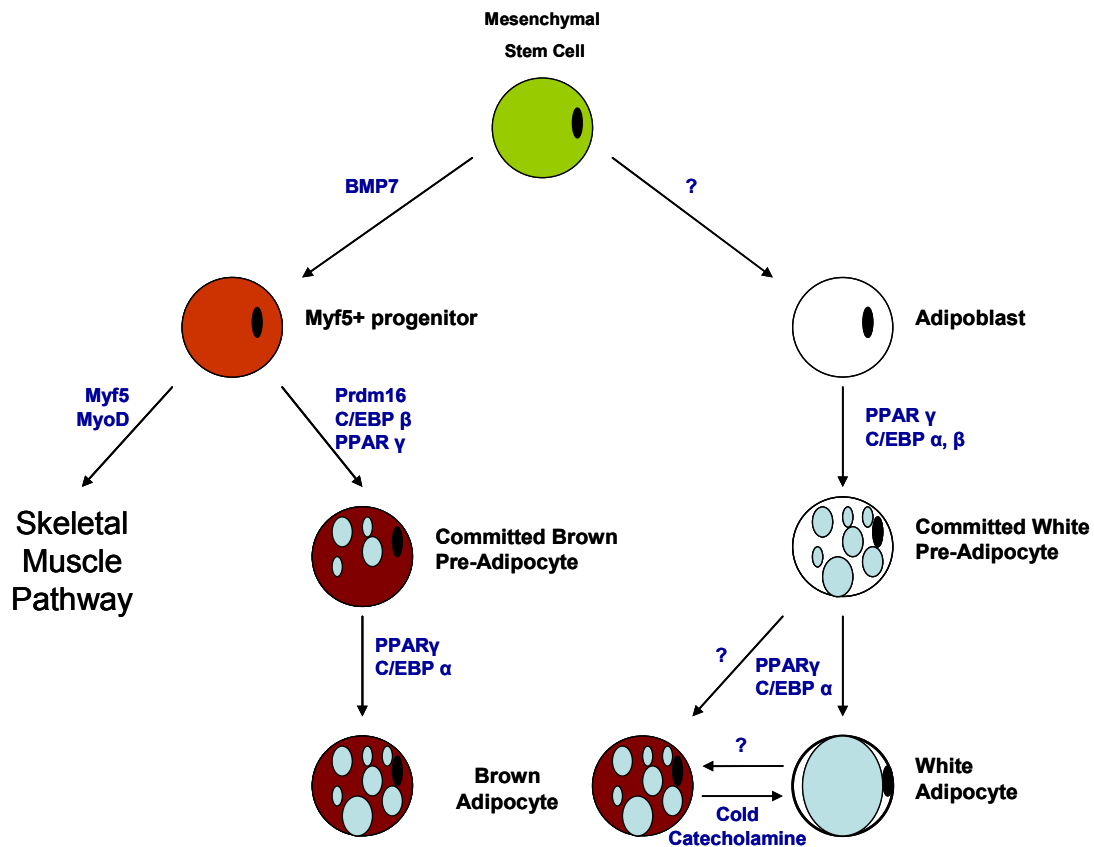


Figure 1.10 Theoretical pathway for differentiation of adipose tissues *in vivo*. Many of the key factors involved in the respective pathways remain unclear, and are therefore highlighted by question marks. Transcription factors in blue represent only the most important factors that promote each following cell type. Nucleus is depicted by black, while lipid droplets are shaded blue. Adapted from ¹⁵⁸.

Strikingly from the image, there are two proposed types of brown adipocyte. It is believed that brown adipocytes, in the classic interscapular depot, come from a Myf5⁺ lineage. A study involving loss of expression of *Prdm16*, a brown adipose determinant, was expected to result in reversion to a white adipocyte-like state. Instead, skeletal muscle characteristics were established ¹⁵⁷. Furthermore, forced expression of *Prdm16* within skeletal muscle cells prompted lipid accumulation and mitochondrial uncoupling ^{156; 158}. The gene was acting as a switch between the myogenic-brown adipogenic lineages.

White adipose depots have been shown to contain brown adipocyte-like cells. In contrast to the iBAT, white adipose tissue arises from a Myf5⁻ lineage (reviewed^{85; 125}). Differences between these two types of brown adipocyte, if there are any, have not yet been elucidated. Difficulty in studying the adipocyte lineages stems from the lack of known pre-adipocyte markers. Currently, only *Pref-1* has been demonstrated as a marker of pre-adipocytes, which is down-regulated upon differentiation^{159; 160}. It will therefore require the discovery of more markers and identify precursor populations within the adipose depots before the whole nature of both brown and white adipocytes can be confirmed.

A final point is that under multiple separate conditions, a brown adipose phenotype can be enhanced in white adipose tissue, in response to a number of different conditions. This will include the induction of *Ucp-1* and non-shivering thermogenesis^{161; 162; 163; 164}.

Imprinted genes and brown fat

Many imprinted genes play key roles regulating fetal growth and placental development^{111; 165; 166; 167; 168}. In addition to their prenatal roles, several imprinted genes have been shown to play significant roles post-natally in particularly with respect to regulating behaviour and metabolism^{169; 170; 171; 172}. The association between imprinted genes and brown fat development was first suggested by David Haig, where he noted that body warmth might be an area on which genomic conflict might act^{173; 174; 175}. A number of imprinted genes have been reported that play a direct or indirect role in regulating thermogenesis^{176; 177; 178; 179}. Due to the limited number of imprinted genes within the genome, it is surprising to find such a clustering of expression away from the role of embryogenesis.

Preliminary Work

The aim of this project was to investigate the consequence of loss and gain-in-expression of *Cdkn1c* in adipose tissue. Constitutive loss of expression of the gene has been widely studied particularly with respect to modeling BWS^{74; 102; 103; 104}. The consequences of over-expressing *Cdkn1c* on embryonic growth have also been described¹⁰⁷. Preliminary studies on the over-expression model noted that adults were lean and did not gain weight as they aged. In a preliminary study, one year old mice that carried an single extra copy of *Cdkn1c* (5D3) on a BAC transgene were found to have a reduced weight of several visceral white adipose depots relative to their total body weight, possessing around 40% less visceral fat (white) than wild types (data not shown). By Magnetic Resonance Imaging (MRI) there was a clear loss of both visceral and subcutaneous adipose (Fig 1.11). No previous role for *Cdkn1c* had been described in adipogenesis, and therefore the project was devised to explore a potential role for *Cdkn1c* in regulating adipogenesis.

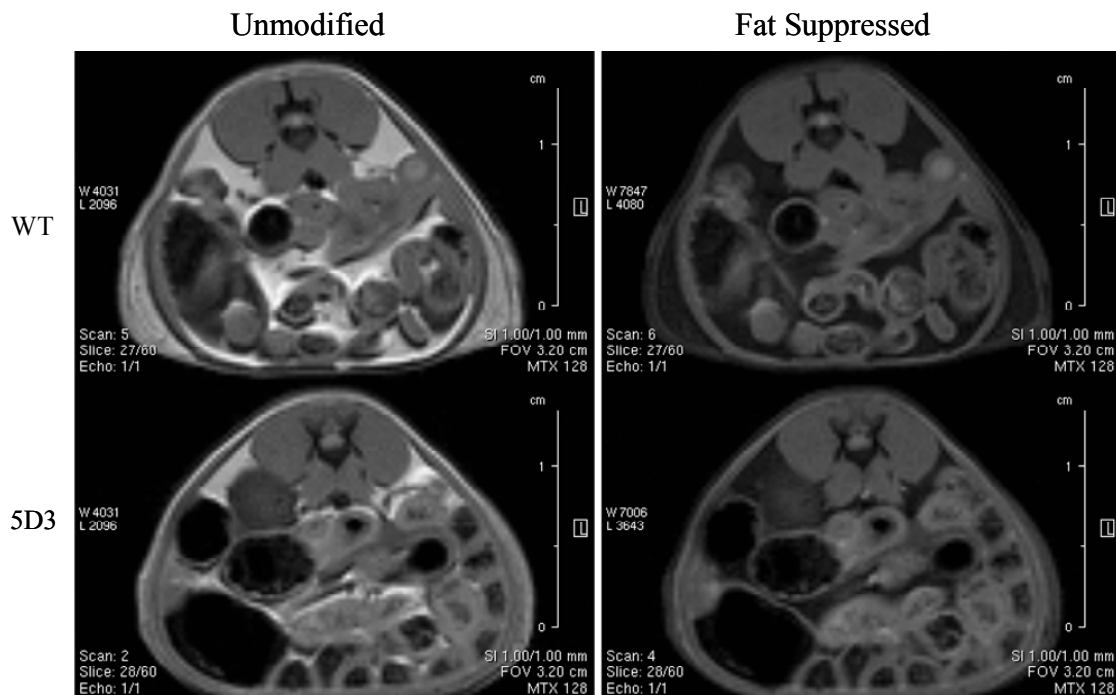


Figure 1.11 MRI scans of 1 year old Wild type and 5D3 129:BL6 female mice. Images were taken around midsection of the mouse body, and revealed less visceral and subcutaneous adipose tissue (white) in 5D3 subject. Through software analysis, signal of the adipose pads were suppressed in the right hand images, leaving only the non-adipose tissue visible.

Experimental Design

As has been previously stated, >90% of *Cdkn1c*^{-m/+p} mice die within 24 hours of birth hampering any study on adult mice. In one study it was reported that surviving *Cdkn1c*-deficient mice (N=5) were all severely growth retarded with severe skeletal abnormalities but their adipose was not investigated¹⁰¹. However, studies on iBAT can be performed since this depot develops during embryogenesis, as opposed to after birth as is the case for white adipose. Therefore experiments were performed at E18.5 of embryogenesis, a time at which *Cdkn1c*-deficient fetuses were still viable.

To study the effects of over-expression of *Cdkn1c* in the adipose tissue, two of the *Cdkn1c* BAC transgenic lines were used. Lines 5D3 and line 5A4 have been previously described^{106; 180}. 5D3 and 5A4 carry one or two copies, respectively, of an unmodified 85kb BAC transgene, described in greater detail in methods section. The BAC transgene spans two additional genes, *Phlda2* and *Slc22a18*, but the existence of the reporter line, 10-15, allows the attribution of *Cdkn1c*-specific phenotypes.

As a first step in the analysis, the 5D3 and 5A4 lines were bred into the BL6 background. As observed when these lines studied on the mixed 129:BL6 background¹⁰⁷, both lines were found to be growth restricted at E18.5. In contrast, 10-15 mice, which possess a modified BAC which does not elevated expression of *Cdkn1c*, were not growth restricted (Fig 1.12). At P7, a similar degree of growth restriction was apparent (Fig 1.13).

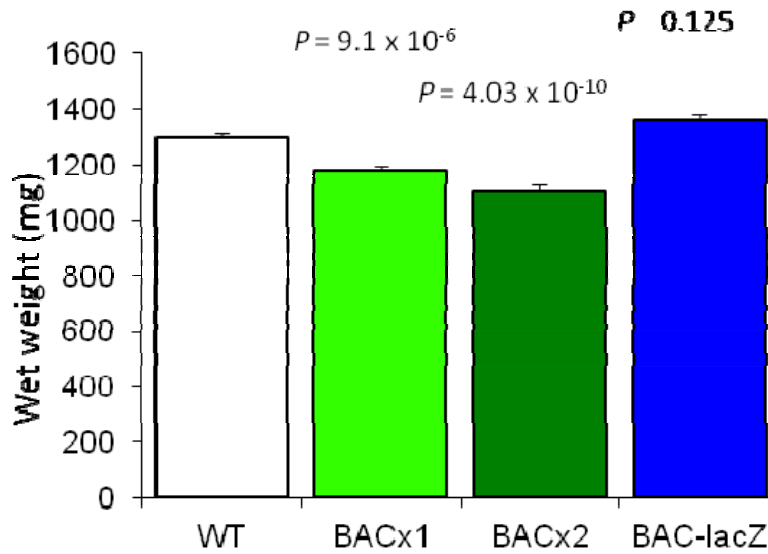


Figure 1.12 Whole body weights of E18.5 transgenic embryos on a pure Bl6 genetic background, compared to wild type (white) littermates. 5D3 (light green) and 5A4 (dark green) embryos were significantly growth restricted, while 10-15 (blue) were not. Error bars represent standard deviation. Statistical analysis was performed by Student's t-test.

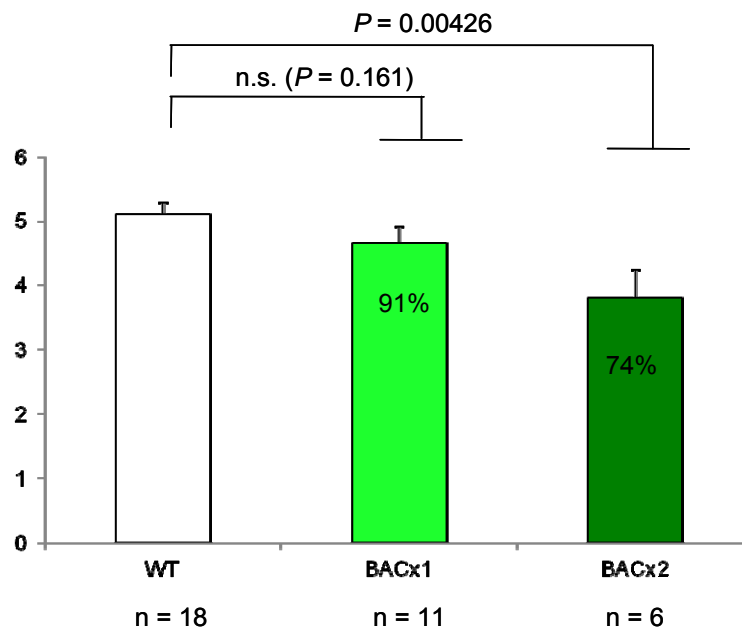


Figure 1.13 Whole body weights of P7 5D3 (light green) and 5A4 (dark green) mice on a pure BL6 background, compared to wild type littermates (white). Error bars represent standard deviation. Statistical analysis was performed by Student's t-test. Both 5D3 and 5A4 pups were smaller, but data for 5D3 did not reach significance.

The aims of the work were:

1. To characterise the cellular and molecular consequences of loss-of-function and gain-in-expression of *Cdkn1c* in iBAT
2. To characterise the cellular and molecular consequences of gain-in-expression of *Cdkn1c* in WAT
3. To determine whether the identified phenotypes occur through the intrinsic action of *Cdkn1c* using mouse embryonic fibroblasts
4. To explore the mechanism by which *Cdkn1c* regulates iBAT and WAT development

Chapter 2: Materials and Methods

Mouse Lines

Three transgenic mouse lines were used for experiments to study the effects of *Cdkn1c* over-expression. The two experimental line 5D3 and 5A4 possess one and two copies, respectively, of a bacterial artificial chromosome (BAC; Genome Systems 144D14) that spans the *Cdkn1c* gene and two other genes, *Phlda2* and *Slc22a18*. This BAC is illustrated in Fig 2.1 (c). These lines were initially generated by electroporating the linearised BAC in mouse 129 RI ES cells, making chimeras and then identifying transgenic offspring¹⁰⁶. These lines were initially bred into an MF1 background as no survivors were found on a pure 129 background. For the purposes of this study, the lines were bred for ≥ 8 generations in the BL6 background. The reporter line 10-15 possesses a modified version of BAC 144D14, illustrated below in Table (b). For creation of this reporter line, the BAC 144D14 clone was modified by homologous recombination of a β -galactosidase reporter construct (*p57Kip2-IRES β geoloxPalkP*) into the *Cdkn1c* locus. Transgenic mice were generated by pronuclear injection of the construct into F₁ C57BL/6 x CBA embryos. The line can be used as a reporter (LacZ staining) to observe where *Cdkn1c* is expressed from the transgene. This line also acted as a control for the experimental lines to ensure that experimental results on the adipose tissue are due exclusively to *Cdkn1c* over-expression (present in line 5D3 and 5A4, absent in line 10-15) and not the other two genes. In all cases transgenic material was obtained by mating male transgenics with wild type females. The majority of the experiments were performed on the BL6 background but some limited analysis was performed on a mixed background of 75% 129 and 25% BL6.

In order to study the consequences of loss of expression of *Cdkn1c*, we utilised the Elledge mutation (*Cdkn1c*^{tm1Sjc})¹⁰³, which had been bred into the 129 genetic background for +8 generation. As *Cdkn1c* is a maternally expressed imprinted gene, effect of the mutation can only be observed upon maternal transmission. Paternal transmission of the same mutation is silent, as this copy of the gene is not naturally expressed. Therefore to generate litters where a phenotype could be observed, females were first generated, which inherited the

mutation by paternal transmission. These *Cdkn1c*^{+m-p} mothers were phenotypically wild type. *Cdkn1c*^{+m-p} females were paired with 129 studs and plug checked each morning. *Cdkn1c*^{-m+p} embryos generated were used to study the effect of loss of *Cdkn1c* expression.

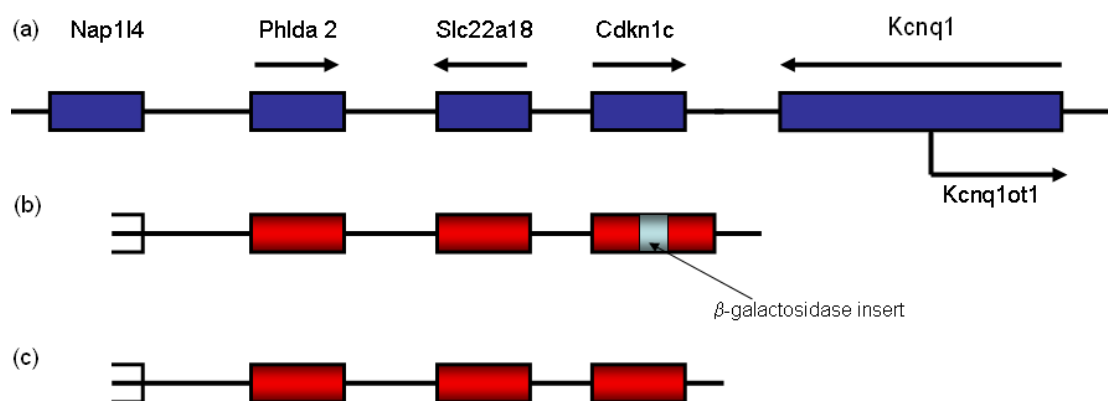


Figure 2.1 IC2 domain and position of transgenes. (a) Representation of five of the imprinted genes found in the IC2 region of Mouse Distal Chromosome 7, which is homologous to Human Chromosome 11p15.5. The five pictured genes are maternally expressed imprinted genes, while the non-coding *Kcnq1ot1* transcript is paternally expressed. (b) Representation of modified BAC transgenes. Line 10-15 carried 3 copies of this modified BAC in which a β -galactosidase insert interrupts expression of *Cdkn1c* expression from the BAC. *Phlda2* and *Slc22a18* expression are the only genes expressed from this modified BAC (Andrews 2007, Tunster 2010). (c) Representation of the unmodified BAC144D14. Line 5D3 contains one copy and line 5A4 contains two copies of the BAC and all three genes are expressed from the transgenic at level similar to the endogenous loci (Andrews 2007, Tunster 2010).

Animal Maintenance

Mice were housed in cages in cohorts not greater than five individuals per cage in non-barrier conditions as per Home Office regulations. Environment was kept at $20^{\circ}\text{C} \pm 1^{\circ}\text{C}$ on a 12 hour light-dark cycle with standard chow (Harlan, Oxfordshire) and water freely accessible. Mice were weaned at four weeks and caged separately from parents in single sex cages.

Genotyping

Tail biopsy from 4 week old animals was digested overnight in lysis buffer (0.05 M Tris.HCl pH 8, 0.025 M EDTA, 0.031% SDS, 0.02 M NaCl, 80 µg/ml Proteinase K (Promega)) at 50°C with rocking. The following morning, samples were vigorously shaken to ensure total lysis, followed by being left for at least 30 minutes to allow undigested material to settle.

10 µl sample was diluted in 190 µl 10mM Tris.HCl pH 8 and boiled at 95°C for 30 minutes. During this time, a PCR master mix was prepared, as given below.

<u>Reagent</u>	<u>Volume (per reaction, µl)</u>
TrueStart 10X Buffer	1.5
MgCl ₂	1.2
dNTP's (25 mM)	0.6
Primers F + R (25 µM)	0.3
TrueStart Taq (Fermentas)	0.1
Boiled Sample	1
ddH ₂ O	to 15

Once boiling had been completed, samples were shaken and allowed briefly to cool. PCR reactions were then set up, and underwent the following PCR: 1. 94°C 15 minutes, 2. 94°C 30 secs, 3. 60°C 30 secs, 4. 72°C 30 secs, 5. 75°C 30 secs, repeat cycle 2-5 35 times, 6. 72°C 5 minutes. The 75°C anti-dimer step was found to be a requirement for successful product generation when the hot start Taq was implemented. PCR products were separated on a 1.5% agarose gel and viewed under U.V light. A H₂O negative and a positive control were used for every reaction.

LacZ staining

Adipose pads were dissected and placed in LacZ fix (2% formaldehyde, 0.2% glutaraldehyde, 0.02% NP-40, 1mM MgCl₂, 0.1mg/ml Sodium Deoxycholate in 1X PBS). Fixation was performed for 1 hour at 4°C with rocking. Tissue was briefly washed in 1X PBS (Gibco) to remove LacZ fix, before being placed in LacZ stain (0.4mg/ml XGal, 4mM Potassium Ferrocyanide, 4mM Potassium Ferricyanide, 1mM MgCl₂, 0.02% NP-40 in 1X PBS). Staining was performed overnight at 4°C with rocking. The following morning, adipose pads were washed 2X five mins in 1X PBS, before transfer to 70% EtOH for storage. Photography of tissue was performed under standard light field conditions.

Feeding Studies

Two separate long-term high fat diet studies were performed on transgenic lines. 10 week old 5D3 BL6 females were subjected to 12 week insult of high fat diet, while 5D3 and 5A4 129:BL6 females underwent a shorter 8 week study. High fat diet (TestDiet 58V8, 45% calories from fat) and water were available *ad libitum*. Mice were weighed weekly, while glucose and insulin tolerance testing was performed post-diet.

When measuring food consumption, one week was allowed after dietary or housing change, as initially during this time it had been noted that large variation in consumption existed. Consumption was calculated by subtraction from the previous days' total. Any mice that had previously demonstrated shredding of food were not utilised in these studies. Tests were performed blind.

For the low protein studies, wild type 129 matings were set up and plug checked each morning. Upon plug discovery, females were removed to a clean cage, either with standard chow, or the low protein diet (4400, 8% casein chow, Abdiets). Pregnant females were exposed to the low protein diet until 18.5 days after plug discovery, when they were returned to standard chow.

Glucose Tolerance Testing (GTT)

Both glucose and insulin tolerance testing were performed in order to provide a view of any changes that may have occurred to the glucose management of 5D3 and 5A4 individuals, under both natural ageing and altered diet. For the ageing cohorts, both GTT and ITT were performed at six months and one year of age, while HFD cohorts were subjected to testing both pre- and post-diet.

Mice were fasted overnight prior to testing, but still had access to water. All subjects were individually housed for the duration of the test, with sufficient and comparable environmental enrichment to reduce any undue stress, and were weighed before testing began. A minimum part (≤ 5 mm) of the tail end was cut off by a clean scalpel and blood was squeezed out. This blood was collected in cuvettes (HemoCue) and blood glucose concentration was measured by Glucose 201+ meter (HemoCue). After samples were taken, mice were injected intraperitoneally with 10 mM/ kg glucose (Sigma Aldrich) and further readings were taken at 30, 60, 90 and 120 mins post-injection.

Once the final sample had been taken, mice were returned to their original cages, and we allowed access to chow again. All experiments were performed blind and not more than twelve individuals were tested in a single test.

Insulin Tolerance Testing (ITT)

Normal practice for insulin tolerance testing involves a short fasting of the mice prior to test commencement, in order to ensure a fair baseline reading. After the initial attempt, it was discovered that 5A4 mice produced a sufficiently extreme response to insulin challenge that this would not be possible. As a result, mice had access to chow ad libitum for the entirety of the procedure. In order to provide some control of baseline readings, it was determined that an early afternoon start provided significantly better grouping of the readings, than one started in the morning. Therefore, all tests were begun at 2pm.

As in the GTT, mice were individually housed with access to water, and in this case chow, ad libitum. A minimum part (≤ 5 mm) of the tail end was cut off by a clean scalpel and blood was squeezed out. This blood was collected in cuvettes (HemoCue) and blood glucose concentration was measured by Glucose 201+ meter (HemoCue). After samples were taken, mice were injected intraperitoneally with 0.75 U/ kg insulin (Novo Nordisk) and further readings were taken at 15, 30, 45 and 60 mins post-injection.

Once the final sample had been taken, mice were returned to their original cages. All experiments were performed blind and not more than twelve individuals were tested in a single test. A supply of 2M glucose solution was required at all tests as a precautionary measure to combat any cases of hypoglycaemia. Any tests subjects that were seen to have blood glucose readings dipping below 3 mMol/ L were removed from the test and injected with 100 μ l glucose initially. These mice were then monitored periodically for the rest of the day, to ensure their well being.

Core Body Temperature + Cold Challenge

In order to determine if 5D3 and 5A4 mice displayed any variations in core body temperature, rectal temperatures were measured, which was immediately followed by cold challenge and re-measurement. 10 week old 5D3 and 5A4 BL6 litters had their core body temperature measured by a rectal probe (IN005A, Vet Tech solution). Mice were firmly scruffed for the procedure, and any signs of greater than mild discomfort caused the test on that subject to be halted. Once measured mice were singly housed in cages in a fridge for 30 mins, with food and water *ad libitum*. The cages had been pre-cooled for a minimum of five hours before starting. Upon completion of the test, rectal temperatures were measured again. Testing was started as close to 2pm as possible and only four mice were tested at any given time, to ensure that warming of the fridge did not occur due to the door having been opened to frequently.

Dissection and Weighing

Mice were culled via cervical dislocation and their abdomen was disinfected with 70% EtOH. Organs and fat pads were dissected out and snap frozen on dry ice prior to being stored at -80°C. Tissues were only weighed once fully frozen to ensure that no loss of material occurred. This was of particular importance for the white adipose tissue, which was found to be more fragile than any other tissue type.

Embryo Dissection

Pregnant females were culled via cervical dislocation and their abdomen was disinfected with 70% EtOH. The uterus was dissected out and transferred to cold 1X PBS (Gibco). Embryos were removed from uterus and separated from placenta. They were then culled by decapitation and brown adipose tissue was removed from between the shoulder blades. Samples were either flash frozen on dry ice and stored at -80°C, or fixed as has already been described. Tail tips were used for genotyping.

Mouse Embryonic Fibroblast Culture (performed by Dr. Rosalind John)

Primary cultures of mouse embryonic fibroblasts (MEF) from E12.5 embryos were maintained and differentiated as described¹⁸¹ with minor modifications. Briefly, embryos were removed from the uterine horn into PBS with the yolk sac, head, and internal organs discarded. Remaining tissue was sheared through the barrel of an 18-gauge needle attached to a 2 ml syringe into cell culture medium, a total of three times. These cell suspensions from each individual embryo were plated into separate wells on 6 well tissue culture plates (Nunclon), incubated for 24 hours (37°C, 5% CO₂) and split (using 0.05% trypsin/EDTA) onto 10 cm plates. Cells were maintained in Dulbecco's modified Eagle's medium (DMEM) and F12 (1:1) containing:

Fetal bovine serum (FBS)	10%
L-glutamine	1.8 mM
Penicillin G	100 units/ml
Streptomycin	100 µg/ml
(all Gibco)	

At confluence cells were split onto 6 well tissue culture plates or poly-L-lysine coated 13 mm coverslips. Two days post-confluence, media was changed to a pro-differentiation media containing:

Insulin	170 η M
Dexamethasone	250 η M
Isobutylmethylxanthine (IBMX)	0.5 mM
(all Sigma)	
Rosiglitazone (Axxora)	2.5 η M

After 2 days, this media was removed and cells were fed media containing only insulin and rosiglitazone for a further 6 days. Cells were fixed, or harvested for RNA on day 0, 2, 5 and 8 respective to addition of the first differentiation regimen.

Confocal microscopy

MEF's were grown up and underwent differentiation as described in the previous section, however for the purposes of confocal microscopy, separate 5cm glass bottom plates (Mat Tek) were utilised. These allowed higher resolution images to be taken, due to the reduced scattering effect of glass over plastic, which allowed clearer visualisation of cellular mitochondrial population.

After 8 days of differentiation, cells were stained with 5 μ g/ ml Hoechst 33342 (Invitrogen) and Rhodimine-123 (Sigma Aldrich) in 2nd differentiation media for 30 minutes

at 37°C. Dyes were removed, and cells were washed for 5 minutes in media. Further staining with 7.5 µg/ ml HCS CellMask Red (Invitrogen) for 10 mins was performed. 3 X 5 mins washes in ddH₂O were performed. Samples were imaged using Leica TCS SP2 AOBS laser confocal microscope, and Leica Confocal software.

Tissue fixation + Sectioning

Samples for H+E staining and *In situ* hybridisation were dissected and immediately immersed in cold 4% PFA fixative. Fixation occurred overnight at 4°C on rotation. The following morning, samples were washed twice in 1X PBS for 5 mins, before storage in 70% EtOH. Paraffin embedding and 10 µm sectioning was performed by Derek Scarborough.

For Oil Red O staining of adipocytes, frozen adipose pads were embedded on aluminium chucks in OCT mounting medium (RA Lamb), using dry ice. 10 µm thick sections were cut using a Bright Microtome 3050 cryostat at -20°C onto TESPA (0.2% TESPA in 100% Acetone (Sigma Aldrich)) coated slides. Samples were immediately sent for fixation and staining.

For immunofluorescence of iBAT, P7 pads were dissected and immediately immersed in cold 4% PFA fixative. Fixation occurred overnight at 4°C on rotation. The following morning, samples were washed twice in 1X PBS for 5 mins, before immersion in 30% sucrose for 24 hours at 4°C for cryopreservation. Upon completion, samples were dried on paper towel and embedded on aluminium chucks in OCT mounting medium (RA Lamb), using dry ice. 7 µm thick sections were cut using a Bright Microtome 3050 cryostat at -20°C onto TESPA coated slides.

Oil Red O (ORO) staining

A stock solution of Oil Red O (ORO) lipid stain was prepared by mixing 1g Oil Red O (Sigma Aldrich) in 500ml Isopropanol. The solution was left to dissolve for 24 hours with mixing to aid. In order to prevent any issues with precipitation of the dye, a working solution was only prepared directly prior to being needed. 24ml of ORO stock solution was mixed with 16ml ddH₂O. After 10 mins, the working solution was filtered through double Whatman paper, where upon passing through was ready for use.

Freshly cut adipose sections were fixed in paraformaldehyde vapour. This was to ensure that formalin liquid did not come into direct contact with the lipid, which hinders the stain. An enclosed incubator was preheated to 50°C containing 10ml paraformaldehyde placed in a beaker. After 15 mins, slides containing the sections were rapidly placed inside the incubator, whilst more paraformaldehyde in the beaker was added if all had vaporised. Samples were fixed for 20 mins in this environment.

Post-fixation, slides were briefly washed in ddH₂O prior to haematoxylin (Sigma Aldrich) staining for 30 secs. It was necessary to perform the nuclear stain first as little signal was generated when performed after lipid staining, whereas this way round, lipid staining performed second was not found to significantly alter results. Slides were washed in running tap water for five mins after nuclear staining and finally rinsed in ddH₂O. Filtered Oil Red O working solution was then applied to slides and left to stain for 15 mins. Upon completion, slides were washed with ddH₂O and mounted using cover slip and Vectamount AQ aqueous mounting medium (Vector). Slides were photographed under standard light microscopy within 24 hours.

ORO staining of day 8 MEF plates was performed in an identical way, however this was performed in 6 well plates, as opposed to slides.

H+E staining

Paraffin embedded 10 µm sections were stained with haematoxylin and eosin (H+E) by Derek Scarborough via standard protocol. Sections were then photographed under standard light microscopy at 20X magnification.

In situ hybridisation and Cell Counting

In situ hybridisation was performed so as to gain insight into *Cdkn1c* expression within the adipose tissue. A probe for *Cdkn1c* had previously been designed by Dr. Simon Tunster. An approximately 500 bp sequence was amplified from mouse placenta cDNA using primers designed by Primer 3. mRNA and genomic *Cdkn1c* had already been aligned to ensure an intron/ exon boundary was the target of amplification. PCR product was purified using PCR purification kit (Qiagen) and resuspended in 30 µl 10mM Tris (pH8).

25 ng DNA was ligated into pGEM-T Easy vector per reaction as follows:

Reagent	Volume (µl)
H ₂ O	to 10
2X Buffer	5
pGEM-T Easy vector	1
T4 DNA ligase	1
DNA	(25 ng)

Reactions were left at 4°C overnight.

The follow day, LB/Carbenicillin plates were prepared by spreading 100 µl IPTG (0.1M) and 20 µl X-Gal (50mg/ml) onto agar and drying at 37 °C for thirty mins.

2 µl of the ligation was added to 50 µl JM109 cells (Promega) on ice and incubated for 20 mins. Cells were heat-shocked for 45 secs at 42°C and then immediately returned to ice for 2 mins. 950 µl SOC medium was added to each reaction and incubated for ninety mins at 37°C on rotation. On separate LB/Carbenicillin/IPTG/X-Gal plates, 100 µl and 900 µl of reaction was plated and incubated overnight at 37°C.

The following day, six white colonies were selected and transferred to 5ml of LB medium containing Carbenicillin using a clean tip, which was then incubated overnight at 37°C on rotation. Plasmid DNA was purified from 4.5 ml of each culture using a mini prep kit (Qiagen), according to the manufacturer's instructions, with DNA eluted in 50 µl ddH₂O. Analytical digest and sequencing was performed to confirm product, orientation and sequence. 0.5 ml of each culture was used to generate a "glycerol stock" by mixing with an equal volume of 50% glycerol in a sterile screw cap tube, labelled appropriately and stored at -80°C.

Agar plates containing the appropriate antibiotic were inoculated using the glycerol stock of the required construct and incubated overnight at 37°C. A single, well-isolated colony was used to inoculate a second agar plate, and incubated overnight at 37°C. A single colony from the second agar plate was used to inoculate 5 ml of LB medium containing antibiotic and grown for 8 hours at 37°C in a shaking incubator at 200 rpm. 100 µl of this culture was used to inoculate 200 ml LB medium, from which plasmid DNA was purified using a midi prep kit (Qiagen) following the manufacturer's instructions, with DNA resuspended in 200 µl 10 mM Tris (pH 8.0), and stored at -20°C. Analytical digests were performed on plasmid DNA preps to confirm product.

Two separate reactions were set up using the restriction enzymes *SacI* (NEB) and *KpnI* (Promega) to linearise each construct either side of the insert thus allowing the independent transcription of sense and anti-sense probes. A total of 30 µg of DNA was linearised in each reaction, with constituents as shown below

Reagent	Volume (µl)
H ₂ O	to 200
10X Buffer (NEB)	20
BSA 100X (NEB)	2
Enzyme	10
DNA	(30 µg)

Restriction digests were incubated overnight at the appropriate temperature, and 5 µl of reaction was run on a 1 % agarose gel alongside undigested vector to confirm complete linearisation.

Linearised plasmid DNA was phenol/chloroform extracted by first adjusting the volume to 500 µl with 10 mM Tris (pH 8.0), then adding an equal volume (500 µl) of phenol and mixing. The mixture was centrifuged at 13,000 r.p.m for 10 mins at room temperature, and the upper aqueous phase was removed to a clean microfuge tube to which an equal volume of chloroform was added and mixed. The mixture was centrifuged as above, and the aqueous phase removed to another microfuge tube. A volume of 3 M NaOAc (pH 5.2) equal to one-tenth of the total volume of the aqueous phase was added in addition to 2.5 volumes of 100% EtOH. DNA was precipitated overnight at -20°C, and centrifuged for 20 mins at 13,000

r.p.m at 4°C. The pellet was washed with 1 ml of 70% EtOH, allowed to air dry and resuspended in 25 µl of 10 mM Tris (pH 8.0). DNA concentration was determined and adjusted to 1 µg/µl using 10 mM Tris (pH 8.0) as required.

The linearised plasmid DNA was used as a template for the transcription of Digoxigenin-labelled riboprobes using T3 (anti-sense) and T7 (sense) RNA polymerase (Roche). Reaction constituents for DIG-labelling of riboprobes are shown below.

Reagent	Volume (µl)
H ₂ O	12
10X Transcription Buffer (Roche)	2
DIG RNA Labelling mix (Roche)	2
RNasin (Promega)	1
RNA Polymerase (Roche)	2
DNA	1 µl (1 µg/µl)

Transcription reactions were incubated for two hours at 37°C, and DNA template digested by incubation with 20 units of DNaseI (Ambion) for 15 mins at 37°C. Probes were precipitated by addition of 2 µl 3 M NaOAc (pH 5.2) and 100 µl 100% EtOH, and incubated at -20°C overnight. RNA was pelleted by centrifugation at 13,000 r.p.m at 4°C for 20 mins, the pellet washed with 70% EtOH, and allowed to air dry for ten mins. The pellet was resuspended in 100 µl of DEPC treated H₂O and divided into 10 µl aliquots, which were stored at -80°C.

Slides with paraffin embedded sections were dewaxed in two changes of xylene for 10 mins each, and rehydrated through graded ethanols of 100% (twice), 95%, 85%, 75%, 50%

and 30% for 1 minute each. Slides were incubated in 1X saline followed by 1X PBS for 5 mins each and incubated in 6% hydrogen peroxide (in 1X PBS) for 30 mins at room temperature in order to inactivate endogenous alkaline phosphatase activity. Slides were washed twice in 1X PBS for 5 mins each, fixed in ice cold 4% PFA (in 1X PBS) for 20 mins and washed twice in 1X PBS for 5 mins each. Slides were incubated for 5 mins in Proteinase K (Promega) (20 µg/ml Proteinase K, 50 mM Tris, 5 mM EDTA in H₂O) at room temperature, washed in 1X PBS for 5 mins, post-fixed in 4% PFA for 5 mins and washed in DEPC treated H₂O for 2 mins.

To reduce non-specific probe binding, slides were treated with acetic anhydride (0.01 M in 0.1 M triethanolamine hydrochloride), by incubating at room temperature for 10 mins. Slides were washed with 1X PBS and 1X saline each for 5 minutes at room temperature. Slides were rehydrated through 30%, 50%, 70%, 85%, 95% and 100% (twice) EtOH solutions, each for one min, except for 70%, in which slides were left for five mins to prevent salt precipitation. Slides were air dried for 30 mins, and placed into sealable boxes lined with absorbent paper soaked in moisture buffer (5X SSC, 50% (v/v) formamide in DEPC H₂O). Probe was heated at 80°C for 3 mins, and stored on ice, whilst hybridisation buffer (5X SSC, 50% formamide, 1% SDS, 0.05 mg/ml heparin, 0.05 mg/ml calf liver tRNA in DEPC H₂O) was thawed at 80°C. An appropriate amount of probe and hybridisation buffer were mixed (per slide: 1 µl probe per 100 µl hybridisation buffer), and applied to relevant slides. A piece of parafilm was placed on top of the probe mixture, the box sealed with electrical tape and incubated at 62°C overnight in a water bath.

Slides were incubated in pre-warmed 5X SSC at 65°C for 30 mins, and parafilm removed from solution using forceps. Slides were washed twice in pre-warmed solution I (50% formamide, 5X SSC, 1% (v/v) SDS in DEPC H₂O) at 65°C for 30 mins each, and then washed three times in solution II (0.5 M NaCl, 0.01 Tris (pH 7.5), 0.1% Tween 20 in DEPC H₂O) at room temperature for 10 mins each. Slides were treated with RNase (0.02 mg/ml in solution II) to digest unhybridised probe, by incubation at 37°C for 45 mins, followed by a

final 10 mins was in solution II at room temperature. Slides were washed twice at 65°C in solution III (50% formamide, 5X SSC in DEPC H₂O) for 30 mins each. Slides were washed twice in PBT (0.1% Tween 20 in 1X PBS) for 10 mins each and pre-blocked in 10% heat-inactivated sheep serum in PBT for three hours, covered with a piece of parafilm as before. Anti-digoxigenin alkaline phosphatase conjugated antibody (Roche) was pre-absorbed for three hours at 4°C in 1% heat inactivated sheep serum in PBT containing 6 mg/ml dried, homogenised wild type placenta. Parafilm was removed from slides by washing in PBT for 5 mins, and the pre-absorbed antibody diluted to a final concentration of 1:2000 in 1% sheep serum in PBT. Antibody solution (100 µl) was applied to each slide, covered with a piece of parafilm, and incubated overnight at 4°C.

Parafilm was removed from slides by washing in PBT for 5 mins, followed by a further two five min washes in PBT, and a subsequent three washes for 30 mins in PBT. Slides were preconditioned in three washes of NTMT (0.1 M NaCl, 0.1 M Tris (pH 9.5), 0.05 M MgCl₂, 0.1% Tween 20) containing 2 mM Levamisole (Sigma) for 5 mins each. BM Purple substrate (Roche) was applied directly onto each slide to completely cover sections. Slides were sealed in a dark box and incubated at room temperature until signal of the desired intensity developed (around 24 hours). Slides were washed in PBT for 10 mins, dH₂O for 30 minutes, and counterstained in Eosin Y Solution (Sigma) for up to 10 secs. Excess eosin was washed in running tap water and slides air dried for 30 mins. Slides were cleared briefly in xylene, air dried and mounted in DPX mounting medium (Sigma).

Slides were imaged at 40X magnification under standard light field conditions and counting of *Cdkn1c* positive cells was performed. Four images per section were counted for positive staining and nuclear count, in six samples from the same *in situ hybridisation*.

Immunofluorescence

Immunofluorescence was performed on cryosectioned 7 μm thick P7 BL6 iBAT, which were prepared as already described. Upon completion of sectioning, slides were air dried for 30 mins to aid adhesion of the section. Lines were drawn around section using Dako pen (Dako). Samples were blocked in blocking buffer (5 % goat serum (Dako), 5 % donkey serum (Dako), 0.1 % Fraction V B.S.A (Sigma) in 1X PBS (Gibco)) for 45 minutes at room temperature. Blocking buffer was removed after time and sections were incubated with primary antibody (see antibody table) in blocking buffer for 3 hours at room temperature. Samples were washed 3 X 5 mins in 1 X PBS before incubation with secondary antibody in blocking buffer. Incubation was for one hour at 4°C in the dark. Following incubation, samples were washed 3 X 5 mins in 1 X PBS.

In order to label the nucleus for images, 4',6-diamidino-2-phenylindole (DAPI) staining was performed immediately following the washes. A 300 ηm working solution of DAPI was made from a 14.28 mM DAPI stock. 1 μl stock solution was mixed with 47.6 ml Mellvaine's buffer (0.02 M Citric Acid, 0.16 M Na_2HPO_4). This working solution was used for up to two weeks when kept in the dark at 4 °C. Sections were incubated with DAPI working solution for 30 seconds before washing 3 X 5 mins in 1 X PBS. Slides were mounted using Fluoromount aqueous media (Sigma) and photographed with the confocal microscope.

Transmission Electron Microscopy (TEM)

TEM was performed to produce high resolution images of single white adipocytes from 5D3 and wild type P7 rWAT. rWAT was dissected from P7 pups into cold 1 X PBS and immediately sent for fixation. Fixation, sectioning and microscopy was performed by Dr. Anthony Hann (Cardiff University) using a TEM 208 electron microscope (Phillips).

RNA extraction + cDNA generation

Analysis of gene expression was determined by qPCR analysis of cDNA, prepared from RNA within tissues. RNA extraction was performed via EZ-RNA Total RNA Isolation Kit (Geneflow), as per manufacturer's specifications with some modifications. Still frozen samples were partially lysed in 0.5ml Denaturing Solution with a pestle (Sigma Aldrich). Once broken up into smaller parts, samples were briefly sonicated using BioRuptor (Diagenode) until total lysis of cells had occurred. Homogenates were then stored for 5 minutes at room temperature prior to the addition of 0.5ml Extraction Solution. Tubes were vigorously shaken for 15-30 seconds, before a ten minute incubation at room temperature and centrifugation at 13,000 r.p.m for 15 mins at 4°C.

Once separated, the upper aqueous phase was transferred to a fresh 1.5ml non-stick tube containing 0.5ml Isopropanol. Once mixed, samples were incubated at room temperature for a further 1 minute before centrifugation at 13,000 r.p.m for 10 mins at 4°C to pellet RNA. Supernatant was poured off and 1ml 75% EtOH added. Tubes were inverted until RNA pellet was dislodged so as to ensure complete washing. Re-pelleting was achieved through further centrifugation at 13,000 r.p.m for 10 mins at 4°C. Once all ethanol residue had been completely removed, pellet was re-dissolved in 10-30 µl 10 mM Tris.HCl pH 8, depending on pellet size.

Reverse transcription of 2 µg RNA was performed by first mixing 1 µl 0.5 µg/µl random hexamers (Promega) with RNA and volume made up to 11 µl with DEPC H₂O. Samples were incubated at 70°C for 10 mins, before returning to ice. 8 µl of RT master mix (4 µl 5X first strand synthesis buffer, 0.5 µl RNasin, 1µl 10 mM dNTP's (all Promega) and 2.5µl DEPC H₂O) was mixed and each sample was returned to heat block at 37°C. After a two minute wait that ensured samples were at block temperature, 1 µl M-MLV Reverse Transcriptase (Promega) was added and complete mixing was ensured through pipetting up and down. After one hour incubation, heat block was increased to 70°C for 15 mins.

Once completed, samples were returned to ice and diluted with 100 µl 10 mM Tris.HCl pH8. For every sample reverse transcribed, a negative was also performed, that underwent identical procedure except M-MLV was not added. These negatives acted as a control for DNA content. In order to test for this, after reverse transcription, 1 µl diluted sample underwent PCR, as already mentioned using β-Actin primers. PCR products were run out on a 1.5% agarose gel, and upon confirmation that no bands were present, negative samples were binned.

gDNA extraction

gDNA was extracted from adipose tissue for two separate reasons. Firstly, changes in mitochondrial copy number were quantified via RT-PCR of mitochondrial and nuclear gDNA. In addition, gDNA was required for bisulphite treatment and sequencing, in order to analyse methylation status of the somatic DMR of *Cdkn1c*.

For total lysis of tissue, adipose pads were incubate in lysis buffer (100 mM Tris.HCl (pH 7.8), 50 mM EDTA, 0.2% SDS, 200 mM NaCl and 100 ug/ml proteinase K) at 55°C overnight with rocking. Following morning, samples were briefly shaken before an equal

volume of phenol was added. A 10 minute incubation period was interspersed with frequent mixing of tubes, followed by 5 minutes of rest, and then another 10 mins of mixing. Upon completion, centrifugation at 13,000 r.p.m for 10 mins followed. Aqueous phase was transferred to a fresh tube containing an equal volume of chloroform, where the mixing procedure as for phenol was repeated. Samples were centrifuged again and aqueous phase transferred to a fresh tube containing 20 µl 3 M NaOAc (pH 6) and 0.5ml EtOH to precipitate DNA.

When sufficient DNA was present, the pellet could be fished out with a clean pipette tip and transferred to another tube directly. The pellet was rinsed in 70% EtOH, centrifuged at 13,000 r.p.m for 10 mins and ethanol was removed. Once fully dry, the DNA was re-suspended in 50-100 µl TE pH8, aided by heating to 55°C for 10-30 mins. In the event that insufficient DNA precipitated to form an easily identifiable pellet, DNA was spun down for one minute in a micro centrifuge. Supernatant was removed and the pellet was washed in 70% EtOH and re-suspended in TE pH 8, as before. However due to the required spinning down of the pellet, RNA treatment was now needed to be performed on these samples.

RNase A (Roche) at a final concentration of 50mg/ml was added and samples were kept at 37°C for 30 mins. Equal volumes of phenol and chloroform were added upon completion of incubation period, with mixing performed as previously described. Following centrifugation at 13,000 r.p.m for 10 mins, aqueous phase was transferred to a fresh tube containing an equal volume of chloroform and the process repeated. After this final centrifugation, DNA was precipitated by transfer of upper aqueous phase to a fresh tube containing 20 µl 3 M NaOAc (pH 5.2) and 2 volumes 96% EtOH. DNA was spun down for 1 min in a microcentrifuge and once supernatant was removed, washed in 0.5ml 70% EtOH, followed by a further spin down for 1 min. Upon removal of all traces of ethanol, DNA was resuspended in 50 µl 10mM Tris.HCl pH 8 as before and analysed by spectrophotography and run out on a 0.75% agarose gel to ensure integrity.

QPCR

For the analysis of relative gene expression and mitochondrial count, qPCR analysis was performed on cDNA and gDNA respectively, using a Chromo4 Continuous Fluorescence Detector mounted on a PTC 200 Thermocycler (MJ Research). In order to generate significant data, a minimum of 4+4 experimental subjects were used. Triplicate wells were utilised for each sample read, and every gene was analysed a minimum of four times. Primer design was performed in the same way as was performed during *in situ* hybridisation, however in this instance, primer pairs were designed to amplify products around 300 bp. PCR master mix was set up per well as follows:

Reagent	Volume (μ l)
TrueStart 10X Buffer	1.5
MgCl ₂	1.2
dNTP's (25 mM)	0.6
Primers F + R (25 μ M)	0.3
TrueStart Taq (Fermentas)	0.1
SybrGreen	0.12
ddH ₂ O	to 15
DNA (50ng)	5

Thermocycler conditions were: 95°C for 15 mins, followed by 35 cycles of 95°C for 30 secs, 60°C for 30 secs, 72°C for 30 secs and an anti primer-dimer step performed at between 75°C

to 82°C for 30 secs. The anti-primer dimer step was performed to denature potential primer dimers, which may contribute to the measured fluorescence. The temperature of this step was set at least two degrees below the pre-determined melting temperature of the PCR product, to prevent denaturation of the specific product. Melting curve analysis was performed between 70°C and 95°C, at 0.5°C intervals. Fluorescence and melting curves were analysed using Opticon 3 software. Melting curves were examined to detect non-specific amplification or the presence of primer-dimers, evidenced by multiple peaks. A threshold fluorescence level was set in the early exponential phase for each assay. The point at which the fluorescence for each amplicon passed through this level was the cycle threshold (CT), and was used to quantify relative transcript abundance using the $2^{-\Delta\Delta C_T}$ method¹⁸², compared to β -Actin expression level for each sample.

Bisulphite treatment and Sequencing of gDNA

For the purposes of studying the methylation status of the *Cdkn1c* somatic DMR, bisulphite treatment and sequencing of gDNA from different environmental scenarios was performed. After extraction of gDNA, as performed in a previous section, all treatment and sequencing of DNA was performed at Tohoku University in the laboratory of Professor Takahiro Arima.

gDNA was bisulphite treated by EZ DNA Methylation Kit (Zymo Research) in line with manufacturers protocol. Briefly, 2 μ g DNA was denatured for 15 mins at 42°C before overnight treatment with 100 μ l CT Conversion Reagent at 50°C. The following morning, samples were cooled to 4°C before mixing with M-Binding Buffer in the provided spin columns. Centrifugation at 13,000 r.p.m for 30 secs was followed by addition of 100 μ l M-Wash buffer. Samples were re-centrifuged, after which 200 μ l M-desulphonation Buffer was added to columns and a 15 mins incubation period followed.

Columns were centrifuged again to remove desulphonation buffer, which was followed by 2X 200 μ l M-Wash Buffer additions, as before. Finally DNA was eluted into a fresh 1.5 ml tube by addition of M-Elution Buffer and centrifuged at 13,000 r.p.m for one min. DNA was immediately used in PCR amplification, due to the fragile nature of bisulphite treated DNA. In order to ensure maximum possible product generation, and due to the fragile nature of the DNA, a hemi-nested PCR was employed. PCR master mix was set up per well as follows for both PCR reactions, with the only difference being primers:

Reagent	Volume (μ l)
10X EpiTaq Buffer	2
MgCl ₂ (25 mM)	2
dNTP's (10 mM)	2.4
Primers F + R (10 μ M)	2
Takara HS EpiTaq (Takara Inc)	0.1
ddH ₂ O	to 20
BiSulphite treated DNA	2

PCR cycle for the round 1 was as follows: 1. 94°C 5 mins, 2. 94°C 2 mins, 3. 55°C 2 mins, 4. 72°C 3 mins, repeat steps 2-4 5 times, 5. 94°C 1 min, 6. 60°C 1 min, 7. 72°C 1 min, repeat steps 5-7 35 times, 8. 72°C 10 mins. PCR products were analysed on a 1.8% agarose gel to

ensure reaction had successfully amplified correct product, with an untreated gDNA sample control and a water negative used with each reaction set.

For the nested PCR, as already stated, mastermix was identical to the primary round. 1µl of first round PCR was added to 20 µl mastermix, containing the hemi-nested primer set. PCR cycle was as follows: 1. 94°C 5 mins, 2. 94°C 1 min, 3. 60°C 1 min, 4. 72°C 1 min, repeat steps 2-4 35 times, 5. 72°C 30 mins. PCR results were separated on a 1.8% agarose gel and expected DNA product was cut out using a clean scalpel, and transferred to a clean 1.5ml tube. DNA clean up was performed using QIAquick Gel Extraction Kit (Qiagen), as per manufacturers specifications.

Upon completion DNA product was inserted into pGEM-T Easy vector and JM 109 cells as already described. Cells were plated on LB/Carbenicillin/IPTG/X-Gal plates and grown up overnight at 37 °C. 24 white colonies per sample were picked the following morning using clean pipette tips and transferred to PCR tubes. DNA was amplified using illustra TempliPhi Amplification Kit (GE Healthcare) as per manufacturer's instructions, for 6 hours at 37 °C. Upon completion, samples were diluted with 16 µl ddH₂O and 2µl was transferred to new 96 well plates. PCR was performed using a primer for the T7 promoter as follows:

Reagent	Volume (μ l)
H ₂ O	4
BigDye® Terminator v3.1 5X Sequencing Buffer (Applied BioSciences)	2
BigDye® Terminator v3.1Premix dye (Applied BioSciences)	1
T7 Primer (10 μ M)	1
DNA	2

Thermocycler conditions were: 96°C for 2 mins, followed by 25 cycles of 96°C for 10 secs, 50°C for 5 secs, 55°C for 2 mins.

Once completed, 10 μ l ddH₂O, 2 μ l 125mM EDTA and 2 μ l 3M NaOAc was added to each PCR product. Then 50 μ l 100% EtOH was added and plates were centrifuged at 14,000 r.p.m for 15 mins at 20°C. Liquid was poured off and 50 μ l 70 % EtOH was added. Plates were centrifuged at 14,000 r.p.m for 5 mins at 20 °C. Liquid was poured off and air dried for at least 10 mins. 10 μ l HiDi formamide (Takara) was added to samples and plates were heated at 96 °C for 2 mins. Plates were then sequenced using ABI Prism 3130xl Genetic Analyzer (Applied Biosystems)

Western blotting

Western blotting was performed to analyze any changes in the expression of four key proteins; Cdkn1c, phospho C/ebp β and total, Prdm16 and Ucp-1. Samples were completely homogenised in 2X SDS sample buffer (0.125M Tris.HCl pH 6.8, 20 % glycerol, 2.5 % (w/v) sodium dodecyl sulfate (SDS), 0.005% bromophenol blue, Complete protease inhibitors (Roche)) and centrifuged at 13,000 r.p.m for 10 mins at 4°C. Lysates were removed to clean tubes, leaving behind the floating fat cake, and boiled at 96°C for 10 mins. Levels of total proteins in each sample were estimated prior to analysis, using a commercial kit (BioRad) based on the Bradford protein assay¹⁸³ and measuring absorbance at 590 nm using a multi-well plate reader (BioTek).

30 μ g samples were separated by SDS-PAGE using resolving gels of various acrylamide concentrations (8-14 %) and a 6 % stacking gel cast into BioRad plates and moulds.

Resolving gel

Acrylamide/bis-acrylamide (Sigma)	8-14 %
Tris-HCl pH 8.8	384 mM
SDS	0.1 %
Ammonium persulphate (APS)	0.1 %
Tetramethylethylenediamine (TEMED)	0.1 %

Stacking gel

Acrylamide/bis-acrylamide	6 %
Tris-HCl pH 6.8	136 mM
SDS	0.1 %
APS	0.1 %
TEMED	0.1 %

Loaded proteins, along with 5 μ l protein ladder (10-250 kDa, PageRuler, Fermentas) were separated at 200 V using a Tris-glycine SDS-PAGE running buffer and electrophoretically transferred to polyvinylidene difluoride (PVDF) using wet transfer system (BioRad) at 50 V for 2 hours at room temperature, with Tris-glycine Methanol transfer buffer (20% methanol, 0.05 M Tris.HCl pH 8.8, 0.384 M Glycine (Sigma)).

Subsequent membranes were blocked in 5% non-fat dry milk (Marvel) in Tris-buffered saline with 0.1% Tween-20 (TBS-T) for one hour, followed by incubation with specific primary antibodies and appropriate horseradish peroxidase (HRP)-conjugated secondary antibodies (1:3000, Amersham), both diluted in 5% non-fat dry milk in TBS-T. Primary antibodies were incubated overnight at 4°C, while secondary antibodies were incubated for two hours at room temperature. Membranes were washed for 20 minutes in TBS-T after both primary and secondary antibody incubation. All antibodies used in Western blotting experiments are listed below. EZ-ECL Chemiluminescence Detection Kit (Geneflow) and ECL plus reagents (Amersham) were used for detection of protein bands. Membranes were exposed to X-ray film (Fuji). Exposure times for each Western were as follows:

Cdkn1c- 1 min

Prdm16- BAT 5 min WAT 15 min

C/EBP β Total + Phospho- 3 min

UCP1- BAT 10 secs, WAT 3 min

B-Actin- 10 secs

Antibodies

Target	Type/Clone	Source	Technique	Dilution
Cdkn1c	Rabbit polyclonal	Sigma	Western	(1 : 1000)
Cdkn1c	Goat polyclonal	Santa Cruz	F-IHC	(1 : 100)
			Western/	(1:1000)
Prdm16	Rabbit polyclonal	Sigma	F-IHC	(1:50)
C/EBP β	Rabbit polyclonal	Santa Cruz	Western	(1:250)
C/EBP β Thr 288	Rabbit polyclonal	Santa Cruz	Western	(1:250)
UCP-1	Rabbit polyclonal	Abcam	Western	(1:3000)
β -Actin	Mouse monoclonal	Sigma	Western	(1:3000)

Primers

Gene	Primer	Sequence
BAC genotyping	Forward	GGGCACCAATAACTGCCTTA
	Reverse	GCGTGTTACGGTGAAAACCT
Cdkn1c KO genotyping	Forward	CGTTCCACAGGCCGAGTGC
	WT	
	Reverse	GCTGCGGAGGTACACGTCG
	KO	
	Reverse	GCGAGGATCTCGTCGTGAC
Cdkn1c	Forward	AGAGAACTGCGCAGGAGAAC
	Reverse	TCTGGCCGTTAGCCTCTAAA
UCP-1	Forward	GGCAAAAACAGAAGGATTGC
	Reverse	TAAGCCGGCTGAGATCTTGT
PGC-1A	Forward	TCATCACCTACCGTTACACCTG
	Reverse	CAAGCTTCTCTGAGCTTCCTTC
Prdm16	Forward	CAGCACGGTGAAGCCATTC
	Reverse	GCGTGCATCCGCTTGTG
Elovl3	Forward	CTGTTGCTCATCGTTGTTGG
	Reverse	ATCTGACTACGGCGTCATCC
Fsp-27	Forward	GACCCAACAGCTGGTGTCTAA
	Reverse	ATTGTGCCATCTTCCTCCAG
Perilipin	Forward	CACTCTCTGGCCATGTGGAT
	Reverse	AGAGGCTGCCAGGTTGTG
aP2	Forward	TCACCTGGAAGACAGCTCCT
	Reverse	AATCCCCATTTACGCTGATG
Cyt C	Forward	TCCATCAGGGTATCCTCTCC

	Reverse	GGAGGCAACCATAAAGACTGG
Cox II	Forward	AATTGCTCTCCCCTCTCTACG
	Reverse	GTAGCTTCAGTATCATTGGTGC
MyoD	Forward	CGCCACTCCGGGACATAG
	Reverse	GAAGTCGTCTGCTGTCTCAAAGG
Myf 5	Forward	CAGCCCCACCTCCAAGT
	Reverse	GGGACCAGACAGGGCTGTTA
pRb	Forward	AAGCAGCCTCAGCCTTCCATA
	Reverse	TGCCATACATAGAGCACATC
PPAR γ	Forward	CCCTGGCAAAGCATTGTAT
	Reverse	GAAACTGGCACCCCTTGAAAA
C/EBP β	Forward	CAAGCTGAGCGACGAGTACA
	Reverse	AGCTGCTCCACCTTCTTCTG
C/EBP α	Forward	CGCTGGTGATCAAACAAGAG
	Reverse	CGATCTGGAAGTCAAGTGG
Cidea	Forward	TGGAAAAGGGACAGAAATGG
	Reverse	TCTCGTACATCGTGGCTTTG
β -Actin	Forward	CCTGTATGCCTCTGGTCGTA
	Reverse	CCATCTCCTGCTCGAAGTCT
RIP140	Forward	TGCTGGCCACAAAGAGGAA
	Reverse	ACAGTGGGACCATTGCTTTGA
PPAR α	Forward	ACGATGCTGTCCTCCTTGATG
	Reverse	CGCGTGTGATAAAGCCATTG
Cdkn1c (bisulphite)	Forward	TGG GTG TAG AGG GTG GAT TTA GTT
	Reverse	CCC ACA AAA ACC CTA CCC CC
	Nested	GTA TTG TTA GGA TTA GGA TTT AGT TGG TAG TAG TAG
T7 promoter	Forward	TAA TAC GAC TCA CTA TAG GG

Statistical Analysis

Student's t-test was performed on cell counting, weights of mice and organs, glucose tolerance testing, insulin tolerance testing, core body temperatures, feeding studies and bisulphite sequencing of *Cdkn1c* sDMR. Mann Whitney test was performed for fold changes for QPCR analysis. SPSS software (IBM) was used for all tests.

Chapter 3: Characterising the effect of altered
***Cdkn1c* dosage on brown adipogenesis**

Imprinted expression of *Cdkn1c* in brown adipose tissue

Prior to this investigation, there was no published data to suggest a direct role for *Cdkn1c* in adipogenesis. Most research had focused instead on the putative role of *Cdkn1c* in BWS, and as a regulator of embryonic growth and placental development^{101; 103; 184; 185; 186}. *Cdkn1c* is highly expressed during embryogenesis in a subset of cells as they exit differentiation but becomes progressively down-regulated in the majority of tissues late in embryogenesis^{90; 91}. In the adult, few sites of *Cdkn1c* expression have been reported including some glomerular podocytes of the adult kidney, early spermatocytes and the adrenal cortex^{90; 91}. *Cdkn1c* was most recently suggested to play a role in self-renewal of adult lung stem cells¹⁸⁷ and the quiescence and maintenance of adult hematopoietic stem cells¹⁸⁸.

***Cdkn1c* expression in iBAT**

At the start of the study, adipose depots from postnatal mice were examined in order to determine firstly whether *Cdkn1c* was expression in these depots and secondly to ask whether imprinted expression was maintained. An *Ava*I restriction fragment length polymorphism (RFLP) had previously been identified within the *Cdkn1c* transcript between *Mus mus domesticus* strains (D) and the wild type strain *Mus mus spretus* (S)²¹. Adipose tissue from post-natal day 90 (P90) animals was generated by crossing a BL6 female (D) with a hybrid male carrying the *spretus* region of mouse distal chromosome 7 (BL6^{S^{spretus}7}, S). Genomic DNA and RNA was isolated, cDNA was prepared and then primers were used to amplify a 381 base pair region spanning the polymorphism from both the genomic and the cDNA samples. The PCR products were purified, and then subjected to *Ava*I digestion and run out on a 2% agarose gel.

A product was amplified from both the interscapular brown adipose tissue (iBAT) and retroperitoneal white adipose tissue (rWAT) at P90. 5 μ l of the cDNA template was required to generate a band visible on the agarose gel as opposed to the 1 μ l usually used to amplify *Cdkn1c* from placental or embryonic samples suggesting a lower level of expression. On digestion with *Ava*I, two bands were observed with the genomic DNA template but only a single band was present in the cDNA amplifications (Fig 3.1). This demonstrated that imprinting of *Cdkn1c* was maintained at least until 3 months in both brown and white adipose tissue.

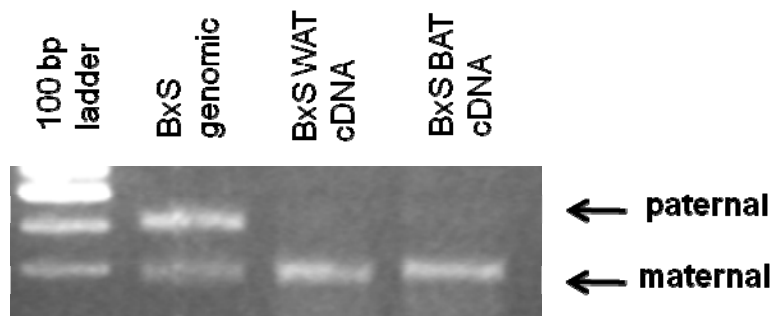


Figure 3.1 RFLP analysis of *Cdkn1c* in rWAT and iBAT. PCR products amplified from genomic DNA and cDNA isolated from adipose tissue from a C57BL/6 x C57BL/6^{Spretus7} cross were subjected to *Ava* I digestion, allowing assignment of parental alleles. This work demonstrated that *Cdkn1c* was expressed and imprinted within cells contained within the rWAT and iBAT depots until at least 3 months of age. Performed by Dr. R John.

The maintenance of imprinted expression of *Cdkn1c* within adipose depots suggested the possibility that *Cdkn1c* may play a role in brown adipogenesis and that the regulated dosage of *Cdkn1c* might have a functional significance.

Investigating the consequences of loss of *Cdkn1c* expression in iBAT

To investigate the molecular and cellular consequences of loss of function of *Cdkn1c* in iBAT, heterozygous female *Cdkn1c*^{m/+p} mice were mated with wild type males to generate litters of *Cdkn1c*^{-m/+p} (knockout) and wild type mice. On the BL6 genetic background, loss of function of *Cdkn1c* results in neonatal lethality in >90% cases¹⁰³. As part of a separate project, the Elledge mutation (*Cdkn1c*^{tm1Sjc}) had been bred into the 129 genetic background for +8 generation. On this 129 background, a similar lethality was observed¹⁰⁴;¹⁰⁷. The few live *Cdkn1c*^{-m/+p} pups recovered on the day of birth were cold to touch and grey in appearance.

iBAT pads are observable as early as embryonic day (E) 15.5 of embryogenesis, although the lineage is believed to begin formation significantly earlier^{144; 150}. Initial examination of undissected iBAT from *Cdkn1c*^{-m/+p} and wild type mice at E18.5 revealed the altered appearance of the *Cdkn1c*^{-m/+p} iBAT (Fig 3.2). The dark nature of the iBAT, clearly seen in the wild type image and attributed to the huge numbers of mitochondria in these cells coupled with their relatively low lipid content and the vascular nature of the tissue, was not observed in the *Cdkn1c*^{-m/+p} iBAT where almost none of the darker tissue was apparent. Instead the tissue more closely resembled white adipose tissue.

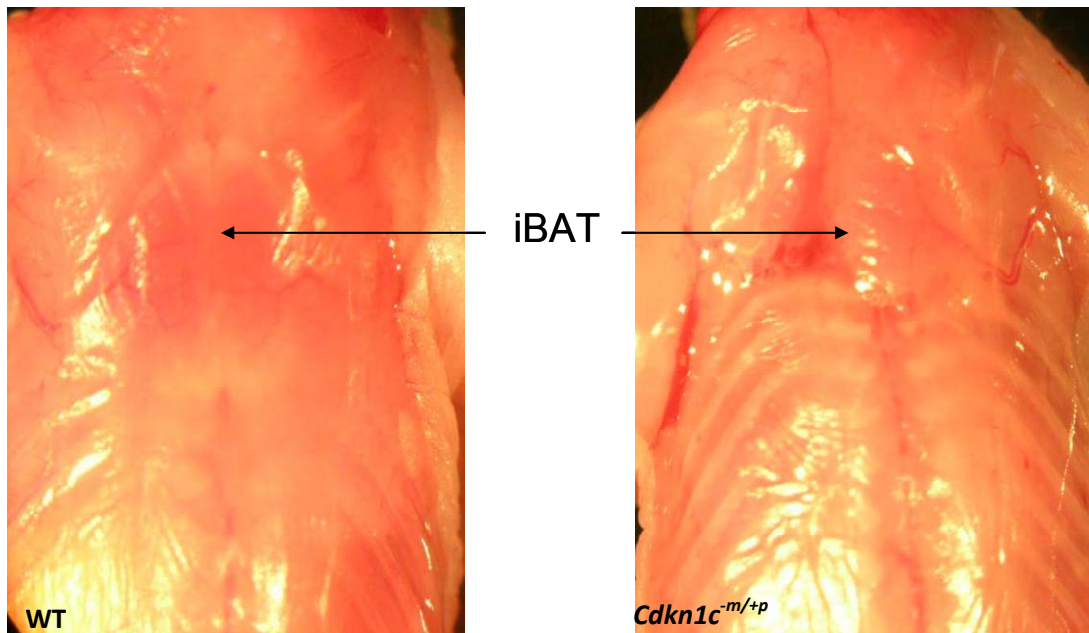


Figure 3.2 Whole body images of E18.5 wild type and *Cdkn1c*^{m/+p} 129 mice. The interscapular brown adipose tissue (iBAT) has been highlighted on both images. The wild type iBAT can be seen as two individual pads with a darkish appearance surrounded by ring of lighter appearing tissue. In contrast, the *Cdkn1c*^{m/+p} pads were less distinct and lighter in appearance.

Fat pads from this litter of E18.5 *Cdkn1c*^{m/+p} embryos were dissected and subjected to H+E (Fig 3.3) and Oil Red O (Fig 3.4) staining. In the wild type section the dark brown colour that distinguishes iBAT from surrounding tissue was clearly apparent at the cellular level. Small pockets of lipid were observed in individual cells. In contrast, the iBAT in *Cdkn1c*^{m/+p} sections appeared poorly differentiated with an unusual morphology, including larger areas of lipid stores. In contrast to wild type adipocytes, which were seen to be highly uniform in nature across the fat pad, cells within the *Cdkn1c*^{m/+p} iBAT displayed a high degree of heterogeneity.

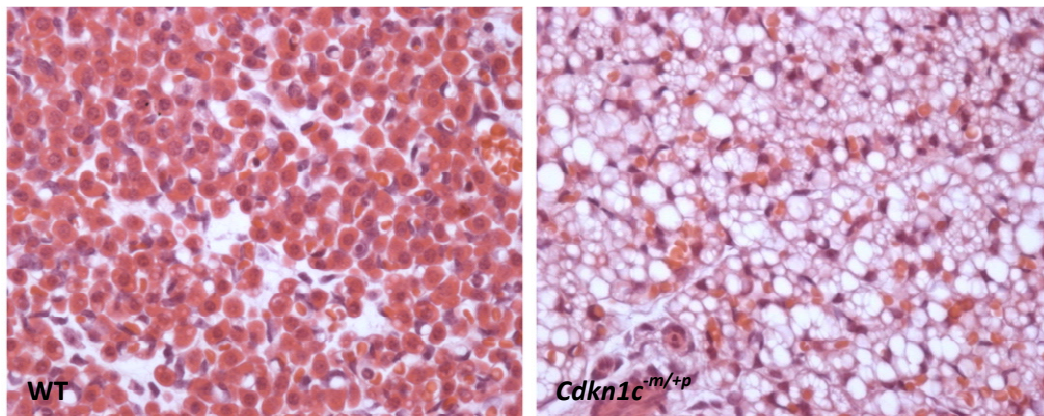


Figure 3.3 H+E stained E18.5 wild type and *Cdkn1c*^{-m/+p} iBAT sections at 40X magnification, photographed under standard light field conditions. Wild type adipocytes have a darker appearance and possess small lipid depots whereas *Cdkn1c*^{-m/+p} adipocytes are lighter in appearance with large lipid stores.

Wild type adipocytes appeared consistent in size and shape across the population whereas *Cdkn1c*^{-m/+p} adipocytes appeared larger and less uniform (Fig 3.3). To quantitate this feature, cell diameter and cell number were analyzed using Image J software (Table 1). *Cdkn1c*^{-m/+p} ($31.17 \pm 1.1 \mu\text{m}$ $P=1.188 \times 10^{-6}$ $N=6$) adipocytes were found to be statistically significantly larger than the wild type cells ($28.88 \pm 0.84 \mu\text{m}$ $N=13$) but no difference in cell number per image was observed between the two groups (92.8 ± 10.86 $P=0.65$) (88.57 ± 8.83) (Table 1).

		Diameter (μm)	Cell Number
Av.	Wild Type	28.88	88.57
	Knockout	31.17	92.8
St.Dev	WT	0.84	8.83
	KO	1.10	10.86
		1.18864E-06	0.65

Table 1 Diameter and cell count of *Cdkn1c*^{-m/+p} E18.5 iBAT, performed in ImageJ software. Loss of expression of *Cdkn1c* was found to increase diameter of cells, compared to wild type, while cell number counted per image was unaffected. Statistical analysis was performed by Student's t-test. Images covered $22,592 \mu\text{m}^2$. Area of image: $80,000 \mu\text{m}^2$.

Loss of *Cdkn1c* expression results in elevated lipid content in iBAT

To verify the areas with a white appearance were lipid stores, Oil Red O staining was performed on cryo-embedded sections (Fig 3.4). Large areas of the *Cdkn1c*^{-m/+p} adipocytes stained positive for lipid whereas wild type brown adipocytes displayed little staining. Though it would appear all cells were lipid positive in the wild type, the intensity of the red colour suggested that the total lipid content was comparatively low to the *Cdkn1c*^{-m/+p} iBAT.

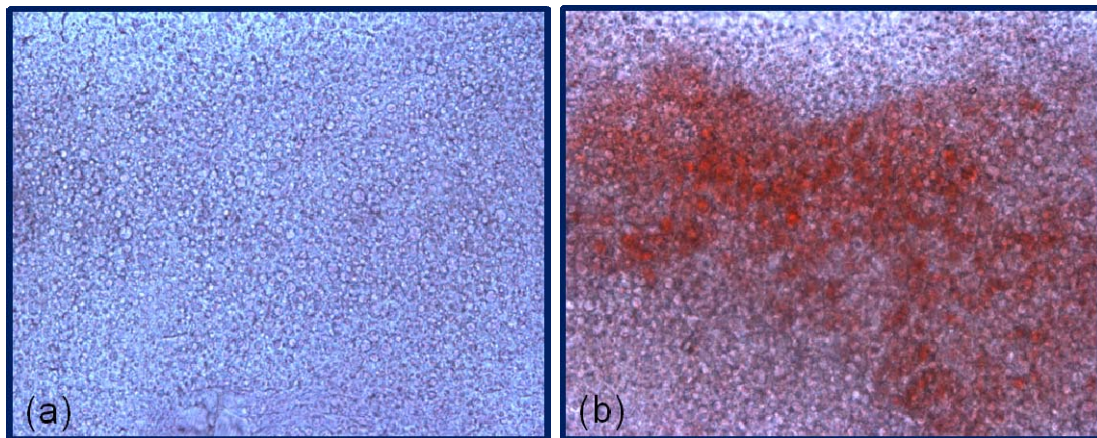


Figure 3.4 Oil Red O stained E18.5 WT (a) and *Cdkn1c*^{-m/+p} (b) iBAT sections at 40X magnification under standard light field conditions. Wild type adipocytes displayed limited staining of lipid positive cells. In contrast, *Cdkn1c*^{-m/+p} brown adipose tissue displayed widespread staining with a deep intensity.

Critical pathways are disrupted in *Cdkn1c*^{-m/+p} iBAT

Histological results so far obtained highlighted a disruption in the normal morphology of the iBAT in *Cdkn1c*^{-m/+p}. It had previously been noted that *Cdkn1c*^{-m/+p} pups when born were cold to touch and grey in appearance. Therefore QPCR analysis of genes involved in the thermogenic programme was performed to determine if defective thermogenesis had occurred (Fig 3.5). *Ucp-1*, *Cidea* and *Elovl3*, markers of mitochondrial uncoupling, were all found to be reduced in expression. *PGC-1 α* , was in contrast, found to be elevated in *Cdkn1c*^{-m/+p} iBAT.

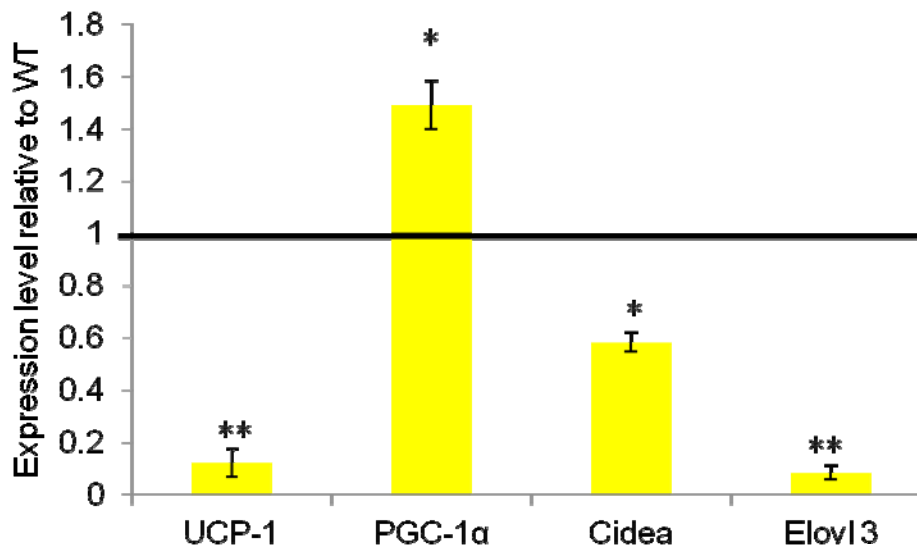


Figure 3.5 QPCR analysis of *Cdkn1c*^{-m/+p} E18.5 iBAT cDNA. Selected thermogenic program genes were found to be reduced in the absence of *Cdkn1c*. Error bars represent standard error of fold changes. Statistical analysis was performed by Mann Whitney test. * P< 0.05. ** P< 0.01. N=4+4

In light of the reduced expression of genes associated with thermogenesis and the widespread accumulation of lipid deposits in the *Cdkn1c*^{-m/+p} iBAT, QPCR analysis of genes associated with lipid accumulation was next performed (Fig 3.6). *Fsp-27*, *Perilipin* and *aP2* were all found to be down-regulated. The expression level of these genes would further suggest that the large

lipid depots observed in the adipocytes were not representing a trans-differentiation event towards the white adipose phenotype, and merely that correct differentiation of the brown adipocytes had not occurred.

Two genes involved in mitochondrial function, *Cytochrome C*^{189; 190} and *Cox 2*¹⁹¹ both displayed significant down-regulation at the cDNA level (Fig 3.7). *Cytochrome C* is transcribed from the nuclear genome and can be used as a measure of activity, while *Cox II* is transcribed from the mitochondrial genome and therefore serves better as a marker of mitochondrion count. Since it was possible that transcription may have been repressed from the mitochondrial genome, as opposed to a reduced organelle population, QPCR analysis was performed on genomic DNA of the iBAT from wild type and *Cdkn1c*^{-m/+p}. The total levels of *Cox 2* mitochondrial DNA when compared to the nuclear DNA of *Rip140* and β -*Actin* was 62.75 ± 0.99 % the wild type level (**P** = 0.029) (Fig 3.7).

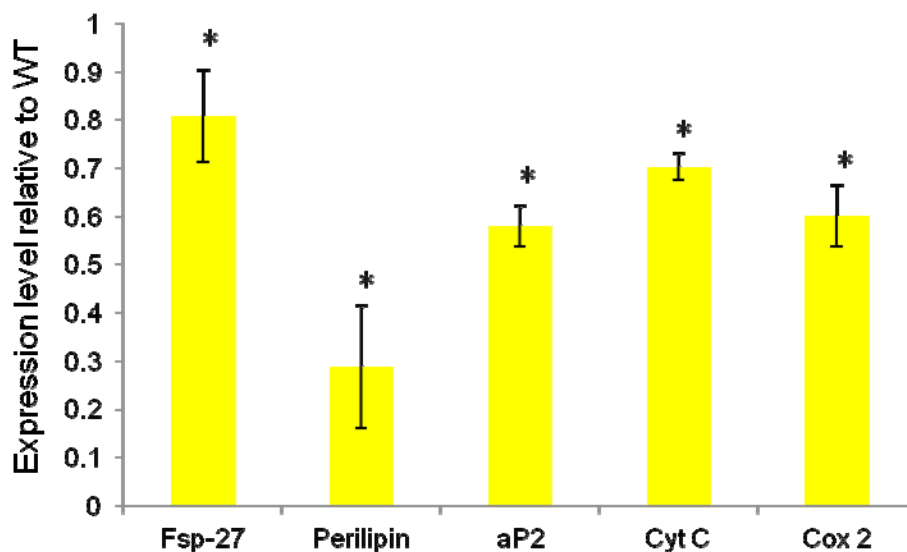


Figure 3.6 QPCR analysis of *Cdkn1c*^{-m/+p} E18.5 iBAT cDNA. Lipid accumulation and mitochondrial genes were found to be down-regulated in the absence of *Cdkn1c*. Error bars represent standard error of fold changes. Statistical analysis was performed by Mann Whitney test. * P< 0.05. N=4+4

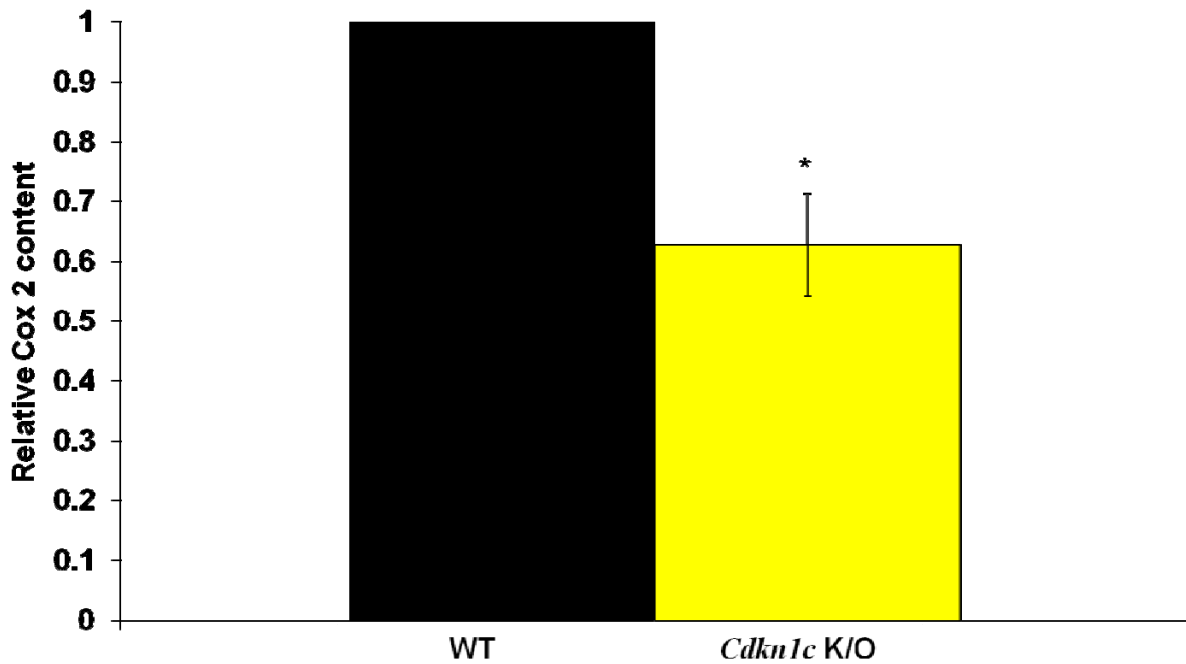


Figure 3.7 QPCR analysis of *Cdkn1c*^{-m/+p} E18.5 iBAT genomic DNA. Amplification of *Cox 2* from the mitochondrial genome was compared to nuclear gDNA content, highlighting a reduction of mitochondrial population in the absence of *Cdkn1c*. Error bars represent standard error of fold changes. Statistical analysis was performed by Mann Whitney test. * P< 0.05. N= 4+4.

Brown adipose tissue in the absence of *Cdkn1c* had been shown to be poorly differentiated and displayed reduced expression of genes associated with the thermogenesis. A similar phenotype, that of poor iBAT differentiation, has been reported in association with loss of function of *Prdm16*, a brown fat determinant^{154; 157; 158} and *C/ebpβ*, one of the earliest transcription factors whose expression is elevated in adipogenesis^{148; 192; 193}. Analysis of these two genes and other selected adipogenic markers was therefore performed to gain insight into the mechanism by which differentiation was being inhibited (Fig 3.8).

The mRNA levels of *Prdm16* were unaltered in the iBAT whereas expression of *C/ebpβ* was reduced. Knockout models of *C/ebpβ* produced mice lacking fully functional brown adipose tissue¹⁴⁸, sharing key features with the histology of *Cdkn1c*^{-m/+p} iBAT (Fig 3.2). However, the analysis of the

expression level of downstream targets of *C/ebpβ* in the *Cdkn1c^{-m/+p}* model was not consistent with loss of expression of *C/ebpβ* as the primary defect¹⁴⁸. *C/ebpa* is found directly downstream of, and is promoted by *C/ebpβ* in the brown adipogenic pathway¹⁹². Were loss of expression of *C/ebpβ* the primary cause of the phenotype observed in the *Cdkn1c^{-m/+p}* iBAT, reduced expression of *C/ebpa* would also be expected. Instead a modest increase in expression of the gene was observed. It should be noted however that previous studies have shown that the gene was dispensable in classic interscapular brown adipose differentiation, instead performing critical roles in the formation of white adipose tissue¹⁹⁴, and therefore the change in expression level was unlikely to account for any of the phenotypes observed. *PPARα*, a transcription factor key to brown adipogenesis, was however significantly down-regulated. *PPARα* has been demonstrated to act as a cold-inducible gene, increasing thermogenesis as required^{195; 196}. The reduced expression that is seen in *Cdkn1c^{-m/+p}* iBAT provides further evidence of a failure to differentiate correctly.

pRb, *PPARγ* and *Rip140* displayed only modest changes in expression level. Due to the extremity of the phenotype observed, it was unlikely that such modest changes in these adipogenic regulators would account for such changes.

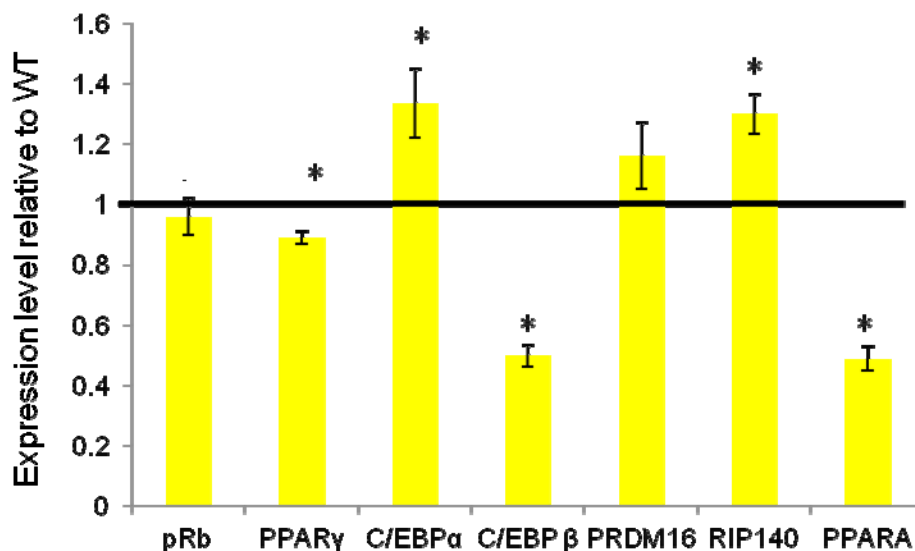


Figure 3.8 QPCR analysis of *Cdkn1c^{-m/+p}* E18.5 iBAT cDNA. Adipogenic and brown adipogenic regulators provided a diverse pattern of expression. Error bars represent standard error of fold changes. Statistical analysis was performed by Mann Whitney test. * P < 0.05. N=4+4.

In certain mouse models where a failure of the brown adipose tissue to form was observed, QPCR analysis of the tissue often found an elevation of skeletal muscle markers^{154; 197}. This phenomenon was suggested to represent a shared progenitor between myogenic lineage of skeletal muscle and brown adipose tissue^{154; 157}. Two skeletal muscle markers, *Myf5* and *MyoD* were analyzed via QPCR to determine if the *Cdkn1c*^{-m/+p} iBAT possessed skeletal muscle characteristics. Both *Myf5* and *MyoD* were found to be significantly elevated (Fig 3.9). Combined with other genes analyzed, the presence of skeletal muscle markers clearly demonstrated a failure to differentiate in the iBAT of *Cdkn1c*^{-m/+p} mice.

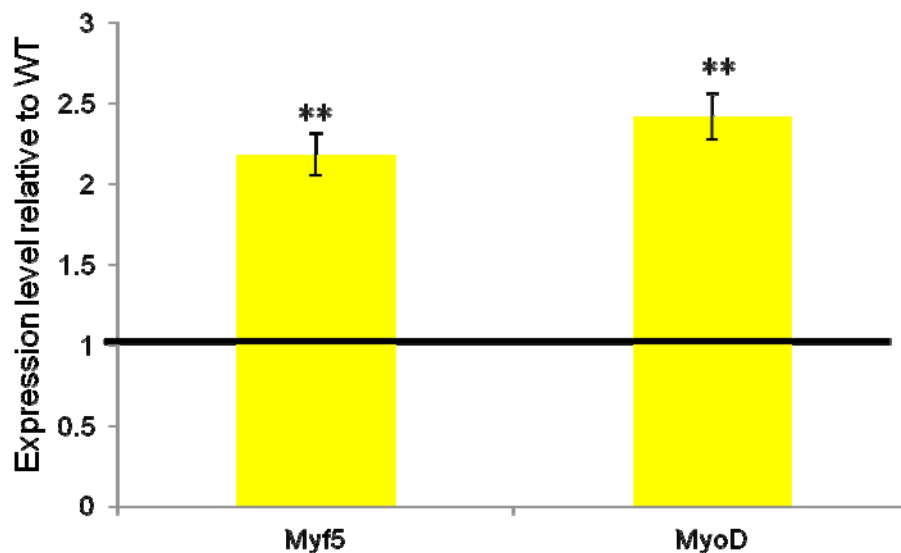


Figure 3.9 QPCR analysis of *Cdkn1c*^{-m/+p} E18.5 iBAT cDNA. Skeletal muscle markers *Myf5* and *MyoD* were both found to be elevated. Error bars represent standard error of fold changes. Statistical analysis was performed by Mann Whitney test. ** P< 0.01. N=4+4.

Reduced C/EBP β and Prdm16 disrupts non-shivering thermogenesis

In addition to the QPCR analysis, Western blotting was performed to ascertain whether the qPCR data was representative of alterations in protein levels. Western analysis for Ucp-1 was performed on E18.5 wild type and *Cdkn1c*^{-m/+p} iBAT (Figure 3.10). Ucp-1 was readily apparent in the wild type samples and barely detectable in the *Cdkn1c*^{-m/+p} samples.

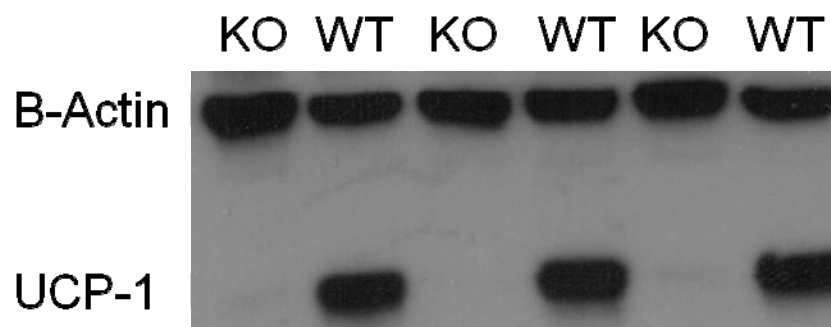


Figure 3.10 Western Blot for Ucp-1 protein in *Cdkn1c*^{-m/+p} E18.5 iBAT lysates. Ucp-1 was barely detectable in the absence of *Cdkn1c* expression. Lanes were normalised for protein amount through β -Actin blot.

Loss of Ucp-1 represented the end point in the failure for correct differentiation of *Cdkn1c*^{-m/+p} iBAT. As opposed to a direct interaction of *Cdkn1c* with the Ucp-1 gene, the QPCR analysis suggested an upstream disruption to many of the key brown adipocyte transcription factors. The importance of the Prdm16-C/ebp β complex to the acquirement of the brown adipose phenotype has previously been shown¹⁵⁶, and given the already discussed reduced expression of *C/ebp β* cDNA (Fig 3.8), focus turned towards analysing the protein levels of these two transcription factors. *Prdm16* cDNA levels were unaltered in *Cdkn1c*^{-m/+p} iBAT whereas *C/ebp β* levels were 50% wild type (Fig

3.8). By Western blotting, Prdm16 protein was greatly reduced in iBAT whereas the C/ebp β staining was consistent with the QPCR data (Fig 3.11).

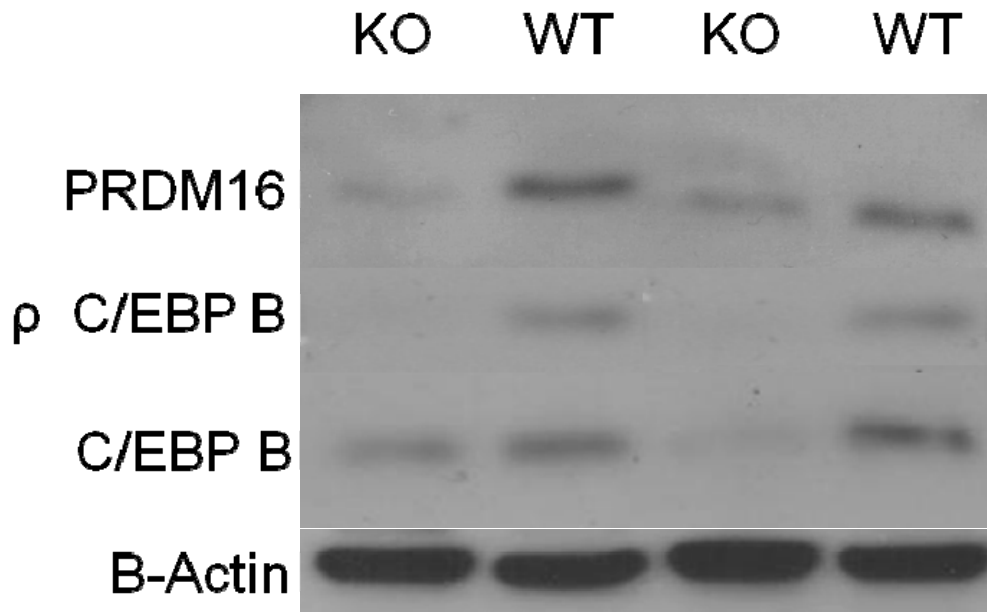


Figure 3.11 Western blotting for Prdm16 and C/ebp β proteins in *Cdkn1c*^{-m/+p} E18.5 iBAT lysates. Reduced detection of Prdm16 and total C/ebp β protein was observed in knockout samples. This also correlated to an absence of the phosphorylated form of C/ebp β . Sample amounts were normalised through β - Actin control.

While a role in modifying the phosphorylation state of C/ebp β had not previously been described for *Cdkn1c*, *Cdkn1c* encodes a cyclin dependent kinase inhibitor. It was possible therefore, that loss of function of *Cdkn1c* resulted in an increase in the phosphorylated form of C/ebp β , which has a tendency to self dimerise and promote the white adipogenesis pathway¹⁹⁸, over the non phosphorylated form which is proposed to dimerise with Prdm16 to promote the brown pathways¹⁵⁶. Levels of the Threonine-217 phosphorylated form of C/ebp β were therefore analysed through Western blotting. Threonine-217 phosphorylation is a secondary phosphorylation event that allows C/ebp β homodimers to form, activating the protein as a transcription factor¹⁹⁸. As can be seen

(Fig 3.11), the phospho-protein was undetectable in the *Cdkn1c* knockout samples. The lack of phospho-C/ebp β in *Cdkn1c*^{-m/+p} iBAT suggests that Cdkn1c did not play a role in inhibiting phosphorylation of C/ebp β .

In summary, this analysis indicated a requirement for *Cdkn1c* in brown adipogenesis and also suggested that *Cdkn1c* might play role in regulating brown fat development either through C/ebp β or *Prdm16*.

Investigating the consequences of elevated *Cdkn1c* expression

The BAC transgenic models were used to investigate the functional consequences of loss of imprinting of *Cdkn1c* in iBAT. Previously mice carrying a BAC transgene spanning the *Cdkn1c* locus were shown to express *Cdkn1c* from this transgene in a subset of tissues where *Cdkn1c* is normally expressed¹⁰⁶. Two version of the BAC transgene were used to generated transgenic mice, on a pure BL6 background. In one version, the transgenic BAC was unmodified and lines were generated with one, two or more copies of the transgene. In the second version, the transgene was initially modified such that the transgenic *Cdkn1c* expression was replaced by a β -galactosidase reporter. The lines with the unmodified transgene were experimental lines in which *Cdkn1c* was elevated whereas the lines carrying the modified version constituted both a reporter line but also a control for the experimental lines, containing the same DNA fragment but without elevation of *Cdkn1c*¹⁰⁷.

As a first step, adipose depots from the reporter line 10-15 were subject to LacZ staining. Discrete patches of blue cells were apparent (Fig 3.12a) suggesting expression of *Cdkn1c* from the transgene in adipose tissue. To ask whether the experimental transgenic lines carrying an unmodified version of this transgene elevated expression of *Cdkn1c* in adipose tissue, adipose depots were isolated from P7 mice from line 5D3 which was known to carry a single copy of the BAC transgene spanning *Cdkn1c* and line 5A4 which was known to carry two copies¹⁰⁷. As a control, depots were also isolated from the lacZ reporter line 10-15 which was known to carry three copies of the modified BAC transgene. QPCR analysis demonstrated elevated *Cdkn1c* in both 5D3 and 5A4 iBAT and expression was at wild type levels in 10-15 iBAT (Fig 3.12b). Western blotting was used to demonstrate that *Cdkn1c* protein was also elevated (Fig 3.13). Increased signal of the protein correlated to the changes seen in the QPCR analysis (Fig 3.12b). This analysis demonstrated that the transgenic lines could be employed to study the effect of over-expression of *Cdkn1c* in the iBAT.

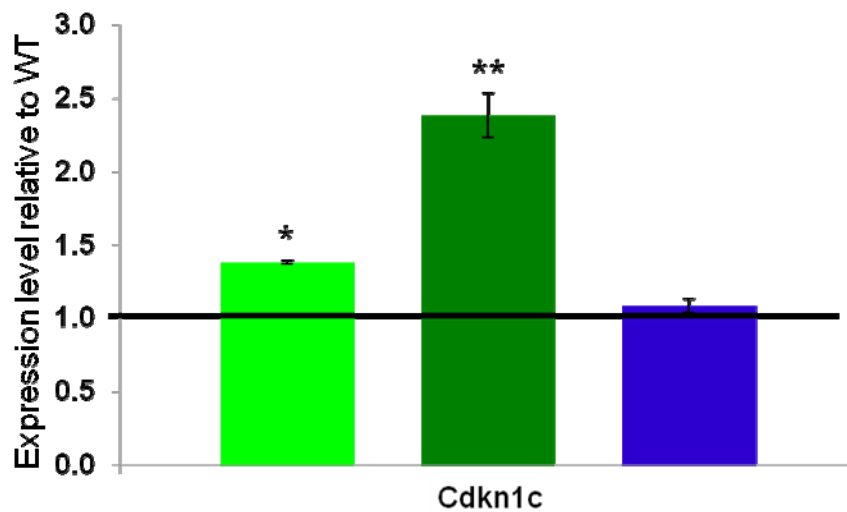
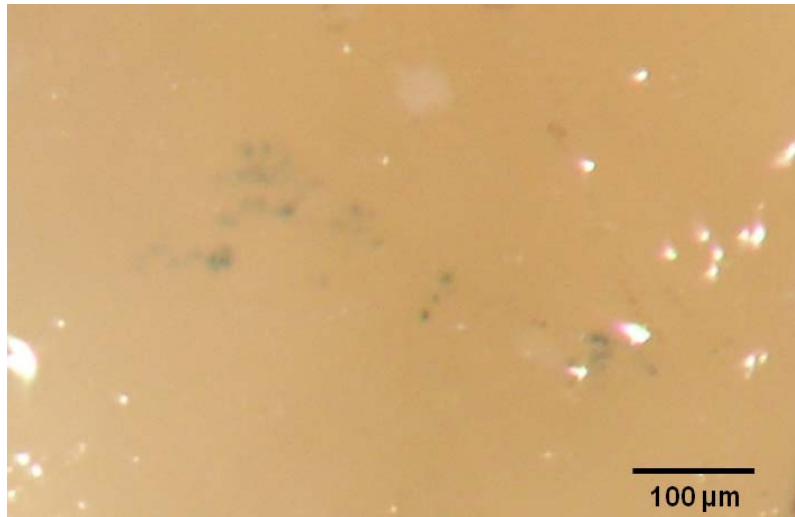


Figure 3.12 a) LacZ staining of iBAT depots from wild type and 10-15 mice. b) QPCR analysis of *Cdkn1c* expression in transgenic P7 iBAT. 5D3 (light green) and 5A4 (dark green) were both found to over-express *Cdkn1c* compared to wild type, while 10-15 (blue) did not. Error bars represent standard error of fold changes. Statistical analysis was performed by Mann Whitney test. * $P < 0.05$, ** $P < 0.01$. $N = 4 + 4$.

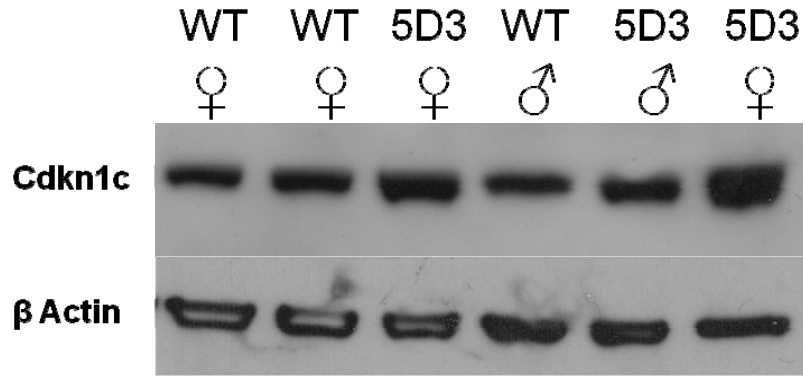


Figure 3.13 Western blot for Cdkn1c in 5D3 and wild type (WT) P7 iBAT lysates. The presence of the BAC in 5D3 was confirmed to result in over-expression of Cdkn1c. Sample amounts were normalised through β - Actin control.

Effect of *Cdkn1c* over-expression in iBAT

To begin the characterisation of the consequences of over-expressing *Cdkn1c* in iBAT, the weights of P7 iBAT from line 5D3 and line 5A4 were obtained. As a percentage of total body weight, both 5D3 and 5A4 iBAT depots was found to be significantly heavier than wild type iBAT depots (Fig 3.14).

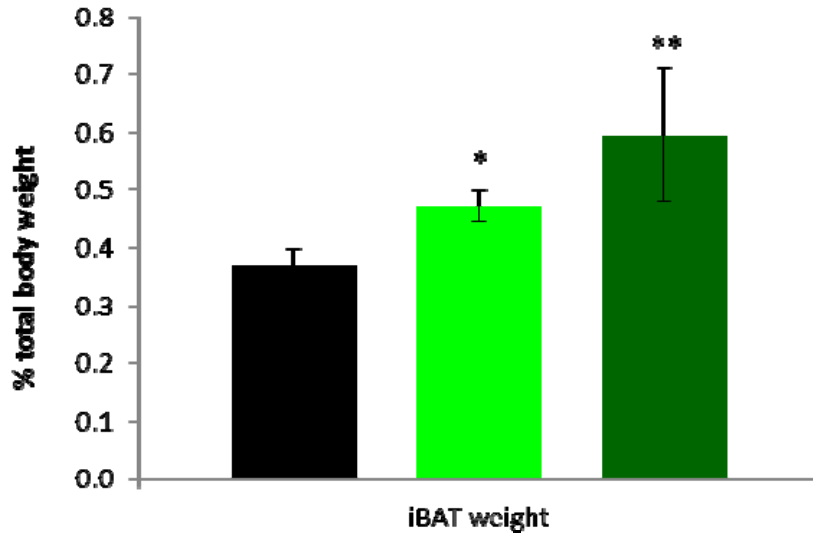


Figure 3.14 Weight of iBAT pad taken from P7 pups, presented as a percentage of total body weight. Both 5D3 and 5A4 pads constituted a significantly larger portion of total body weight than wild type mice. * $P \geq 0.05$. ** $P \geq 0.01$. Statistical analysis was performed by Students t-test. Error bars represent standard error. $N=20+18+8$

In order to further explore the consequences of increased *Cdkn1c* dosage on iBAT, pads were fixed, sectioned and subjected to histological analysis. H+E staining was performed on both *Cdkn1c* over-expressing lines, in addition to wild type and 10-15 controls (Fig 3.15). The tissue in all genotypes was constituted by multi-locular classic brown adipocytes. No detectable differences could be seen between the 10-15 and wild type sections. 5D3 and 5A4 sections appeared generally darker in colour as compared to wild type, most noticeably so in the 5A4 image. In addition, images of 5D3 and 5A4 iBAT appeared to contain more cells in a given area. To confirm this observation, cell counting was performed on the H+E images. Both 5D3 and 5A4 iBAT were found to contain significantly more cells than wild type (Fig 3.16).

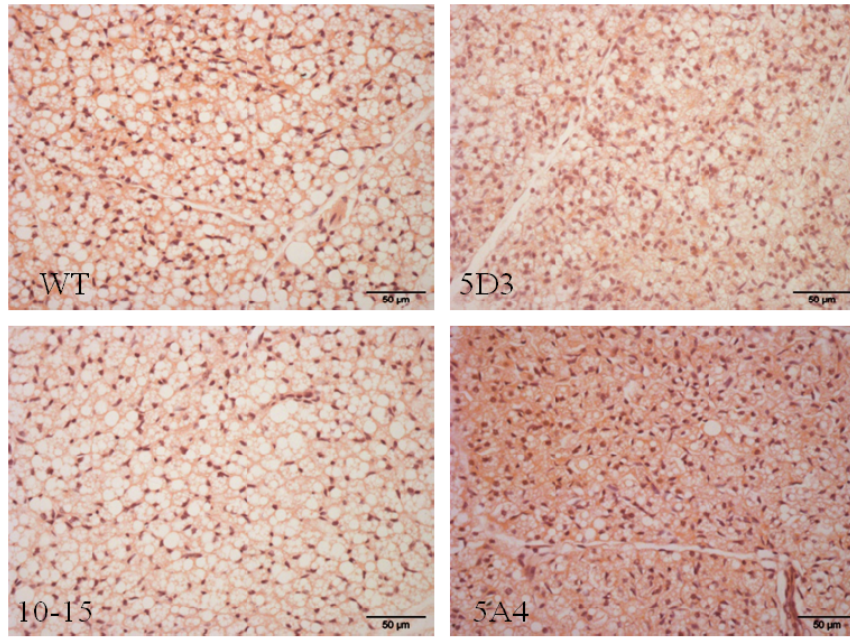


Figure 3.15 H+E of transgenic P7 iBAT sections at 20X magnification, photographed under standard light field conditions. 5D3 and 5A4 brown adipocytes appeared more numerous and the tissue appeared darker in colour than wild type or 10-15 sections, which were not discernible from one another. Scale bar represents 50 μm

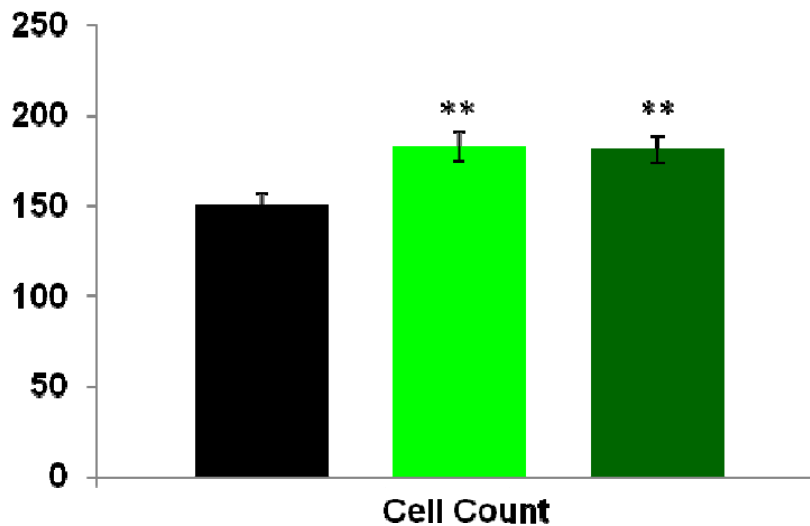


Figure 3.16 Cell counting performed on H+E images of P7 iBAT. Both 5D3 and 5A4 iBAT were found to possess significantly more cells per image than wild type tissue. ** $P \geq 0.01$. Statistical analysis was performed by Student's t-test. Error bars represent standard error. N: 8+8+8. Area of image: 160,000 μm^2 .

In summary, upon completion of these initial observations, *Cdkn1c* expression was shown to be elevated in iBAT from the experimental lines and this increased dosage was associated with a larger brown adipose deposit. Furthermore, the results were consistent with increased cellularity, as opposed to an increase in the amount of lipid stored.

Cellular expression of *Cdkn1c* in iBAT

In situ hybridisation was performed on paraffin embedded sections from P7 wild type and 5D3 iBAT (Fig 3.17). The expression pattern found was consistent with the LacZ staining (Fig 3.12a), where only a sub-set of cells were positive for expression. Cell counting of wild type images demonstrated that less than 5% of cells within the wild type tissue were found to be *Cdkn1c* positive (Fig 3.18). Both 5D3 and 5A4 sections were found to possess a greater percentage of *Cdkn1c* positive cells, although only 5A4 achieved significance (Fig 3.18).

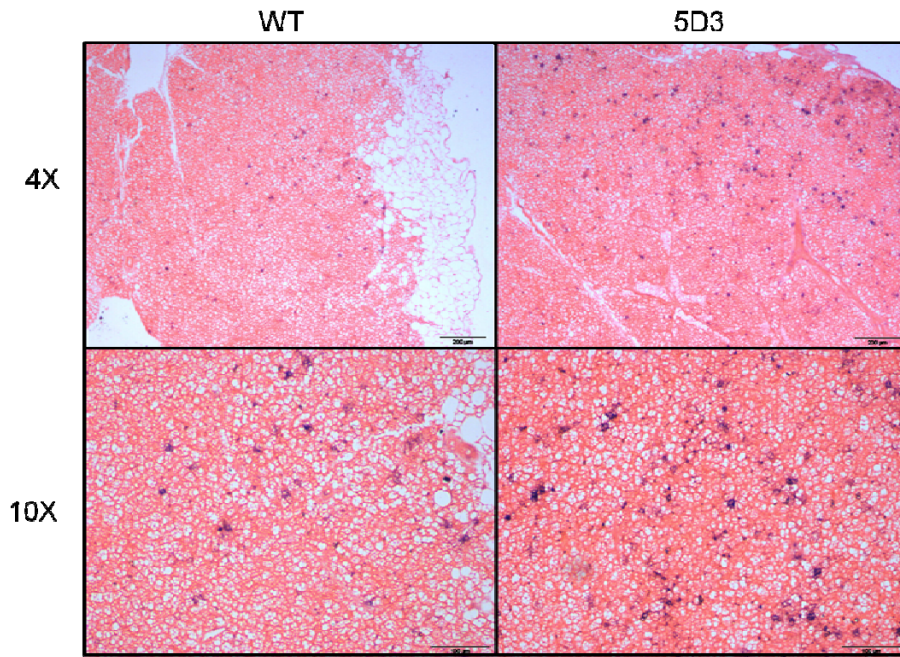


Figure 3.17 *In situ* hybridisation for *Cdkn1c* of 5D3 P7 iBAT sections, photographed under standard light field conditions. Expression of *Cdkn1c* was detected in a sub-population of cells within the tissue. Scale bars represent 200 μm (4X) and 100 μm (10X)

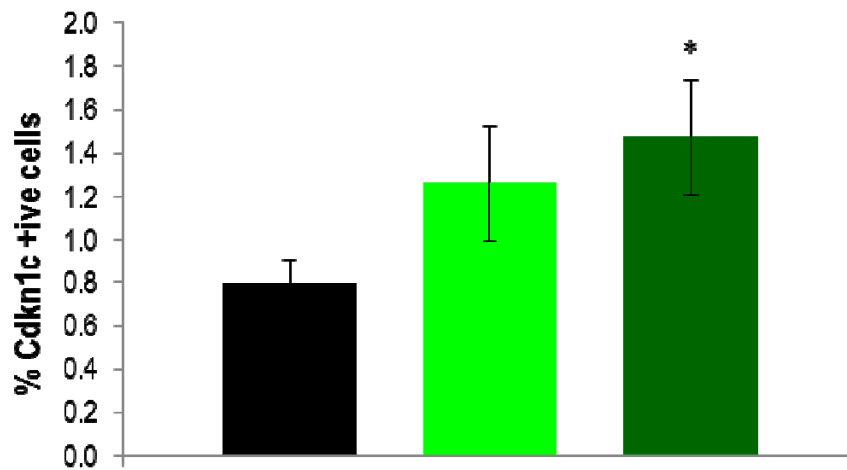


Figure 3.18 Counting of *Cdkn1c* positive cells within P7 iBAT from *In situ* hybridisation. Less than 1% of cells were found to express *Cdkn1c*. Error bar represents standard error. N=6+6+6.

QPCR analysis of *Cdkn1c* over-expressing iBAT

cDNA was generated from iBAT and QPCR analysis was performed on genes associated with brown adipogenesis (Fig 3.19). While *Ucp-1* and *Cidea* were not significantly increased in 5D3 iBAT at this time point, *PGC-1 α* and *Elovl3* were. All four genes were found to be further elevated in line 5A4, indicating a dosage dependent phenotype. The results of the 5A4 analysis, together with a lack of amplification of the thermogenic programme in the 10-15 reporter line, excluded the possibility of a phenotype having arisen as a result of an insertion event. It should be noted at this stage that while *Cdkn1c* was only found to be expressed within a subset of cells in the interscapular brown adipose tissue, the four genes analyzed, that were involved in the thermogenic programme, would be uniformly expressed throughout the tissue, and therefore the cell number differences already described would not affect these results (Fig 3.16).

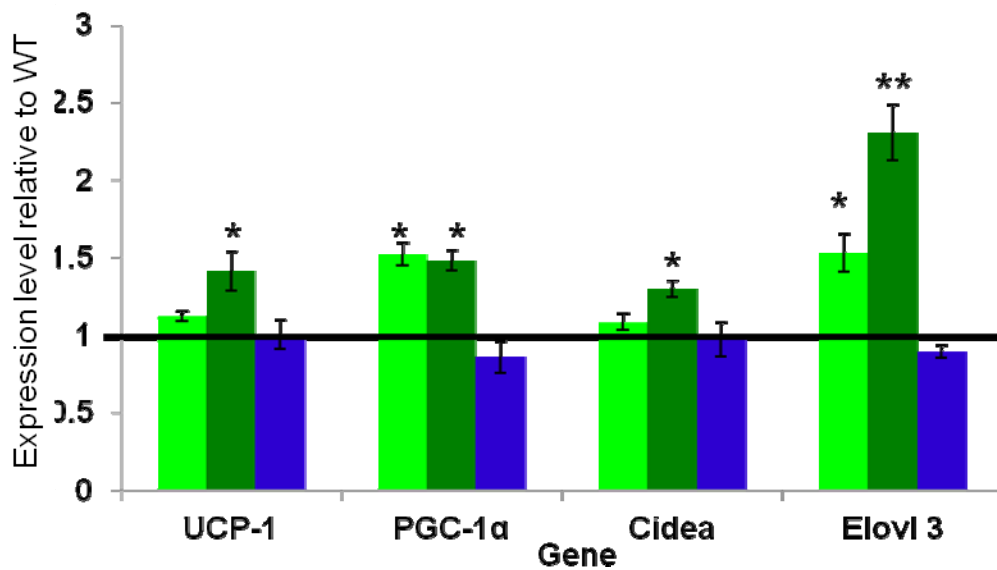


Figure 3.19 QPCR analysis of transgenic P7 iBAT. 5D3 and 5A4 were shown to possess an enhanced thermogenic program, which was not the case for 10-15. Amplification of thermogenic genes occurred in a dosage dependent manner. Error bars represent standard error of fold changes. Statistical analysis was performed by Mann Whitney test. * $P < 0.05$. ** $P < 0.01$. $N=4+4+4+4$

Beyond the examination of genes associated with the thermogenic programme, key regulators of lipid storage and mitochondrial content were analysed (Fig 3.20). Expression of *Fsp-27* was reduced in 5D3 and 5A4 iBAT whereas expression of *aP2* was increased. *Perilipin* expression was also elevated in 5D3 and 5A4 lines. Given the known role of *Perilipin* in lipolysis and lipid mobilisation, to provide the fuel for heat generation ^{163; 199; 200}, this elevation in expression was consistent with an enhanced thermogenic programme.

H+E staining of iBAT sections (Fig 3.15) had previously revealed a darker brown colour in the transgenic mice which might reflect increased mitochondrial content. *Cox II* levels were increased in both 5D3 and 5A4 mice, with no changes in *Cytochrome C* levels in either line. *Cytochrome C* is encoded by the nuclear genome while *Cox 2* is transcribed off the mitochondrial genome. To ascertain whether these changes in gene expression related to a change in mitochondrial copy number, gDNA QPCR analysis of iBAT pads was performed (Fig 3.21). The increased amplification of *Cox 2* observed from 5D3 and 5A4 iBAT gDNA corroborated the changes that were seen in the cDNA analysis.

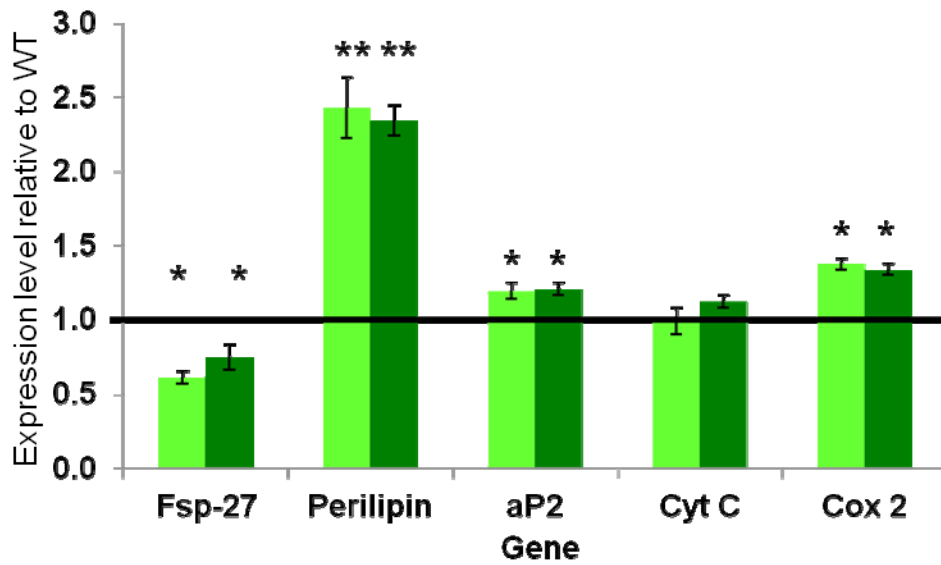


Figure 3.20 QPCR analysis of transgenic P7 iBAT cDNA. 5D3 and 5A4 were shown to possess an enhanced mitochondrial program. Large induction of Perilipin was believed to relate to increased lipid turnover within the adipocytes. Limited amplification of lipid accumulation and mitochondrial genes was observed. Error bars represent standard error of fold changes. Statistical analysis was performed by Mann Whitney test. * P< 0.05. ** P< 0.01. N= 4+4+4

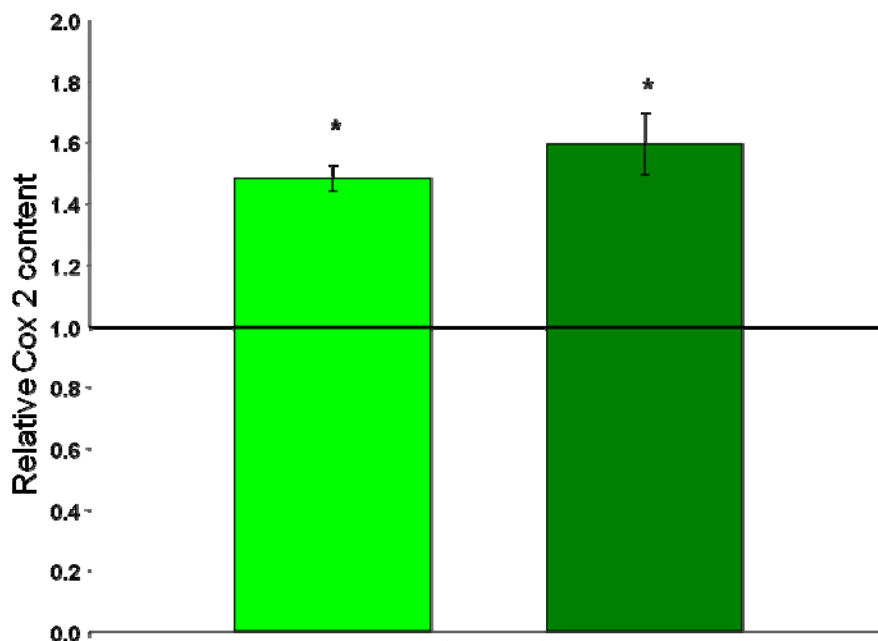


Figure 3.21 QPCR analysis of transgenic P7 iBAT gDNA. Total cellular Cox 2 content, compared to nuclear gDNA, was increased in 5D3 and 5A4. Error bars represent standard error of fold changes. Statistical analysis was performed by Mann Whitney test. * P< 0.05. N= 4+4+4

All experiments so far performed suggested that the increased dosage of *Cdkn1c* enhanced brown adipogenesis. Further investigation into the expression levels of key adipogenic regulators was performed in order to gain insight into the mechanism by which this process was occurring (Fig 3.22). Neither *pRb* nor *PPAR γ* were altered in the 5D3 or 5A4 iBAT. However both *C/ebp β* and *Prdm16* displayed increased expression in 5D3 and 5A4 iBAT. These two genes have been shown to be critical to the formation of brown adipose tissue, and were also demonstrated to be binding partners in brown adipogenesis¹⁵⁶. Further to these genes *C/ebp α* , a downstream family member of *C/ebp β* , was also found to be elevated in both 5D3 and 5A4 iBAT. Finally, the nuclear co-repressor *Rip140* was found to be modestly elevated in 5D3 and 5A4 iBAT.

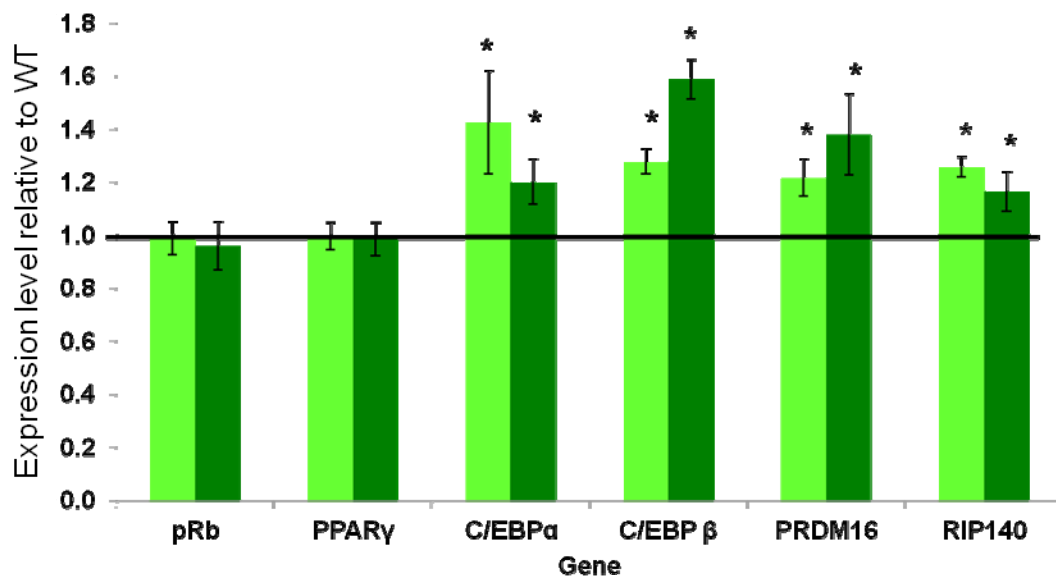


Figure 3.22 QPCR analysis of transgenic P7 iBAT cDNA. 5D3 and 5A4 displayed modest amplification of certain adipogenic regulators. Error bars represent standard error of fold changes. Statistical analysis was performed by Mann Whitney test. * $P < 0.05$. $N = 4+4+4$

Cdkn1c functions with Prdm16 and C/EBPβ in iBAT

As a result of the previously described roles of *Prdm16* and *C/ebpβ* in brown adipogenesis¹⁵⁶ the dosage dependent increases in these two genes that were found in 5D3 and 5A4 iBAT were further explored at the protein level. Analysis of 5D3 iBAT was performed through Western blotting of *Prdm16* and *C/ebpβ* proteins (Fig 3.23), in order to corroborate the changes that were observed at the mRNA level (Fig 3.22). *Prdm16* Western indicated increased levels of the protein in 5D3 iBAT, when compared to wild type. Further Western blotting including 5A4 iBAT demonstrated a *Cdkn1c* dosage related increase in *Prdm16* protein (Fig 3.24). Total *C/ebpβ* protein levels were comparable to wild type. The fold change observed for the mRNA was comparatively modest (1.28 ± 0.049), and therefore the Western blot may have been insufficiently sensitive to detect this difference. In reference to the phosphorylated form of *C/ebpβ*, unaltered levels in the 5D3 iBAT from wild type again suggested that *Cdkn1c* does not play a role in regulating the phosphorylation state of *C/ebpβ*.

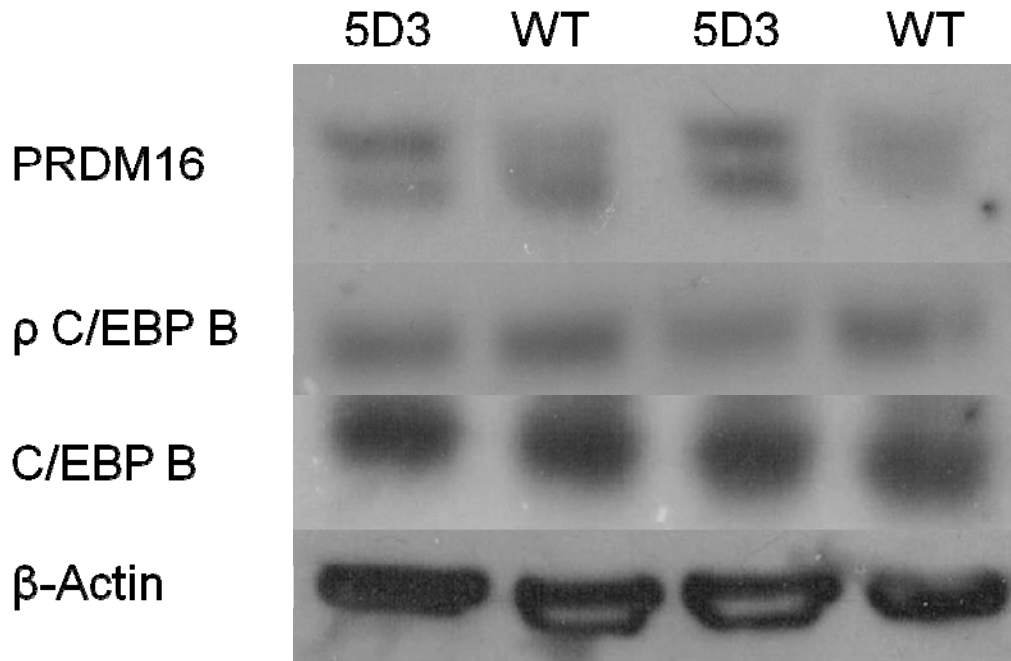


Figure 3.23 Western blotting for Prdm16 and C/ebpβ proteins in 5D3 P7 iBAT lysates. Levels of phosphorylated and total C/ebpβ were not seen to be altered in transgenic samples from wild type. Prdm16 protein content was increased in 5D3. The blot produced a double band that had not previously been reported. The nature of this band has not yet been elucidated. Sample amounts were normalised through β- Actin control.

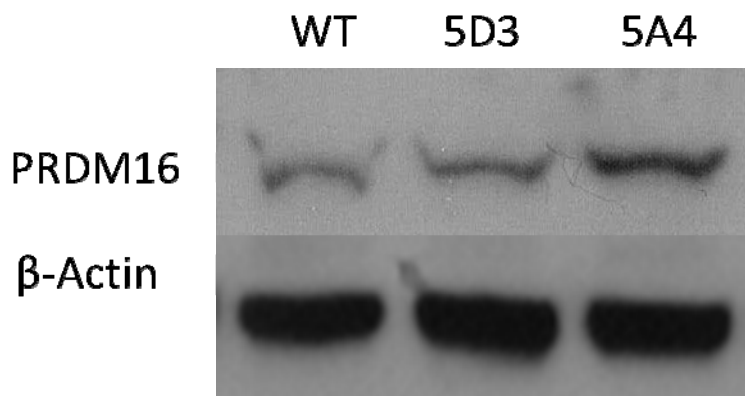


Figure 3.24 Western blot for Prdm16 protein in P7 iBAT lysates. Prdm16 content was increased in a dosage dependent manner in transgenic iBAT. Sample amounts were normalised through β-Actin control.

Co-localisation of Cdkn1c and Prdm16 proteins in iBAT

The qPCR analysis and Western analysis of $Cdkn1c^{m/+p}$ and BAC transgenic iBAT suggested a potential relationship between *Cdkn1c* and *Prdm16*. Fluorescent immunohistochemistry (Fig 3.25) was performed on P7 wild type iBAT to explore this relationship further. *Cdkn1c* expression seen by *in situ* (Fig 3.17), was detected in only a sub-set of cells. However, there appeared to be two separate populations that expressed *Cdkn1c*. The main population, that expressed the gene at low levels, and a much rarer cell that expressed the gene very highly (data not shown). By immunofluorescence, this very rare single cell was observed, highlighted by white arrows, that was found to fluoresce for *Cdkn1c* and *Prdm16* expression more highly than surrounding cells. A high magnification image of this cell (Fig 3.25) confirmed overlapping expression of the two proteins, and this expression was found to be nuclear. This cell type that displayed overlapping nuclear expression of *Cdkn1c* and *Prdm16* was also found to be BrdU label-retaining in a long term study (Fig. 3.26).

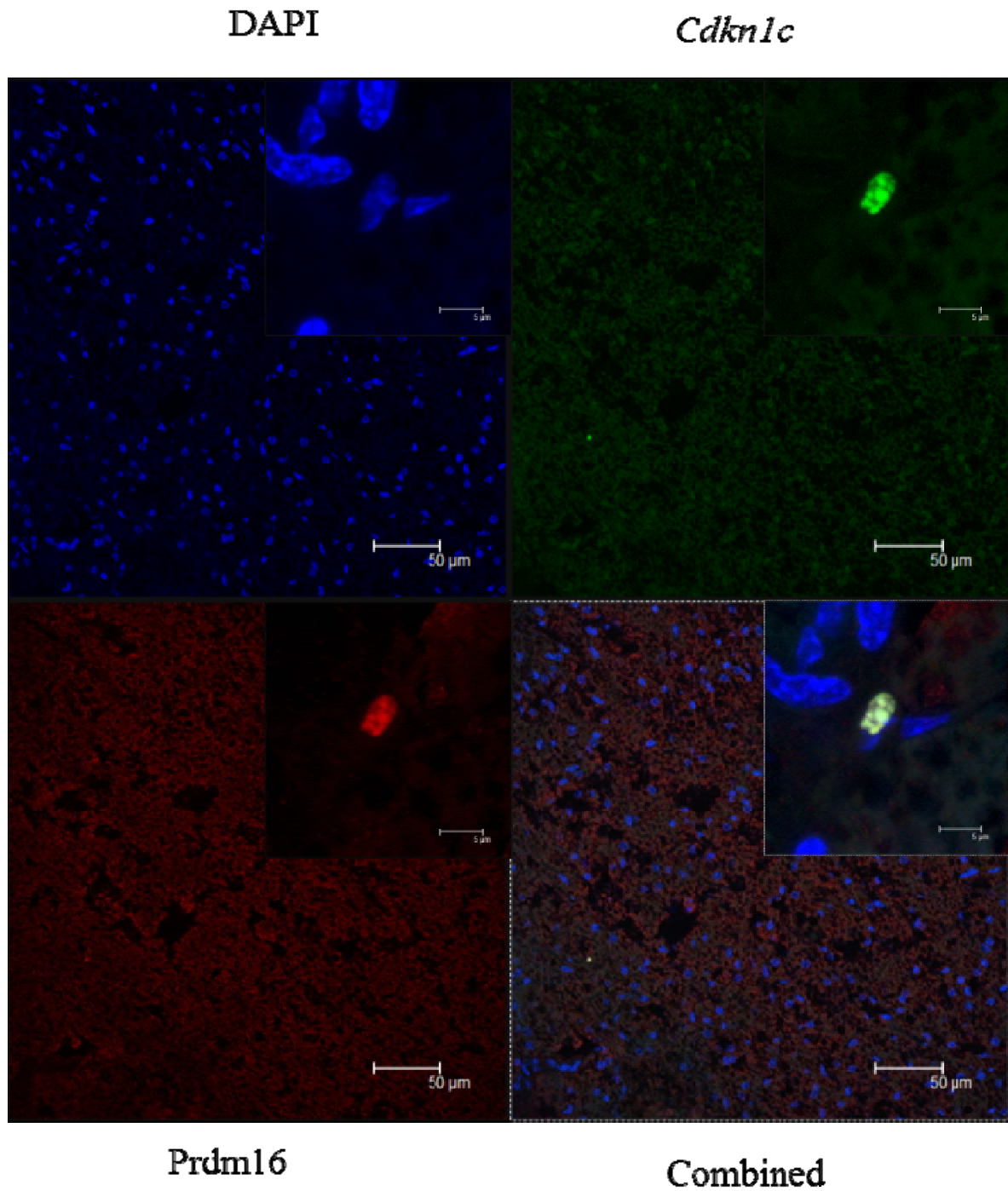


Figure 3.25 Fluorescent Immunohistochemistry of Wild type P7 iBAT for *Cdkn1c* and *Prdm16* expression with the tissue. Elevated *Cdkn1c* expression was observed in a subset of cells while *Prdm16* expression was observed throughout the tissue. A single cell was found to display overlapping *Cdkn1c* and *Prdm16* expression (highlighted by arrows) at high levels.

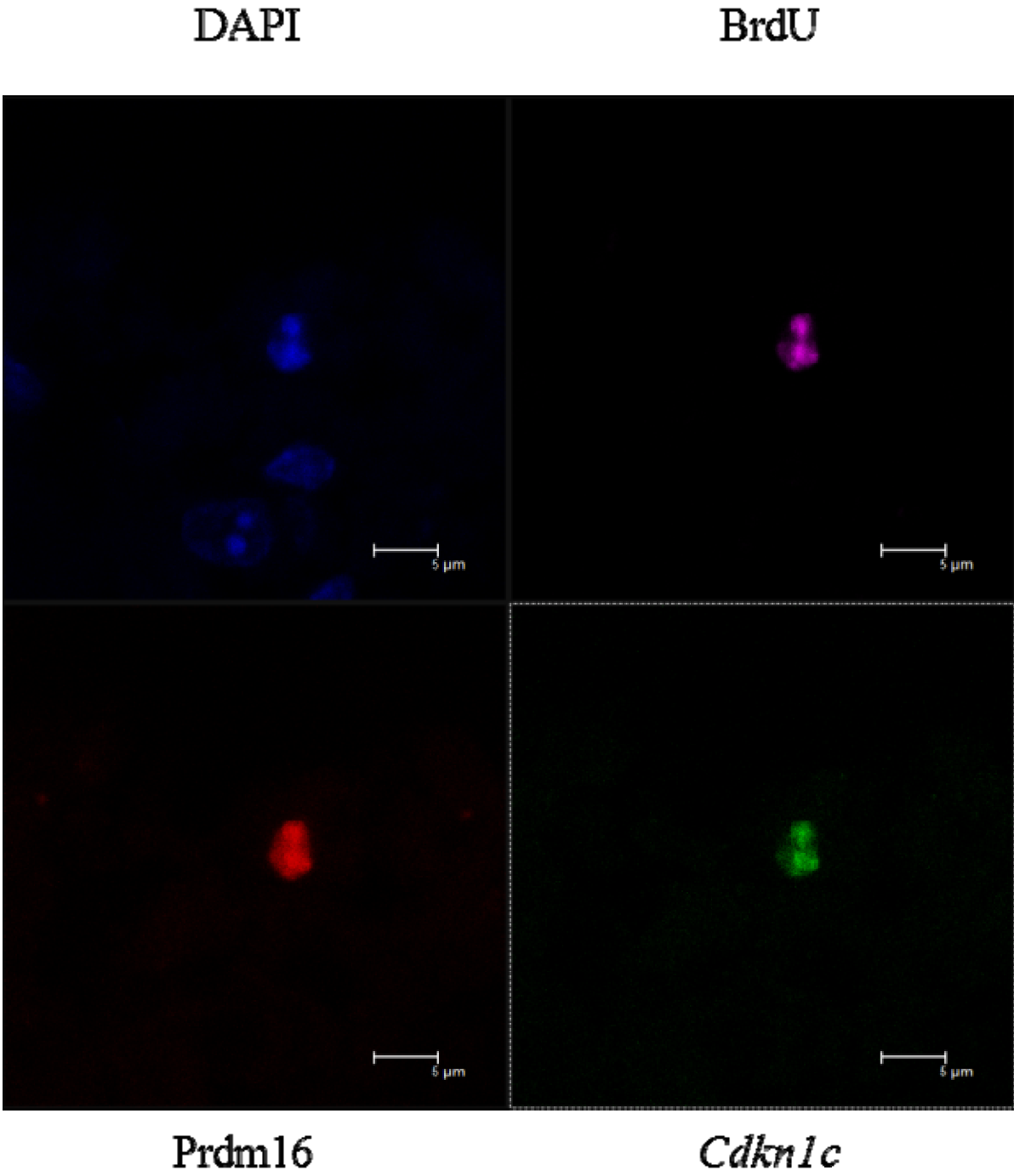


Figure 3.26 Fluorescent immunohistochemistry of wild type P56 iBAT. High magnification image of the single cell which displayed over-lapping expression of both *Cdkn1c* and *Prdm16*, and was found to be BrdU label-retaining. Other cells were not found to be BrdU positive.

Discussion

Cdkn1c was shown to be expressed and imprinted in a small population of cells within postnatal iBAT. Using both loss-of-function and gain-in-expression models, a critical and dosage-related function for *Cdkn1c* in brown adipogenesis was identified.

In the loss-of-expression model, an almost complete absence of Ucp-1 protein suggested that the tissue was largely thermogenically inactive (Fig 3.10). A lack of thermogenesis would account for the increased lipid content of *Cdkn1c* deficient iBAT (Fig 3.4). Without the uncoupling of the electron transport chain, use of lipid energy stores would have been reduced, resulting in the observed build up. Due to the neonatal lethality and other developmental abnormalities associated with loss-of-function of *Cdkn1c*, it was not possible to determine whether the alterations in iBAT would result in a lower body temperature but this seems a likely conclusion. Such work will require the development of a conditional *Cdkn1c* allele and suitable cre-expressing lines.

In terms of the mechanism for loss of iBAT in *Cdkn1c*^{-m/+p} pups, there was an association between *Cdkn1c* dosage and *C/ebpβ* expression, both at the mRNA and protein level. The phenotype of the *Cdkn1c* loss-of-expression iBAT could be attributed to loss of *C/ebpβ* expression (Fig 3.8, 3.11) which has been shown to result in a failure in iBAT differentiation¹⁴⁸. Mirroring this effect, increased *Cdkn1c* expression in the 5D3 and 5A4 lines resulted in enhanced *C/ebpβ* expression at the mRNA level (Fig 3.22). The increase in mRNA was not apparent at the protein level although Western blotting is not a sufficiently sensitive method for detecting such subtle changes in expression (Fig 3.23). In addition to directly or indirectly regulating *C/ebpβ* transcription, *Cdkn1c* might have been involved in regulating phosphorylation state of *C/ebpβ* since a similar function has already been assigned to p27^{KIP1}²⁰¹. This CDKi protein family member was found to maintain the unphosphorylated state of *C/ebpβ*, thereby preventing protein dimerisation and G1/S phase progression. *Cdkn1c* could also have been anticipated to play a similar role. However, this was found not to be the case. While deficiency of the *Cdkn1c* would be predicted to result in hyper-phosphorylation of *C/ebpβ*, instead. *Cdkn1c*^{-m/+p} iBAT, lysates were essentially devoid of detectable phosphorylated

C/ebp β (Fig 3.11). It was essential to bear in mind that the total pool of protein was also shown to be reduced, thereby limiting the available target to be phosphorylated (Figure 3.11). With this in mind though, there remained still a sizable target population, and had *Cdkn1c* been negatively regulating the phosphorylation events, it would certainly have been expected that at least some of the population would be found in this phosphorylated state. In addition, in the reciprocal scenario, elevated *Cdkn1c* would be predicted to result in hypo-phosphorylation of C/ebp β . Such a change in the phosphorylation state of C/ebp β in 5D3 iBAT was not apparent (Fig 3.23). These data suggest that it is unlikely that *Cdkn1c* regulates the phosphorylation of C/ebp β in iBAT.

Loss of *Cdkn1c* in iBAT also showed striking phenotypic similarities to loss of expression of the brown fat determinant, Prdm16¹⁵⁴. Furthermore, the immuno-fluorescence (Fig 3.25-26) demonstrated co-localisation of *Cdkn1c* and Prdm16 to the nucleus of a discrete population of iBAT cells which could indicate an interaction. Prdm16 mRNA expression was not disrupted as a consequence of the loss of *Cdkn1c* in iBAT and Prdm16 mRNA was only slightly higher in response to elevated *Cdkn1c* expression (Fig 3.8, 3.22). However, detectable differences in Prdm16 protein content were observed in both models. Western blot *Cdkn1c*^{m/+p} iBAT lysates detected reduced Prdm16 protein (Fig 3.11), while 5D3 and 5A4 iBAT was shown to exhibit elevated Prdm16 content (Fig 3.23-24). This disparity between Prdm16 mRNA and Prdm16 protein in the models was consistent with a role for *Cdkn1c* in the post-transcriptional stabilisation of Prdm16. A previous study has shown that *Cdkn1c* directly binds to and stabilises MyoD protein promoting the development of skeletal muscle^{100; 202}. A similar function could be suggested for *Cdkn1c* in the formation of brown adipose tissue through the stabilisation of Prdm16. Both skeletal muscle and brown adipose share a myogenic lineage, and the data generated would now implicate *Cdkn1c* as contributing to the formation of both tissue types. Expression of MyoD protein results in skeletal muscle formation, while Prdm16 protein will produce brown adipose tissue, and both proteins can therefore be termed “molecular switches” towards their respective cell type. *Cdkn1c* on the other hand, does not appear to function as a switch in this molecular determination since it seems to act in both lineages. Instead, certainly from the brown adipose perspective, the gene appears to function as an augmentor of an

already established cell fate (Fig 3.26). This theory is supported by the 5D3 and 5A4 iBAT, where an enhancement of the brown adipogenic phenotype was observed.

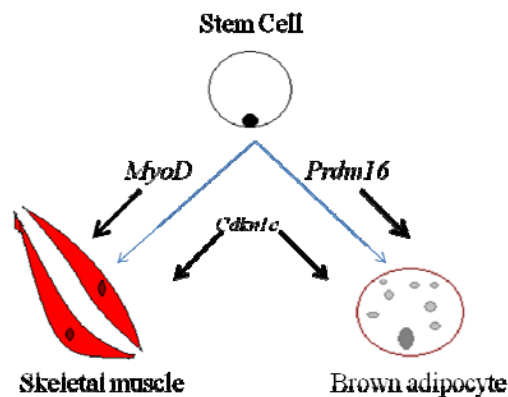


Figure 3.26 Possible role of *Cdkn1c* in determining myogenic lineage cell fate. *Cdkn1c* acts to stabilise both *MyoD* and *Prdm16*, providing an augmentation of both the skeletal muscle and brown adipogenic pathways.

The *in situ* hybridisation of *Cdkn1c* expression within the iBAT displayed expression in only a subset of cells (Fig 3.17). This population of cells was expanded under the increased *Cdkn1c* dose in iBAT (Fig 3.18). Although not investigated further in this thesis, this population may represent a precursor cell. The immunofluorescence of the iBAT (Fig 3.24-25) demonstrated a very rare cell type that was expressing *Cdkn1c* and *Prdm16*, which was a label-retaining cell. This was in addition to the *in situ* data that highlighted a greater population of cells that was *Cdkn1c* positive, at much lower levels. Thus our preliminary data suggest that *Cdkn1c* marks two populations of cells within the brown adipose tissue, those that are *Cdkn1c*-only positive, and a much rarer population that co-express *Cdkn1c* and *Prdm16*, which may represent the brown adipose stem cell. This subject will be discussed in greater detail in the final discussion.

This work identified a key role for *Cdkn1c* in the classic brown adipose lineage most likely through regulation of *Prdm16*. Brown adipose tissue is also present within white adipose depots. This non-classical lineage is thought to arise from a different precursor to iBAT which does not express *Myf5* and the role of *Cdkn1c* in this lineage is explored in the next chapter.

Chapter 4: *Cdkn1c* in white adipogenesis

Cdkn1c expression in white adipose tissue

The previous chapter focused exclusively on *Cdkn1c* expression within the classic interscapular brown adipose depot. In the absence of expression of *Cdkn1c*, cells were poorly differentiated and were found to be lacking in the thermogenic programme. Use of the *Cdkn1c* over-expression lines demonstrated that elevated expression enhanced the thermogenic programme in a dosage dependent manner. Work has suggested that populations of brown adipocytes are found contained within the white adipose depots (reviewed ¹²⁵). It is believed that this cell type may represent a different lineage to those cells within the iBAT. While iBAT cells are found to be Myf5⁺ ¹⁵⁴, brown adipocytes found in the white adipose depots are believed to be Myf5⁻ ¹⁵⁶ (reviewed ¹⁹³). The next focus point was to determine if *Cdkn1c* had a role in regulating the brown adipocytes found within white adipose tissue.

Cdkn1c expression within the white adipose tissue was not known upon commencement of these studies. RFLP analysis had demonstrated a detectable level of *Cdkn1c* in the rWAT depot and that the gene was imprinted (Fig 3.1). *In situ* hybridisation was performed on P7 wild type rWAT. Expression of *Cdkn1c* was confirmed in the rWAT, however and as had been the case for the iBAT, expression was only detected in a sub-set of cells (Fig 4.1). The 10-15 reporter line was again utilised to ask whether *Cdkn1c* was expressed from the transgene. Expression was only detected in a sub-set of cells (Fig 4.2), consistent with the *in situ* image.

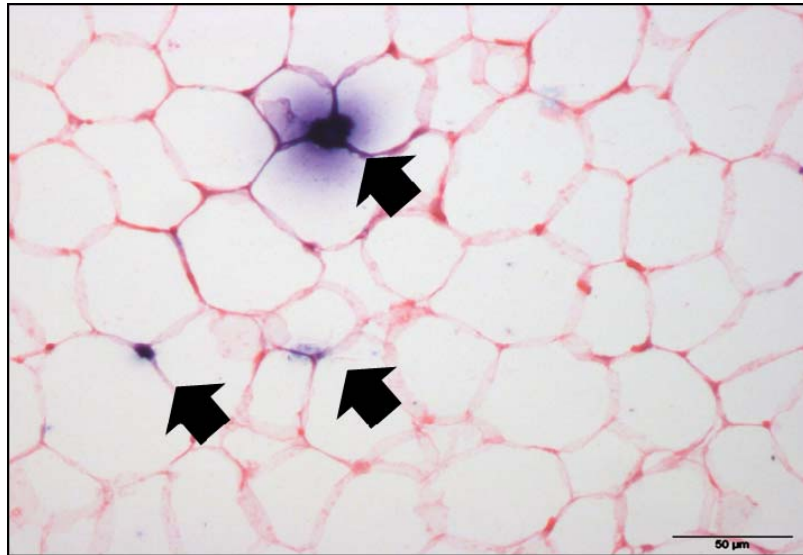


Figure 4.1 *In situ* hybridisation for *Cdkn1c* of wild type P7 rWAT sections, photographed under standard light field conditions. Only a sub-population of cells within the tissue were found to express *Cdkn1c*. Scale bar represented 50 µm.

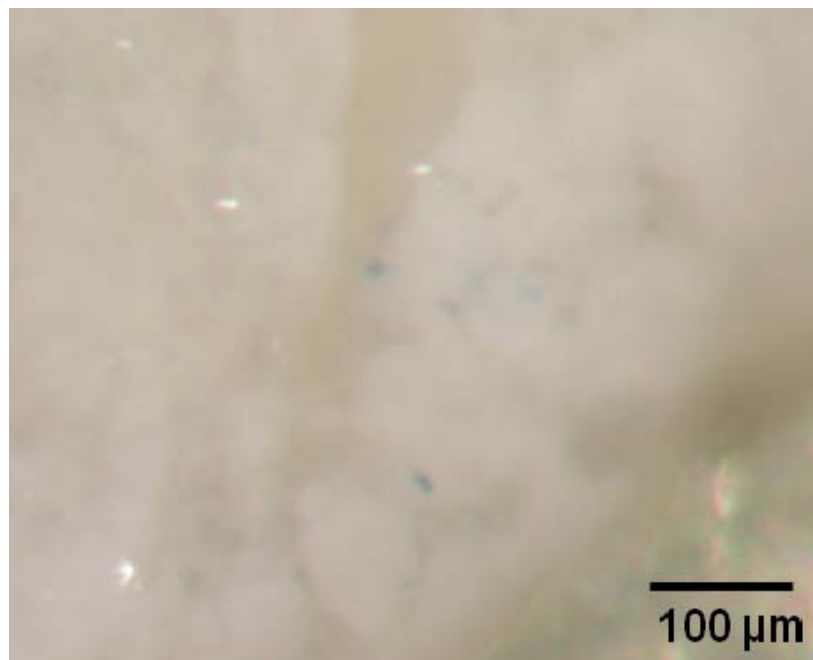


Figure 4.2 *LacZ* staining of whole 10-15 reporter line P7 rWAT, photographed under standard light field conditions. Positive blue staining represented a sub-population within the adipose tissue of cells expressing *Cdkn1c*. Surrounding white adipocytes were not found to be expressing the gene. No staining was observed in wild type adipose pads.

Expression of *Cdkn1c*, both endogenously and from the transgene, had now been confirmed in the rWAT depot through *in situ* hybridisation and *lacZ* staining (Fig 4.1-2). QPCR analysis was performed to ask whether or not the experimental transgenic lines 5D3 and 5A4 over-expressed *Cdkn1c* which would therefore allow the study of the consequences of increased *Cdkn1c* expression in this white adipose depot. As can be seen below (Fig 4.3), over-expression of *Cdkn1c* was found in both the 5D3 and 5A4 lines at a similar level to the over-expression observed in iBAT. Critically, no increase in *Cdkn1c* expression was observed in the 10-15 rWAT. Western blotting for *Cdkn1c* was used to demonstrate that there was increased *Cdkn1c* protein, with increased signal in 5D3 lysates as compared to wild type (Fig 4.4).

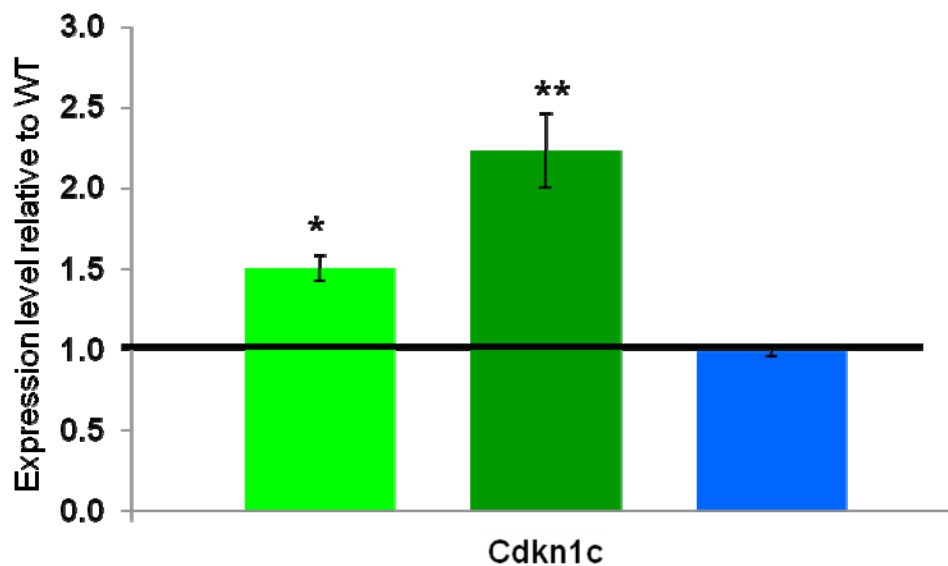


Figure 4.3 qPCR analysis of *Cdkn1c* expression in transgenic p.7 rWAT cDNA. 5D3 and 5A4 were both found to over-express *Cdkn1c* compared to wild type, while 10-15 did not. Error bars represent standard error of fold changes. Statistical analysis was performed by Mann Whitney test. * $P < 0.05$, ** $P < 0.01$. $N = 4 + 4 + 4 + 4$.

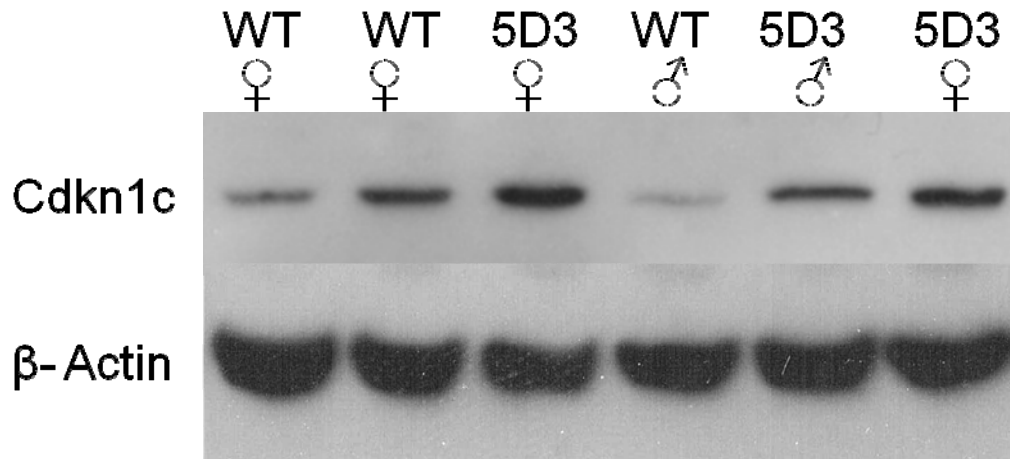


Figure 4.4 Western blot for *Cdkn1c* in 5D3 P7 rWAT lysates. Elevated detection of the protein was found in 5D3 males and females, compared to wild type littermates. Sample amounts were normalised through β -Actin control.

Increased *Cdkn1c* alters normal white adipose tissue

Upon confirmation that the transgenic lines could be employed to study the consequences of *Cdkn1c* over-expression in a white adipose tissue depot, rWAT pads from the transgenic lines were subjected to sectioning and H+E staining. Both wild type and 10-15 sections were populated primarily by uni-locular white adipocytes with few regions with a BAT-like appearance. In contrast 5D3 and 5A4 rWAT sections, although also containing uni-locular cells, were found to contain more extensive areas of multi-locular cells (Fig 4.5). Under higher magnification, these cells were found to more closely resemble brown adipocytes (Fig 4.6).

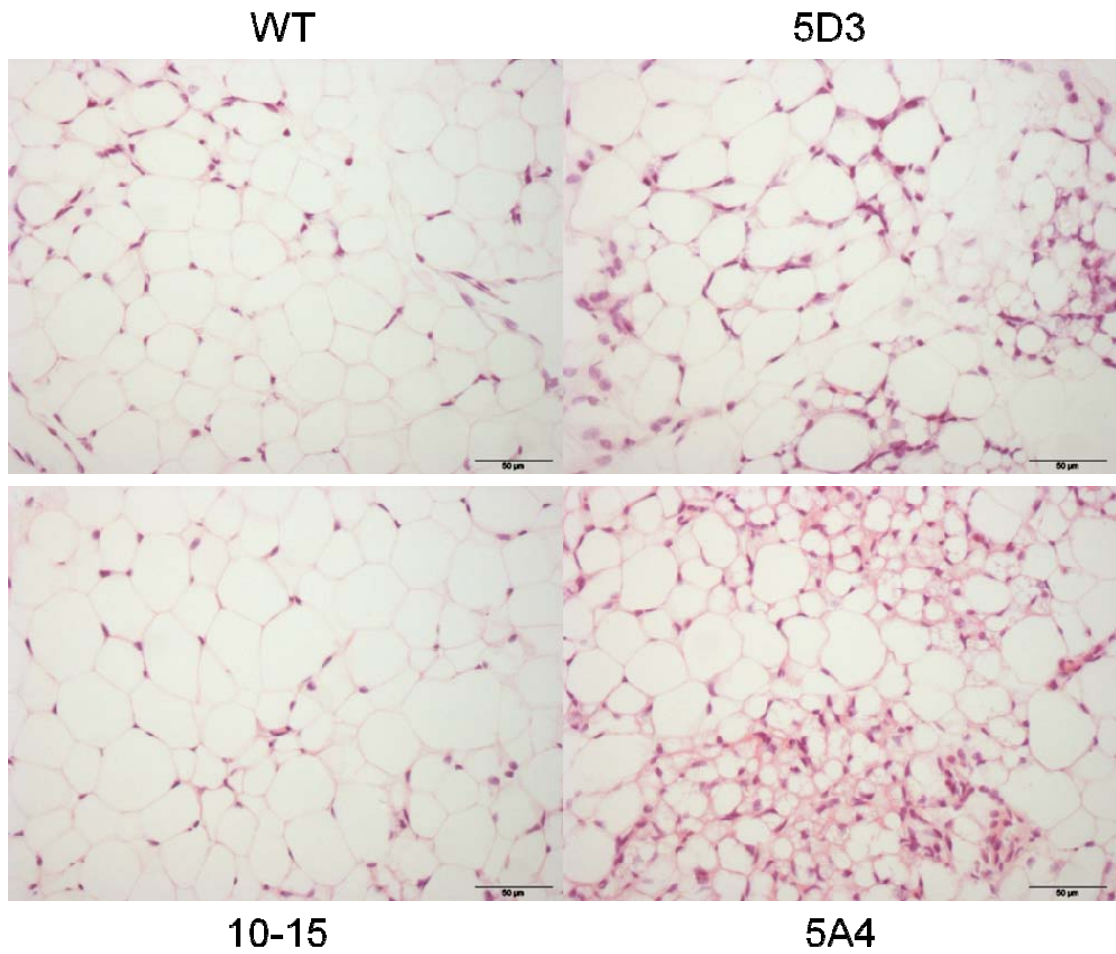


Figure 4.5 H+E staining of transgenic P7 rWAT sections, photographed under standard light microscopy. Wild type and 10-15 sections revealed a uniform tissue comprised of unilocular white adipocytes. 5D3 and 5A4 sections meanwhile presented with both unilocular and multi-locular adipocytes. Scale bar represented 50 µm.

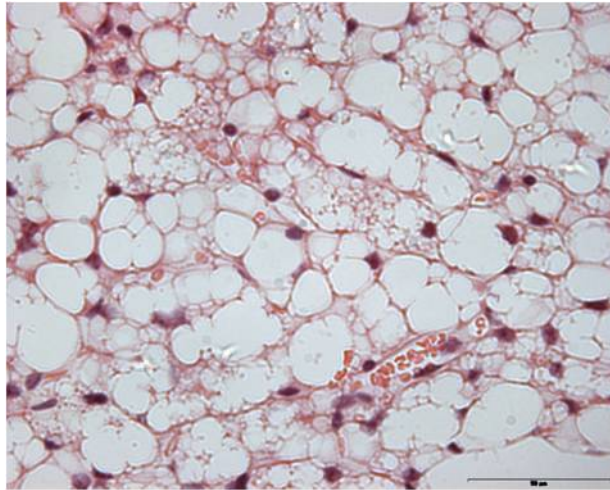


Figure 4.6 High magnification image of 5D3 multi-locular white adipocytes. Almost all cells within the field of view were found to be multi-locular. Wild type and 10-15 samples did not present with such cells. Scale bar represents 50 μm .

To shed further light on the observed differences, transmission electron microscopy was performed on sections from P7 rWAT. This technique allowed resolution of the cells at far higher magnification, clearly displaying any morphological discrepancies. Seen below are adipocytes from wild type and 5D3 P7 rWAT (Fig 4.7). In the wild type image, the membrane of two separate cells can be seen bordering one another. A thin segment of cytosolic region could be observed within each membrane; however the huge majority of the cell volume was occupied by the white unilocular lipid droplet. Near the bottom right of the image, the flattened nucleus of the upper adipocyte could be seen. From the 5D3 image, the multi-locular nature of the lipid stores was clearly resolved, confirming observations from the H+E images under light microscopy. A far larger cytosolic region could also be seen.

Contained within this cytosolic space is the mitochondrial population, seen as the dark organelles. While mitochondria were apparent within both wild type and 5D3 adipocytes (Fig 4.7), they were more abundant in 5D3 adipocytes and this was observed in different sections

from different experimental animals where clusters of these abundant mitochondria was observed.

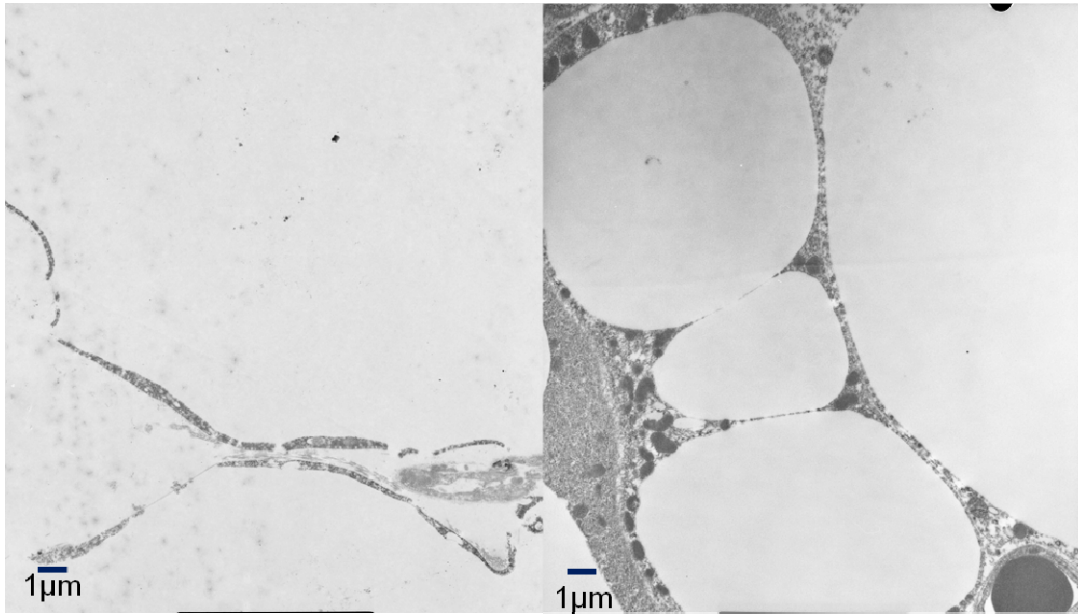


Figure 4.7 TEM images of wild type (left) and 5D3 (right) p.7 white adipocytes from the retroperitoneal adipose pad, imaged at 4000X magnification. Unilocular white adipocytes were observed in the wild type rWAT, while 5D3 adipocytes were found to be multi-locular. Performed by Dr. Anthony Hann.

Induction of thermogenic genes

In the previous experimental chapter, over-expression of *Cdkn1c* resulted in an amplification of the brown adipocyte gene program including increase *Ucp-1* expression. The increased prevalence of brown-adipocyte-like cells in 5D3 rWAT alongside the multi-locular cells and increased mitochondrial content (Fig 4.7) suggested *Cdkn1c* functioned to drive the accumulation of brown adipose in the white adipose depot. To determine whether such an event had taken place, QPCR analysis of thermogenic genes was performed on P7 rWAT obtained from females for the different transgenic lines. Elevated *Ucp-1* expression was detected in 5D3 (10-fold) rWAT, which was further elevated in 5A4 (23-fold). *PGC-1 α* , *Cidea* and *Elovl3* were also expressed more highly in transgenic rWAT than in wild type. Crucially 10-15 rWAT was not found to possess elevated levels of any of the genes analyzed (Fig 4.8). QPCR analysis was performed on subcutaneous white adipose tissue (Fig 4.8-purple) and 5D3 males (supplemental data), where increased expression of the thermogenic programme genes was also present.

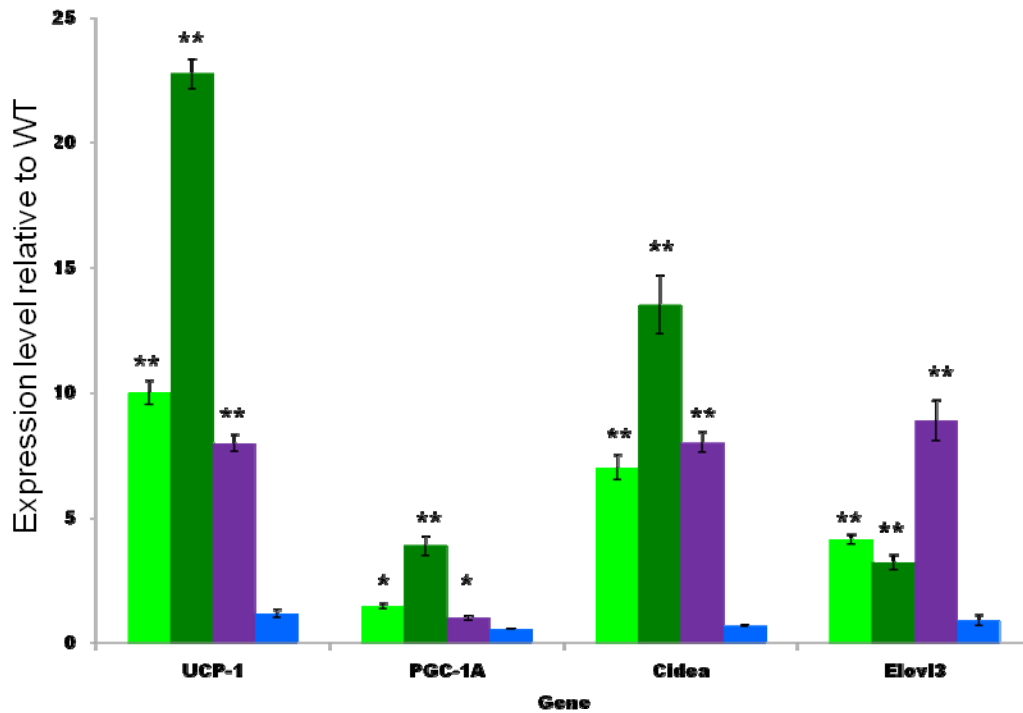


Figure 4.8 QPCR analysis of female transgenic P7 rWAT cDNA. 5D3, 5A4 and 5D3 subcutaneous (purple) were shown to possess an enhanced thermogenic program, which was not the case for 10-15. Amplification of thermogenic genes occurred in a dosage dependent manner. Error bars represent standard error of fold changes. Statistical analysis was performed by Mann Whitney test. * P< 0.05. ** P< 0.01. N=4+4+4+4

Disruption of adipogenic genes

Increased dosage of *Cdkn1c* was found to be associated with increased expression of genes associated with brown adipocytes and an active thermogenic programme, in both iBAT and now rWAT. Further to this, the histology performed on 5D3 rWAT identified regions of cells within the pad that were multi-locular with increased mitochondria (Fig 4.5-7). With this in mind, QPCR analysis of lipid accumulation and mitochondrial genes was performed. All three of *Fsp-27*, *Perilipin* and *aP2* were found to have reduced expression levels in 5D3 rWAT. In addition, *Cytochrome C* and *Cox 2* were both found to be elevated.

This was consistent with the TEM images that appeared to show an increased mitochondrial population in 5D3 white adipocytes.

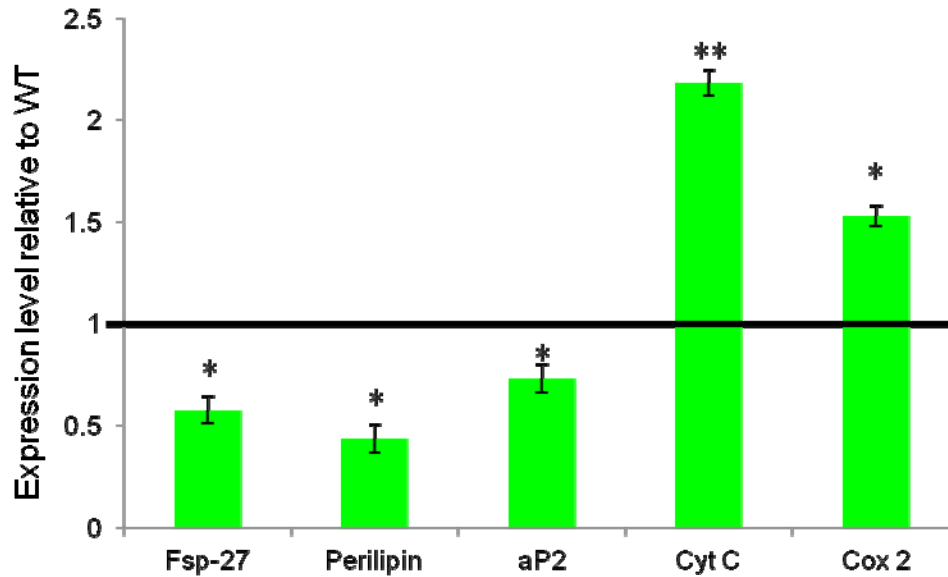


Figure 4.9 QPCR analysis of adipogenic regulators and lipid accumulation genes within 5D3 P7 rWAT cDNA. Lower expression of all three lipid accumulation genes measured was observed. Adipogenic regulators, with the exception of *PPAR γ* whose expression was reduced, were found to possess elevated expression levels. Error bars represent standard error of fold changes. Statistical analysis was performed by Mann Whitney test. * $P < 0.05$. ** $P < 0.01$. $N=4+4$

Next QPCR of adipogenic regulators was performed (Fig 4.10). *pRb* expression was unchanged, however *PPAR γ* was found to be significantly down-regulated. This change was consistent with the reduced expression level of the lipid accumulation genes observed at the same time-point (Fig 4.9), as *PPAR γ* represents the master adipogenic regulator^{203; 204}. *C/ebpa* displayed a modest increase in expression. Brown adipogenic regulators *C/ebp β* , *Prdm16*, *Rip140* and *PPAR α* were all found to be significantly up-regulated in 5D3 P7 rWAT. These increases were largely consistent with a brown adipocyte phenotype.

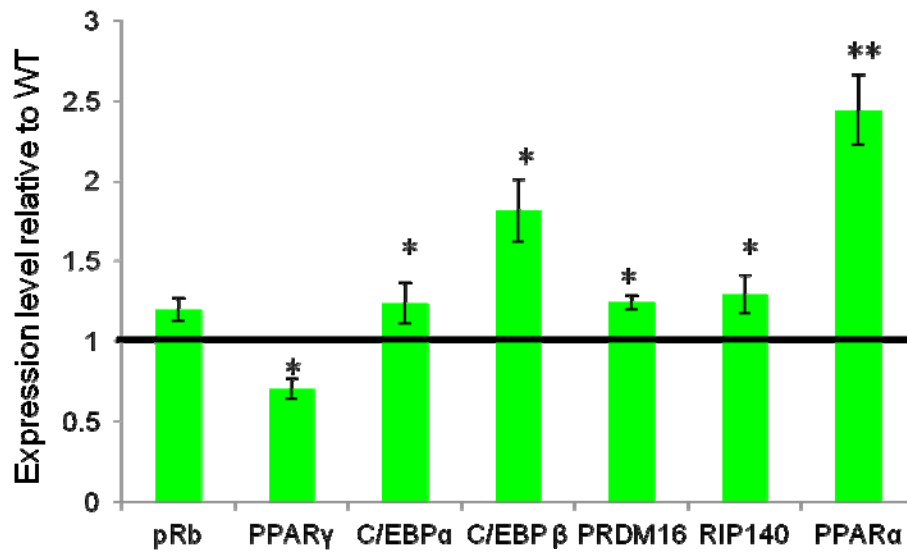


Figure 4.10 QPCR analysis of brown adipogenic and mitochondrial markers, in 5D3 P7 rWAT cDNA. Both sets of genes were found to be increased, compared to wild type levels. Error bars represent standard error of fold changes. Statistical analysis was performed by Mann Whitney test. * $P < 0.05$. ** $P < 0.01$. $N=4+4$

Cdkn1c acts through C/ebp β and Prdm16

Due to the amplification of the thermogenic programme, and as had been the case for the iBAT studies, exploration of C/ebp β (Fig 4.11) and Prdm16 (Fig 4.12) protein levels was performed. Total C/ebp β levels in the 5D3 rWAT were consistent with the QPCR data (Fig 4.10). Levels of phosphorylated protein were unchanged from those in the wild type (Fig 4.11).

Prdm16 has previously been shown to not be detectable at the protein level through Western blotting in mouse visceral adipose tissue²⁰⁵. This was confirmed in P7 wild type rWAT (Fig 4.12), in both male and female depots. In addition, Western blotting for Ucp-1 was performed, with no detectable protein in the male sample, while trace amounts were

observed in the female white adipose tissue (Fig 4.12). 5D3 male and female mice differ from the wild type, in that both Prdm16 and Ucp-1 proteins were detectable in male and female rWAT.

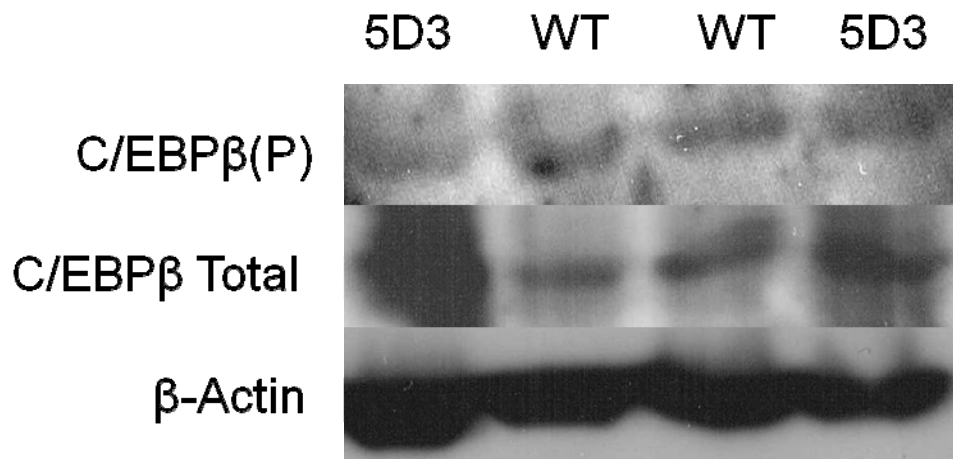


Figure 4.11 Western blotting for C/ebpβ protein in 5D3 p.7 rWAT lysates. Levels of phosphorylated C/ebpβ were not seen to be altered in transgenic samples from wild type. Greater detection of total C/ebpβ however were observed in the tissue Sample amounts were normalised through β-Actin control.

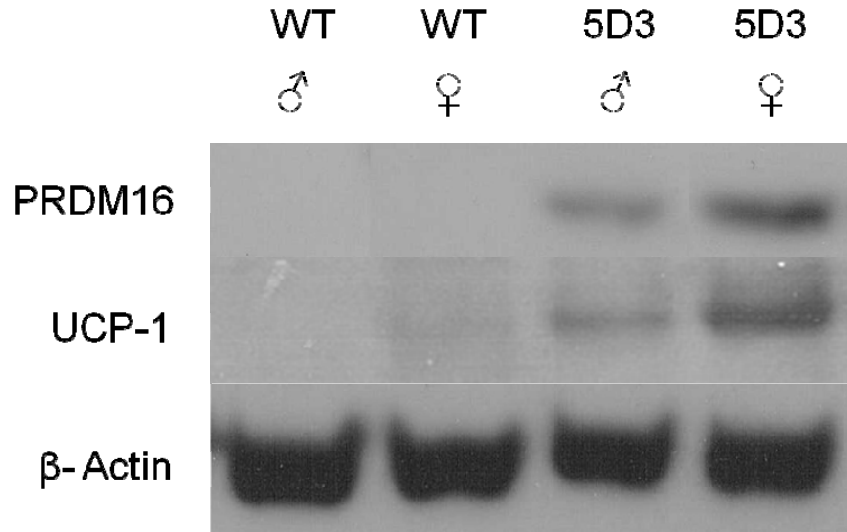


Figure 4.12 Western blot for Prdm16 and Ucp-1 proteins in 5D3 P7 rWAT lysates. Prdm16 and Ucp-1 protein were detected in both male and female 5D3 samples, and were largely absent from the wild type lanes, although trace amounts of Ucp-1 were found in the female wild type sample. Sample amounts were normalised through β -Actin control.

Results presented thus far implicated a role for *Cdkn1c* in the enhancement of a brown adipose phenotype in both the classic brown depot and also within the white adipose tissue. However, the BAC transgene drives expression of *Cdkn1c* at other sites including the hypothalamus, the adrenal gland, the pancreas and the pituitary gland¹⁰⁶, all known to play a role in regulating metabolism. As a result, ex vivo studies were performed in order to ask whether the amplification of the brown adipose gene program was due to the intrinsic action of *Cdkn1c* within adipose or due to expression elsewhere. Mouse embryonic fibroblasts (MEFs) from E12.5 embryos when exposed to a cocktail of hormones are forced to differentiate down the adipocyte lineage, towards a white adipose phenotype (reviewed¹³³). Thus by examining MEFs from the transgenic lines, the results obtained could be exclusively attributed to altered dosage of *Cdkn1c* in the adipocytes. In addition, this technique presented the opportunity to study the consequences of loss of expression of *Cdkn1c* on adipocyte differentiation *in vitro*.

Ex-vivo: Mouse Embryonic Fibroblast (MEF) culture to adipocytes

As a means of determining whether the phenotype was intrinsic to adipose, MEFs were isolated from wild type, 5D3, *Cdkn1c*^{-m/+p} and 5D3/*Cdkn1c*^{-m/+p} (double transgenic = 'rescue') E12.5 embryos obtained by crossing a 5D3 male with a *Cdkn1c*^{+m/-p} male, and subjected to the differentiation protocol. After 8 days being subjected to differentiation media, cells were fixed and stained with Oil Red O. As can be observed below, all genotypes studied underwent differentiation to adipose-like cell, demonstrated by the accumulation of lipid in each sample (Fig 4.13).

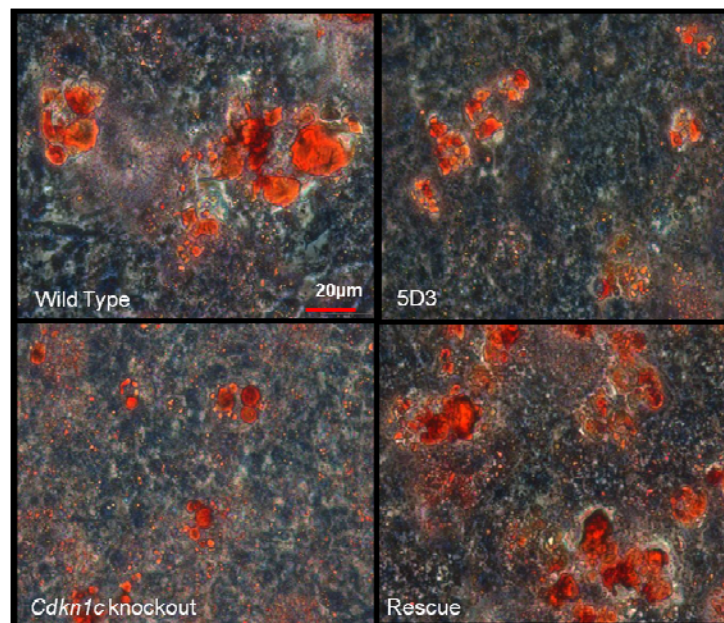


Figure 4.13 Oil Red O stained day 8 MEF induced-adipocytes. MEFs from wild type, 5D3, *Cdkn1c* knockout and Rescue all differentiated into mature adipocytes. Undifferentiated MEFs appeared blue from haematoxylin staining.

Further light microscopic analysis of the MEFs was performed through the use of confocal microscopy. Day 8 culture plates were stained using Rhodamine-123 (Sigma), a mitochondrial stain, with individual mitochondria were seen as a lighter green colour compared to the darker green non-specific binding. HCS CellMask Red (Invitrogen), a cell membrane stain, and Hoechst 33342 (Invitrogen) were also used. In all three genotypes studied, unstained lipid globules (black) were observed in the cytosol. Regarding mitochondrial staining, no marked differences were observed between the wild type and *Cdkn1c^{m/+p}* images in mitochondrial staining whereas there appeared to contain more mitochondria in 5D3 MEFs. Higher magnification images of the 5D3 MEFs confirmed that the signal of Rhodamine-123 was associated with mitochondria (Fig 4.14). These mitochondria were so large that, in some cases, the two sides of the mitochondrial membrane surrounding the matrix were observable. It was not possible to find similar large Rhodamine-123 staining organelles in the wild type or the *Cdkn1c^{+m/p}* cells. This suggested that mitochondria were both more frequent and much larger in 5D3 cells. This was consistent with the observations made by EM (Fig 4.7).

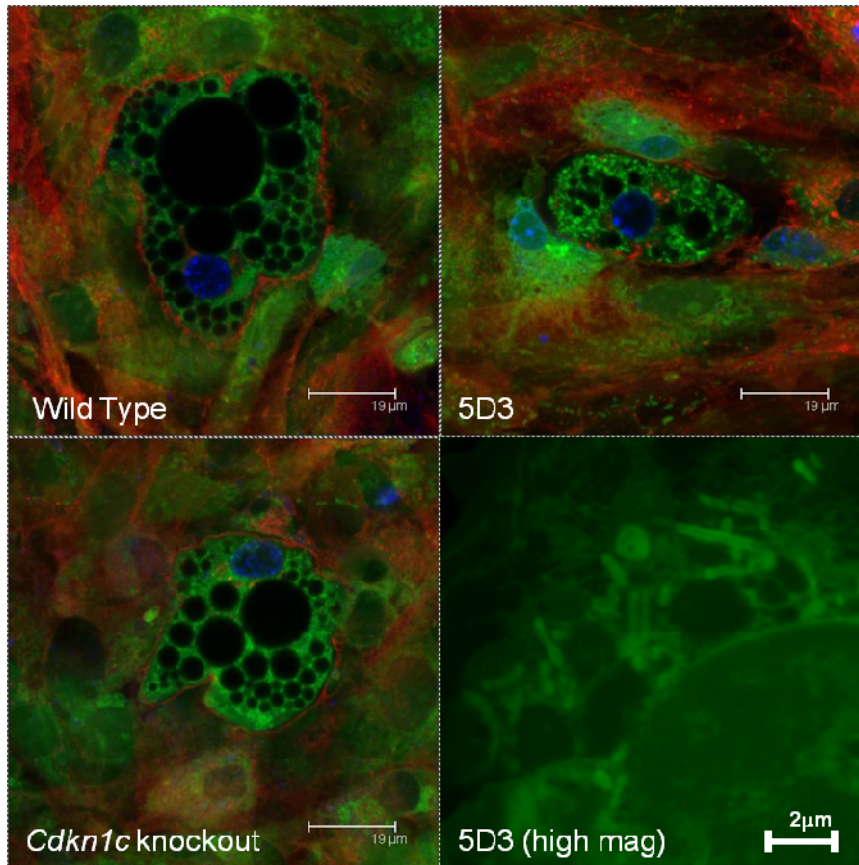


Figure 4.14 Confocal microscopy of day 8 MEF- induced adipocytes. Individual adipocytes were imaged in wild type, 5D3 and *Cdkn1c*-m/+p cultures. Lipid droplets were not stained and so appear black. Mitochondrial population (Rhodamine-123, Sigma) was stained green and detectable in all genotypes. Higher magnification imaging of mitochondria within 5D3 adipocytes enabled the resolution of the mitochondrial matrix, which was not possible in the other genotypes. Nuclei can be seen in blue (Hoechst 33342, Invitrogen) while cell membrane was stained red (HCS CellMask Red, Invitrogen).

Next QPCR analysis of differentiating MEFs was performed. By including the ‘rescue’ genotype in which both the single copy transgene and a targeted deletion of the endogenous maternal allele were present, any changes in 5D3 adipocyte gene expression could be attributed to endogenous *Cdkn1c* expression by comparing data from these ‘rescue’ MEFs with the single transgenic MEFs and wild type MEFs. Expression of *Cdkn1c* was examined in these samples, and also in wild type and 5A4 differentiated MEFs. 5D3 MEFs

over-expressed *Cdkn1c* at day 8 of differentiation at levels similar to that observed in vivo (1.33-fold wild type \pm 0.14 P=0.029).

An expression profile for *Cdkn1c* during the eight days of differentiation was generated for wild type MEFs. *Cdkn1c* was rapidly induced upon differentiation, with day 2 and day 4 represent peak expression levels, both around forty five-fold higher than the day 0 levels. Expression was decreased by day 8 but was still significantly higher than in confluent, undifferentiated MEFs (Fig 4.15).

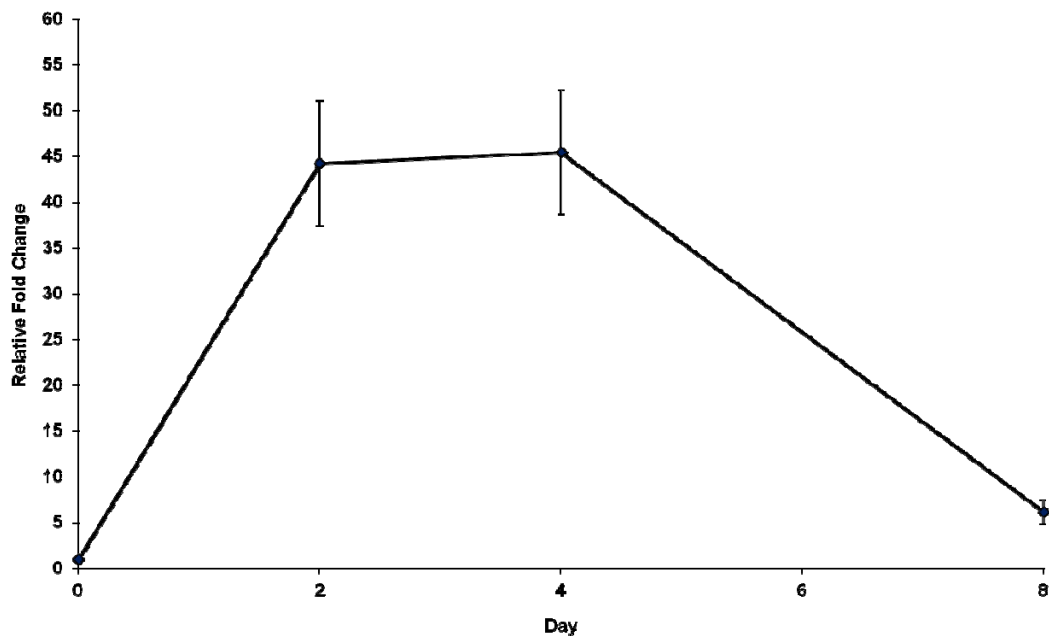


Figure 4.15 Expression profile of *Cdkn1c* during wild type MEF differentiation. Fold changes were determined with respect to expression level at day 0. Error bars represent standard error of fold changes. N=4+4+4+4

Analysis of the expression of the four key genes associated with brown adipogenesis was performed. As seen in the graph, *Ucp-1* levels in 5D3 MEFs at day 8 were elevated compared to those of wild type. *PGC-1 α* , *Cidea* and *Elovl3* were also elevated. A dosage dependent phenotype, as previously noted in vivo (Fig 4.8), was also found in 5A4 MEFs at

day 8. When the ‘rescue’ MEFs (red) were analysed, gene expression was similar to wild type thus assigning these changes to elevated *Cdkn1c* and excluding a role for other genes on the BAC or a site of integration effect (Fig 4.16). *Cdkn1c*^{-m/+p} MEFs, although demonstrating a varied range of expression for thermogenic genes, were not found to possess increased *Ucp-1* mRNA levels.

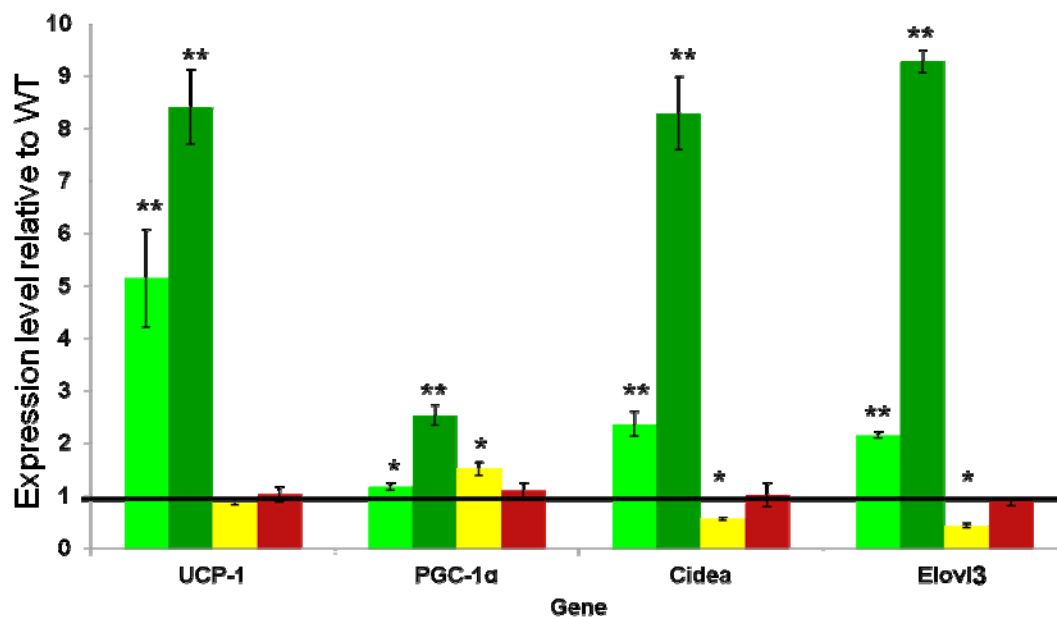


Figure 4.16 QPCR analysis of thermogenic program genes in transgenic day 8 differentiated MEFs. Genes were elevated in a dosage dependent manner in 5D3 and 5A4 MEFs, while *Cdkn1c*^{+m/p} samples displayed reduced expression of some genes. This was rescued by the presence of the BAC (red). Error bars represent standard error of fold changes. Statistical analysis was performed by Mann Whitney test. * P< 0.05. ** P< 0.01. N=4+4+4+4

The induction of the thermogenic gene programme in the presence of excess *Cdkn1c* was confirmed in MEFs through Western blotting. *Ucp-1* was detectable in 5D3 MEFs, but not in wild type (Fig 4.19). The level of amplification of the four genes analysed by QPCR was consistent with those seen in vivo (Fig 4.8). Next, QPCR analysis of lipid

accumulation and mitochondrial genes was performed on 5D3 and *Cdkn1c*^{-m/+p} day 8 MEFs. These genes had been studied *in vivo*, and therefore it was important to confirm if an overlapping pattern of expression was observed. Both 5D3 and *Cdkn1c*^{-m/+p} MEFs displayed significant down-regulation of lipid accumulation genes. For 5D3 MEFs, this pattern of expression was similar to that observed *in vivo* data for these three genes (Fig 4.9). Meanwhile increased expression of mitochondrial genes was detected in 5D3 MEFs, while decreased expression was found in *Cdkn1c*^{-m/+p} MEFs (Fig 4.17).

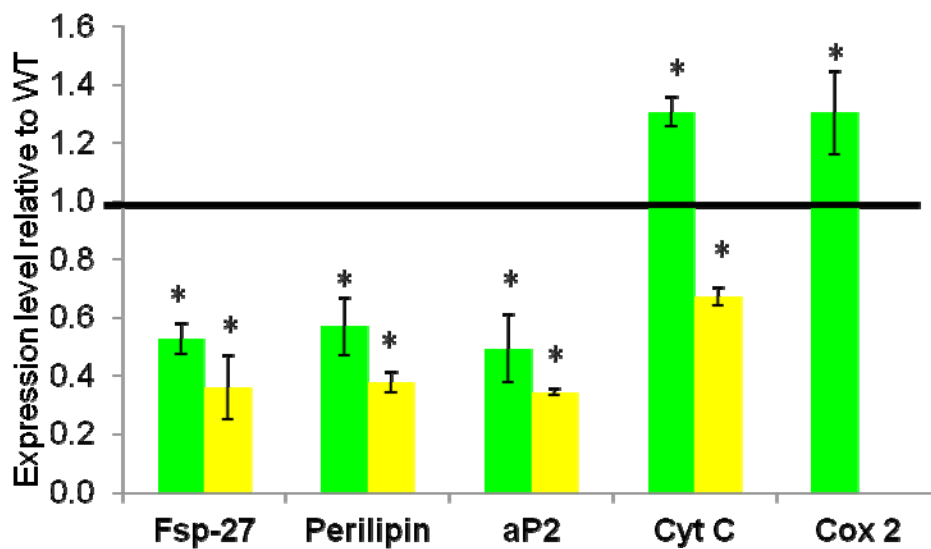


Figure 4.17 QPCR analysis of lipid accumulation and mitochondrial genes in transgenic day 8 differentiated MEFs. Expression of lipid accumulation genes was impaired in both 5D3 and *Cdkn1c*^{-m/+p} MEFs. 5D3 mitochondrial genes were elevated, while *Cdkn1c*^{-m/+p} were reduced in expression level. Error bars represent standard error of fold changes. Statistical analysis was performed by Mann Whitney test. * P< 0.05. N=4+4

To complete the QPCR analysis of these MEFs, adipogenic regulators were studied, with the same genes targeted as was done for in vivo. 5D3 MEFs displayed significant down-regulation of the adipogenic regulators *PPAR γ* and *C/ebpa*, but not *pRb*. The brown adipogenic regulators *C/ebp β* and *Prdm16* were both elevated. In contrast, *Cdkn1c^{m/+p}* MEFs were not found to possess altered expression of *pRb*, *C/ebp β* or *Prdm16*. However *PPAR γ* was down-regulated while *C/ebpa* was elevated (Fig 4.18).

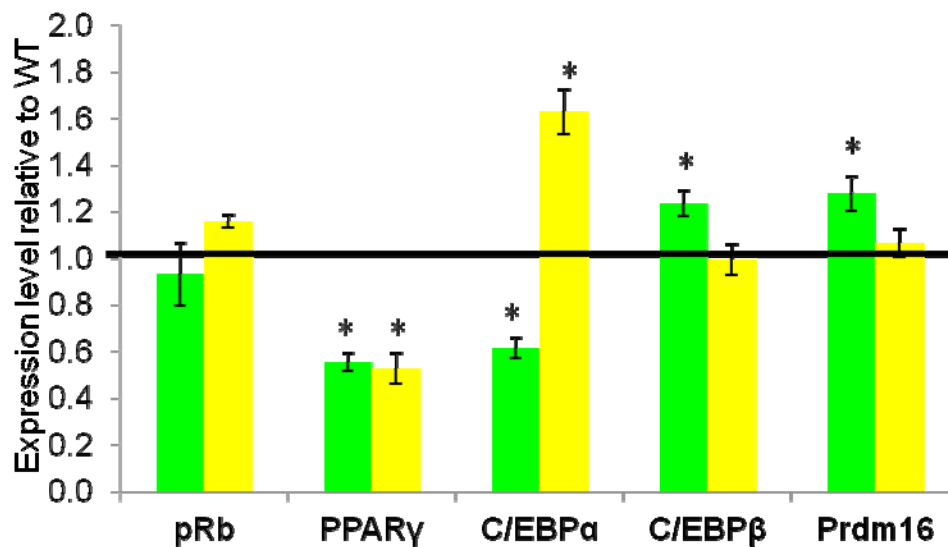


Figure 4.18 QPCR analysis of adipogenic and brown adipogenic genes in transgenic day 8 differentiated MEFs. Restricted expression of 5D3 adipogenic genes was found, while brown adipogenic genes were elevated. No amplification of brown adipogenic genes was detected in *Cdkn1c^{m/+p}* MEFs, while correct expression of adipogenic genes was disrupted. Error bars represent standard error of fold changes. Statistical analysis was performed by Mann Whitney test. * $P < 0.05$.

N=4+4

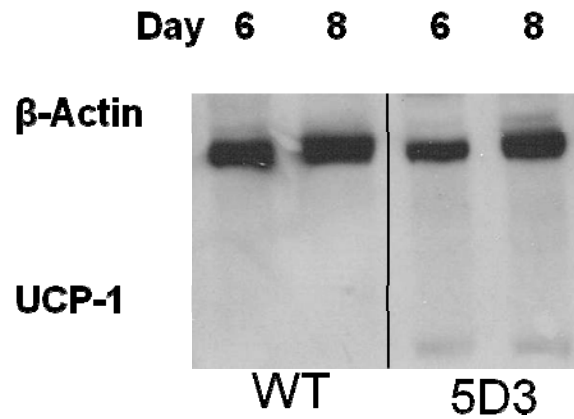


Figure 4.19 Western blotting of Ucp-1 in differentiating MEF plates. Protein could be detected at low levels in 5D3 samples, where it was not seen in wild type. Sample amounts were normalised through β -Actin control.

Regarding an in vivo versus ex vivo comparison, the data set of fold changes were graphed together to provide a direct comparison (Figure 4.20), with 5D3 in vivo represented by the greens columns 5D3 ex vivo represented by the blue columns, 5D3 P7 iBAT represented by brown columns and *Cdkn1c*^{-m/+p} iBAT represented by yellow columns. The fold changes represent original comparisons to the respective wild type data, and were otherwise unchanged. Statistical analysis was not performed as the groups are distinct from one another. A relatively high degree of similarity was seen between the 5D3 iBAT, rWAT and MEF expression levels was observed, while little obvious pattern was observed in the *Cdkn1c*^{-m/+p} iBAT.

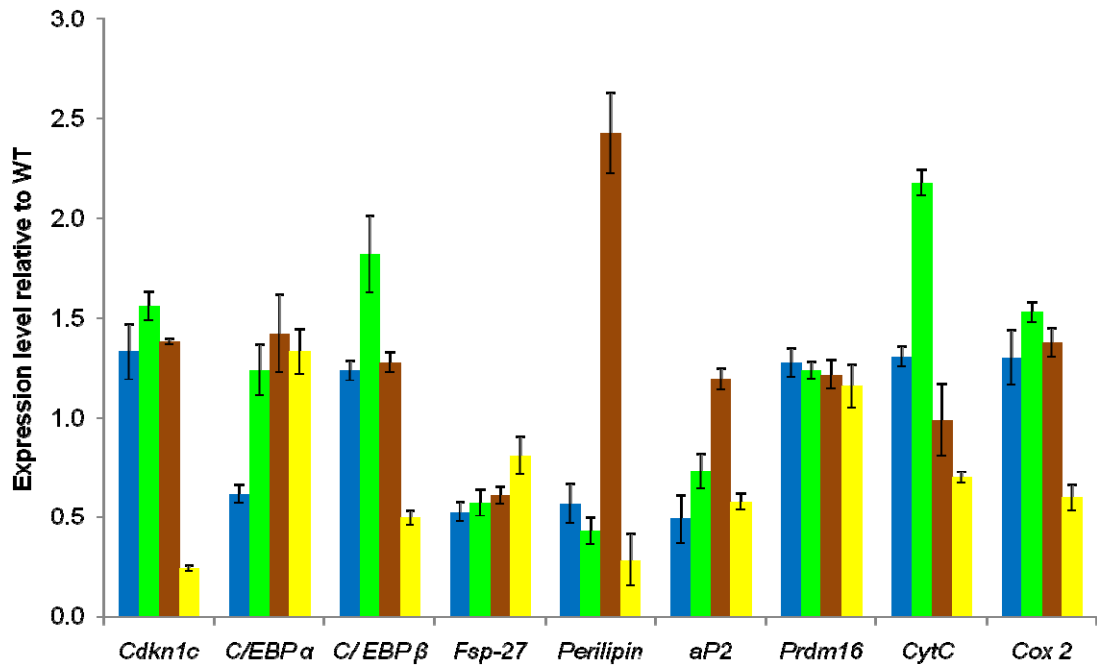


Figure 4.20 Comparison of 5D3 day 8 differentiating MEFs (blue), 5D3 P7 rWAT (green), 5D3 P7 iBAT (brown) and *Cdkn1c*^{-m/+p} iBAT (yellow) expression of adipogenic genes. Expression levels represent expression; in comparison to their respective wild type. Error bars represent standard error of calculated fold changes. No statistical analysis was performed.

A final experiment for the 5D3 MEF culture was performed to explore the inducibility of the system, with regards to Ucp-1. Adipocytes differentiated from MEFs have previously been shown to be sensitive to retinoic acid, and upon treatment, express Ucp-1²⁰⁶ because *retinoic acid* is a positive regulator of *Ucp-1* gene transcription^{207; 208}. *QPCR* analysis of the Retinoic Acid (RAR's) and Retinoic X (RXR's) receptors at day 8 of differentiation had shown a significant increase in all six receptors in 5D3 adipocytes (Fig 4.21). D8 differentiated MEFs were therefore subjected to 0.1 μM retinoic acid treatment for 48 hours, before cells were harvested. Western blot analysis of these time points clearly showed induction of Ucp-1 in both wild type and 5D3 MEFs, as was expected. 5D3 MEFs

however, displayed a greater signal of the protein than the wild type cells after 48hr treatment (Fig 4.22).

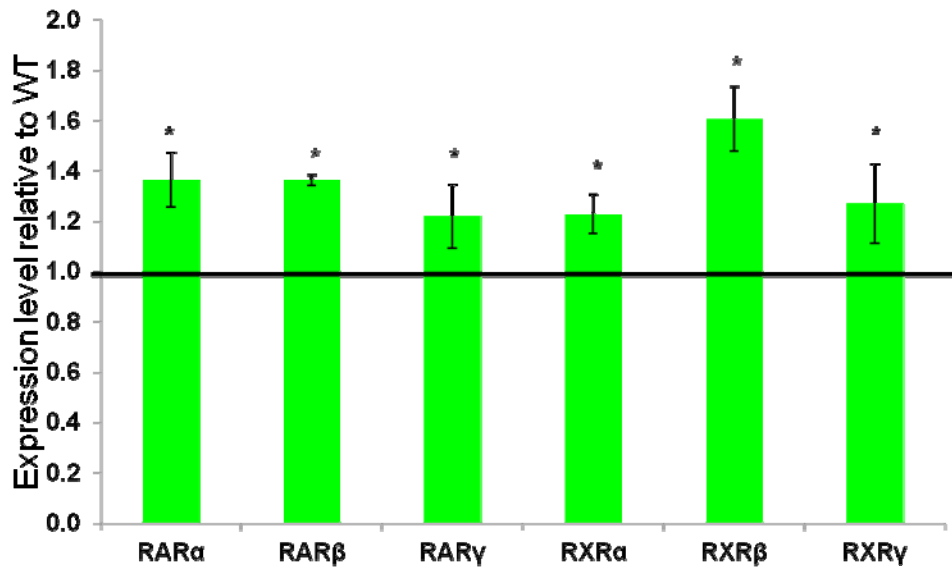


Figure 4.21 Relative expression levels of Retinoic Acid (RAR) and Retinoid X (RXR) receptors in 5D3 day 8 differentiating MEFs. All were found to be significantly up regulated at this time. Error bars represent standard error of calculated fold changes. Statistical analysis was performed by Mann Whitney test. * $P < 0.05$. $N = 4+4$

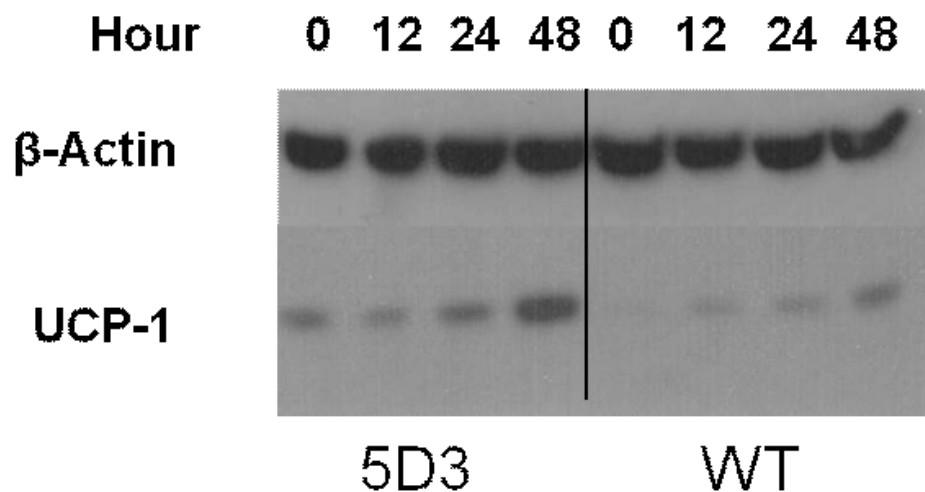


Figure 4.22 Western blot of Ucp-1 expression in day 8 MEFs subjected to 0.1 μ M Retinoic acid treatment for the given time periods. Ucp-1 was found to be induced in both genotypes, with a stronger detection at all time points in 5D3 samples. Sample amounts were normalised through β -Actin control.

Discussion

The *ex vivo* system for differentiating MEFs into adipocytes was extremely important for these studies, as they presented a system for studying the intrinsic effects of altering *Cdkn1c* dosage during adipogenesis. 5D3 MEFs at day 8 of differentiation were found to display a phenotype similar to that seen *in vivo* in rWAT (Fig 4.21), including detectable induction of Ucp-1 protein (Fig 4.19). *In vivo* Western blot analysis showed increased Prdm16 protein in response to the elevated *Cdkn1c* dose, which was consistent with the induction of thermogenic genes. Although similar downstream changes in gene expression were apparent in the differentiated MEFs, Prdm16 protein was not detectable by Western (data not shown). Ucp-1 protein was only weakly detectable in D8 5D3 MEFs in contrast to the high level in 5D3 rWAT. It seemed likely that the Western blot was insufficiently sensitive to detect Prdm16 protein.

The gene expression changes observed in the *in vivo* studies were similar to those obtained utilising 5D3 and 5A4 MEFs. While this work does not exclude a contribution of other sites of transgenic expression to the *in vivo* phenotypes described in chapter 3 and this chapter, this work did identify an intrinsic role for *Cdkn1c* in inducing brown adipogenesis. It should be noted however that although this protocol drives differentiation towards a white adipocyte phenotype, fibroblasts are a *Myf5*⁺ cell type. Normal white adipocytes are *Myf5*⁻ ¹⁵⁶, while brown adipocytes are *Myf5*⁺ ²⁰⁵, highlighting the limitations of this technique. Given the results presented in the previous chapter, where loss of *Cdkn1c* expression was shown to heavily impair the formation of brown adipocytes, the poor differentiation of MEFs in the absence of *Cdkn1c* cannot conclusively be stated as exclusively a white adipocyte phenotype.

The *in vivo* data demonstrated a role for *Cdkn1c* within the white adipose depot. As had been the case in the iBAT, there was over-expression of genes in the 5D3 and 5A4 lines and an increase in Prdm16 protein consistent with augmentation of the thermogenic programme (Fig 4.8). Prdm16 has also previously been shown to suppress the white adipocyte

phenotype, through binding partners CtBP1 and 2¹⁵⁵, consistent with the data generated for 5D3 and 5A4 white adipose tissue, where expression of lipid accumulation genes and adipogenic markers were altered (Fig 4.9-10). Therefore it is possible that *Cdkn1c* may exclusively function in brown adipocytes purely by augmenting Prdm16 levels, thereby enhancing the brown adipocyte phenotype. However, Cdkn1c is a multifunctional protein and alterations in the timing of cell cycle exit, for example, may also account for some of the changes observed.

The MEF system also allowed insight into the consequences of loss of expression of *Cdkn1c* on adipogenesis. Although the *Cdkn1c*^{-m/+p} MEFs did differentiate (Fig 4.13-14), the appearance of the cells, coupled with the QPCR data (Fig 4.16-18) suggested that this did not occur as normal and that adipogenesis was impaired. Reduced *PPAR γ* (Fig 4.18) expression could account for the impaired adipogenesis.

Prdm16 and Cdkn1c were found in the previous chapter to be co-expressed in the nucleus of a rare cell type within iBAT. In addition, Cdkn1c was also found to mark a separate population of cells, which did not co-express Prdm16 (Fig 3.24-25). Comparable immuno-histochemistry was not performed in the white adipocytes. However, the *in situ* hybridisation for *Cdkn1c* (Fig 4.1) also produced a restricted pattern of expression, as seen in iBAT (Fig 3.17). This sub-population of cells could be the iBAT progenitor population. The question arising from the rWAT *in situ* therefore is if *Cdkn1c* is marking the same population. It is now believed that populations of brown adipocyte-like cells exist within the white adipose depots (reviewed¹²⁵). Given the expression pattern seen in the rWAT and the data in this chapter showing an increase in brown adipose-like cells within rWAT, it is possible that *Cdkn1c* may be marking an iBAT progenitor population in WAT. One intriguing possibility is that, in addition to role in driving accumulation of Prdm16 protein and thus attenuating the brown fat gene program, elevated Cdkn1c also increases the number of iBAT progenitors in both iBAT, accounting for the increase mass and cellularity of this tissue, and in rWAT accounting for the presence of patches of BAT-like cells within the rWAT depot and

increased expression of the iBAT markers. Future studies using the transgenic models will be useful in testing this hypothesis.

An increase in thermogenically active brown adipose is associated with obesity resistance^{164; 209; 210; 211}. Given that both the 5D3 and the 5A4 mice showed indications of increased brown fat, the next step was to ask whether these mice were resistant to either age-induced or diet induced obesity.

Chapter 5: Consequences of over-expression of

Cdkn1c

Weight gain in *Cdkn1c* BAC transgenic mice.

The experiments described in Chapters 3 and 4 identified *Cdkn1c* as a novel regulator of both the classic brown adipose lineage and the non classic adipose lineage found within white adipose deposits. The data obtained was consistent with *Cdkn1c* enhancing the brown-phenotype in both lineages at least in part through the stabilisation of Prdm16 protein. The interscapular brown adipose pad was found to be greater in mass with a higher cellularity in response to elevated *Cdkn1c*, alongside an enhanced thermogenic programme, while white adipose depots were found to contain a greater proportion of brown-like adipose. An increased proportion of thermogenically active brown adipose would be predicted to provide protection against obesity. In this chapter, an investigation of weight gain and glucose management was made in the context of both aging and a high fat diet in the over expression models.

Fat pad mass in *Cdkn1c* BAC transgenic mice at 10 weeks of age maintained on a standard chow diet

For the analysis, cohorts of mice from line 5D3 and line 5A4 were generated and maintained on a standard chow diet for 10 weeks. In previous work, transgenic mice from both these lines displayed a degree of post natal growth restriction on a mixed 129/BL6 genetic background¹⁰⁷. Similar results were obtained when the weights of male and female transgenic mice was compared with wild type littermates on the ‘pure’ (>8 generations) BL6 background (Table 2). 5D3 males were approximately 14% lighter than wild type males while 5A4 males were 18% lighter. 5D3 females were 14% lighter than wild type females and 5A4 females were 20% lighter.

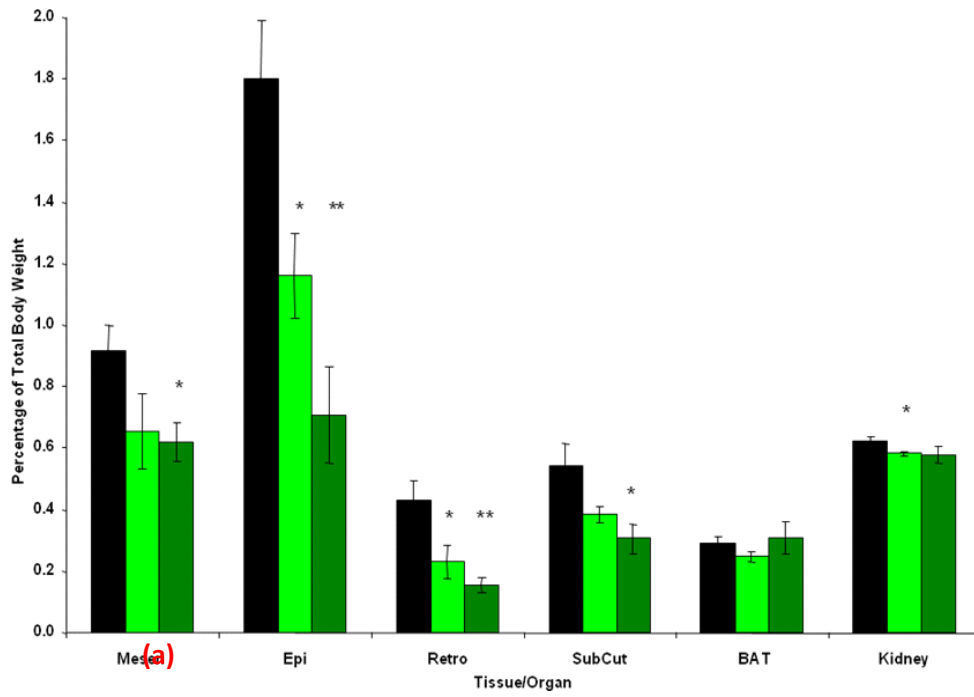
Male		WT	5D3	5A4
	Weight (g)	30.601	26.400	25.160
	St. Error	0.510	1.04	0.340
	P. Value		4.6*10 ⁻³	1.6*10 ⁻⁵
	N	8	8	6
Female				
	Weight (g)	23.250	20.450	18.570
	St. Error	0.350	0.390	0.750
	P. Value		1.8*10 ⁻³	1*10 ⁻⁵
	N	8	7	7

Table 2 Total body weights of 10 week old mice, housed under standard conditions. Statistical analysis was performed by Student's t-test.

On dissection of the 10 week old female mice, the weights of the kidney and iBAT were found to be a similar proportion of total body weight for both lines, although 5D3 kidneys were found to be significantly lighter than wild type. A comparable pattern was observed in the male transgenic lines (Fig 5.1). Results at P7 had demonstrated 5D3 and 5A4 mice to possess significantly larger iBAT than wild type (Fig 3.14), a result that was not replicated at 10 weeks of age (Fig 5.1 (b)). H+E staining of 10 weeks brown adipose depots revealed a lower lipid burden in 5D3 female iBAT (Fig 5.2) which could account for the reduced overall mass of the iBAT at 10 weeks.

On examination of the weight of the white adipose depots, female 5D3 mice had an overall reduction in total visceral weights of 37.1 % (\pm 4.38 %). Although statistically only the mesenteric white adipose depot was found to be significantly lighter in 5D3 females, all the other depots weighed showed a reduction in weight. In the case of line 5A4, the combined visceral adipose depots were 48.4 % (\pm 8.44 %) lighter than wild type and the reduction in weights of each depot with respect to wild type was significant, suggesting a dosage dependent reduction in white fat mass. Similarly 5D3 and 5A4 males were found to possess comparably lighter visceral adipose depots than wild type (Fig 5.1(a)). In contrast to the visceral depots, the subcutaneous white adipose tissue was not found to be significantly lighter in 5D3 or 5A4 females compared to wild type. A modest restriction was observed in

5A4 males compared to wild type, but not in 5D3.



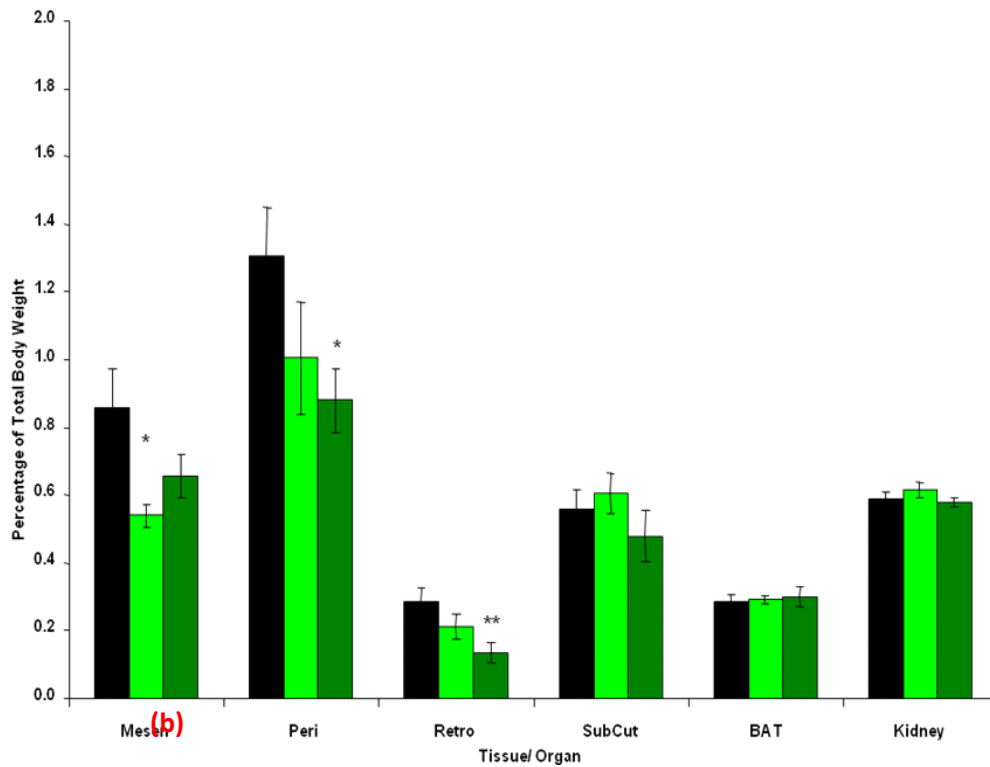


Figure 5.1 (a: males) (b: females): Wet weight of adipose pads at 10 weeks of age, presented as a percentage of total body weight. Reduced weight of white adipose pads were observed in both the 5D3 and 5A4 lines in both males and females. Brown adipose tissue and kidney weights were not found to be altered in either 5D3 or 5A4. Statistical analysis was performed by Student's t-test. * $P < 0.05$. ** $P < 0.01$ $N = 9 + 9 + 8$ (for each gender)

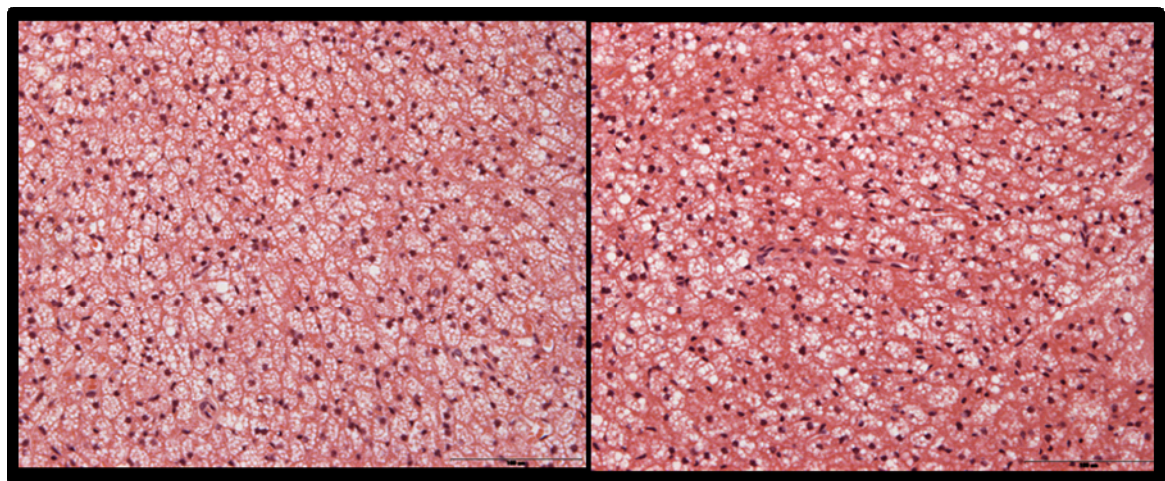


Figure 5.2 H+E staining of 10 week old 5D3 (right) and wild type (left) iBAT. 5D3 iBAT appeared darker in colour. Scale bar represents $100\mu\text{m}$.

Induction of thermogenic genes

In the previous experimental chapters, increased dosage of *Cdkn1c* had been shown to enhance the brown adipogenesis. In particular, the effect of this change in dosage was the induction of the mitochondrial uncoupling thermogenic gene programme. At P7, *Ucp-1* mRNA was found to be expressed 10-fold higher in 5D3 female rWAT than wild type and Ucp-1 protein was readily detectable by Western blot (Fig 4.8, 4.12). To ask whether the induction of the thermogenic gene program identified at P7 was maintained into adulthood, QPCR was performed on cDNA prepared from rWAT isolated from 10 week old transgenic and wild type females from line 5D3. Firstly, QPCR was used to confirm that elevation in *Cdkn1c* expression was maintained until at least 10 weeks (Fig 5.4). *Ucp-1*, *PGC-1 α* , *Cidea* and *Elovl 3* were all found to be more highly expressed in the 10 week old transgenic samples, and the degree of difference was greater than seen at P7 (Fig 4.8). QPCR analysis of the same key thermogenic genes was also performed on males (Table 3). An even greater increase in the expression of *Ucp-1* was found in 5D3 male mice. The other remaining thermogenic genes analysed, *PGC-1 α* , *Cidea* and *Elovl3*, were also elevated in 5D3 males. In addition to the thermogenic genes, QPCR analysis was performed for *C/ebp β* and *Prdm16* in female rWAT from line 5D3. Both *C/ebp β* and *Prdm16* were found to be elevated in the presence of higher *Cdkn1c* dose (Fig 5.4).

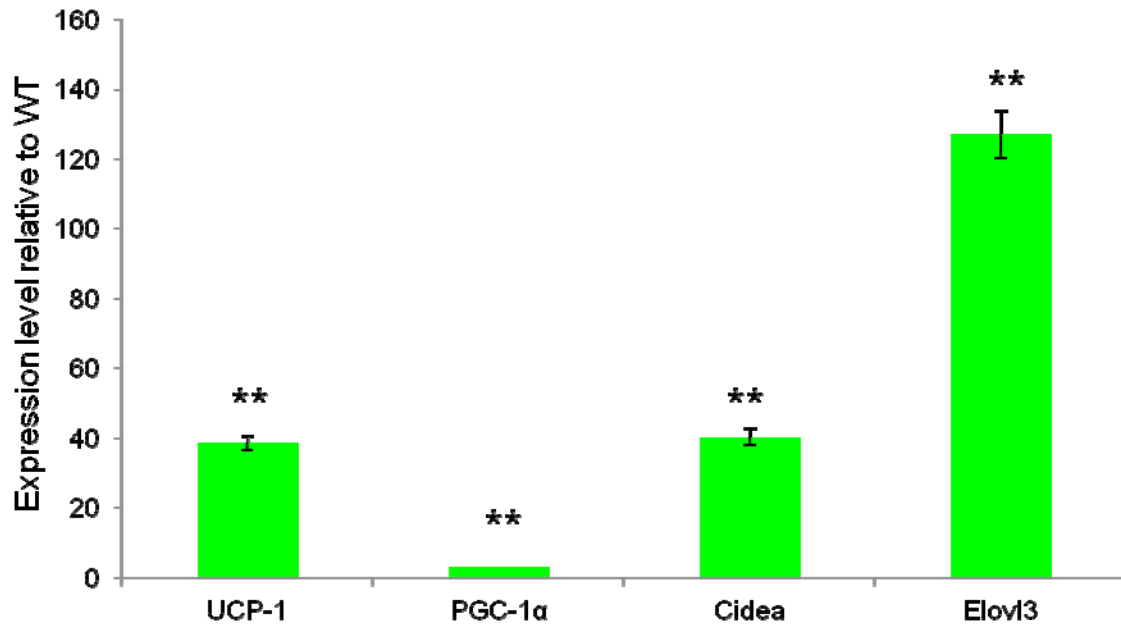


Figure 5.3 QPCR analysis of selected thermogenic program genes in 5D3 female 10 week rWAT. All genes analysed were found to be highly induced in the presence of excess *Cdkn1c*. Error bars represent standard error of fold changes. Statistical analysis was performed by Mann Whitney test. ** P<0.01. N=4+4.

Gene	<i>Cdkn1c</i>	<i>Ucp-1</i>	<i>PGC-1α</i>	<i>Cidea</i>	<i>Elovl3</i>
Av. Fold Change	1.47	159.79	2.17	6.00	45.30
St.Error	0.08	7.62	0.30	0.68	8.97
P.value	0.029	0.008	0.008	0.008	0.008

Table 3 Fold changes in male 5D3 10 week retroperitoneal white adipose tissue of thermogenic program genes. Large induction of thermogenic program had also occurred in male 5D3 mice, as was seen in females. Error bars represent standard error of fold changes. Statistical analysis was performed by Mann Whitney test. N=4+4.

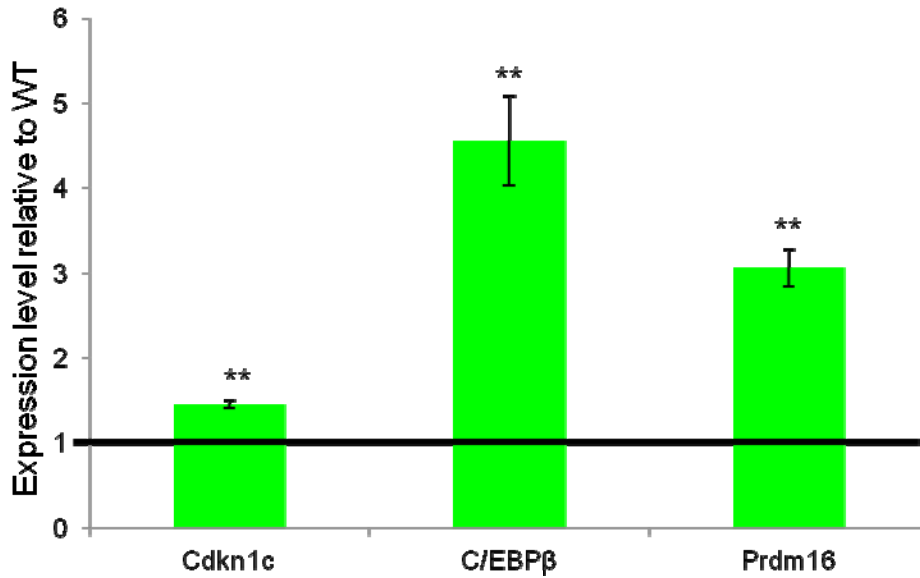


Figure 5.4 QPCR analysis of selected brown adipogenic genes in 5D3 female 10 week rWAT. Excess *Cdkn1c* increased the expression of both *C/ebpβ* and *Prdm16*. Error bars represent standard error of fold changes. Statistical analysis was performed by Mann Whitney test. ** P<0.01. N=4+4.

Elevated core body temperature.

Increased thermogenesis would be predicted to result in an elevation in body temperature as a consequence of greater heat production. Therefore a measurement of rectal temperatures of the 10 week old male and female mice was performed. In addition, mice were subjected to a cold challenge after baseline temperature measurement, which involved subjecting the mice to 4°C environment for a 30 minute period and then obtaining a measurement of body temperature.

5D3 males were found to be significantly hotter both pre- and post- cold challenge than wild type (Fig 5.5). Data for 5A4 males was not obtained. Both 5D3 and 5A4 female mice were hotter under standard conditions than wild type. After the cold challenge, 5D3 and 5A4 were hotter than wild type but this did not reach statistical significance (Fig 5.6).

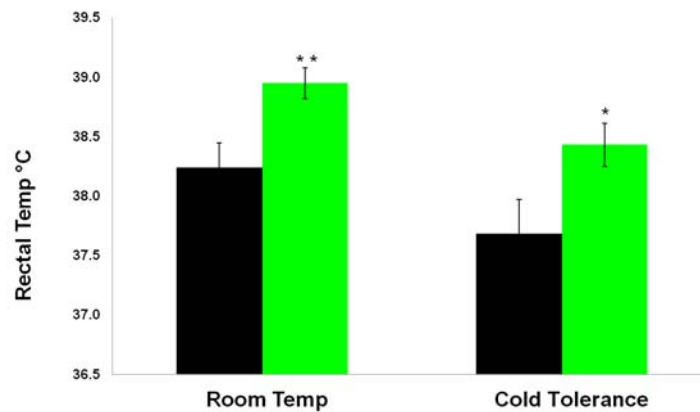


Figure 5.5 Rectal temperature of 5D3 male 10 week old mice, under standard conditions and after a 30 minute cold challenge. 5D3 mice were found to be significantly hotter than wild type litter mates, pre- and post- cold challenge. Error bars represent standard error of fold changes. Statistical analysis was performed by Student's t-test. * P<0.05, ** P<0.01. N=8+6.

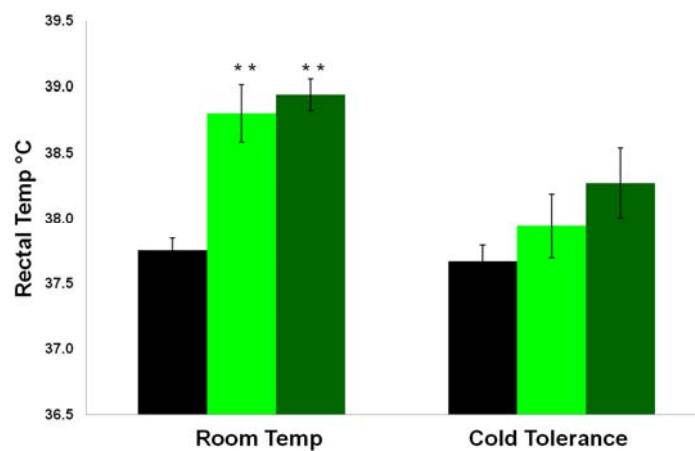


Figure 5.6 Rectal temperature of female 10 week old mice, under standard conditions and cold challenge. 5D3 and 5A4 mice were found to be significantly hotter than wild type litter mates under standard conditions. However, after being subjected to cold challenge, there was not a statistically significant difference. Error bars represent standard error of fold changes. Statistical analysis was performed by Student's t-test. ** P<0.01. N=7+6+5.

Fat pad mass in *Cdkn1c* BAC transgenic mice at one year of age maintained on a standard chow diet

In order to study the long term consequences of elevated *Cdkn1c* expression on weight gain, 5D3 and 5A4 mice were housed in cohorts containing not more than four individuals, with both wild type and transgenic animals, for one year maintained on a standard chow diet. Mice were weighted monthly. At six months and one year of age, mice were subjected to glucose and insulin tolerance testing and at 12 months mice were sacrificed to obtain fat pad data.

At 10 weeks of age, mice over-expressing *Cdkn1c* were reduced in total body weights (Table 2). At 6 months of age 5D3 and 5A4 male mice were found to weigh significantly less than wild type. This difference was maintained through to one year of age (Fig 5.7). In total wild type male mice increased in total body weight by 19.04 % (\pm 5.57 %) between six and twelve months while 5D3 male mice increased by 8.70 % (\pm 2.09 %) and 5A4 increased in weight by 4.03 % (\pm 1.26 %). Female 5D3 mice were lighter than wild type at 6 months but this difference was not found to be significant. 5A4 female mice were significantly lighter at this time-point (Figure 5.8). This pattern was maintained to 1 year of age, where 5D3 and 5A4 females were lighter than wild type. The lack of significance for the 5D3 females likely reflects the relatively higher standard deviation and the small number of animals (N=5). Consequently obtaining data for additional animals at this time point will be important in future work.

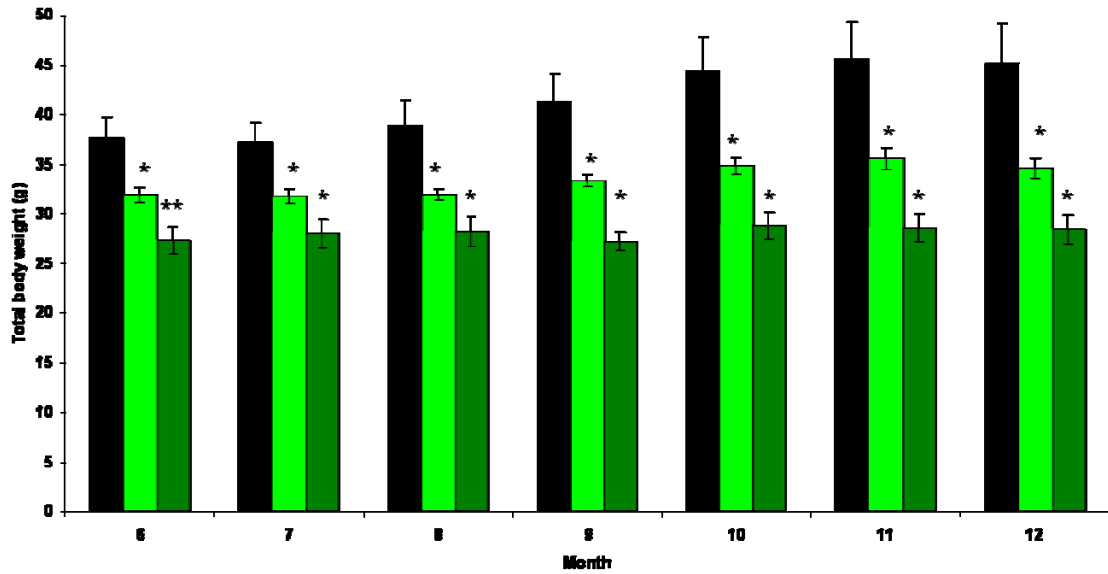


Figure 5.7 Monthly weights of male transgenic groups in 1 year ageing cohort. 5D3 and 5A4 mice were found to be significantly lighter at all time-points. Error bars represent standard error of fold changes. Statistical analysis was performed by Student's t-test. * P<0.05, ** P<0.01 N=5+5+4.

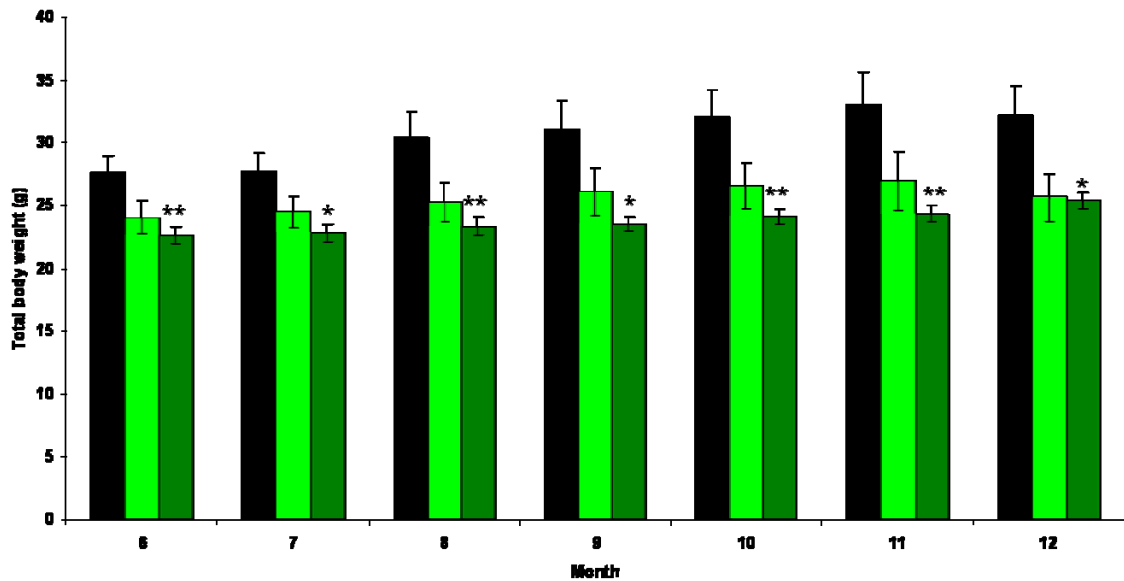


Figure 5.8 Monthly weights of female transgenic groups in 1 year ageing cohort. 5A4, but not 5D3 mice were found to be significantly lighter at all time points. Error bars represent standard error of fold changes. Statistical analysis was performed by Student's t-test. * P<0.05, ** P<0.01 N=6+5+5.

Glucose and Insulin tolerance

Increased fat mass has linked to irregularities in the management of glucose ²¹². In order to ascertain whether the reduction in fat mass in the transgenic models had any consequences for glucose metabolism at the whole body level, glucose and insulin tolerance testing were performed at 6 months and 1 year of age. At 6 months of age, there was no significant alterations in the handling of glucose after an IP glucose challenge in male 5D3 mice or 5A4 (Fig 5.9). Female 5D3 and 5A4 mice displayed an improved response at the thirty minute mark post injection from wild type (Figure 5.10).

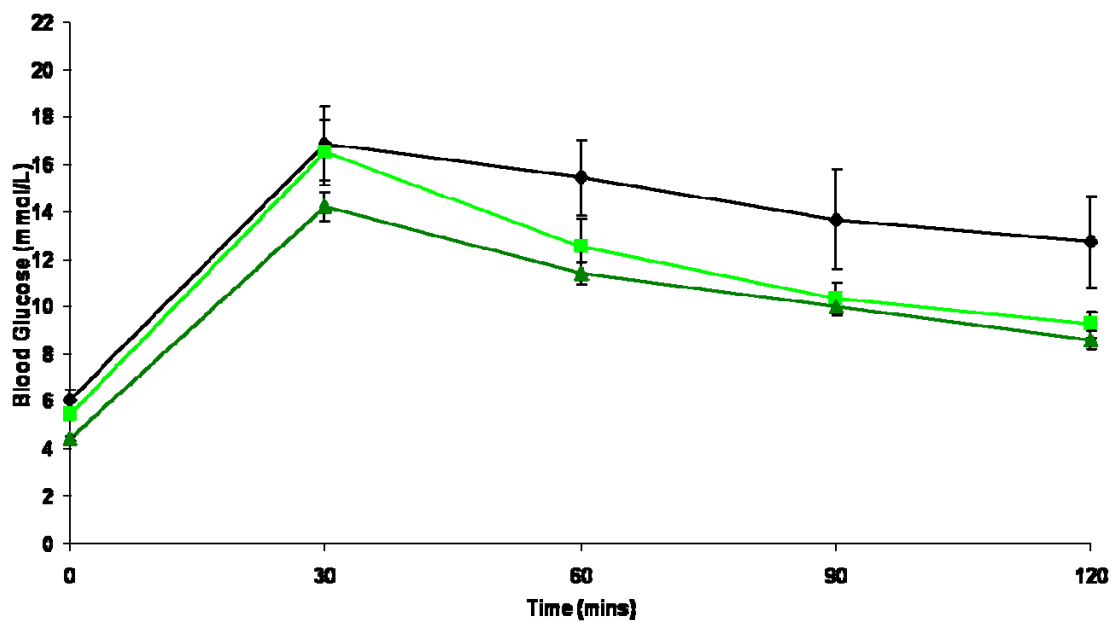


Figure 5.9 10 mM/ kg Glucose tolerance testing of transgenic male groups at 6 months of age. No differences between transgenic groups were detected. Error bars represent standard error. Statistical analysis was performed by Student's t-test. N=5+5+4

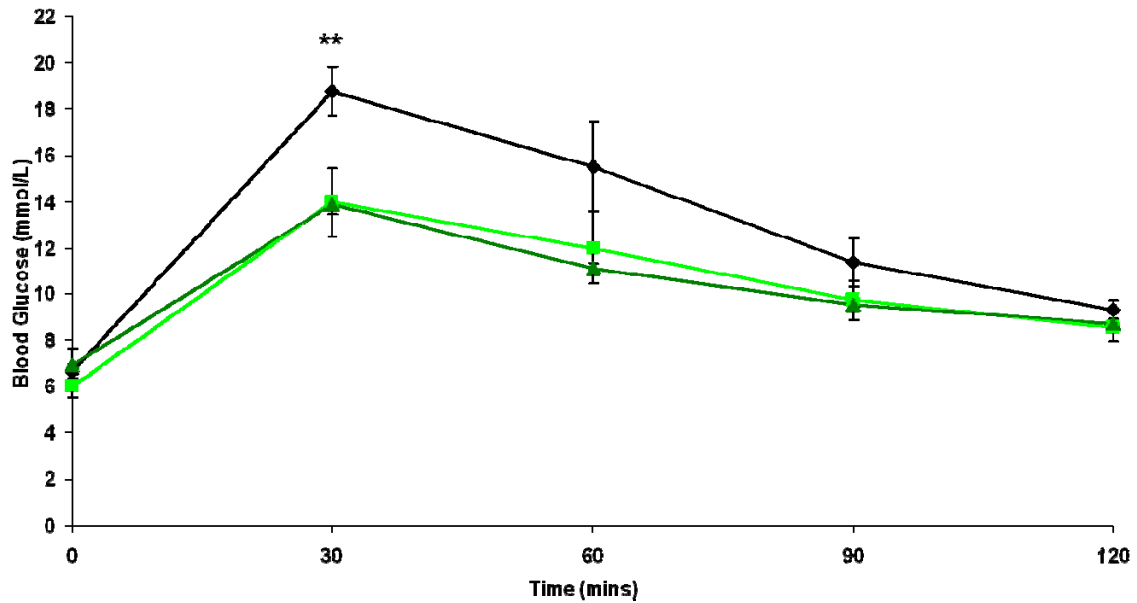


Figure 5.10 10 mM/kg Glucose tolerance testing of transgenic female groups at 6 months of age. 5D3 and 5A4 mice had a significantly reduced elevation in blood glucose level 30 minutes after injection. No further differences were detected. Error bars represent standard error. Statistical analysis was performed by Student's t-test. ** P<0.01 N=6+5+5

At one year of age, both 5D3 and 5A4 mice showed significantly improved responses at ninety minutes to wild type (Figure 5.11). These significantly improved responses were maintained through to the tests conclusion at one hundred and twenty minutes respectively. 5A4 male mice also presented with a more measured initial peak compared to wild type mice, thirty minutes after glucose injection. 5D3 mice at this time point were found to possess a similar peak to wild type.

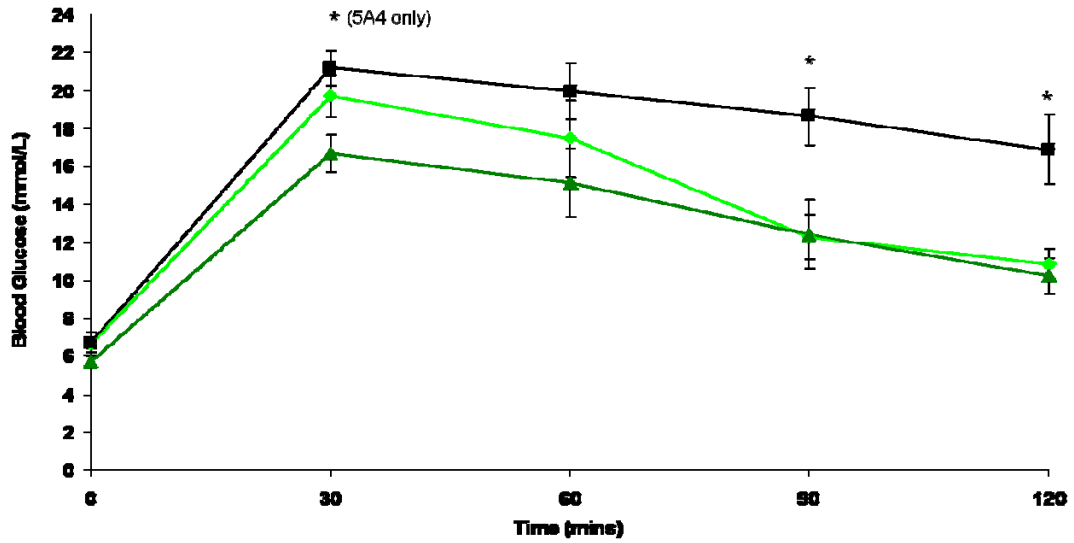


Figure 5.11 10 mM/kg Glucose tolerance testing of transgenic male groups at 1 year of age. 5D3 and 5A4 mice were found to possess a significantly improved response to glucose challenge. Error bars represent standard error. Statistical analysis was performed by Student's t-test. * $P < 0.05$ $N = 5 + 5 + 4$

Female 5D3 and 5A4 mice also displayed a significantly improved glucose tolerance response at 1 year (Fig 5.12). Unlike the male mice, both 5D3 and 5A4 females were found to possess an improved response compared to wild type mice at all time points measured. Thirty minutes after glucose injection, both 5D3 and 5A4 presented with a hugely reduced initial response, compared to wild type. Thus while the wild type mice showed a slower clearance of the IP glucose challenge as they aged, both the 5D3 and 5A4 males and females appeared to resist this age induced glucose intolerance.

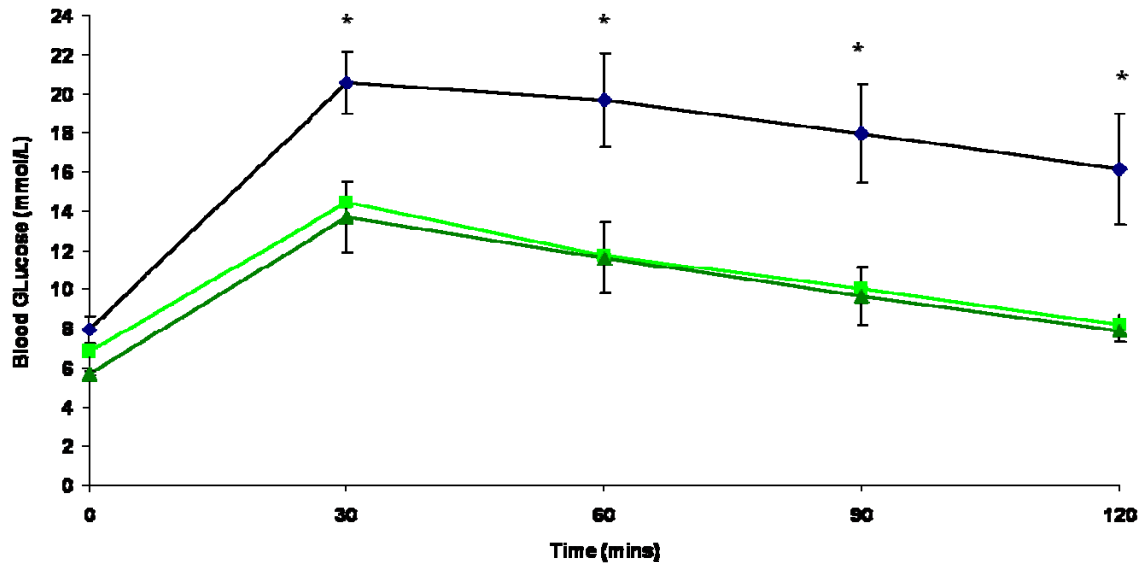


Figure 5.12 10 mM/ kg Glucose tolerance testing of transgenic female groups at 1 year of age. 5D3 and 5A4 mice were found to possess a significantly improved response to glucose challenge. Error bars represent standard error. Statistical analysis was performed by Student's t-test. * P<0.05 N= 6+5+5

Insulin tolerance testing (ITT) was also performed at 6 months and 12 months. During the initial ITT of 6 month old 5A4 mice, a very rapid and large decrease in blood glucose was observed in response to the insulin injection and the mice appeared to be losing consciousness. It was consequently necessary to remove them from the test and administer glucose injection due to the risks associated with hypoglycaemia. As a result, no data at six months of age was generated for the 5A4 mice. For the male 5D3 mice, fifteen minutes post-injection they were found to possess an improved response to insulin challenge as compared to wild type. This improved response was apparent at each time point measured till the end of the test (Fig 5.13). 5D3 females did not display a significantly improved response to wild type (Fig 5.14).

At 1 year of age, the ITT was performed under the same experimental conditions. This time data was obtained from both the 5D3 and the 5A4 cohorts. Fifteen minutes post-

injection 5D3 and 5A4 males were both found to be more sensitive to insulin challenge than wild type (Fig 5.15). This improved response was retained throughout the test in both transgenic lines. In 1 year old females, 5D3 and 5A4 also were found to be more sensitive to insulin challenge than wild type. This improved response was retained at the thirty minute post-injection time point in both 5D3 and 5A4, but thereafter lost (Fig 5.16).

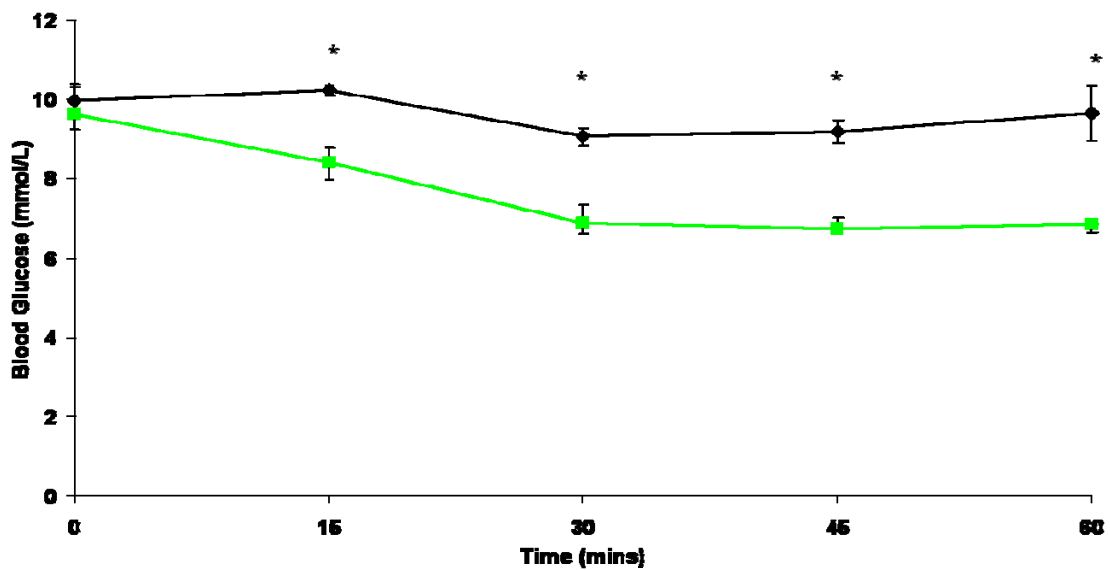


Figure 5.13 0.75U Insulin Tolerance Testing for transgenic male groups at 6 months of age. 5D3 mice possessed a significantly improved response to insulin challenge. Error bars represent standard error. Statistical analysis was performed by Student's t-test. * $P < 0.05$ $N = 5+5$

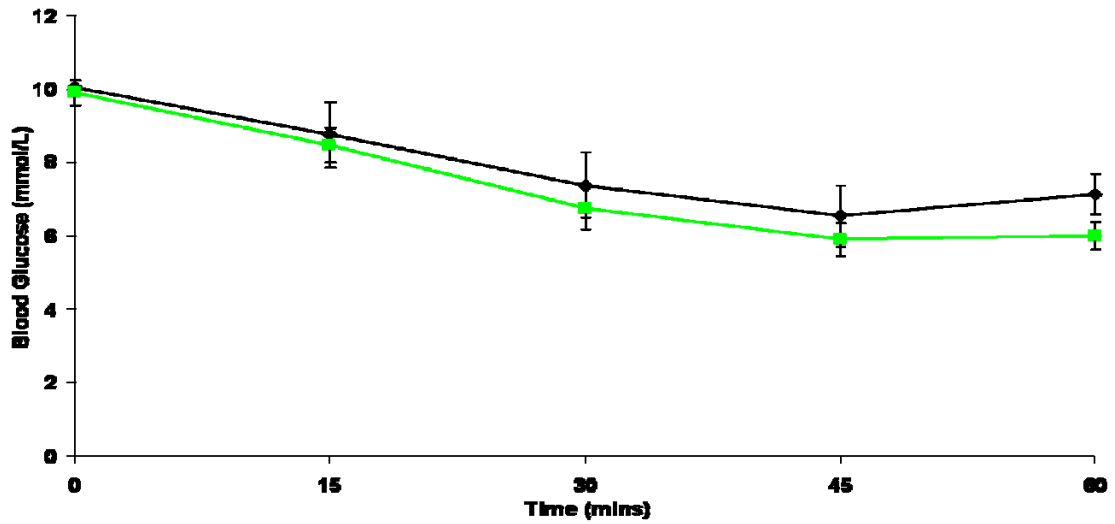


Figure 5.14 0.75U Insulin Tolerance Testing for transgenic female groups at 6 months of age. No difference was detected between wild type and 5D3 mice. Error bars represent standard error. Statistical analysis was performed by Student's t-test. N= 6+5

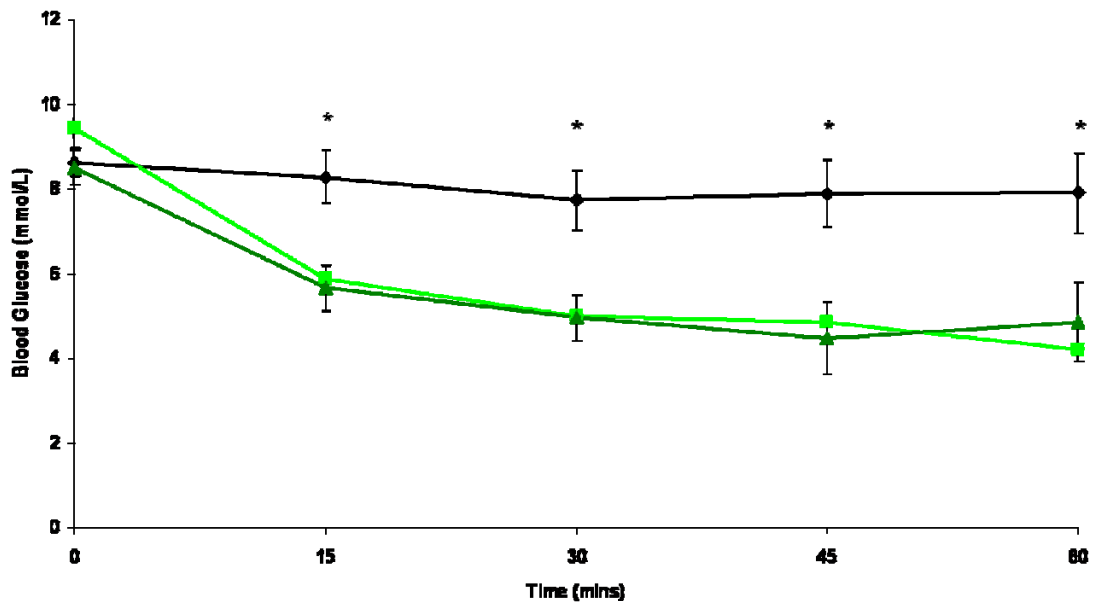


Figure 5.15 0.75U Insulin Tolerance Testing for transgenic male groups at 1 year of age. Both 5D3 and 5A4 mice possessed a significantly improved response to wild type at all time points after injection. Error bars represent standard error. Statistical analysis was performed by Student's t-test. * P<0.05 N=5+5+4

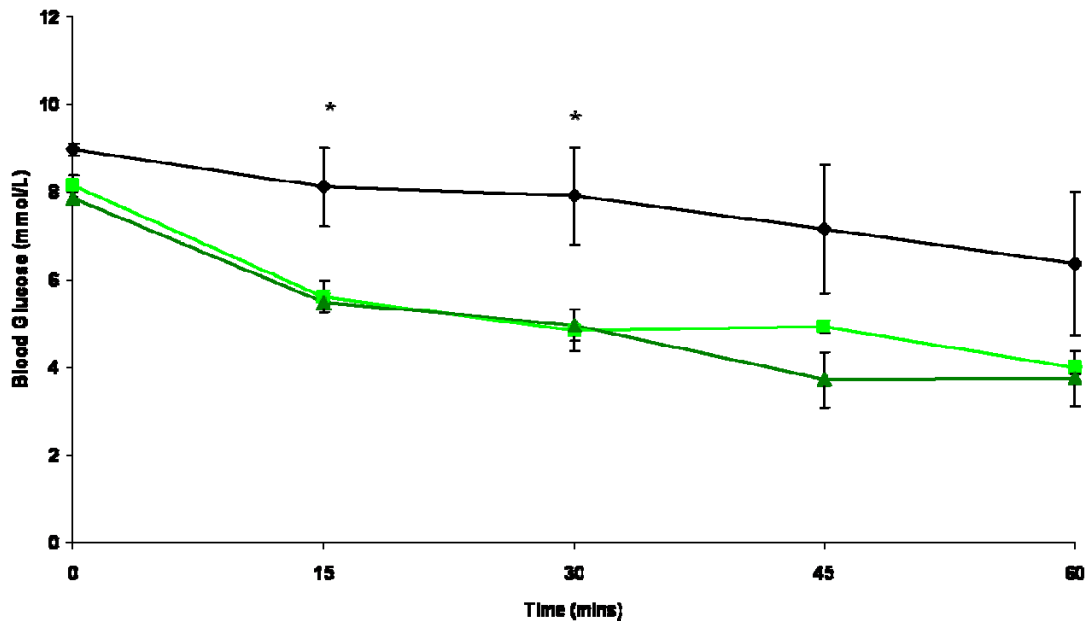


Figure 5.16 0.75U Insulin Tolerance Testing for transgenic female groups at 1 year of age. Both 5D3 and 5A4 mice possessed a significantly improved response to wild type at 15 and 30 minute time points. Error bars represent standard error. Statistical analysis was performed by Student's t-test. * $P < 0.05$ $N = 6+5+$

Adipose weights

Upon completion of glucose and insulin tolerance testing, mice were dissected and organs harvested for weights. Transgenic males and females from both lines showed a similar proportion in weight of kidney and liver as wild types (Fig 5.17-18). Visceral adipose depots taken were found to weigh significantly less in 5D3 ($42.98 \% \pm 7.81 \%$) and 5A4 ($71.50 \% \pm 7.43 \%$) females than wild type. At this stage in life, all visceral adipose depots when taken individually were lighter in both 5D3 and 5A4 females than wild type. In addition the inguinal subcutaneous white adipose depot was found to be lighter in 5D3 females than wild type. iBAT was significantly lighter in 5D3 females than wild type (Fig 5.18). Male 5D3

(44.43 % \pm 5.58) and 5A4 (76.26 % \pm 4.11) mice largely shared this pattern to wild type mice, with reduced visceral and subcutaneous white adipose depots (Fig 5.17).

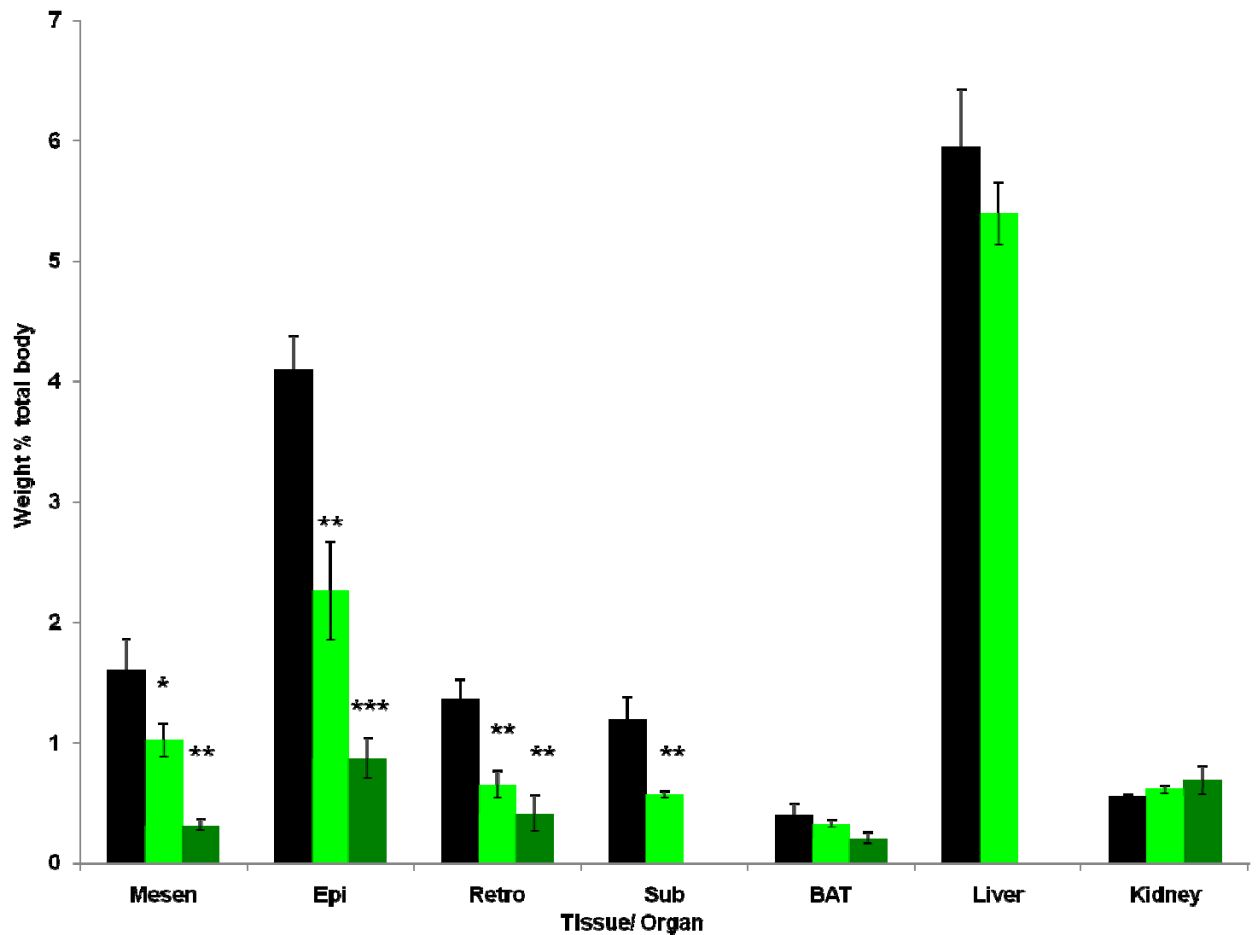


Figure 5.17 Wet weight of transgenic male adipose pads at 1 year of age, presented as a percentage of total body weight. Significantly reduced white adipose pads were observed in both the 5D3 and 5A4 lines in both males and females. Brown adipose tissue and kidney content were not found to be affected under any of the conditions. Statistical analysis was performed by Student's t-test. * P<0.05. ** P<0.01 *** P<0.001. N=5+5+4

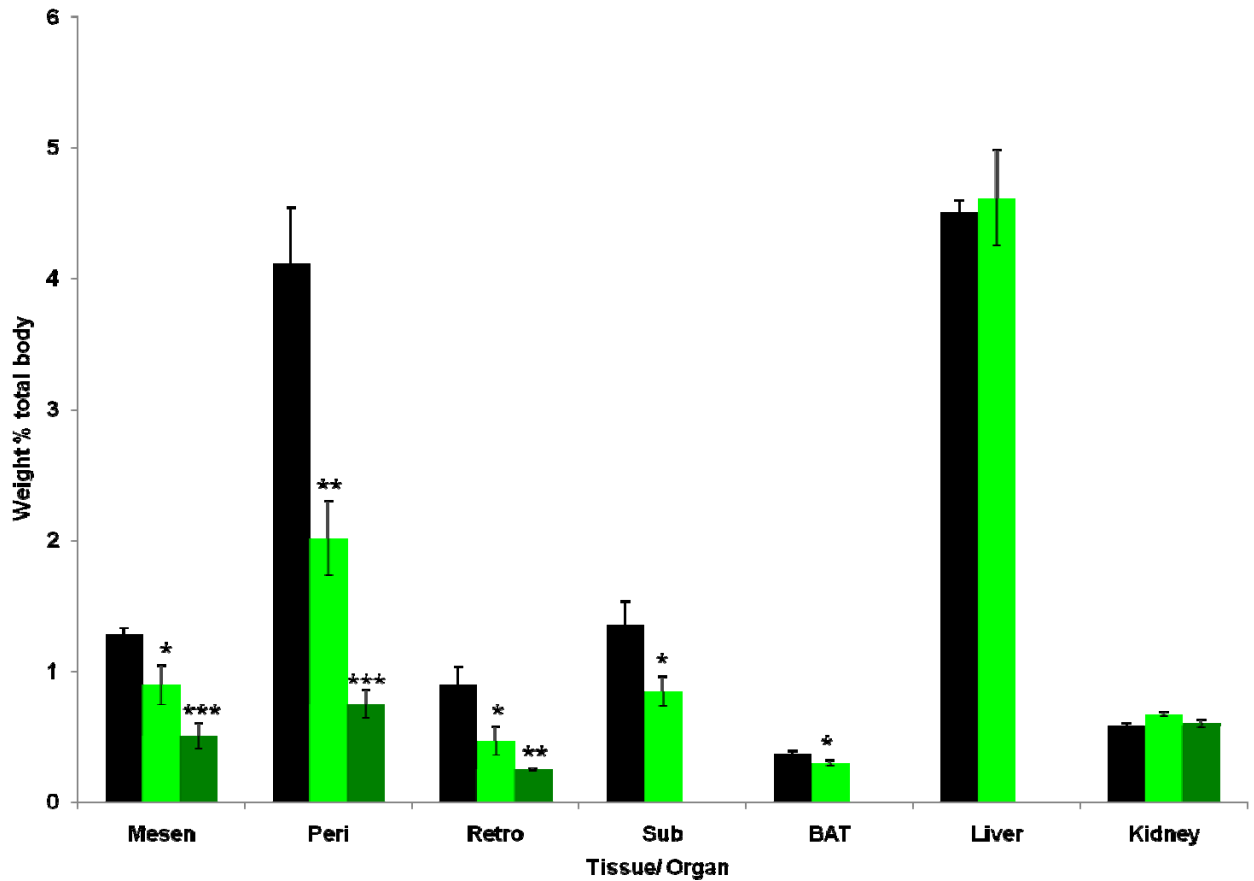


Figure 5.18 Wet weight of transgenic female adipose pads at 1 year of age, presented as a percentage of total body weight. Significantly reduced white adipose pads were observed in both the 5D3 and 5A4 lines in both males and females. Kidney content was not found to be affected under any of the conditions. Statistical analysis was performed by Student's t-test. * P<0.05. ** P<0.01 *** P<0.001. N=6+5+5

Examination of fat pad mass in *Cdkn1c* BAC transgenic mice in response to a high fat diet

Given the apparent protection against age-induced obesity provided by elevated *Cdkn1c*, it was interesting to determine whether elevated *Cdkn1c* provided any protection against obesity induced by a high fat diet. Wild type BL6 mice subject to a high fat diet rapidly gain weight as a consequence of increase fat deposition and develop both glucose

intolerance and insulin resistance¹⁴². A cohort of 10 week old female mice initially bred and maintained on a standard chow diet that delivers 18% of calories from fat were switched for a 12 week period to the high fat diet where 45% of calories come from fat. One week into the high fat diet, a measurement was made of food consumption on the high fat diet for a two week period. No differences were observed in the amount of food consumed between the 5D3 and wild type female mice (Fig 5.19).

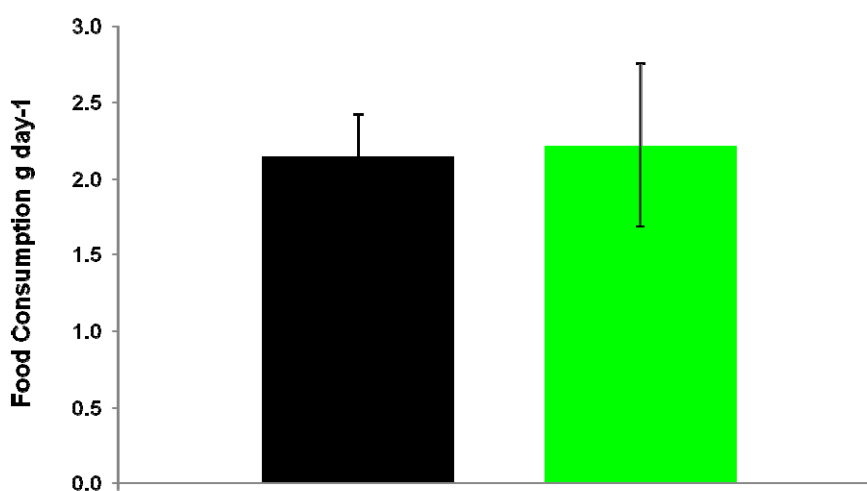


Figure 5.19 Feeding study for singly housed transgenic animals subjected to high fat diet study. Consumption was measured over a 2 week period, after an initial one week period post diet change. No difference was observed between 5D3 and wild type. Statistical analysis was performed by Student's t-test. N= 6+6.

From week 0 through week 12 of the high fat diet, 5D3 female mice total body weights were obtained. 5D3 female were found to be highly significantly lighter than wild types throughout (Fig 5.20). While wild type mice gained 9.85 g (\pm 1.04 g) over the duration of the diet whereas 5D3 mice gained 2.48 g (\pm 0.73 g). By the end of the study, wild type females were 50% heavier than 5D3 females.

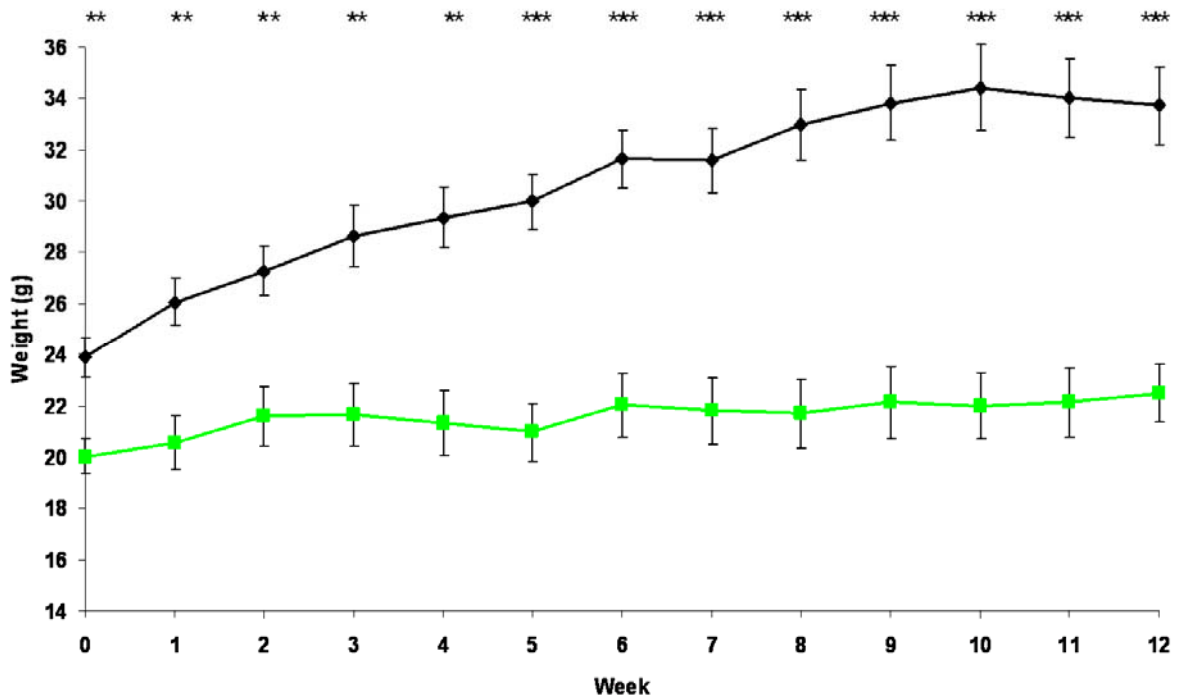


Figure 5.20 Weekly weights of 5D3 female cohort subjected to high fat diet. Error bars represent standard error of fold changes. Statistical analysis was performed by Student's t-test. ** P<0.01, *** P<0.001 N=9+9

Glucose and insulin tolerance testing were performed to observe the different groups' response to these respective challenges after the high fat diet challenge. Both wild type and 5D3 mice achieved similar peak blood glucose readings with no significant difference between the two groups. However 5D3 mice were found to clear glucose from sixty minutes to the end of the test. At one hundred and twenty minutes, 5D3 mice had significantly lower blood glucose than wild type (Fig 5.21).

Upon administration of insulin, 5D3 mice were found to be more sensitive to insulin challenge than wild type mice, at all time points measured (Fig 5.22). After forty-five minutes, the time point at which maximum decrease in blood glucose was determined, 5D3 mice had a greater response to insulin challenge than wild type.

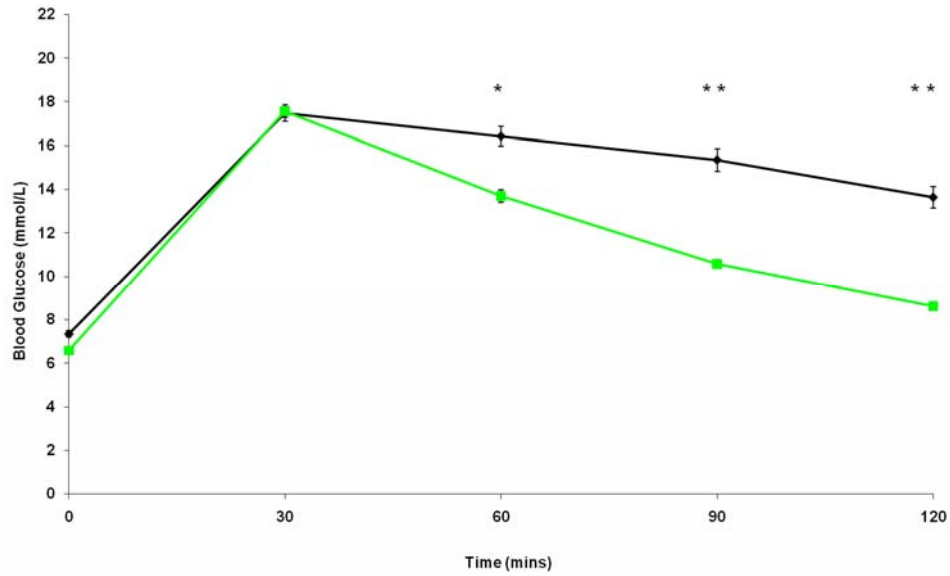


Figure 5.21 10 mM/kg Glucose tolerance testing of 5D3 female cohort subjected to high fat diet. 5D3 mice were found to clear glucose challenge more rapidly than wild type. Error bars represent standard error. Statistical analysis was performed by Student's t-test. * P<0.05, ** P<0.01 N=9+9

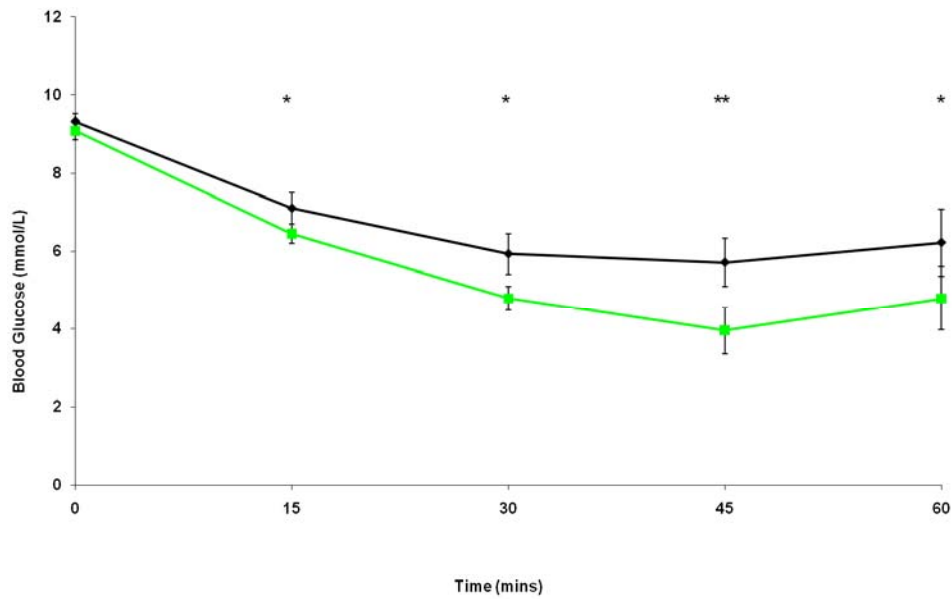


Figure 5.22 0.75 U Insulin tolerance testing of 5D3 female cohort subjected to high fat diet. 5D3 mice displayed a significantly improved response to insulin challenge than wild type. Error bars represent standard error. Statistical analysis was performed by Student's t-test. * P<0.05, ** P<0.01. N=9+9.

In addition to ITT and GTT after the HFD, an assessment of rectal temperature was made. While increased dietary lipids will elevate Ucp-1 expression throughout the adipose organ and thereby increase mitochondrial uncoupling, this potential increase in body heat can be counter-acted as energy expenditure is reduced in BL6 mice under these conditions²¹³. At 10 weeks of age 5D3 and 5A4 mice were significantly hotter than wild type (Fig 5.6). After 12 weeks of high fat diet 5D3 subjects were found to be significantly warmer than wild type mice (Fig 5.23).

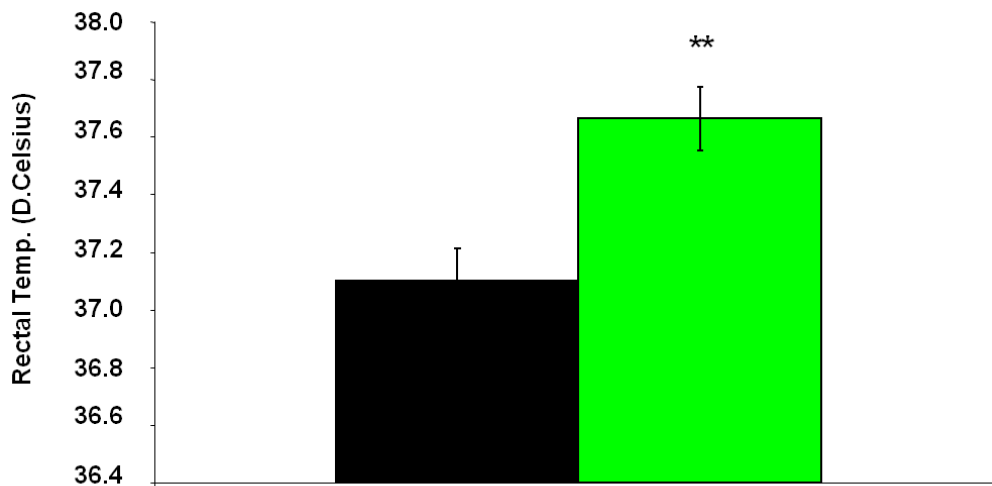


Figure 5.23 Rectal temperature of 5D3 female cohort subjected to high fat diet, under otherwise standard conditions. 5D3 mice were found to be significantly hotter than wild type, at rest. Error bars represent standard error of fold changes. Statistical analysis was performed by Student's t-test. ** P<0.01. N=9+9.

Mice were culled and dissected and organ weights were obtained. There was no significant difference in the weight of the kidney and liver as a proportion of total body weight between 5D3 and wild type. All adipose depots dissected were found to be significantly lighter in 5D3 mice (Fig 5.24), including visceral white adipose depots found to

be 62.70 % (\pm 6.74 %) lighter than wild type.

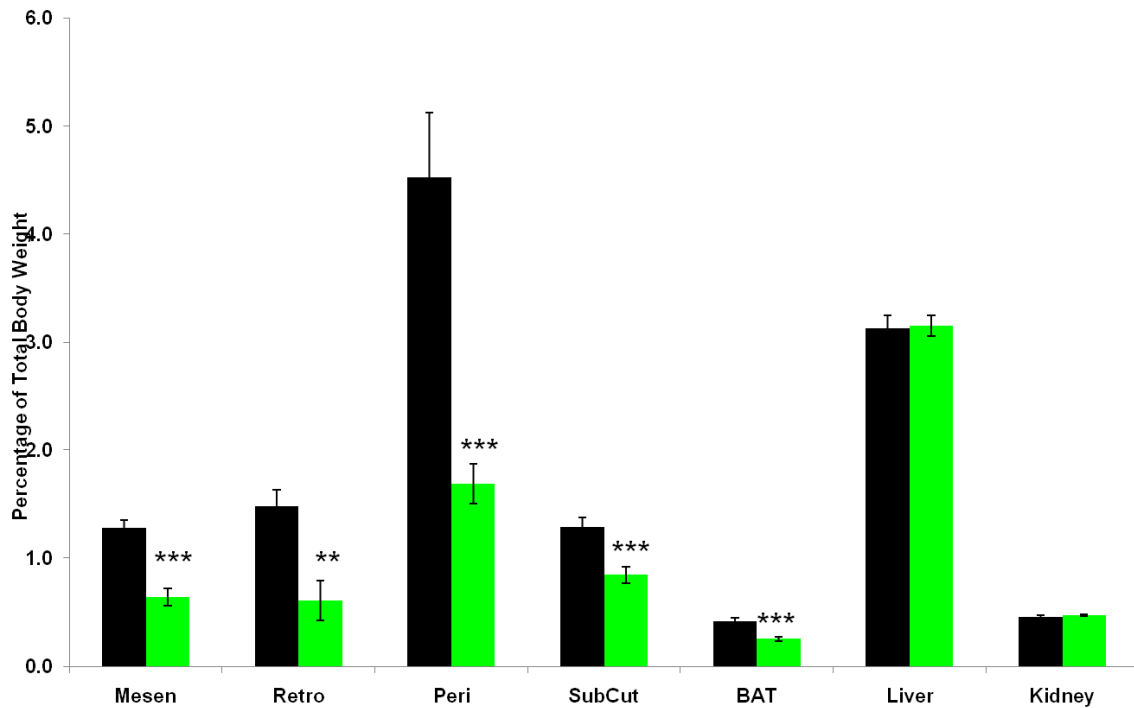


Figure 5.24 Wet weight of 5D3 female cohort adipose pads subjected to high fat diet, presented as a percentage of total body weight. Significantly reduced white adipose pads were observed in both 5D3 females. Kidney and liver displayed no difference between groups. Statistical analysis was performed by Student's t-test. * $P < 0.05$. ** $P < 0.01$ *** $P < 0.001$ $N = 9+9$

As a percentage of total body weight, there was no significant difference in the weight of the liver between wild type and 5D3 mice after the high fat diet (Fig 5.24). When weights were compared without taking into account total body weight, the wild type livers were significantly heavier (wild type $1.016 \text{ g} \pm 0.064$ versus 5D3 mice $0.692 \text{ g} \pm 0.037$; $P = 0.001$). H+E images of these livers showed substantial lipid deposition in the wild type liver which was less apparent in the 5D3 livers (Fig 5.25). Similarly, while the wild type white and brown adipose depots appeared to have larger cells indicating increased lipid stores, this was not the case for the 5D3 depots.

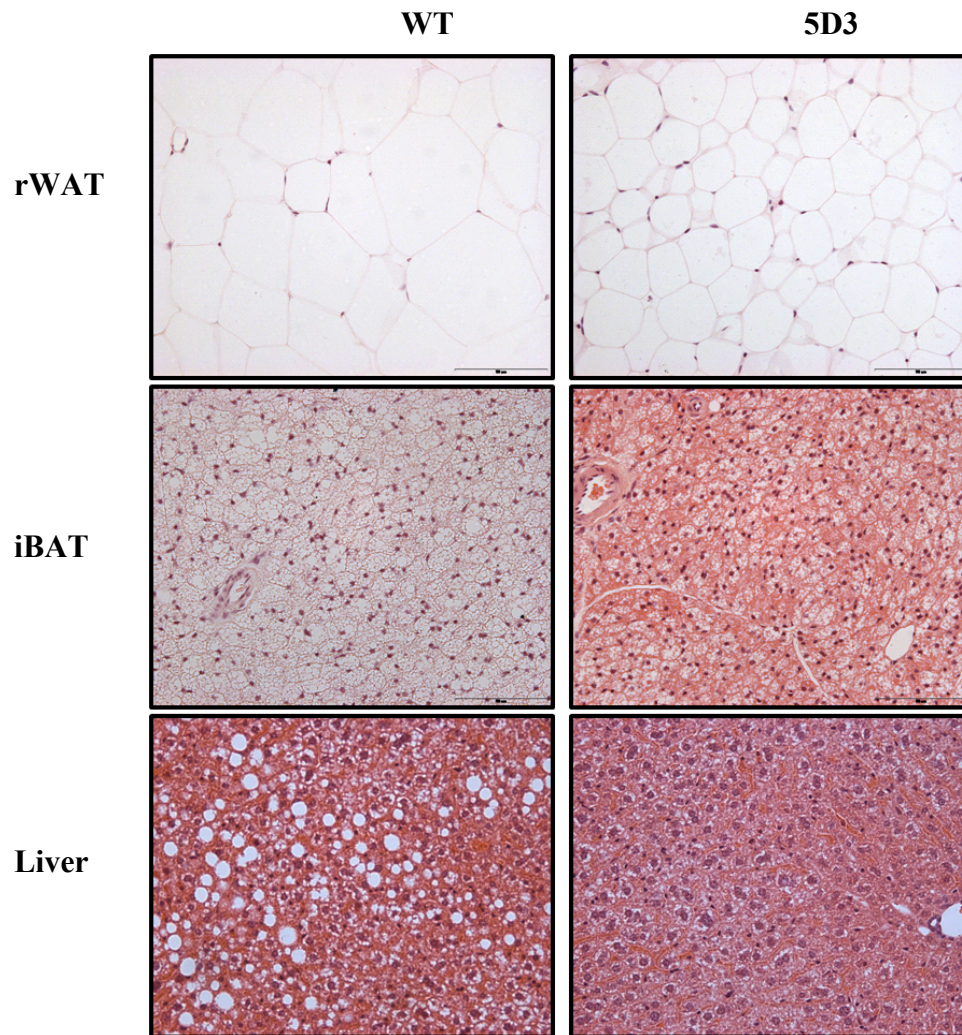


Figure 5.25 H+E staining of 5D3 rWAT, iBAT and liver sections, from cohort subjected to high fat diet, photographed under standard light field conditions. The appearance of the wild type sections suggests a greater lipid load as compared to 5D3 tissues. Scale bar represents 50 μm .

QPCR was used to examine the expression of key markers of non shivering thermogenesis. *PGC-1 α* , *Ucp-1*, *Cidea* and *Elovl3* were all found to be elevated in 5D3 rWAT after high fat diet (Fig 5.26).

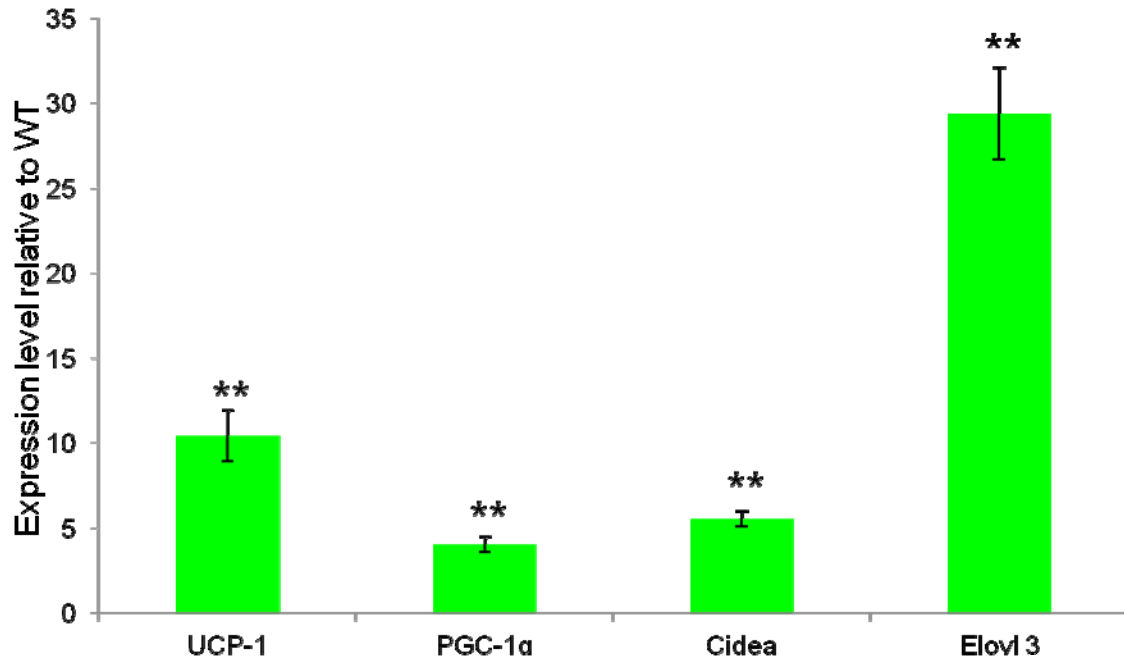


Figure 5.26 QPCR analysis of selected thermogenic program genes in 5D3 female high fat diet rWAT. All genes analysed were found to be elevated in 5D3 rWAT. Error bars represent standard error of fold changes. Statistical analysis was performed by Mann Whitney test. ** P<0.01. N=4+4.

Fat pad mass in *Cdkn1c* BAC transgenic mice on the 129 genetic background in response to a high fat diet

Work presented in the results so far examined BAC transgenic mice maintained on a ‘pure’ BL6 background. Prior to breeding of the lines onto this genetic background, provisional work that had identified a potential lean phenotype in line 5D3 when this line was studied on a mixed 129:BL6 background (Fig 1.15). It was not possible to study 5D3 or 5A4 transgenic mice on a pure 129 background as this was known to be a non viable combination¹⁰⁷. BL6 is the strain of mice commonly used in metabolic studies due to the propensity of this

strain to gain weight and develop metabolic irregularities on a HFD ¹⁴². In contrast, the 129 strain has been shown to be relatively resistant to the adverse consequences of a HFD ²¹⁴. In order to compare the relative “fat-fighting” effect of *Cdkn1c* on the two genetic backgrounds, a cohort of 5D3 and 5A4 mice and their wild type litter mates, was generated on a 75% 129/25% BL6 background and on a standard chow diet. At 10 weeks of age, these mice were switched to a high fat diet and weekly weights were recorded. Both 5D3 (1.8 g ± 0.66 g; P=0.03) and 5A4 (0.17 g ± 1.05 g; P=0.001) mice gained less weight than wild type (5.68 g ± 1.47 g). After 8 weeks under the dietary change 5D3 and 5A4 mice weighed significantly less than wild type mice (Fig 5.27).

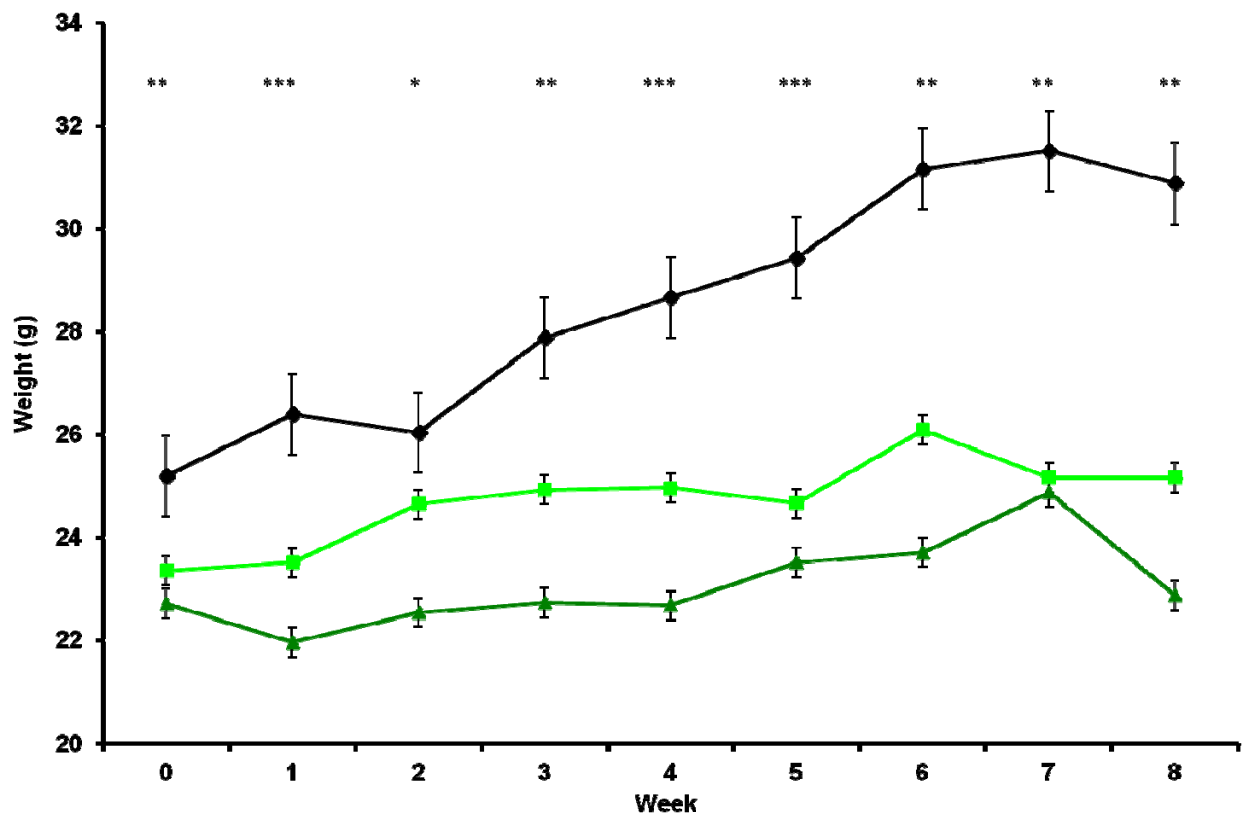


Figure 5.27 Weekly weights of 75% 129 transgenic female cohorts subjected to high fat diet. Both 5D3 and 5A4 mice were significantly lighter than wild type. Error bars represent standard error of fold changes. Statistical analysis was performed by Student’s t-test. * P<0.05, ** P<0.01 *** P<0.001 N=8+7+6

As was the case for the BL6 cohort, glucose and insulin tolerance testing was performed upon completion of the high fat diet. In glucose tolerance testing, no difference was observed between 5D3, 5A4 or wild type, 30 minutes after injection. Similar responses were achieved for all groups, through to one hundred and twenty (Fig 5.28). Insulin tolerance testing also returned highly similar plots for all three genetic groups forty five minute readings, where maximum insulin induced drop in blood glucose had been achieved. No differences were found between any of the groups, with the exception of a higher 5A4 measuring at one hour (Fig 5.29).

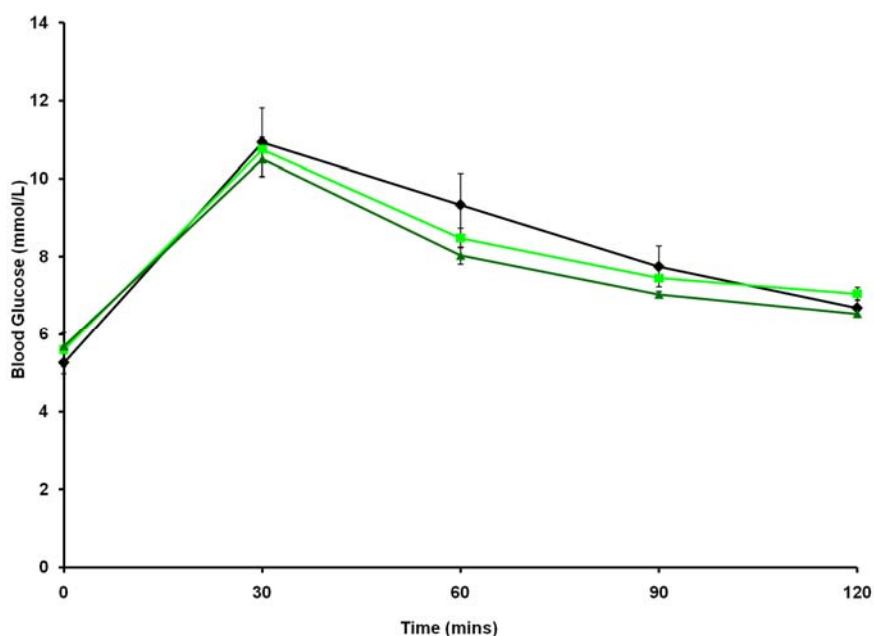


Figure 5.28 10 mM/ kg Glucose tolerance testing of 75% 129: 25% BL6 transgenic 5D3 and 5A4 females subjected to high fat diet. No differences in response to glucose challenge were detected in 5D3 or 5A4 mice, to wild type. Error bars represent standard error. Statistical analysis was performed by Student's t-test. N=8+7+6

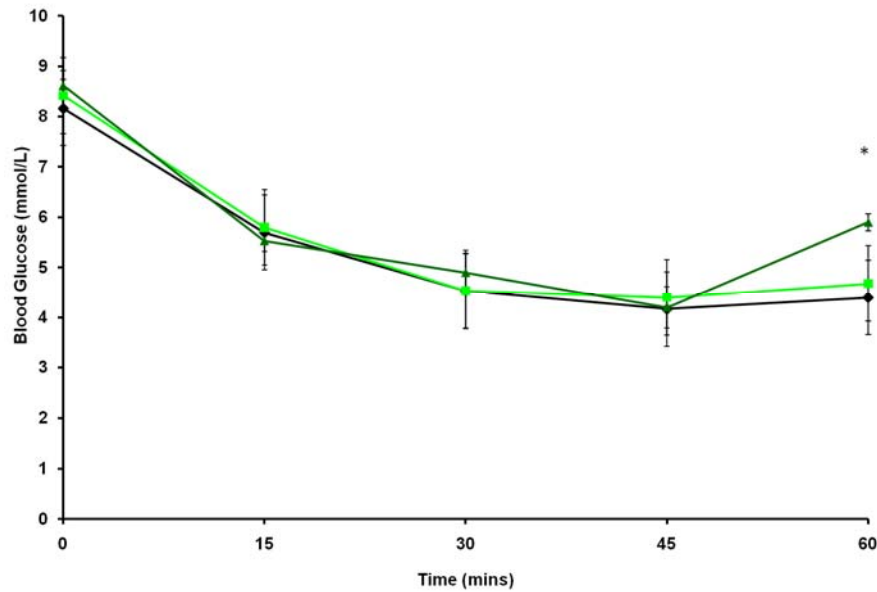


Figure 5.29 0.75U Insulin tolerance testing of 75% 129 transgenic female cohort subjected to high fat diet. Response to insulin challenge was highly similar in 5D3, 5A4 and wild type mice. Error bars represent standard error. Statistical analysis was performed by Student's t-test. N=8+7+6.

Mice were culled after the tolerance testing and dissected to determine adipose pad weights (Fig 5.30). The reductions in weight seen were similar to that observed when 5D3 was studied on the BL6 background (Fig 5.24). All three visceral white adipose and the inguinal subcutaneous white adipose depots were found to be lighter in both 5D3 and 5A4 mice than wild type. No differences were detected between groups in iBAT or kidney weights (Fig 5.30).

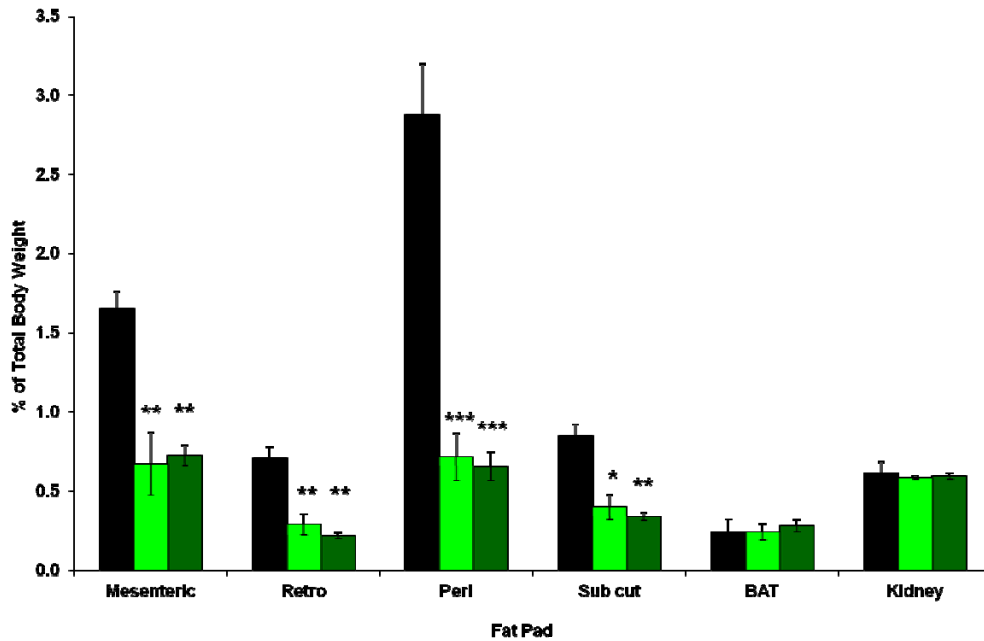


Figure 5.30 Wet weight of 75% 129:25% BL6 female adipose pads after high fat diet, presented as a percentage of total body weight. Significantly reduced white adipose pads were observed in both 5D3 and 5A4 females compared to wild type. Kidney and iBAT content was not found to be altered. Statistical analysis was performed by Student's t-test. * P<0.05. ** P<0.01. N=8+7+6

Discussion

The Spiegelman group had previously reported that ectopic expression of *Prdm16* from the α P2 promoter resulted in a lean phenotype, due to an induction of the mitochondrial uncoupling programme²⁰⁵. They also noted that, although near equal levels of *Prdm16* mRNA were detected in inguinal and epididymal adipose depots, the protein was detectable by Western in only the inguinal white adipose tissue. It was this discrepancy that prompted them to theorise that as yet unknown factor(s) were present to suppress the pooling of *Prdm16* in the visceral white adipose depots, where mitochondrial uncoupling is not anticipated.

Work in the previous two chapters suggested *Cdkn1c* as a novel regulator of adipogenesis through regulating the accumulation of Prdm16 protein in the adipose tissue. 5D3 females were found to contain the protein in their rWAT (Fig 4.12), which was not detectable by Western in wild type mice. In addition, Prdm16 accumulation was found to be greater in transgenic iBAT, in a dosage dependent manner (Fig 3.24). An accumulation of Prdm16 would account for the induction of the thermogenic programme in the transgenic white adipocyte depots alongside detectable levels of Ucp-1 protein (Fig 4.12). Consistent with increased thermogenesis, even as early as 10 weeks on a standard chow diet, there was a clear reduction in the weight of the visceral adipose depots in the single copy BAC transgenic line, with a further reduction apparent in the two copy transgenic line (Fig 5.1). This dosage phenotype correlated with the dosage dependent increase in Prdm16 accumulation (Fig 3.24).

The relative differences in adipose weight between wild type and the experimental lines were found to increase as mice aged (Fig 5.17-18). The profile of weight gain suggested that, rather than losing weight as they aged, the transgenic mice failed to gain weight like their wild type counterparts. Similarly, the transgenic mice also appeared to resist aged induced glucose intolerance and insulin resistance (Fig 5.9-16).

In addition to resisting age-induced weight gain, both 5D3 and 5A4 mice demonstrated an extreme resistance to diet-induced obesity (Fig 5.20-30). There were reduced lipid stores in the white adipose depots and also within iBAT and the liver of 5D3 females, compared to wild type (Fig 5.25). A single extra copy of the *Cdkn1c* gene was sufficient to confer almost total resistance to the effects of the high fat diet. This is in contrast to many other “anti-obesity” genes, where effects are seen after highly ectopic over-expression from the aP2 promoter, or potentially dangerous deletions such as *pRb* haploinsufficiency^{205; 209; 215; 216}. These results highlight *Cdkn1c* as a potential obesity therapy, which will be discussed in more detail later.

The final experimental chapter will focus on *Cdkn1c* expression in different adipose depots and between young and aging mice.

Chapter 6: *Cdkn1c* expression in adipose tissue

In the previous chapter *Cdkn1c* was found to protect against both age- and diet-induced obesity, in a dosage dependent manner consistent with a role for *Cdkn1c* in promoting the formation of thermogenically active brown adipose as suggested by the results in chapters 3 and 4. In light of these functions, a final enquiry that this project posed was to explore whether variations in the relative expression levels of *Cdkn1c* occurred in across the different adipose deposits and whether the expression level varied either as mice aged or in response to specific diets.

***Cdkn1c* expression across different depots**

In order to determine whether the level of *Cdkn1c* varied between the different adipose subtypes, four separate adipose depots were isolated at P7: retroperitoneal, subcutaneous, mesenteric (mWAT) and iBAT. mWAT is a visceral white adipose depot and was chosen as it represents a visceral adipose depot with less brown adipocyte content than rWAT¹²⁵. In a recently published work, *Prdm16* content had been shown to vary across adipose depots, at levels that correlated to an increased brown adipose characteristic²⁰⁵. Initially it was determined by QPCR that mWAT expressed *Cdkn1c* at the lowest level as compared to the other depots. In rWAT and scWAT *Cdkn1c* was expressed at nearly 8-fold higher level than in mWAT while iBAT displayed the highest level of *Cdkn1c* expression at approximately 16-fold more than in mWAT (Fig 6.1).

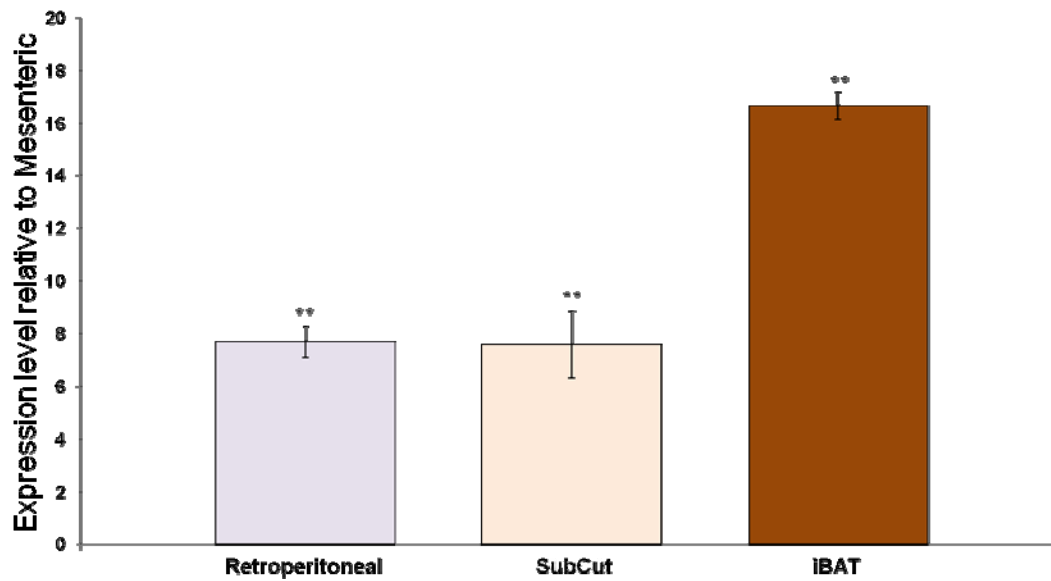


Figure 6.1 QPCR analysis of *Cdkn1c* expression in C57/Bl6 adipose deposits at P7, compared to the mesenteric adipose depot. rWAT (purple) and scWAT (pink) were found to possess similar expression levels, whilst expression in the iBAT (brown) was highest.

***Cdkn1c* expression in adipose as mice age**

In order to determine whether the level of *Cdkn1c* varied as mice aged, the same four adipose depots were isolated from mice aged one year. The expression of *Cdkn1c* in these older adipose depots was compared by QPCR to those from P7. In mWAT and iBAT there was a small but significant increase in expression between the two time-points. In contrast, expression of *Cdkn1c* in rWAT and scWAT was very much reduced at one year as compared to P7 (Fig 6.2).

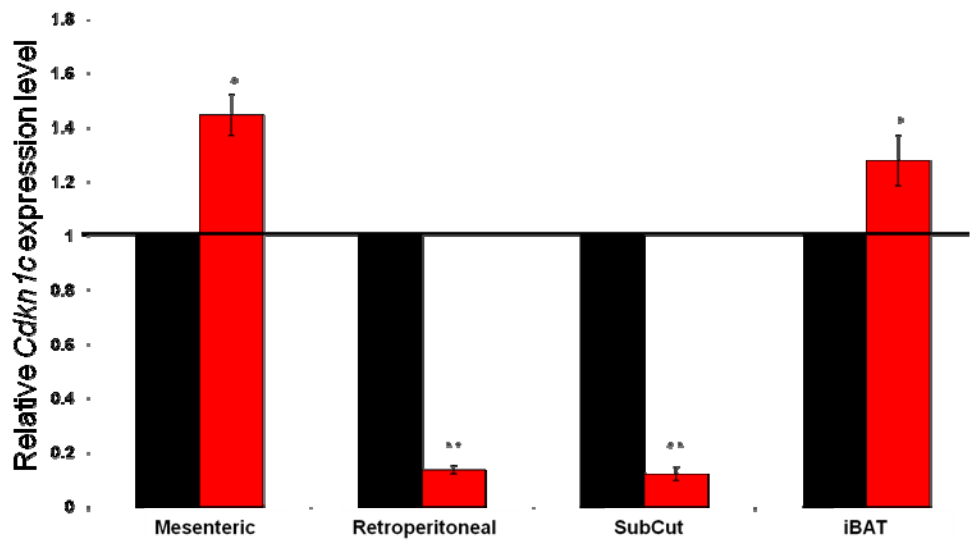


Figure 6.2 QPCR analysis of *Cdkn1c* expression in C57/Bl6 adipose deposits, comparing P7 (black) expression, to 1 year (red). Both mesenteric and iBAT were modestly increased, while rWAT and scWAT demonstrated significant down-regulation. Error bars represent standard error of fold changes. Statistical analysis was performed by Mann Whitney test. * $P < 0.05$. ** $P < 0.01$. $N = 4+4$

There are two interpretations of these findings. Firstly the reduced expression in retroperitoneal and subcutaneous WAT might indicate a progressive silencing of the locus. Alternatively, there may be fewer cells expressing *Cdkn1c* relative the total mass of the depots.

Cdkn1c sDMR and Lit1 gDMR in adipose as mice age

It has previously been mentioned that *Cdkn1c* imprinted expression is regulated by differential methylation of the *Lit1* gDMR, and the *Cdkn1c* sDMR^{22; 65; 217; 218; 219;}
220

To explore whether changes in the methylation of these DMR's could account for the reduced expression patterns observed, gDNA was isolated from the four depots at P7 and at one year. This DNA was subjected to bi-sulphite treatment, PCR amplified and PCR clones were sequenced. Methylation of the *Cdkn1c* sDMR was found to be slightly reduced in iBAT at one year (22.92 % of CpG's methylated \pm 1.13 P = 0.00019) as compared to P7 iBAT (37.24 % \pm 0.68) (Fig 6.3). Similarly, a slight reduction in methylation was observed in rWAT (1 year 22.78 % \pm 2.08 versus P7 32.51 % \pm 0.87; P = 0.006) (Fig 6.4). A decrease in the percentage of methylated CpG's in *Lit1* gDMR in iBAT was also observed at one year (25.60 % \pm 7.73 P=0.11) and P7 (46.83 % \pm 10.28) (Fig 6.5), however this did not achieve significance. This was again replicated in the rWAT (1 year 29.43 % \pm 2.01 versus P7 37.85 % \pm 4.90; P = 0.12).



Figure 6.3 Example of sequencing results of *Cdkn1c* sDMR, from wild type female iBAT gDNA after bisulphite treatment. Filled circles represent methylated CpG's, while empty circles represent unmethylated. The area analysed contained 50 CpG's and was located just upstream of the predicted transcription start site.



Figure 6.4 Example of Sequencing results of *Cdkn1c* sDMR, from wild type female rWAT gDNA after bisulphite treatment. Filled circles represent methylated CpG's, while empty circles represent unmethylated.

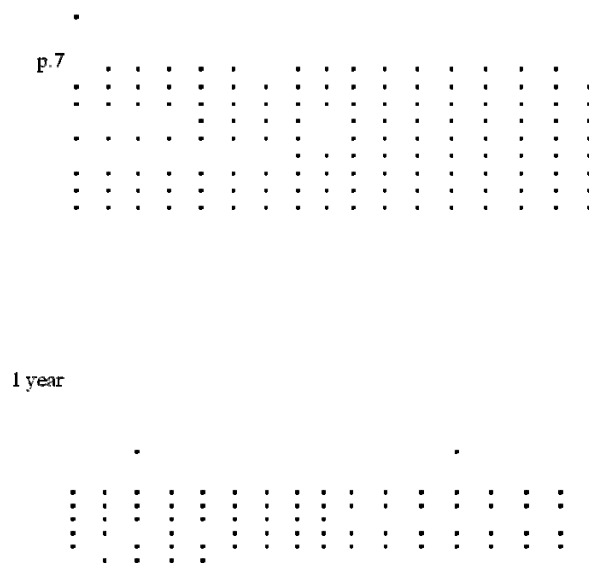


Figure 6.5 Example of sequencing results of *Lit1* gDMR, from wild type female iBAT gDNA after bisulphite treatment. Filled circles represent methylated CpG's, while empty circles represent unmethylated.

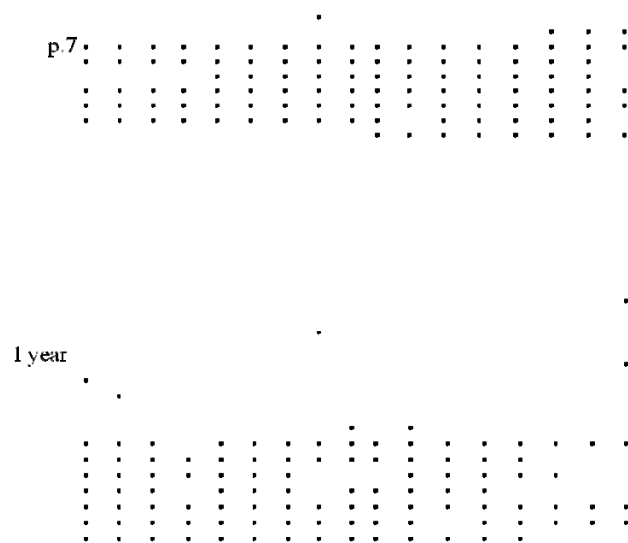


Figure 6.6 Example of sequencing results *Lit1* gDMR, from wild type female rWAT gDNA after bisulphite treatment. Filled circles represent methylated CpG's, while empty circles represent unmethylated.

These minor changes in methylation showed that increased DNA methylation during aging was not consistent with the shutting down of the *Cdkn1c* locus during aging by DNA methylation.

***Cdkn1c* expression in adipose in response to maternal conditions**

A previous study had noted that maternal exposure to low protein diet resulted in elevated *Cdkn1c* expression in the brain of her offspring in three of four regions studied and there was also reduced methylation of *Cdkn1c* sDMR²²¹. Since this study was performed on only one tissue, the brain, and since both expression and methylation were examined only in adult mice, it was important to determine whether this phenomenon was restricted to the brain and whether this occurred in younger animals. Pregnant 129 females were fed a low protein

diet during gestation from the day of the discernable plug until term. A second cohort of mice was set up at the same time but mothers were maintained on a standard chow diet. Pups were harvested at P7 and QPCR analysis was performed on iBAT. In iBAT of pups that had been exposed to the low protein diet, *Cdkn1c* expression was found to be significantly up-regulated as compared to standard chow pups (Fig 6.7). Although this up-regulation was more subtle than reported by Vucetic in the adult brain ²²¹, it was significant (P = 0.011). Bi-sulphite sequencing of the *Cdkn1c* sDMR was also performed. A reduction in methylation was observed in the low protein samples (LP 10.19 % ± 2.31 % versus St chow 23.2 % ± 3.01 %; P = 0.05) (Fig 6.8).

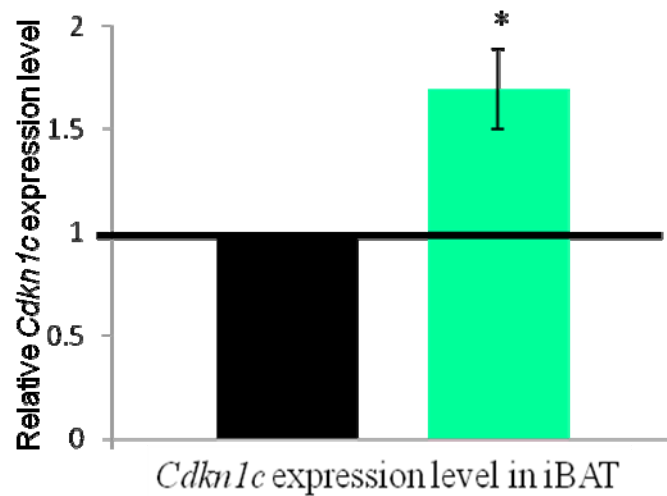


Figure 6.7 QPCR analysis of *Cdkn1c* expression in P7 iBAT, after maternal exposure to low protein diet, during pregnancy. *Cdkn1c* was found to be significantly up-regulated. Error bars represent standard error of fold changes. Statistical analysis was performed by Mann Whitney test. * P< 0.05. ** P< 0.01. N=4+4



Figure 6.8 High throughput sequencing of *Cdkn1c* sDMR, from P7 iBAT bisulphite treated gDNA, after maternal exposure to low protein diet. Loss of sDMR methylation arose. Filled circles represent methylated CpG's, while empty circles represent unmethylated.

Discussion

Cdkn1c expression was found to vary both across the different adipose depots, in response to aging and also in response to maternal diet. At P7, highest expression was observed in iBAT with subcutaneous and retroperitoneal WAT showing medium levels and mesenteric the lowest. *Cdkn1c* is expressed on a small subset of cells within iBAT and rWAT (Fig 3.17, 3.25, 4.1). Given the co-localisation of *Cdkn1c* with the brown fat determinant *Prdm16* in some of these cells (Fig 3.25-26) and the low frequency of label retaining cell in the iBAT³⁵, it is tempting to speculate that *Cdkn1c* marks the brown adipose stem cells in both iBAT and rWAT and that the level of expression reflects the number of cells present in the different depots rather than the absolute level of expression of *Cdkn1c* per cell. There was

not time to pursue this idea but further experiments are in progress to ask whether the *Cdkn1c* +ve cell is a label retaining cell.

Expression of *Cdkn1c* was much lower in one year old rWAT and scWAT than in P7 depots but this was not reflected in an increase in DNA methylation (Fig 6.2). A small increase in expression of *Cdkn1c* was observed in iBAT and mesenteric WAT. Again little change was observed in DNA methylation. More work is required to determine the mechanism by which *Cdkn1c* is down regulated by 9-fold in r and scWAT but one intriguing possibility is that this reduced expression reflects an age-related loss of the cells expressing *Cdkn1c* which may be brown adipose stem cells. Such a loss of stem cell could account for the loss in brown fat capacity and tendency towards adiposity seen in aging animals. Again, further work is required to explore this hypothesis.

While the methylation pattern of the sDMR appeared to change very little in response to aging, the experiments involving exposure to low protein diet demonstrated that there was epigenetic flexibility at the *Cdkn1c* locus (Fig 6.7). Timing of the exposure to low protein diet occurs prior to the time-point at which methylation of the sDMR is detectable between E8.5 and E9.5, and after monoallelic expression has been established²³. In this short study, the temporal changes in methylation were not assessed. There remain four main possibilities. Firstly, that mono-allelic expression of *Cdkn1c* is not established under conditions of low protein diet possibly due to a failure in signalling from the IC. Secondly, monoallelic expression of *Cdkn1c* is established but the secondary DNA methylation event does not occur and consequently the imprinted expression of *Cdkn1c* is not locked down – similar to that seen in the *Dnmt1* KO experiments^{220; 222}. Thirdly, it may be that both mono-allelic expression and differential DNA methylation are established but that this is not maintained. Finally, imprinted status may have been retained and the increase in expression of *Cdkn1c* results from an increase in transcription from the maternally inherited allele.

The low protein diet altered DNA methylation and expression of *Cdkn1c* while aging, albeit over a relatively short time of 12 months, altered expression in some depots but not all and the changes in DNA methylation were not consistent for a role for DNA methylation in inducing progressive silencing of the locus. This could be interpreted to mean that the *Cdkn1c* imprint is relative responsive during embryogenesis but less responsive after birth.

Finally, in response to the low protein diet, *Cdkn1c* expression was elevated in the iBAT (Fig 6.7). The level of over-expression in these low protein iBAT was similar to the over-expression levels in 5D3 iBAT (Fig 3.12). This is quite an important finding since it is usually presumed that such small changes in genes expression (less than 2-fold) would have a negligible effect on any process. However, our transgenic work demonstrates a very great effect on brown adipogenesis at this level of over-express. The consequence of elevated expression in response to the low protein diet may have a similar consequence – to increase iBAT.

Chapter 7: Discussion

This study has used four separate mouse lines to gain insight into a role for *Cdkn1c* in adipogenesis. Prior to this study, an adipogenic phenotype had not been characterised in *Cdkn1c*^{-m/+p} offspring. The results presented in Chapter 3 have therefore highlighted a new feature of these mice. This may prove to be important in future studies, regarding loss of expression of *Cdkn1c*.

The studies using the transgenic lines provided validity to the use of BAC transgenic lines in adipose tissue biology. A single copy of a BAC transgene was sufficient to produce phenotypes in all adipose tissue studied, and was able to protect against diet and age-induced obesity. The double copy line added to this by displaying a dosage dependent phenotype. Over-expression of a gene at the levels employed in these studies provides biological relevance given the imprinted nature of *Cdkn1c*.

***Cdkn1c* in adipogenesis**

The work in chapters 3-5 identified *Cdkn1c* as a novel regulator of brown adipogenesis. *Cdkn1c* was expressed in only a subset of cells within the BAT and WAT adipose depots. *In situ hybridisation* demonstrated that less than one percent of the cells at P7 were *Cdkn1c* positive. Further to this, there was over-lapping nuclear expression of *Cdkn1c* and *Prdm16* in a rarer subset of *Cdkn1c*-positive cells in iBAT, detected by immunofluorescence. This co-localisation alongside the very low frequency of this double positive cell was very intriguing. Long term studies demonstrated this cell to be BrdU label retaining). One hypothesis is that the co-expressing cell represents the brown adipose stem cell, while *Cdkn1c*-only cells are brown pre-adipocytes. There was insufficient time to look for *Cdkn1c* and *Prdm16* co-localisation in WAT but it is interesting to speculate that the *Cdkn1c* positive cells within rWAT are also brown fat stem cells. The ability to label these putative stem cells with a LacZ marker (reporter line) would provide another important tool in enhancing the understanding of brown adipogenesis.

Mechanism for action

Altering the dose of *Cdkn1c* resulted in alterations in two key molecules involved in promoting brown adipogenesis, *C/ebpβ* and *Prdm16*. Expression of the mRNA for *C/ebpβ* was altered in response to different doses of *Cdkn1c* while for *Prdm16*, it was the protein level that was changed. Although the mechanism by which *Cdkn1c* induced these changes was not investigated, the changes observed in *C/ebpβ* and *Prdm16* were consistent with *Cdkn1c* promoting the formation the *C/ebpβ*: *Prdm16* complex which would result in the downstream enhancement of the thermogenic gene programme. This work suggested that *Cdkn1c* acts to modulate an existing brown adipose program rather than acting as a brown fat determinant although further work is required.

One very striking discovery made during this work was identifying the relationship between *Cdkn1c* and *Prdm16*. Altering the dosage of *Cdkn1c* was not largely found to affect *Prdm16* mRNA levels. Instead, *Cdkn1c* dosage correlated with *Prdm16* protein. The higher the dose of *Cdkn1c*, the more *Prdm16* protein was found. In contrast, the lower the dose (KO), the less protein was found. This suggested a post-transcriptional role for *Cdkn1c* in the maintenance of *Prdm16* protein. The mechanism for this regulation was not resolved. However, *Prdm16* is a 140kDa protein with multiple potential phosphorylation and ubiquitination sites and recent work has shown *Prdm16* protein stability is enhanced through the administration of PPAR γ agonists which correlated with an inhibition of ubiquitination¹²⁴. This recent data suggests that the *Prdm16* protein undergoes posttranslational modification and degradation. By blocking phosphorylation of PPAR γ , *Prdm16* half-life can be lengthened. Maintaining PPAR γ in this hypo-phosphorylated state would be consistent with already identified functions of *Cdkn1c*^{87; 88}, and is therefore a potential future experimental pathway to explore if this is the case.

Cdkn1c has been shown to directly bind to and stabilise the MyoD protein enhancing the skeletal muscle phenotype¹⁰⁰. It is interesting to speculate that *Cdkn1c* may function in both skeletal

muscle and brown adipose tissue by directly binding MyoD or Prdm16 respectively, and stabilising these proteins to further enhance the predetermined cell fate.

Loss of expression of *Cdkn1c*

The consequences of loss of expression of *Cdkn1c* in white adipose tissue *in vivo* in adults were not studied due to the difficulties in obtaining *Cdkn1c*-deficient animal after birth. However, through the *ex vivo* system of differentiating MEF's to adipocytes (Fig 4.13-18), it was determined that a loss of *Cdkn1c* did not promote white adipogenesis. Rather it seemed that *Cdkn1c* was required for both white and brown adipogenesis. Given the role the *Cdkn1c* plays in both cell cycle regulation and also directing differentiation, it will not be straightforward to dissect apart the roles that *Cdkn1c* plays in both white and brown adipogenesis. Both *in vitro* systems such as 3T3-L1 cells and also a conditional *Cdkn1c* knockout model would be helpful to dissect apart mechanisms and to study loss of expression phenotypes in the adult.

Although not fully explored here, it might be possible to generate a model in which *Cdkn1c* expression is lower than wild type but not completely absent. Low protein diet during pregnancy results in increased expression of *Cdkn1c* in the iBAT and brain²²¹. It has not currently been confirmed, but this increase in expression is likely attributable to a release of silencing of the paternally inherited copy of the *Cdkn1c* gene. If this were to be the case, maternal low protein exposure during pregnancy may be sufficient to rescue the lethality associated with *Cdkn1c*^{-m/+p} mutation, by partially reactivating the silenced copy of the gene. This would allow the study of the consequences of reduced expression of *Cdkn1c* in brown and white adipose tissue and also the whole organism level.

Flexibility of *Cdkn1c* in iBAT.

Data in chapter 6 suggested that the *Cdkn1c* imprint is responsive to environmental cues during embryogenesis. Although much work is still required, this flexibility has important implications. *Cdkn1c* is already known to regulate birth weight¹⁰⁷. In this thesis, a role for *Cdkn1c* in enhancing thermogenesis has been identified. This means that *Cdkn1c* has the ability to regulated both birth weight and thermogenesis. Sub-optimal conditions during pregnancy are widely known to result in growth restriction^{223; 224; 225}. A consequence of growth restriction is an increased surface to body ratio, which leads to greater heat loss. As a result, greater demand is placed on heat generation, to ensure body temperature is maintained. It was found during these studies that low protein diet was sufficient to increase expression of *Cdkn1c* in the iBAT. *Cdkn1c*, due to its' role in brown adipogenesis, may therefore function in accommodating these changes. By possessing flexibility in the expression level of *Cdkn1c*, iBAT capacity could potentially be modulated to allow for increased demands, as a result of a sub-optimal pregnancy.

Imprinting of *Cdkn1c*

The imprinted nature of *Cdkn1c* adds an extra element of intrigue to the phenotypes seen. 5D3/5A4 iBAT essentially model the consequence of loss of imprinting of *Cdkn1c*. Increased Ucp-1 protein and iBAT mass suggests a greater heat generating capacity than a wild type pad. Wild type newborn mice are able to survive early life before the development of fur through their ability to

produce heat through both shivering and non-shivering thermogenesis. Non-shivering thermogenesis has often been referred to as a highly efficient form of heat generation, when compared to shivering. However, due to the inability of the subject to freely switch Ucp-1 function on and off, that it is possible to do when shivering, non shivering thermogenesis is essentially fixed during development. If not required, excess energy will simply be radiated out of the body at the expense of the individual through lost lipid stores.

Imprinting of *Cdkn1c* involved a decrease from two active copies to one active copy. Our data suggest that such a change in active copies would result in lower *Cdkn1c* expression and a reduction in active iBAT, in other words, less thermogenesis at birth. Previous work performed in the lab identified *Cdkn1c* as a dosage dependent growth restrictor. Elevated *Cdkn1c* was linked to lower birth weight and loss of *Cdkn1c* was linked to fetal overgrowth^{104; 107}. *Cdkn1c* expression therefore modulates both birth weight and iBAT mass. Heat production is of far greater importance to new born mice than at any other time in their lives, due to their high surface area to volume ratio, and low level of fur covering. The presence of their littermates and parents helps maintain body warmth, due to huddling, and combined non-shivering thermogenesis. As the mouse ages, greater covering of hair, higher motility and the development of subcutaneous white fat reduce the comparative amount of non shivering thermogenesis required to maintain body temperature. Under Allan and Bergman's rules, smaller pups have a higher degree of heat loss due to a high surface area to volume ratio, and more so more heat generation is required to maintain body temperature as compared to larger pups²²⁶ (Fig 7.1). Since a larger pup requires less thermogenesis to maintain body temperature, linking of birth weight to thermogenesis via *Cdkn1c* would provide a distinct advantage. Essentially when *Cdkn1c* acquired imprinted status, birth weight was increased and thermogenesis decreased such that energy acquired from suckling would all go toward supporting growth rather than keeping warm, providing a distinct advantage. In the event of a sub-optimal pregnancy however, the ability to increase *Cdkn1c* dosage in the iBAT is retained through flexibility of the sDMR.

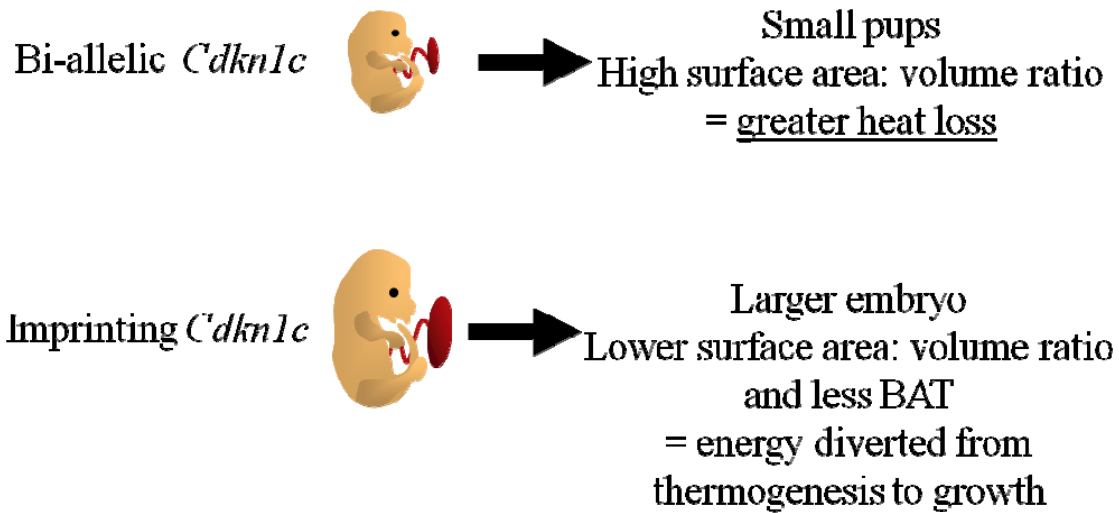


Figure 7.1 Effect of imprinting *Cdkn1c* on body size and thermogenic requirements. Mono-allelic expression of *Cdkn1c* results in larger offspring that loose less heat.

Cdkn1c and obesity

In addition to the brown adipose depots, *Cdkn1c* was expressed from the transgenes at other sites with relevance to obesity including the hypothalamus, the adrenal gland and the pituitary (John 2001) which may contribute to the obesity resistance observed in the 5D3 and 5A4 models. The action of *Cdkn1c* at these sites requires further investigation. Nonetheless, the changes observed in both brown and white adipose depots, in particular the increase in Prdm16 protein, suggest that the resistance to age- and diet-induced obesity is in part directed by elevated *Cdkn1c* in these depots. Consequently *CDKN1C* may be a target for obesity therapy in humans.

It currently remains to be seen whether the human gene functions in adipose tissue to regulate the accumulation of PRDM16 and enhance thermogenesis. However, observations from Silver-Russell patients suggest that it might. Three observed symptoms of the disease are a striking lack of

subcutaneous adipose tissue, night sweats and hypoglycaemia (recently reviewed ^{227; 228}). These three symptoms are consistent with excessive thermogenesis and also consistent with the phenotype observed in 5D3/5A4 mice. Further work will be required to conclusively demonstrate if such a role for *CDKN1C* in adipogenesis is present in humans. Were the function to be conserved between species however, the potential of *CDKN1C* providing a novel therapy is extremely appealing. Due to the imprinted nature of the gene, we all possess an extra copy of the gene that is currently unused, the paternally inherited silenced copy. Given the results presented in this chapter, where a single extra copy of *Cdkn1c* from a BAC transgene was sufficient to provide the phenotype, it is possible to speculate that activation of the paternally inherited allele may be enough to provide a buffer towards age and diet-induced obesity.

One final point of interest regarding weight regulation comes from a prediction that *Prdm16* is imprinted, in both mice and humans ^{229; 230}. As a result of the potential relationship between *Cdkn1c* and *Prdm16* in adipose, and the prediction that it is the maternal allele of *Prdm16* that is silenced, this could represent a synergy between imprinted genes. Further work will be required, first of all to confirm if the gene is in fact imprinted.

Brown adipose tissue and the Parental Conflict Hypothesis.

The divergence of eutherians and marsupials represents the expansion of the brown adipose pathway, with only limited mitochondrial uncoupling detected in marsupials, and none in monotremes ^{137; 231; 232; 233}. It is interesting to speculate that these marsupial brown adipose cells are more closely related to the *Myf5⁻* population of BAT seen in white adipose depots of rodents, as opposed to the *Myf5⁺* iBAT lineage. Regardless of the origins, it appears that thermogenically active brown fat likely was present in the common ancestor of marsupials and eutherians at the time of an expansion of the imprinting system, so we also see an expansion in the biological significance of brown adipose tissue.

The mechanisms that have given rise to the differences between eutherian and marsupial brown adipose tissue have not been elucidated. However, the so far established roles of imprinted genes in adipose tissue are largely consistent with this tissue being a site of parental conflict, including *Pref-1*^{234; 235} and *Necdin*^{38; 159; 236}.

David Haig predicted in his theory of Kinship that maternally expressed imprinted transcripts would promote brown adipogenesis^{173; 237; 238}. *Cdkn1c*, a maternally expressed imprinted gene would therefore fit within this hypothesis, with respect to the adipose tissue. *Pref-1* and *Necdin*, which are paternally expressed imprinted genes, inhibit adipogenesis, and therefore also fit within this framework. Previous work has shown *Cdkn1c*, and other members of the IC2 imprinted cluster are not be imprinted in marsupials^{34; 36}. We can therefore speculate that the imprinting of *Cdkn1c*, and potentially other imprinted genes, may have been influenced by conflict caused by the brown adipose lineage. It is particularly interesting that *Cdkn1c* also regulates embryonic growth and thus weight at birth¹⁸⁰. One can imagine that when *Cdkn1c* became mono-allelically expressed, this resulted in larger mammals with a lower surface area and also less brown fat thus energy normally required for thermogenesis could be used to support post-natal growth. Much work still needs to be done. For example, although *Cdkn1c* is imprinted in humans and not marsupials, nothing is known about the epigenetic status of *Cdkn1c* in Afrotheria (elephants), a lineage of eutherians most distant from euarchontians (human, mice).

This work has explored a novel function for *Cdkn1c* and has demonstrated the gene to be involved in brown adipogenesis. The exact mechanism for its' function remains to be discovered but the work has highlighted an exciting new gene in the adipose field.

1. Surani, M. A. (1998). Imprinting and the initiation of gene silencing in the germ line. *Cell* **93**, 309-12.
2. Feil, R. & Berger, F. (2007). Convergent evolution of genomic imprinting in plants and mammals. *Trends Genet* **23**, 192-9.
3. Killian, J. K., Byrd, J. C., Jirtle, J. V., Munday, B. L., Stoskopf, M. K., MacDonald, R. G. & Jirtle, R. L. (2000). M6P/IGF2R imprinting evolution in mammals. *Mol Cell* **5**, 707-16.
4. Monk, D., Arnaud, P., Apostolidou, S., Hills, F. A., Kelsey, G., Stanier, P., Feil, R. & Moore, G. E. (2006). Limited evolutionary conservation of imprinting in the human placenta. *Proc Natl Acad Sci USA* **103**, 6623-8.
5. Surani, A. (1983). Genetic Manipulation of Embryos. *Veterinary Record* **113**, 268-268.
6. Surani, M. A. H., Barton, S. C. & Norris, M. L. (1984). Development of Reconstituted Mouse Eggs Suggests Imprinting of the Genome during Gametogenesis. *Nature* **308**, 548-550.
7. Thomson, J. A. & Solter, D. (1988). The Developmental Fate of Androgenetic, Parthenogenetic, and Gynogenetic Cells in Chimeric Gastrulating Mouse Embryos. *Genes & Development* **2**, 1344-1351.
8. Barton, S. C., Surani, M. A. & Norris, M. L. (1984). Role of paternal and maternal genomes in mouse development. *Nature* **311**, 374-6.
9. Kaufman, M. H., Barton, S. C., Azim, M. & Surani, H. (1977). Normal Postimplantation Development of Mouse Parthenogenetic Embryos to Forelimb Bud Stage. *Nature* **265**, 53-55.
10. Hu, J. F., Oruganti, H., Vu, T. H. & Hoffman, A. R. (1998). Tissue-specific imprinting of the mouse insulin-like growth factor II receptor gene correlates with differential allele-specific DNA methylation. *Mol Endocrinol* **12**, 220-32.
11. Jaenisch, R. (1997). DNA methylation and imprinting: why bother? *Trends Genet* **13**, 323-9.
12. Driscoll, D. J., Waters, M. F., Williams, C. A., Zori, R. T., Glenn, C. C., Avidano, K. M. & Nicholls, R. D. (1992). A DNA methylation imprint, determined by the sex of the parent, distinguishes the Angelman and Prader-Willi syndromes. *Genomics* **13**, 917-24.
13. Reik, W. & Dean, W. (2001). DNA methylation and mammalian epigenetics. *Electrophoresis* **22**, 2838-43.
14. Bartolomei, M. S. & Ferguson-Smith, A. C. (2011). Mammalian genomic imprinting. *Cold Spring Harbor perspectives in biology* **3**.
15. Okano, M., Bell, D. W., Haber, D. A. & Li, E. (1999). DNA methyltransferases Dnmt3a and Dnmt3b are essential for de novo methylation and mammalian development. *Cell* **99**, 247-57.

16. Kaneda, M., Okano, M., Hata, K., Sado, T., Tsujimoto, N., Li, E. & Sasaki, H. (2004). Essential role for de novo DNA methyltransferase Dnmt3a in paternal and maternal imprinting. *Nature* **429**, 900-3.
17. Bourc'his, D., Xu, G. L., Lin, C. S., Bollman, B. & Bestor, T. H. (2001). Dnmt3L and the establishment of maternal genomic imprints. *Science* **294**, 2536-9.
18. Hata, K., Okano, M., Lei, H. & Li, E. (2002). Dnmt3L cooperates with the Dnmt3 family of de novo DNA methyltransferases to establish maternal imprints in mice. *Development* **129**, 1983-93.
19. Green, K., Lewis, A., Dawson, C., Dean, W., Reinhart, B., Chaillet, J. R. & Reik, W. (2007). A developmental window of opportunity for imprinted gene silencing mediated by DNA methylation and the Kcnq1ot1 noncoding RNA. *Mamm Genome* **18**, 32-42.
20. Mancini-Dinardo, D., Steele, S. J., Levorse, J. M., Ingram, R. S. & Tilghman, S. M. (2006). Elongation of the Kcnq1ot1 transcript is required for genomic imprinting of neighboring genes. *Genes Dev* **20**, 1268-82.
21. Umlauf, D., Goto, Y., Cao, R., Cerqueira, F., Wagschal, A., Zhang, Y. & Feil, R. (2004). Imprinting along the Kcnq1 domain on mouse chromosome 7 involves repressive histone methylation and recruitment of Polycomb group complexes. *Nat Genet* **36**, 1296-300.
22. John, R. M. & Lefebvre, L. (2011). Developmental regulation of somatic imprints. *Differentiation* **81**, 270-280.
23. Bhogal, B., Arnaudo, A., Dymkowski, A., Best, A. & Davis, T. L. (2004). Methylation at mouse Cdkn1c is acquired during postimplantation development and functions to maintain imprinted expression. *Genomics* **84**, 961-70.
24. Caspary, T., Cleary, M. A., Baker, C. C., Guan, X. J. & Tilghman, S. M. (1998). Multiple mechanisms regulate imprinting of the mouse distal chromosome 7 gene cluster. *Mol Cell Biol* **18**, 3466-74.
25. Fitzpatrick, G. V., Soloway, P. D. & Higgins, M. J. (2002). Regional loss of imprinting and growth deficiency in mice with a targeted deletion of KvDMR1. *Nat Genet* **32**, 426-31.
26. Searle, A. G. & Beechey, C. V. (1990). Genome imprinting phenomena on mouse chromosome 7. *Genet Res* **56**, 237-44.
27. Ono, R., Shiura, H., Aburatani, H., Kohda, T., Kaneko-Ishino, T. & Ishino, F. (2003). Identification of a large novel imprinted gene cluster on mouse proximal chromosome 6. *Genome Res* **13**, 1696-705.
28. Paulsen, M., Davies, K. R., Bowden, L. M., Villar, A. J., Franck, O., Fuermann, M., Dean, W. L., Moore, T. F., Rodrigues, N., Davies, K. E., Hu, R. J., Feinberg, A. P., Maher, E. R., Reik, W. &

- Walter, J. (1998). Syntenic organization of the mouse distal chromosome 7 imprinting cluster and the Beckwith-Wiedemann syndrome region in chromosome 11p15.5. *Hum Mol Genet* **7**, 1149-59.
29. Ainscough, J. F., John, R. M. & Surani, M. A. (1998). Mechanism of imprinting on mouse distal chromosome 7. *Genet Res* **72**, 237-45.
30. Alleman, M. & Doctor, J. (2000). Genomic imprinting in plants: observations and evolutionary implications. *Plant Mol Biol* **43**, 147-61.
31. Vinkenoog, R., Bushell, C., Spielman, M., Adams, S., Dickinson, H. G. & Scott, R. J. (2003). Genomic imprinting and endosperm development in flowering plants. *Mol Biotechnol* **25**, 149-84.
32. Killian, J. K., Nolan, C. M., Stewart, N., Munday, B. L., Andersen, N. A., Nicol, S. & Jirtle, R. L. (2001). Monotreme IGF2 expression and ancestral origin of genomic imprinting. *J Exp Zool* **291**, 205-12.
33. John, R. M. & Surani, M. A. (2000). Genomic imprinting, mammalian evolution, and the mystery of egg-laying mammals. *Cell* **101**, 585-8.
34. Suzuki, S., Renfree, M. B., Pask, A. J., Shaw, G., Kobayashi, S., Kohda, T., Kaneko-Ishino, T. & Ishino, F. (2005). Genomic imprinting of IGF2, p57(KIP2) and PEG1/MEST in a marsupial, the tammar wallaby. *Mech Dev* **122**, 213-22.
35. Staszkiwicz, J., Gimble, J., Cain, C., Dietrich, M., Burk, D., Kirk-Ballard, H. & Gawronska-Kozak, B. (2009). Flow cytometric and immunohistochemical detection of in vivo BrdU-labeled cells in mouse fat depots. *Biochemical and Biophysical Research Communications* **378**, 539-544.
36. Suzuki, S., Shaw, G., Kaneko-Ishino, T., Ishino, F. & Renfree, M. B. (2011). Characterisation of marsupial PHLDA2 reveals eutherian specific acquisition of imprinting. *BMC evolutionary biology* **11**, 244.
37. Zeller, U. & Freyer, C. (2001). Early ontogeny and placentation of the grey short-tailed opossum, *Monodelphis domestica* (Didelphidae : Marsupialia): contribution to the reconstruction of the marsupial morphotype. *Journal of Zoological Systematics and Evolutionary Research* **39**, 137-158.
38. Cypess, A. M., Zhang, H., Schulz, T. J., Huang, T. L., Espinoza, D. O., Kristiansen, K., Unterman, T. G. & Tseng, Y. H. (2011). Insulin/IGF-I regulation of neclin and brown adipocyte differentiation via CREB- and FoxO1-associated pathways. *Endocrinology* **152**, 3680-9.
39. Carter, A. M. & Mess, A. (2007). Evolution of the placenta in eutherian mammals. *Placenta* **28**, 259-62.
40. Moore, T. & Haig, D. (1991). Genomic imprinting in mammalian development: a parental tug-of-war. *Trends Genet* **7**, 45-9.
41. Haig, D. (1994). Refusing the ovarian time bomb. *Trends Genet* **10**, 346-7; author reply 348-9.

42. Haig, D. (1999). Multiple paternity and genomic imprinting. *Genetics* **151**, 1229-31.
43. Giannoukakis, N., Deal, C., Paquette, J., Goodyer, C. G. & Polychronakos, C. (1993). Parental genomic imprinting of the human IGF2 gene. *Nat Genet* **4**, 98-101.
44. Barlow, D. P., Stoger, R., Herrmann, B. G., Saito, K. & Schweifer, N. (1991). The mouse insulin-like growth factor type-2 receptor is imprinted and closely linked to the Tme locus. *Nature* **349**, 84-7.
45. DeChiara, T. M., Robertson, E. J. & Efstratiadis, A. (1991). Parental imprinting of the mouse insulin-like growth factor II gene. *Cell* **64**, 849-59.
46. DeChiara, T. M., Efstratiadis, A. & Robertson, E. J. (1990). A growth-deficiency phenotype in heterozygous mice carrying an insulin-like growth factor II gene disrupted by targeting. *Nature* **345**, 78-80.
47. Lau, M. M., Stewart, C. E., Liu, Z., Bhatt, H., Rotwein, P. & Stewart, C. L. (1994). Loss of the imprinted IGF2/cation-independent mannose 6-phosphate receptor results in fetal overgrowth and perinatal lethality. *Genes Dev* **8**, 2953-63.
48. Wang, Z. Q., Fung, M. R., Barlow, D. P. & Wagner, E. F. (1994). Regulation of embryonic growth and lysosomal targeting by the imprinted Igf2/Mpr gene. *Nature* **372**, 464-7.
49. Sun, F. L., Dean, W. L., Kelsey, G., Allen, N. D. & Reik, W. (1997). Transactivation of Igf2 in a mouse model of Beckwith-Wiedemann syndrome. *Nature* **389**, 809-15.
50. Murrell, A., Heeson, S., Cooper, W. N., Douglas, E., Apostolidou, S., Moore, G. E., Maher, E. R. & Reik, W. (2004). An association between variants in the IGF2 gene and Beckwith-Wiedemann syndrome: interaction between genotype and epigenotype. *Hum Mol Genet* **13**, 247-55.
51. Plagge, A., Isles, A. R., Gordon, E., Humby, T., Dean, W., Gritsch, S., Fischer-Colbrie, R., Wilkinson, L. S. & Kelsey, G. (2005). Imprinted Nesp55 influences behavioral reactivity to novel environments. *Molecular and cellular biology* **25**, 3019-26.
52. Varmuza, S. & Mann, M. (1994). Genomic imprinting--defusing the ovarian time bomb. *Trends Genet* **10**, 118-23.
53. Barlow, D. P. (1993). Methylation and imprinting: from host defense to gene regulation? *Science* **260**, 309-10.
54. Moore, T. & Haig, D. (1991). Genomic imprinting in mammalian development: a parental tug-of-war. *Trends in genetics : TIG* **7**, 45-9.
55. Cerrato, F., Sparago, A., Di Matteo, I., Zou, X. G., Dean, W., Sasaki, H., Smith, P., Genesio, R., Bruggemann, M., Reik, W. & Riccio, A. (2005). The two-domain hypothesis in Beckwith-Wiedemann syndrome: autonomous imprinting of the telomeric domain of the distal chromosome 7 cluster. *Human Molecular Genetics* **14**, 503-511.

56. Engemann, S., Stroedicke, M., Paulsen, M., Franck, O., Reinhardt, R., Lane, N., Reik, W. & Walter, J. (2000). Sequence and functional comparison in the Beckwith-Wiedemann region: implications for a novel imprinting centre and extended imprinting. *Hum Mol Genet* **9**, 2691-706.
57. Ferguson-Smith, A. C., Cattanach, B. M., Barton, S. C., Beechey, C. V. & Surani, M. A. (1991). Embryological and molecular investigations of parental imprinting on mouse chromosome 7. *Nature* **351**, 667-70.
58. Ferguson-Smith, A. C., Sasaki, H., Cattanach, B. M. & Surani, M. A. (1993). Parental-origin-specific epigenetic modification of the mouse H19 gene. *Nature* **362**, 751-5.
59. Beatty, L., Weksberg, R. & Sadowski, P. D. (2006). Detailed analysis of the methylation patterns of the KvDMR1 imprinting control region of human chromosome 11. *Genomics* **87**, 46-56.
60. Mancini-DiNardo, D., Steele, S. J. S., Ingram, R. S. & Tilghman, S. M. (2003). A differentially methylated region within the gene *Kcnq1* functions as an imprinted promoter and silencer. *Human molecular genetics* **12**, 283-294.
61. Thakur, N., Tiwari, V. K., Thomassin, H., Pandey, R. R., Kanduri, M., Gondor, A., Grange, T., Ohlsson, R. & Kanduri, C. (2004). An antisense RNA regulates the bidirectional silencing property of the *Kcnq1* imprinting control region. *Mol Cell Biol* **24**, 7855-62.
62. Higashimoto, K., Soejima, H., Saito, T., Okumura, K. & Mukai, T. (2006). Imprinting disruption of the *CDKN1C/KCNQ10T1* domain: the molecular mechanisms causing Beckwith-Wiedemann syndrome and cancer. *Cytogenetic and Genome Research* **113**, 306-312.
63. John, R. M., Hodges, M., Little, P., Barton, S. C. & Surani, M. A. (1999). A human p57(KIP2) transgene is not activated by passage through the maternal mouse germline. *Hum Mol Genet* **8**, 2211-9.
64. Nicholls, D. G. (1974). Hamster brown-adipose-tissue mitochondria. The control of respiration and the proton electrochemical potential gradient by possible physiological effectors of the proton conductance of the inner membrane. *European journal of biochemistry / FEBS* **49**, 573-83.
65. Fan, T., Hagan, J. P., Kozlov, S. V., Stewart, C. L. & Muegge, K. (2005). Lsh controls silencing of the imprinted *Cdkn1c* gene. *Development* **132**, 635-44.
66. Weksberg, R., Shen, D. R., Fei, Y. L., Song, Q. L. & Squire, J. (1993). Disruption of insulin-like growth factor 2 imprinting in Beckwith-Wiedemann syndrome. *Nat Genet* **5**, 143-50.
67. Weksberg, R. & Squire, J. A. (1996). Molecular biology of Beckwith-Wiedemann syndrome. *Med Pediatr Oncol* **27**, 462-9.
68. Gicquel, C., Rossignol, S., Cabrol, S., Houang, M., Steunou, V., Barbu, V., Danton, F., Thibaud, N., Le Merrer, M., Burglen, L., Bertrand, A. M., Netchine, I. & Le Bouc, Y. (2005). Epimutation

- of the telomeric imprinting center region on chromosome 11p15 in Silver-Russell syndrome. *Nat Genet* **37**, 1003-7.
69. Cannon, B. & Nedergaard, J. (2004). Brown adipose tissue: function and physiological significance. *Physiological reviews* **84**, 277-359.
 70. Osborn, D. P., Li, K., Hinitz, Y. & Hughes, S. M. (2011). Cdkn1c drives muscle differentiation through a positive feedback loop with Myod. *Developmental biology* **350**, 464-75.
 71. Wiedemann, H. R. (1964). [Familial Malformation Complex with Umbilical Hernia and Macroglossia--a "New Syndrome"?]. *J Genet Hum* **13**, 223-32.
 72. Choufani, S., Shuman, C. & Weksberg, R. (2010). Beckwith-Wiedemann syndrome. *American journal of medical genetics. Part C, Seminars in medical genetics* **154C**, 343-54.
 73. Lee, M. P., DeBaun, M., Randhawa, G., Reichard, B. A., Elledge, S. J. & Feinberg, A. P. (1997). Low frequency of p57KIP2 mutation in Beckwith-Wiedemann syndrome. *Am J Hum Genet* **61**, 304-9.
 74. Hatada, I., Ohashi, H., Fukushima, Y., Kaneko, Y., Inoue, M., Komoto, Y., Okada, A., Ohishi, S., Nabetani, A., Morisaki, H., Nakayama, M., Niikawa, N. & Mukai, T. (1996). An imprinted gene p57KIP2 is mutated in Beckwith-Wiedemann syndrome. *Nat Genet* **14**, 171-3.
 75. Hatada, I., Nabetani, A., Morisaki, H., Xin, Z., Ohishi, S., Tonoki, H., Niikawa, N., Inoue, M., Komoto, Y., Okada, A., Steichen, E., Ohashi, H., Fukushima, Y., Nakayama, M. & Mukai, T. (1997). New p57KIP2 mutations in Beckwith-Wiedemann syndrome. *Hum Genet* **100**, 681-3.
 76. Lee, M. P., DeBaun, M. R., Mitsuya, K., Galonek, H. L., Brandenburg, S., Oshimura, M. & Feinberg, A. P. (1999). Loss of imprinting of a paternally expressed transcript, with antisense orientation to KVLQT1, occurs frequently in Beckwith-Wiedemann syndrome and is independent of insulin-like growth factor II imprinting. *Proc Natl Acad Sci U S A* **96**, 5203-8.
 77. Diaz-Meyer, N., Day, C. D., Maher, E. R., Junien, C., Graham, G., Kaloustian, V. D. & Higgins, M. J. (2002). Epimutation at KvDMR1 leads to ablation of CDKN1C expression in patients with Beckwith-Wiedemann syndrome. *American Journal of Human Genetics* **71**, 492-492.
 78. Diaz-Meyer, N., Day, C. D., Khatod, K., Maher, E. R., Cooper, W., Reik, W., Junien, C., Graham, G., Algar, E., Der Kaloustian, V. M. & Higgins, M. J. (2003). Silencing of CDKN1C (p57KIP2) is associated with hypomethylation at KvDMR1 in Beckwith-Wiedemann syndrome. *J Med Genet* **40**, 797-801.
 79. Sibley, C. P., Coan, P. M., Ferguson-Smith, A. C., Dean, W., Hughes, J., Smith, P., Reik, W., Burton, G. J., Fowden, A. L. & Constancia, M. (2004). Placental-specific insulin-like growth factor 2 (Igf2) regulates the diffusional exchange characteristics of the mouse placenta. *Proc Natl Acad Sci U S A* **101**, 8204-8.

80. Bonaldi, A., Mazzeu, J. F., Costa, S. S., Honjo, R. S., Bertola, D. R., Albano, L. M., Furquim, I. M., Kim, C. A. & Vianna-Morgante, A. M. (2011). Microduplication of the ICR2 domain at chromosome 11p15 and familial Silver-Russell syndrome. *American journal of medical genetics. Part A* **155A**, 2479-83.
81. Eggermann, T., Schonherr, N., Meyer, E., Roos, A., Schmidt, A. & Wollmann, H. A. (2007). The centromeric 11p15 imprinting centre is also involved in Silver-Russell syndrome. *Journal of Medical Genetics* **44**, 59-63.
82. Obermann, C., Meyer, E., Prager, S., Tomiuk, J., Wollmann, H. A. & Eggermann, T. (2004). Searching for genomic variants in IGF2 and CDKN1C in Silver-Russell syndrome patients. *Molecular Genetics and Metabolism* **82**, 246-250.
83. Russell, C. (1954). A simple inexpensive bacterial colony counting device. *Biochimica et biophysica acta* **14**, 295.
84. Silver, H. K., Kiyasu, W., George, J. & Deamer, W. C. (1953). Syndrome of congenital hemihypertrophy, shortness of stature, and elevated urinary gonadotropins. *Pediatrics* **12**, 368-76.
85. Lazar, M. A. (2008). Developmental biology. How now, brown fat? *Science* **321**, 1048-9.
86. Hatada, I. & Mukai, T. (1995). Genomic imprinting of p57KIP2, a cyclin-dependent kinase inhibitor, in mouse. *Nat Genet* **11**, 204-6.
87. Lee, M. H., Reynisdottir, I. & Massague, J. (1995). Cloning of p57KIP2, a cyclin-dependent kinase inhibitor with unique domain structure and tissue distribution. *Genes Dev* **9**, 639-49.
88. Matsuoka, S., Edwards, M. C., Bai, C., Parker, S., Zhang, P., Baldini, A., Harper, J. W. & Elledge, S. J. (1995). p57KIP2, a structurally distinct member of the p21CIP1 Cdk inhibitor family, is a candidate tumor suppressor gene. *Genes Dev* **9**, 650-62.
89. Hatada, I., Inazawa, J., Abe, T., Nakayama, M., Kaneko, Y., Jinno, Y., Niikawa, N., Ohashi, H., Fukushima, Y., Iida, K., Yutani, C., Takahashi, S., Chiba, Y., Ohishi, S. & Mukai, T. (1996). Genomic imprinting of human p57KIP2 and its reduced expression in Wilms' tumors. *Hum Mol Genet* **5**, 783-8.
90. Westbury, J., Watkins, M., Ferguson-Smith, A. C. & Smith, J. (2001). Dynamic temporal and spatial regulation of the cdk inhibitor p57(kip2) during embryo morphogenesis. *Mech Dev* **109**, 83-9.
91. Nagahama, H., Hatakeyama, S., Nakayama, K., Nagata, M., Tomita, K. & Nakayama, K. (2001). Spatial and temporal expression patterns of the cyclin-dependent kinase (CDK) inhibitors p27Kip1 and p57Kip2 during mouse development. *Anat Embryol (Berl)* **203**, 77-87.

92. Itoh, Y., Masuyama, N., Nakayama, K., Nakayama, K. I. & Gotoh, Y. (2007). The cyclin-dependent kinase inhibitors p57 and p27 regulate neuronal migration in the developing mouse neocortex. *The Journal of biological chemistry* **282**, 390-6.
93. Sakai, K., Peraud, A., Mainprize, T., Nakayama, J., Tsugu, A., Hongo, K., Kobayashi, S. & Rutka, J. T. (2004). Inducible expression of p57KIP2 inhibits glioma cell motility and invasion. *Journal of neuro-oncology* **68**, 217-23.
94. Vlachos, P. & Joseph, B. (2009). The Cdk inhibitor p57(Kip2) controls LIM-kinase 1 activity and regulates actin cytoskeleton dynamics. *Oncogene* **28**, 4175-88.
95. Yokoo, T., Toyoshima, H., Miura, M., Wang, Y., Iida, K. T., Suzuki, H., Sone, H., Shimano, H., Gotoda, T., Nishimori, S., Tanaka, K. & Yamada, N. (2003). p57Kip2 regulates actin dynamics by binding and translocating LIM-kinase 1 to the nucleus. *The Journal of biological chemistry* **278**, 52919-23.
96. Dyer, M. A. & Cepko, C. L. (2000). p57(Kip2) regulates progenitor cell proliferation and amacrine interneuron development in the mouse retina. *Development* **127**, 3593-605.
97. Joseph, B., Wallen-Mackenzie, A., Benoit, G., Murata, T., Joodmardi, E., Okret, S. & Perlmann, T. (2003). p57(Kip2) cooperates with Nurr1 in developing dopamine cells. *Proceedings of the National Academy of Sciences of the United States of America* **100**, 15619-24.
98. Joseph, B., Andersson, E. R., Vlachos, P., Sodersten, E., Liu, L., Teixeira, A. I. & Hermanson, O. (2009). p57Kip2 is a repressor of Mash1 activity and neuronal differentiation in neural stem cells. *Cell death and differentiation* **16**, 1256-65.
99. Reynaud, E. G., Pospel, K., Guillier, M., Leibovitch, M. P. & Leibovitch, S. A. (1999). p57(Kip2) stabilizes the MyoD protein by inhibiting cyclin E-Cdk2 kinase activity in growing myoblasts. *Molecular and Cellular Biology* **19**, 7621-7629.
100. Reynaud, E. G., Leibovitch, M. P., Tintignac, L. A. J., Pospel, K., Guillier, M. & Leibovitch, S. A. (2000). Stabilization of MyoD by direct binding to p57(Kip2). *Journal of Biological Chemistry* **275**, 18767-18776.
101. Takahashi, K., Nakayama, K. & Nakayama, K. (2000). Mice lacking a CDK inhibitor, p57Kip2, exhibit skeletal abnormalities and growth retardation. *J Biochem (Tokyo)* **127**, 73-83.
102. Yan, Y., Frisen, J., Lee, M. H., Massague, J. & Barbacid, M. (1997). Ablation of the CDK inhibitor p57Kip2 results in increased apoptosis and delayed differentiation during mouse development. *Genes Dev* **11**, 973-83.
103. Zhang, P., Liegeois, N. J., Wong, C., Finegold, M., Hou, H., Thompson, J. C., Silverman, A., Harper, J. W., DePinho, R. A. & Elledge, S. J. (1997). Altered cell differentiation and

- proliferation in mice lacking p57KIP2 indicates a role in Beckwith-Wiedemann syndrome. *Nature* **387**, 151-8.
104. Tunster, S. J., Van de Pette, M. & John, R. M. (2011). Fetal overgrowth in the Cdkn1c mouse model of Beckwith-Wiedemann syndrome. *Disease models & mechanisms* **4**, 814-21.
 105. Tunster, S. J., Van De Pette, M. & John, R. M. (2011). BACs as Tools for the Study of Genomic Imprinting. *Journal of Biomedicine and Biotechnology* **2011**.
 106. John, R. M., Ainscough, J. F. X., Barton, S. C. & Surani, M. A. (2001). Distant cis-elements regulate imprinted expression of the mouse p57(KiP2) (Cdkn1C) gene: implications for the human disorder, Beckwith-Wiedemann syndrome. *Human Molecular Genetics* **10**, 1601-1609.
 107. Andrews, S. C., Wood, M. D., Tunster, S. J., Barton, S. C., Surani, M. A. & John, R. M. (2007). Cdkn1c (p57Kip2) is the major regulator of embryonic growth within its imprinted domain on mouse distal chromosome 7. *BMC Dev Biol* **7**, 53.
 108. Qian, N., Frank, D., O'Keefe, D., Dao, D., Zhao, L., Yuan, L., Wang, Q., Keating, M., Walsh, C. & Tycko, B. (1997). The IPL gene on chromosome 11p15.5 is imprinted in humans and mice and is similar to TDAG51, implicated in Fas expression and apoptosis. *Hum Mol Genet* **6**, 2021-9.
 109. Frank, D., Fortino, W., Clark, L., Musalo, R., Wang, W., Saxena, A., Li, C. M., Reik, W., Ludwig, T. & Tycko, B. (2002). Placental overgrowth in mice lacking the imprinted gene Ipl. *Proceedings of the National Academy of Sciences of the United States of America* **99**, 7490-5.
 110. Salas, M., John, R., Saxena, A., Barton, S., Frank, D., Fitzpatrick, G., Higgins, M. J. & Tycko, B. (2004). Placental growth retardation due to loss of imprinting of Phlda2. *Mech Dev* **121**, 1199-210.
 111. Tunster, S. J., Tycko, B. & John, R. M. (2010). The imprinted Phlda2 gene regulates extraembryonic energy stores. *Molecular and cellular biology* **30**, 295-306.
 112. Coan, P. M., Ferguson-Smith, A. C. & Burton, G. J. (2004). Developmental dynamics of the definitive mouse placenta assessed by stereology. *Biol Reprod* **70**, 1806-13.
 113. Apostolidou, S., Abu-Amero, S., O'Donoghue, K., Frost, J., Olafsdottir, O., Chavele, K. M., Whittaker, J. C., Loughna, P., Stanier, P. & Moore, G. E. (2007). Elevated placental expression of the imprinted PHLDA2 gene is associated with low birth weight. *J Mol Med* **85**, 379-87.
 114. McMinn, J., Wei, M., Schupf, N., Cusmai, J., Johnson, E. B., Smith, A. C., Weksberg, R., Thaker, H. M. & Tycko, B. (2006). Unbalanced placental expression of imprinted genes in human intrauterine growth restriction. *Placenta* **27**, 540-9.
 115. Lewis, R. M., Cleal, J. K., Ntani, G., Crozier, S. R., Mahon, P. A., Robinson, S. M., Harvey, N. C., Cooper, C., Inskip, H. M., Godfrey, K. M., Hanson, M. A. & John, R. M. (2012). Relationship

- between placental expression of the imprinted PHLDA2 gene, intrauterine skeletal growth and childhood bone mass. *Bone* **50**, 337-42.
116. Dao, D., Frank, D., Qian, N., O'Keefe, D., Vosatka, R. J., Walsh, C. P. & Tycko, B. (1998). IMPT1, an imprinted gene similar to polyspecific transporter and multi-drug resistance genes. *Hum Mol Genet* **7**, 597-608.
 117. Gessner, C. (1551). *Conradi Gesneri medici Tigurine Historiae Animalium: Lib. I De Quadrupedibus viviparis*.
 118. Bulychhev, A., Kramar, R., Drahota, Z. & Lindberg, O. (1972). Role of a specific endogenous fatty acid fraction in the coupling-uncoupling mechanism of oxidative phosphorylation of brown adipose tissue. *Experimental cell research* **72**, 169-87.
 119. Cunningham, S. A., Wiesinger, H. & Nicholls, D. G. (1986). Quantification of Fatty-Acid Activation of the Uncoupling Protein in Brown Adipocytes and Mitochondria from the Guinea-Pig. *European Journal of Biochemistry* **157**, 415-420.
 120. Locke, R. M., Rial, E., Scott, I. D. & Nicholls, D. G. (1982). Fatty-Acids as Acute Regulators of the Proton Conductance of Hamster Brown-Fat Mitochondria. *European Journal of Biochemistry* **129**, 373-380.
 121. Gerard, M., Hernandez, L., Wevrick, R. & Stewart, C. L. (1999). Disruption of the mouse necdin gene results in early post-natal lethality. *Nature genetics* **23**, 199-202.
 122. MacDonald, H. R. & Wevrick, R. (1997). The necdin gene is deleted in Prader-Willi syndrome and is imprinted in human and mouse. *Human molecular genetics* **6**, 1873-8.
 123. Jay, P., Rougeulle, C., Massacrier, A., Moncla, A., Mattei, M. G., Malzac, P., Roeckel, N., Taviaux, S., Lefranc, J. L., Cau, P., Berta, P., Lalande, M. & Muscatelli, F. (1997). The human necdin gene, NDN, is maternally imprinted and located in the Prader-Willi syndrome chromosomal region. *Nature genetics* **17**, 357-61.
 124. Ohno, H., Shinoda, K., Spiegelman, B. M. & Kajimura, S. (2012). PPARgamma agonists induce a white-to-brown fat conversion through stabilization of PRDM16 protein. *Cell metabolism* **15**, 395-404.
 125. Cinti, S. (2005). The adipose organ. *Prostaglandins Leukotrienes and Essential Fatty Acids* **73**, 9-15.
 126. Aebischer, J., Sturny, R., Andrieu, D., Rieusset, A., Schaller, F., Geib, S., Raoul, C. & Muscatelli, F. (2011). Necdin protects embryonic motoneurons from programmed cell death. *PloS one* **6**, e23764.

127. Andrieu, D., Meziane, H., Marly, F., Angelats, C., Fernandez, P. A. & Muscatelli, F. (2006). Sensory defects in Necdin deficient mice result from a loss of sensory neurons correlated within an increase of developmental programmed cell death. *BMC developmental biology* **6**, 56.
128. Ma, Y., Chen, L., Wright, G. M., Pillai, S. R., Chellappan, S. P. & Cress, W. D. (2010). CDKN1C negatively regulates RNA polymerase II C-terminal domain phosphorylation in an E2F1-dependent manner. *The Journal of biological chemistry* **285**, 9813-22.
129. Kozak, L. P., Britton, J. H., Kozak, U. C. & Wells, J. M. (1988). The mitochondrial uncoupling protein gene. Correlation of exon structure to transmembrane domains. *The Journal of biological chemistry* **263**, 12274-7.
130. Nicholls, D. G., Bernson, V. S. & Heaton, G. M. (1978). The identification of the component in the inner membrane of brown adipose tissue mitochondria responsible for regulating energy dissipation. *Experientia. Supplementum* **32**, 89-93.
131. Moore, T. (2012). Review: Parent-offspring conflict and the control of placental function. *Placenta* **33 Suppl**, S33-6.
132. Klingenberg, M., Echtay, K. S., Bienengraeber, M., Winkler, E. & Huang, S. G. (1999). Structure-function relationship in UCP1. *International journal of obesity and related metabolic disorders : journal of the International Association for the Study of Obesity* **23 Suppl 6**, S24-9.
133. Rosen, E. D. & MacDougald, O. A. (2006). Adipocyte differentiation from the inside out. *Nature reviews. Molecular cell biology* **7**, 885-96.
134. Hope, P. J., Pyle, D., Daniels, C. B., Chapman, I., Horowitz, M., Morley, J. E., Trayhurn, P., Kumaratilake, J. & Wittert, G. (1997). Identification of brown fat and mechanisms for energy balance in the marsupial, *Sminthopsis crassicaudata*. *American Journal of Physiology-Regulatory Integrative and Comparative Physiology* **273**, R161-R167.
135. Kabat, A. P., Rose, R. W. & West, A. K. (2003). Non-shivering thermogenesis in a carnivorous marsupial *Sarcophilus harrisii*, in the absence of UCP1. *Journal of Thermal Biology* **28**, 413-420.
136. Rose, R. W. & Ikonopoulou, M. P. (2005). Shivering and non-shivering thermogenesis in a marsupial, the eastern barred bandicoot (*Perameles gunnii*). *Journal of Thermal Biology* **30**, 85-92.
137. Kabat, A. P., Rose, R. W. & West, A. K. (2007). Shivering, muscle tone, and uncoupling proteins in a developing marsupial, the Tasmanian bettong (*Bettongia gaimardi*). *Journal of Thermal Biology* **32**, 282-292.
138. Saito, S., Saito, C. T. & Shingai, R. (2008). Adaptive evolution of the uncoupling protein 1 gene contributed to the acquisition of novel nonshivering thermogenesis in ancestral eutherian mammals. *Gene* **408**, 37-44.

139. Nedergaard, J., Bengtsson, T. & Cannon, B. (2007). Unexpected evidence for active brown adipose tissue in adult humans. *American Journal of Physiology-Endocrinology and Metabolism* **293**, E444-E452.
140. Cinti, S., Zingaretti, M. C., Crosta, F., Vitali, A., Guerrieri, M., Frontini, A., Cannon, B. & Nedergaard, J. (2009). The presence of UCPI demonstrates that metabolically active adipose tissue in the neck of adult humans truly represents brown adipose tissue. *Faseb Journal* **23**, 3113-3120.
141. Pond, C. M. (1992). An evolutionary and functional view of mammalian adipose tissue. *The Proceedings of the Nutrition Society* **51**, 367-77.
142. Surwit, R. S., Kuhn, C. M., Cochrane, C., McCubbin, J. A. & Feinglos, M. N. (1988). Diet-induced type II diabetes in C57BL/6J mice. *Diabetes* **37**, 1163-7.
143. Zhang, Y., Proenca, R., Maffei, M., Barone, M., Leopold, L. & Friedman, J. M. (1994). Positional cloning of the mouse obese gene and its human homologue. *Nature* **372**, 425-32.
144. Kaufman, M. H. (1992). *The Atlas of Mouse Development*. 2nd edit, 1. 1 vols, Academic Press, London.
145. Park, B. H., Qiang, L. & Farmer, S. R. (2004). Phosphorylation of C/EBPbeta at a consensus extracellular signal-regulated kinase/glycogen synthase kinase 3 site is required for the induction of adiponectin gene expression during the differentiation of mouse fibroblasts into adipocytes. *Molecular and Cellular Biology* **24**, 8671-80.
146. Li, X., Kim, J. W., Gronborg, M., Urlaub, H., Lane, M. D. & Tang, Q. Q. (2007). Role of cdk2 in the sequential phosphorylation/activation of C/EBPbeta during adipocyte differentiation. *Proceedings of the National Academy of Sciences of the United States of America* **104**, 11597-602.
147. Murre, C., McCaw, P. S. & Baltimore, D. (1989). A new DNA binding and dimerization motif in immunoglobulin enhancer binding, daughterless, MyoD, and myc proteins. *Cell* **56**, 777-83.
148. Akira, S., Tanaka, T., Yoshida, N. & Kishimoto, T. (1997). Defective adipocyte differentiation in mice lacking the C/EBP beta and/or C/EBP delta gene. *Embo Journal* **16**, 7432-7443.
149. Carmona, M. C., Hondares, E., De La Concepcion, M. L. R., Rodriguez-Sureda, V., Peinado-Onsurbe, J., Poli, V., Iglesias, R., Villarroya, F. & Giralt, M. (2005). Defective thermoregulation, impaired lipid metabolism, but preserved adrenergic induction of gene expression in brown fat of mice lacking C/EBP beta. *Biochemical Journal* **389**, 47-56.
150. Barak, Y., Nelson, M. C., Ong, E. S., Jones, Y. Z., Ruiz-Lozano, P., Chien, K. R., Koder, A. & Evans, R. M. (1999). PPAR gamma is required for placental, cardiac, and adipose tissue development. *Molecular cell* **4**, 585-95.

151. Rosen, E. D., Sarraf, P., Troy, A. E., Bradwin, G., Moore, K., Milstone, D. S., Spiegelman, B. M. & Mortensen, R. M. (1999). PPAR gamma is required for the differentiation of adipose tissue in vivo and in vitro. *Mol Cell* **4**, 611-7.
152. Coe, N. R., Simpson, M. A. & Bernlohr, D. A. (1999). Targeted disruption of the adipocyte lipid-binding protein (aP2 protein) gene impairs fat cell lipolysis and increases cellular fatty acid levels. *Journal of Lipid Research* **40**, 967-972.
153. Wu, Z., Rosen, E. D., Brun, R., Hauser, S., Adelmant, G., Troy, A. E., McKeon, C., Darlington, G. J. & Spiegelman, B. M. (1999). Cross-regulation of C/EBP alpha and PPAR gamma controls the transcriptional pathway of adipogenesis and insulin sensitivity. *Mol Cell* **3**, 151-8.
154. Seale, P., Kajimura, S., Yang, W., Chin, S., Rohas, L. M., Uldry, M., Tavernier, G., Langin, D. & Spiegelman, B. M. (2007). Transcriptional Control of Brown Fat Determination by PRDM16. *Cell metabolism* **6**, 38-54.
155. Spiegelman, B. M., Kajimura, S., Seale, P., Tomaru, T., Erdjument-Bromage, H., Cooper, M. P., Ruas, J. L., Chin, S., Tempst, P. & Lazar, M. A. (2008). Regulation of the brown and white fat gene programs through a PRDM16/CtBP transcriptional complex. *Genes & Development* **22**, 1397-1409.
156. Spiegelman, B. M., Kajimura, S., Seale, P., Kubota, K., Lunsford, E., Frangioni, J. V. & Gygi, S. P. (2009). Initiation of myoblast to brown fat switch by a PRDM16-C/EBP-beta transcriptional complex. *Nature* **460**, 1154-U125.
157. Seale, P., Bjork, B., Yang, W., Kajimura, S., Chin, S., Kuang, S., Scime, A., Devarakonda, S., Conroe, H. M., Erdjument-Bromage, H., Tempst, P., Rudnicki, M. A., Beier, D. R. & Spiegelman, B. M. (2008). PRDM16 controls a brown fat/skeletal muscle switch. *Nature* **454**, 961-967.
158. Fruhbeck, G., Sesma, P. & Burrell, M. A. (2009). PRDM16: the interconvertible adipo-myocyte switch. *Trends in Cell Biology* **19**, 141-146.
159. Tseng, Y. H., Butte, A. J., Kokkotou, E., Yechoor, V. K., Taniguchi, C. M., Kriauciunas, K. M., Cypess, A. M., Niinobe, M., Yoshikawa, K., Patti, M. E. & Kahn, C. R. (2005). Prediction of preadipocyte differentiation by gene expression reveals role of insulin receptor substrates and necdin. *Nature cell biology* **7**, 601-11.
160. Sul, H. S. (2009). Minireview: Pref-1: role in adipogenesis and mesenchymal cell fate. *Molecular endocrinology* **23**, 1717-25.
161. Bonet, M. L., Mercader, J., Ribot, J., Murano, I., Felipe, F., Cinti, S. & Palou, A. (2006). Remodeling of white adipose tissue after retinoic acid administration in mice. *Endocrinology* **147**, 5325-5332.

162. Klingenspor, M. (2003). Cold-induced recruitment of brown adipose tissue thermogenesis. *Experimental Physiology* **88**, 141-148.
163. Blanchette-Mackie, E. J., Dwyer, N. K., Barber, T., Coxey, R. A., Takeda, T., Rondinone, C. M., Theodorakis, J. L., Greenberg, A. S. & Londos, C. (1995). Perilipin is located on the surface layer of intracellular lipid droplets in adipocytes. *Journal of lipid research* **36**, 1211-26.
164. Lebrasseur, N. K. (2012). Building muscle, browning fat and preventing obesity by inhibiting myostatin. *Diabetologia* **55**, 13-7.
165. Reik, W., Constancia, M., Fowden, A., Anderson, N., Dean, W., Ferguson-Smith, A., Tycko, B. & Sibley, C. (2003). Regulation of supply and demand for maternal nutrients in mammals by imprinted genes. *Journal of Physiology-London* **547**, 35-44.
166. Tycko, B. & Morison, I. M. (2002). Physiological functions of imprinted genes. *J Cell Physiol* **192**, 245-58.
167. Bartolomei, M. S. (2009). Genomic imprinting: employing and avoiding epigenetic processes. *Genes Dev* **23**, 2124-33.
168. Sekita, Y., Wagatsuma, H., Nakamura, K., Ono, R., Kagami, M., Wakisaka, N., Hino, T., Suzuki-Migishima, R., Kohda, T., Ogura, A., Ogata, T., Yokoyama, M., Kaneko-Ishino, T. & Ishino, F. (2008). Role of retrotransposon-derived imprinted gene, Rtl1, in the feto-maternal interface of mouse placenta. *Nat Genet* **40**, 243-8.
169. Smith, F. M., Garfield, A. S. & Ward, A. (2006). Regulation of growth and metabolism by imprinted genes. *Cytogenet Genome Res* **113**, 279-91.
170. Kelsey, G., Frontera, M., Dickins, B. & Plagge, A. (2008). Imprinted genes, postnatal adaptations and enduring effects on energy homeostasis. *Genomic Imprinting* **626**, 41-61.
171. Isles, A. R. & Holland, A. J. (2005). Imprinted genes and mother-offspring interactions. *Early Hum Dev* **81**, 73-7.
172. Isles, A. R., Davies, W. & Wilkinson, L. S. (2006). Genomic imprinting and the social brain. *Philos Trans R Soc Lond B Biol Sci* **361**, 2229-37.
173. Haig, D. (2000). The kinship theory of genomic imprinting. *Annual Review of Ecology and Systematics* **31**, 9-32.
174. Haig, D. (2004). Genomic imprinting and kinship: how good is the evidence? *Annual review of genetics* **38**, 553-85.
175. Haig, D. (2008). Huddling: brown fat, genomic imprinting and the warm inner glow. *Current biology : CB* **18**, R172-4.
176. Villena, J. A., Carmona, M. C., Rodriguez de la Concepcion, M., Rossmeisl, M., Vinas, O., Mampel, T., Iglesias, R., Giralt, M. & Villarroya, F. (2002). Mitochondrial biogenesis in brown

- adipose tissue is associated with differential expression of transcription regulatory factors. *Cell Mol Life Sci* **59**, 1934-44.
177. Vrang, N., Meyre, D., Froguel, P., Jelsing, J., Tang-Christensen, M., Vatin, V., Mikkelsen, J. D., Thirstrup, K., Larsen, L. K., Cullberg, K. B., Fahrenkrug, J., Jacobson, P., Sjostrom, L., Carlsson, L. M., Liu, Y., Liu, X., Deng, H. W. & Larsen, P. J. The imprinted gene neuronatin is regulated by metabolic status and associated with obesity. *Obesity (Silver Spring)* **18**, 1289-96.
 178. Small, K. S., Hedman, A. K., Grundberg, E., Nica, A. C., Thorleifsson, G., Kong, A., Thorsteindottir, U., Shin, S. Y., Richards, H. B., Soranzo, N., Ahmadi, K. R., Lindgren, C. M., Stefansson, K., Dermitzakis, E. T., Deloukas, P., Spector, T. D. & McCarthy, M. I. Identification of an imprinted master trans regulator at the KLF14 locus related to multiple metabolic phenotypes. *Nat Genet* **43**, 561-4.
 179. Charalambous, M., Ferron, S. R., da Rocha, S. T., Murray, A. J., Rowland, T., Ito, M., Schuster-Gossler, K., Hernandez, A. & Ferguson-Smith, A. C. Imprinted gene dosage is critical for the transition to independent life. *Cell Metab* **15**, 209-21.
 180. John, R. M., Andrews, S. C., Wood, M. D., Tunster, S. J., Barton, S. C. & Surani, M. A. (2007). Cdkn1c (p57(Kip2)) is the major regulator of embryonic growth within its imprinted domain on mouse distal chromosome 7. *Bmc Developmental Biology* **7**.
 181. Soukas, A., Socci, N. D., Saatkamp, B. D., Novelli, S. & Friedman, J. M. (2001). Distinct transcriptional profiles of adipogenesis in vivo and in vitro. *The Journal of biological chemistry* **276**, 34167-74.
 182. Livak, K. J. & Schmittgen, T. D. (2001). Analysis of relative gene expression data using real-time quantitative PCR and the 2(-Delta Delta C(T)) Method. *Methods* **25**, 402-8.
 183. Bradford, M. M. (1976). A rapid and sensitive method for the quantitation of microgram quantities of protein utilizing the principle of protein-dye binding. *Analytical biochemistry* **72**, 248-54.
 184. Duckers, E. J., Yang, Z. Y., San, H., Gordon, D., Nabel, G. J. & Nabel, E. G. (1997). A novel function of the cyclin dependent kinase inhibitor p57(KIP2) in human atherosclerosis. *Circulation* **96**, 1584-1584.
 185. Caspary, T., Cleary, M. A., Perlman, E. J., Zhang, P., Elledge, S. J. & Tilghman, S. M. (1999). Oppositely imprinted genes p57(Kip2) and igf2 interact in a mouse model for Beckwith-Wiedemann syndrome. *Genes Dev* **13**, 3115-24.
 186. Takahashi, K., Kobayashi, T. & Kanayama, N. (2000). p57(Kip2) regulates the proper development of labyrinthine and spongiotrophoblasts. *Mol Hum Reprod* **6**, 1019-25.

187. Zacharek, S. J., Fillmore, C. M., Lau, A. N., Gludish, D. W., Chou, A., Ho, J. W., Zamponi, R., Gazit, R., Bock, C., Jager, N., Smith, Z. D., Kim, T. M., Saunders, A. H., Wong, J., Lee, J. H., Roach, R. R., Rossi, D. J., Meissner, A., Gimelbrant, A. A., Park, P. J. & Kim, C. F. (2011). Lung stem cell self-renewal relies on BMI1-dependent control of expression at imprinted loci. *Cell stem cell* **9**, 272-81.
188. Matsumoto, A. & Nakayama, K. I. (2012). Role of key regulators of the cell cycle in maintenance of hematopoietic stem cells. *Biochimica et biophysica acta*.
189. Hochli, M., Hochli, L. & Hackenbrock, C. R. (1985). Independent lateral diffusion of cytochrome bc1 complex and cytochrome oxidase in the mitochondrial inner membrane. *European journal of cell biology* **38**, 1-5.
190. Hackenbrock, C. R., Chazotte, B. & Gupte, S. S. (1986). The random collision model and a critical assessment of diffusion and collision in mitochondrial electron transport. *Journal of bioenergetics and biomembranes* **18**, 331-68.
191. Xie, W. L., Chipman, J. G., Robertson, D. L., Erikson, R. L. & Simmons, D. L. (1991). Expression of a mitogen-responsive gene encoding prostaglandin synthase is regulated by mRNA splicing. *Proceedings of the National Academy of Sciences of the United States of America* **88**, 2692-6.
192. Zuo, Y., Qiang, L. & Farmer, S. R. (2006). Activation of CCAAT/enhancer-binding protein (C/EBP) alpha expression by C/EBP beta during adipogenesis requires a peroxisome proliferator-activated receptor-gamma-associated repression of HDAC1 at the C/ebp alpha gene promoter. *The Journal of biological chemistry* **281**, 7960-7.
193. Parker, M. G. & Christian, M. (2010). The Engineering of Brown Fat. *Journal of Molecular Cell Biology* **2**, 23-25.
194. Dixon, T. M., Daniel, K. W., Farmer, S. R. & Collins, S. (2001). CCAAT/enhancer-binding protein alpha is required for transcription of the beta(3)-adrenergic receptor gene during adipogenesis. *Journal of Biological Chemistry* **276**, 722-728.
195. Barbera, M. J., Schluter, A., Pedraza, N., Iglesias, P., Villarroya, F. & Giralt, M. (2001). Peroxisome proliferator-activated receptor alpha activates transcription of the brown fat uncoupling protein-1 gene - A link between regulation of the thermogenic and lipid oxidation pathways in the brown fat cell. *Journal of Biological Chemistry* **276**, 1486-1493.
196. Tsuchida, A., Yamauchi, T., Takekawa, S., Hada, Y., Ito, Y., Maki, T. & Kadowaki, T. (2005). Peroxisome proliferator-activated receptor (PPAR)alpha activation increases adiponectin receptors and reduces obesity-related inflammation in adipose tissue - Comparison of activation of PPAR alpha, PPAR-gamma, and their combination. *Diabetes* **54**, 3358-3370.

197. Shabalina, I. G., Hoeks, J., Kramarova, T. V., Schrauwen, P., Cannon, B. & Nedergaard, J. (2010). Cold tolerance of UCP1-ablated mice: a skeletal muscle mitochondria switch toward lipid oxidation with marked UCP3 up-regulation not associated with increased basal, fatty acid- or ROS-induced uncoupling or enhanced GDP effects. *Biochimica et biophysica acta* **1797**, 968-80.
198. Tang, Q. Q., Gronborg, M., Huang, H., Kim, J. W., Otto, T. C., Pandey, A. & Lane, M. D. (2005). Sequential phosphorylation of CCAAT enhancer-binding protein beta by MAPK and glycogen synthase kinase 3beta is required for adipogenesis. *Proceedings of the National Academy of Sciences of the United States of America* **102**, 9766-71.
199. Souza, S. C., Christoffolete, M. A., Ribeiro, M. O., Miyoshi, H., Strissel, K. J., Stancheva, Z. S., Rogers, N. H., D'Eon, T. M., Perfield, J. W., Imachi, H., Obin, M. S., Bianco, A. C. & Greenberg, A. S. (2007). Perilipin regulates the thermogenic actions of norepinephrine in brown adipose tissue. *Journal of Lipid Research* **48**, 1273-1279.
200. Miyoshi, H., Souza, S. C., Zhang, H. H., Strissel, K. J., Christoffolete, M. A., Kovsan, J., Rudich, A., Kraemer, F. B., Bianco, A. C., Obin, M. S. & Greenberg, A. S. (2006). Perilipin promotes hormone-sensitive lipase-mediated adipocyte lipolysis via phosphorylation-dependent and -independent mechanisms. *The Journal of biological chemistry* **281**, 15837-44.
201. Park, Y. K. & Park, H. (2010). Prevention of CCAAT/enhancer-binding protein beta DNA binding by hypoxia during adipogenesis. *The Journal of biological chemistry* **285**, 3289-99.
202. Hughes, S. M., Osborn, D. P. S., Li, K. Y. & Hinitz, Y. (2011). Cdkn1c drives muscle differentiation through a positive feedback loop with Myod. *Developmental Biology* **350**, 464-475.
203. Tontonoz, P., Hu, E. & Spiegelman, B. M. (1994). Stimulation of adipogenesis in fibroblasts by PPAR gamma 2, a lipid-activated transcription factor. *Cell* **79**, 1147-56.
204. Tontonoz, P., Hu, E., Graves, R. A., Budavari, A. I. & Spiegelman, B. M. (1994). mPPAR gamma 2: tissue-specific regulator of an adipocyte enhancer. *Genes & development* **8**, 1224-34.
205. Seale, P., Conroe, H. M., Estall, J., Kajimura, S., Frontini, A., Ishibashi, J., Cohen, P., Cinti, S. & Spiegelman, B. M. (2011). Prdm16 determines the thermogenic program of subcutaneous white adipose tissue in mice. *The Journal of clinical investigation* **121**, 96-105.
206. Mercader, J., Palou, A. & Luisa Bonet, M. (2010). Induction of Uncoupling Protein-1 in Mouse Embryonic Fibroblast-derived Adipocytes by Retinoic Acid. *Obesity* **18**, 655-662.
207. Alvarez, R., de Andres, J., Yubero, P., Vinas, O., Mampel, T., Iglesias, R., Giralt, M. & Villarroya, F. (1995). A novel regulatory pathway of brown fat thermogenesis. Retinoic acid is a transcriptional activator of the mitochondrial uncoupling protein gene. *The Journal of biological chemistry* **270**, 5666-73.

208. Puigserver, P., Vazquez, F., Bonet, M. L., Pico, C. & Palou, A. (1996). In vitro and in vivo induction of brown adipocyte uncoupling protein (thermogenin) by retinoic acid. *The Biochemical journal* **317** (Pt 3), 827-33.
209. Bonet, M. L., Mercader, J., Ribot, J., Murano, I., Feddersen, S., Cinti, S., Madsen, L., Kristiansen, K. & Palou, A. (2009). Haploinsufficiency of the retinoblastoma protein gene reduces diet-induced obesity, insulin resistance, and hepatosteatosis in mice. *American Journal of Physiology-Endocrinology and Metabolism* **297**, E184-E193.
210. Toh, S. Y., Gong, J., Du, G., Li, J. Z., Yang, S., Ye, J., Yao, H., Zhang, Y., Xue, B., Li, Q., Yang, H., Wen, Z. & Li, P. (2008). Up-regulation of mitochondrial activity and acquirement of brown adipose tissue-like property in the white adipose tissue of fsp27 deficient mice. *PloS one* **3**, e2890.
211. Ginter, E. & Simko, V. (2012). Brown fat tissue - a potential target to combat obesity. *Bratislavske lekarske listy* **113**, 52-6.
212. Hu, F. B., Manson, J. E., Stampfer, M. J., Colditz, G., Liu, S., Solomon, C. G. & Willett, W. C. (2001). Diet, lifestyle, and the risk of type 2 diabetes mellitus in women. *The New England journal of medicine* **345**, 790-7.
213. Hu, C. C., Qing, K. & Chen, Y. (2004). Diet-induced changes in stearyl-CoA desaturase 1 expression in obesity-prone and -resistant mice. *Obesity research* **12**, 1264-70.
214. Almind, K. & Kahn, C. R. (2004). Genetic determinants of energy expenditure and insulin resistance in diet-induced obesity in mice. *Diabetes* **53**, 3274-85.
215. Strom, K., Hansson, O., Lucas, S., Nevsten, P., Fernandez, C., Klint, C., Moverare-Skrtic, S., Sundler, F., Ohlsson, C. & Holm, C. (2008). Attainment of Brown Adipocyte Features in White Adipocytes of Hormone-Sensitive Lipase Null Mice. *Plos One* **3**.
216. Gloyn, A. L., Suliman, S. G. L., Stanik, J., McCulloch, L. J., Wilson, N., Edghill, E. L., Misovicova, N., Gasperikova, D., Sandrikova, V., Elliott, K. S., Barak, L., Ellard, S., Volpi, E. V. & Klimes, I. (2009). Severe Insulin Resistance and Intrauterine Growth Deficiency Associated With Haploinsufficiency for INSR and CHN2 New Insights Into Synergistic Pathways Involved in Growth and Metabolism. *Diabetes* **58**, 2954-2961.
217. Smilnich, N. J., Day, C. D., Fitzpatrick, G. V., Caldwell, G. M., Lossie, A. C., Cooper, P. R., Smallwood, A. C., Joyce, J. A., Schofield, P. N., Reik, W., Nicholls, R. D., Weksberg, R., Driscoll, D. J., Maher, E. R., Shows, T. B. & Higgins, M. J. (1999). A maternally methylated CpG island in KvLQT1 is associated with an antisense paternal transcript and loss of imprinting in Beckwith-Wiedemann syndrome. *Proc Natl Acad Sci U S A* **96**, 8064-9.

218. Xin, Z., Soejima, H., Higashimoto, K., Yatsuki, H., Zhu, X., Satoh, Y., Masaki, Z., Kaneko, Y., Jinno, Y., Fukuzawa, R., Hata, J. & Mukai, T. (2000). A novel imprinted gene, KCNQ1DN, within the WT2 critical region of human chromosome 11p15.5 and its reduced expression in Wilms' tumors. *J Biochem* **128**, 847-53.
219. Higgins, M. J., Diaz-Meyer, N., Day, C. D., Khatod, K., Maher, E. R., Cooper, W., Reik, W., Junien, C., Graham, G., Algar, E. & Kaloustian, V. M. D. (2003). Silencing of CDKN1C (p57(KIP2)) is associated with hypomethylation at KvDMR1 in Beckwith-Wiedemann syndrome. *Journal of Medical Genetics* **40**, 797-801.
220. John, R. M., Wood, M. D., Hiura, H., Tunster, S., Arima, T., Shin, J. Y. & Higgins, M. (2010). Autonomous silencing of the imprinted Cdkn1c gene in stem cells. *Epigenetics* **5**, 214-221.
221. Vucetic, Z., Totoki, K., Schoch, H., Whitaker, K. W., Hill-Smith, T., Lucki, I. & Reyes, T. M. (2010). Early life protein restriction alters dopamine circuitry. *Neuroscience* **168**, 359-70.
222. Hirasawa, R., Chiba, H., Kaneda, M., Tajima, S., Li, E., Jaenisch, R. & Sasaki, H. (2008). Maternal and zygotic Dnmt1 are necessary and sufficient for the maintenance of DNA methylation imprints during preimplantation development. *Genes Dev* **22**, 1607-16.
223. Simmons, R. A., Templeton, L. J. & Gertz, S. J. (2001). Intrauterine growth retardation leads to the development of type 2 diabetes in the rat. *Diabetes* **50**, 2279-86.
224. Metges, C. C., Lang, I. S., Hennig, U., Brussow, K. P., Kanitz, E., Tuchscherer, M., Schneider, F., Weitzel, J. M., Steinhoff-Ooster, A., Sauerwein, H., Bellmann, O., Nurnberg, G., Rehfeldt, C. & Otten, W. (2012). Intrauterine growth retarded progeny of pregnant sows fed high protein:low carbohydrate diet is related to metabolic energy deficit. *PloS one* **7**, e31390.
225. Langley-Evans, S. C., Daniel, Z. C., Wells, C. A., Ryan, K. J., Plant, R. & Welham, S. J. (2011). Protein restriction in the pregnant mouse modifies fetal growth and pulmonary development: role of fetal exposure to β -hydroxybutyrate. *Experimental physiology* **96**, 203-15.
226. Alho, J. S., Herczeg, G., Laugen, A. T., Rasanen, K., Laurila, A. & Merila, J. (2011). Allen's rule revisited: quantitative genetics of extremity length in the common frog along a latitudinal gradient. *Journal of evolutionary biology* **24**, 59-70.
227. Wakeling, E. L. (2011). Silver-Russell syndrome. *Archives of disease in childhood* **96**, 1156-61.
228. Binder, G., Begemann, M., Eggermann, T. & Kannenberg, K. (2011). Silver-Russell syndrome. *Best practice & research. Clinical endocrinology & metabolism* **25**, 153-60.
229. Luedi, P. P., Hartemink, A. J. & Jirtle, R. L. (2005). Genome-wide prediction of imprinted murine genes. *Genome research* **15**, 875-84.

230. Luedi, P. P., Dietrich, F. S., Weidman, J. R., Bosko, J. M., Jirtle, R. L. & Hartemink, A. J. (2007). Computational and experimental identification of novel human imprinted genes. *Genome research* **17**, 1723-30.
231. Rose, R. W. (2010). Development of endothermy and non-shivering thermogenesis in the Tasmanian bettong: a review. *Macropods: The Biology of Kangaroos, Wallabies and Rat-Kangaroos*, 109-115.
232. Jastroch, M., Withers, K. W., Taudien, S., Frappell, P. B., Helwig, M., Fromme, T., Hirschberg, V., Heldmaier, G., McAllan, B. M., Firth, B. T., Burmester, T., Platzer, M. & Klingenspor, M. (2008). Marsupial uncoupling protein 1 sheds light on the evolution of mammalian nonshivering thermogenesis. *Physiological Genomics* **32**, 161-169.
233. Nicol, S. C. & Andersen, N. A. (2008). Rewarming rates and thermogenesis in hibernating echidnas. *Comparative Biochemistry and Physiology a-Molecular & Integrative Physiology* **150**, 189-195.
234. Rakhshandehroo, M., Koppen, A. & Kalkhoven, E. (2012). Pref-1 preferentially inhibits heat production in brown adipose tissue. *The Biochemical journal* **443**, e3-5.
235. Armengol, J., Villena, J. A., Hondares, E., Carmona, M. C., Sul, H. S., Iglesias, R., Giralt, M. & Villarroya, F. (2012). Pref-1 in brown adipose tissue: specific involvement in brown adipocyte differentiation and regulatory role of C/EBPdelta. *The Biochemical journal* **443**, 799-810.
236. Fujiwara, K., Hasegawa, K., Ohkumo, T., Miyoshi, H., Tseng, Y. H. & Yoshikawa, K. (2012). Necdin controls proliferation of white adipocyte progenitor cells. *PloS one* **7**, e30948.
237. Haig, D. (2008). Huddling: Brown fat, genomic imprinting and the warm inner glow. *Current Biology* **18**, R172-R174.
238. Haig, D. (2004). Genomic imprinting and kinship: How good is the evidence? *Annual Review of Genetics* **38**, 553-585.